

UNIVERSITY OF OKLAHOMA

GRADUATE COLLEGE

THE ORGANIC GEOCHEMICAL VARIABILITY IN DEPOSITIONAL ENVIRONMENTAL
PROCESSES WITHIN A STRATIGRAPHIC SEQUENCE OF THE WOODFORD SHALE IN
THE ARDMORE BASIN, OKLAHOMA

A THESIS

SUBMITTED TO THE GRADUATE FACULTY

In partial fulfillment of the requirement for the

Degree of

MASTER OF SCIENCE

By

TARA ANGGITA PUTRI

Norman, Oklahoma

2020

THE ORGANIC GEOCHEMICAL VARIABILITY IN DEPOSITIONAL ENVIRONMENTAL
PROCESSES WITHIN A STRATIGRAPHIC SEQUENCE OF THE WOODFORD SHALE IN
THE ARDMORE BASIN, OKLAHOMA

A THESIS APPROVED FOR THE
SCHOOL OF GEOCIENCES

BY THE COMMITTEE CONSISTING OF

Dr. Xiaolei Liu, Chair

Dr. R. Paul Philp, Co-Chair

Dr. Michael Engel

© Copyright by TARA ANGGITA PUTRI 2020

All Rights Reserved.

To my parents and my sisters for their undying support, and bountiful of love...

*To my beloved friends who have supported me and helped me throughout my
academic journey...*

Thank you all for being the light in my life!

ACKNOWLEDGEMENTS

I want to first of all express my sincerest gratitude to Dr. R. Paul Philp, who has supported me from the beginning, His guidance, mentorship, and support has made the completion of my thesis wholesome. He has taken me in from the beginning as an undergraduate research assistant and believed in my capabilities and potential throughout the way. For that I thank you for all the time you have given me.

I would also like to thank Dr. Xiaolei Liu and Dr. Michael Engel for serving in my committee and giving me the time to review my thesis. I truly appreciate the guidance and valuable feedback you have given to me for this thesis. Moreover, I would like to express my deepest gratitude for Dr. Roger Slatt. Thank you for supporting and giving me valuable advice throughout my graduate program.

My gratitude to the OU Organic Geochemistry Laboratories is endless, especially to Mr. Jon Allen and Mr. Larry Hyde for guiding me with the technical support that helped me accomplish my data collection. Multitude of gratitude toward Brian and Dan Jarvie for providing the Rock-Eval analysis at no charge. Furthermore, the support, time, and advice from Dr. Tomasz Kuder, Emilio Torres, Richard Brito, Carl Symcox, Andreina Liborius, Gregory Connock, Brittney Tamborello, Chenxi Xu, and Dallas Cook.

I want to give my appreciation to the director, faculty, and staff members of the OU Mewbourne College of Earth and Energy, including the School of Geosciences. For your generosity in providing me with the recognition, honors, scholarship and support that have helped me make this journey possible, I thank you all.

Many folds of gratitude and appreciation to all my friends from the University that have made positive impact throughout my journey and has given me the strength to push through: Delcio Teixeira, Dalila De Jesus, Omar Amer, Roberto Clairmont, Nishit Garg, Madhunika Suresh, Peter Mueller, Aditya Narasimhan, Brandon Maples, Tatiana Martinez McBride, and Stefan Varickappallil. You all have given me the strength and support throughout all of my downfalls and brightened my days. These are the friendships I will cherish throughout my life, and I am gratefully for each of the role you all play in my life. I would also like to thank the supportive international community: International Student Services, International Advisory Community, and College of International Studies.

Most of all, I would express my special and deepest gratitude to my beloved family, my parents, Karina, and Deandra. Thank you for supporting me, lifting me up when I'm down, and for believing in me. I would not be where I am today without your guidance.

Thank you very much to all!

Table of Contents

Acknowledgements	v
Table of Contents	vii
List of Figures	ix
List of Tables	xvii
Abstract	xix
CHAPTER I	1
1. Introduction	1
1.1. <i>The Woodford Shale of Oklahoma</i>	1
1.2. <i>Biomarkers</i>	3
1.3. <i>Regional Geology</i>	5
1.4. <i>Paleogeography and climate</i>	9
1.5. <i>Sequence Stratigraphy and the Woodford Shale</i>	12
1.6. <i>Objectives</i>	16
1.7. <i>Purpose of study</i>	17
CHAPTER II	18
2. Methodology	18
2.1. <i>Study Area and sample Location</i>	18
2.2. <i>Lithofacies Classification and discussion</i>	20
2.2.1. <i>Argillaceous Shales</i>	23
2.2.2. <i>Siliceous Shales</i>	23
2.2.3. <i>Brown Siliceous Shales</i>	23
2.2.4. <i>Siliceous-Dolomitic Shales</i>	23
2.2.5. <i>Siliceous Mudstones</i>	24
2.2.6. <i>Cherts</i>	24
2.2.7. <i>Dolomitic Mudstone</i>	24
2.3. <i>Experimental</i>	25
2.3.1. <i>Rock-Eval Pyrolysis and Leco-TOC</i>	25
2.3.2. <i>Laboratory Experimental Procedures</i>	25
2.3.2.1. <i>Preliminary Samples Preparation</i>	25
2.3.2.2. <i>Extraction of Organic Matter</i>	26
2.3.2.3. <i>De-Asphaltening Process – Bitumen Fractionation</i>	28
2.3.2.4. <i>Maltene Fractionation</i>	28
2.3.2.5. <i>Gas Chromatography</i>	29
2.3.2.6. <i>Gas Chromatography – Mass Spectrometry</i>	30
CHAPTER III	32
3. Results and Discussion	32
3.1. <i>Geochemical Screening</i>	32

3.2. Organic Richness	35
3.3. Organic Matter Type	42
3.4. Kerogen Type.....	43
3.5. Thermal Maturity from Rock-Eval	45
3.6. Gas Chromatography	48
3.6.1. n-Alkane distribution	49
3.6.2. Pristane and Phytane	50
3.6.3. Steranes	55
3.6.3.1. Organic Matter Source	58
3.6.3.2. Thermal maturity indicators	67
3.6.3.3. Lithology	69
3.6.4. Terpanes.....	72
3.6.4.1. Organic Matter Source	74
3.6.4.2. Depositional Environments.....	76
3.6.4.2.1. Ts and Tm.....	77
3.6.5. C ₄₀ Aromatic carotenoids and aryl isoprenoid	85
3.6.6. Tetracyclic Polyprenoids	92
3.6.7. Dibenzothiophene and phenanthrene	96
CHAPTER IV	100
4. Discussion	100
4.1. High Resolution Analysis of Biomarker Distributions	100
4.1.1. Organic Matter Source	101
4.1.2. Depositional Environment	104
4.1.3. Marine vs. Lacustrine	105
4.2. Evidence of Frasnian – Famennian Extinction Boundary	106
CHAPTER V	113
5. Conclusion	113
References	116
Appendix I: Naphthalene and Phenanthrene	135
Appendix II: Structures	142
Appendix III: Abbreviations and formulas for calculation of geochemical biomarkers	147
Appendix IV: Fragmentograms	149
GC chromatograms	159
Speake Ranch Outcrop m/z 191	175
Speake Ranch Outcrop m/z 217	192
Additional Chromatogram.....	208

LIST OF FIGURES

Figure 1. Major geologic provinces of Oklahoma encasing the Southern Oklahoma Aulacogen that comprises the Anadarko, Marietta, and Ardmore Basin (Ham et al., 1964).....	6
Figure 2. Map of Oklahoma and the tectonic activities during the early Paleozoic showing the Southern Oklahoma Aulacogen (Allen, 2000; Brueske et al., 2016). Two of the arms of the three-arm rift joined to form the Early Paleozoic continental margin, while the third arm formed the SOA. CO: Colorado; OK: Oklahoma; MO: Missouri; AR; Arkansas; LA: Louisiana; TX: Texas; NM: New Mexico; WM: Wichita Mountains, AM; Arbuckle Mountains; WVF: Washita Valley Fault; MVF: Mountain View Fault.....	7
Figure 3. The tectonic events that occurred from the Cambrian until the Permian to illustrate the basinal history of the Ardmore Basin in Oklahoma (Hoffman et al., 1974).....	8
Figure 4. Tectonic map illustrating the location of the study within the Ardmore Basin at the southern flank of the Arbuckle Mountains (Northcutt and Campbell, 1995).....	8
Figure 5. Cross-section across the Southern Oklahoma Aulacogen including the Woodford Shale in the Ardmore Basin. (Ham et al., 1973).....	9
Figure 6. Paleogeography of the mid-continent North America within the Late Devonian and Early Mississippian illustrating the marine transgression that overwhelmed the Oklahoma region (Robinson and Kirschbaum, 1995; modified from Comer, 2008; Blakey, 2011; and illustrated by Galvis, 2017).....	11
Figure 7(a). Sea Level curve displaying relative positions during a Highstand System Tract, Transgressive System Tract, and Lowstand System Tract; and (b). model of the sea level fluctuation stages relative to the depositional and erosional process (Slatt et al., 2016; Slatt and Rodriguez, 2012).....	14

Figure 8. Model of water stratification, and anoxic environment within the minibasins for the Woodford Shale in the Ardmore Basin, Oklahoma.....15

Figure 9. Top figure is location of Ardmore Basin in Oklahoma between the Carter and Murray county which is included in the SCOOP play. Middle figure is the location of Speake Ranch Quarry just west off of I-35 in Southern Oklahoma. Bottom figure is the exposed Speake Ranch Outcrop displaying the complete section of the Woodford Formation including the underlying Hunton Formation, and the overlying Sycamore Formation (Cardott, 2012; Galvis, 2017).19

Figure 10. Stratigraphic column and outcrop Gamma Ray depth log of the Woodford Shale from Speake Ranch. The colors of the lithofacies correlate to those in Figure 11. The Upper Woodford is overwhelmed with phosphate concretions within the chert lithofacies indicated by the red circles (Galvis, 2017).....21

Figure 11. The 13 identified lithofacies within the Woodford Shale of South Central Oklahoma distinguished between the soft and hard layers (Galvis, 2017).....22

Figure 12(a). Process workflow of sample processing of the Woodford Shale for organic biomarker analysis; **(b).** Enhanced process workflow of sample processing of the Woodford Shale for organic biomarker analysis displaying the detailed fractionation process.....27

Figure 13. Gas chromatograms displaying the distribution and separation of the n-alkanes. Upper right chromatogram shows the saturate and aromatic fractions (Philp, 2000).....30

Figure 14. Programmed temperature of Rock-Eval 6 pyrolysis displaying the resulting products and heat signatures (McCarthy et al., 2011).....33

Figure 15. TOC abundance distribution across all the Woodford members from Speake Ranch studied by Galvis (2017). The Lower Woodford displays the most organic rich intervals within the soft lithofacies intervals. The Middle Woodford shows nearly equivalent ratio of hard to soft lithofacies. The Upper Woodford has the lowest average TOC values and a higher hard to soft lithofacies ratio. The TOC and Gamma Ray plots illustrate that high TOC is not always correlative

to high Gamma Ray response. The higher Gamma Ray plots may be an effect of the radioactive component, phosphatic particles (Galvis, 2017).....36

Figure 16. Depth Plots of Gamma-Ray, TOC%, S₁, and XRF-Hardness data for the 536 Speake Ranch samples (Galvis, 2017).....38

Figure 17. Soft vs. hard relationship with TOC. The softer bed intervals have positive correlations with increasing TOC, while the hard lithofacies intervals have negative correlations with TOC (Galvis, 2017). Hard bed lithofacies are enriched in quartz content and depleted in clay content, while the soft bed lithofacies are enriched in clay content. The outlier symbols of the hard bed and soft beds with significantly low quartz content, may be an indication of dolomites.39

Figure 18. Model of depositional environment and water column s for both higher water levels and lower water levels. Higher water levels cause vertical mixing of the water column and introduces oxygen to the system. Lower water levels cause a restricted water column accompanied with stratification (Tulipani et al., 2013).....40

Figure 19. Depth Plots of defined parameters from Rock-Eval pyrolysis and Leco TOC. (Organic richness: TOC wt%, maturity: T_{max}, Hydrogen Index: S₂/TOC*100, Oxygen Index: S₃/TOC*100, and Si/Al) The grey intervals signify the soft bed intervals while the white intervals indicate hard beds.41

Figure 20. Kerogen classification and maturity assessment utilizing T_{max} vs. Hydrogen Index (HI) parameter plot useful in aiding primary interpretation of source rock analysis. The Speake Ranch samples are primarily a Type II kerogen with several samples plotting as Type III.....42

Figure 21. Pseudo van Krevelen type kerogen type plot plotting the HI vs. the OI to assess the kerogen type of the Woodford samples from Speake Ranch. 37 of the studied samples indicate a Type I and Type II kerogen. Outlier sample points within the circles are most likely to a result from organic matter source input.....45

Figure 22. Depth plot of T_{max} showing variations within the 40ft sequence. There is little to no variation in the distribution of the maturity parameter, which justifies suggesting that thermal alteration is not a factor contributing to observed biomarker variations.....47

Figure 23. Distribution of vitrinite reflectance in South Central Oklahoma. Petrographic vitrinite reflectance of Speake Ranch ranges from immature to early oil window, with a mean of 0.60%Ro (Cardott, 2012; Galvis, 2017).....48

Figure 24. Gas chromatogram of the saturate fraction from the extract of the sample at a depth of 229.0 ft from the Woodford Shale at Speake Ranch.....50

Figure 25. Pr/n-C₁₇ vs. Ph/n-C₁₈ illustrating the redox conditions for the Woodford Shale from the Speake Ranch. All the studied source rock samples illustrate a Type II and Type II/III kerogen of marine and marine-terrigenous mixed organic matter deposited within a reducing environment.....52

Figure 26. Integration of TOC depth plot and Pr/Ph depth plot generated in this study. Pr/Ph parallels the oscillation of TOC which coincides with the preservation of abundant organic matter within anoxic intervals. Gray intervals indicate soft bed layers, while the white intervals indicate hard bed layers. The red line is the Upper Woodford and Middle Woodford boundary.....54

Figure 27. Pr/Ph vs. C₂₇ diasteranes/steranes (Appendix III; modified from Moldowan et al. 1994). The arrow shows the expected direction of thermal maturity effect, which is not considered for these specific samples since they are all of relatively low-maturity rocks. The diagram shows that Pr/Ph varies as clay content stays nearly consistent.....55

Figure 28. Distribution of the steranes and diasteranes resulting from monitoring the ion at m/z 217. Molecular structure of sterane from Pratt et al. (1992) (IV, V, VI; Appendix II).57

Figure 29(a). Ternary plot of the C₂₇-C₂₈-C₂₉ steranes to indicate organic matter source for the Woodford Shale. Majority of the samples are seen clustering in an abundance of C₂₇ steranes indicating an open marine environment (sterane ternary plot recreated from Huang and Meinschein, 1979); **(b).** distribution determined by Moldowan et al. (1985) for source rocks of varying ages..... 59

Figure 30. Geochemical logs representing the environmental condition variations that yield the distribution of organic matter source. Gray intervals indicate the soft bed lithofacies.....60

Figure 31. Geochemical logs correlating TOC fluctuations, with the associated marine vs. terrigenous source input (C_{27}/C_{29} sterane), and the role of anoxia (Pr/Ph) in its distribution. Highlighted zones indicate that low preservations of organic matter are associated with high C_{29} input and oxidizing environmental deposition conditions. Gray zones are the soft bed intervals, and the white zones are the hard bed intervals.....64

Figure 32. The plot on the right display the relative abundances of C_{27} and C_{29} [C_{27} 14 α ,17 α - +14 β ,17 β -Steranes(20S+20R)/total steranes; C_{29} 14 α ,17 α - +14 β ,17 β -Steranes (20S+20R)/total steranes; **Appendix III**; triangles: C_{27} /total steranes; circles: C_{29} /total steranes]. Decrease in C_{27}/C_{29} steranes coincide with a relative increase in C_{29} steranes.....65

Figure 33. C_{27}/C_{29} steranes vs. Pr/Ph plot characterizing the Woodford Shale from Speake Ranch as algal rich organic matter deposited in an anoxic environment. (modified from Hossain et al., 2009). Samples plotting below 0.55 indicate terrigenous input into the anoxic environment.....65

Figure 34. Maturity plot of the 20S/(20S+20R) vs. C_{29} $\beta\beta/(\beta\beta+ \alpha\alpha)$ isomers. This plot illustrates clustering of the Woodford Shale samples from Speake Ranch due to their similar levels of maturity. Upper Woodford and Middle Woodford may indicate samples of migrated HC (modified from Peters et al., 1999). Blue circles symbol indicates Middle Woodford and, red triangle symbols indicate Upper Woodford samples. Outlier may be due to partial sterane biodegradation that results in increase of the 20S, by selective removal of the 20R epimer by bacteria.....69

Figure 35. C_{27} diasterane to non-arranged sterane ratio [C_{27} 13 β ,17 α -Diacholestane (20S+20R)]/[C_{27} 14 α ,17 α - + 14 β ,17 β -Cholestane (20S+20R)] as a correlative tool to indicate lithology and level of anoxia. High diasterane values over the regular steranes indicate clay rich intervals, which coincide with the soft beds of the Speake Ranch samples deposited in an anoxic environment, determined by the Pr/Ph ratio.....71

Figure 36 (a). Pr/Ph ratio vs. diasterane/sterane ratio is used to determine the lithology and the extent of anoxia the sediments were deposited (modified from Moldowan et al., 1994) **(b).** C₂₇/C₂₉ sterane ratio vs. C₂₇/C₂₉ diasterane ratio to further support organic matter source influx of predominantly marine with mixed marine (modified from Ghori, 2002). Ratio description are included in the Appendix.....72

Figure 37. GC-MS chromatograms displaying the distribution of the terpane biomarkers within the Woodford shale screened at m/z 191.....73

Figure 38. Depth logs of C₂₃ TT/C₂₄ Tet, C₃₅/C₃₄ homohopane, C₂₇ diasterane/sterane and Pr/Ph to correlate origin of organic source matter using terpane parameters and its correlation to anoxia. Highlighted interval show increase in C₂₃ TT/C₂₄ Tet of marine indication along with low values of C₃₅/C₃₄ Homohopane, C₂₇ diasterane/sterane and Pr/Ph parameters reflecting anoxic marine sediments.....75

Figure 39. C₃₅/C₃₄ Homohopane vs. C₂₉ Ts/C₃₀ D plot to determine lithology and oxicity level of depositional environment. The Speake Ranch samples were largely deposited in anoxic environment with oxic to sub-oxic disturbances (Zumberge, 2000).....77

Figure 40. Geochemical logs to determine anoxia proxies (Ts/Tm) of Speake Ranch deposition, and if (at all) output values have been affected by thermal maturation determined using C₂₉ sterane 20S/(20S+20R).....78

Figure 41. Depth plots for indication of water salinity, water column stratification, and anoxia. GI define the water column stratification, TPP/C₂₇Diasterane and Hopane/C₂₇αααS+R sterane define the organic matter source, and Pr/Ph defines the water column anoxia. The highlighted intervals indicate persistence of GI with varying anoxia levels, independent from organic matter source input.....80

Figure 42. Plot of the relationship between Gammacerane Index and Pr/Ph of the Woodford Shale. Despite varying levels of anoxia, water stratification persisted throughout the interval of Speake Ranch (modified from Mello et al., 1988).....81

Figure 43. Speake Ranch anoxia proxies utilizing C₂₈ BNH/C₃₀ hopane, C₂₈ BNH/C₂₉ norhopane, and Pr/Ph to observe frequency of anoxia.....83

Figure 44. Identification of the C₄₀ carotenoids screened at summed m/z 133+134 at depth 204.5ft within the Middle Woodford. Top chromatogram is at depth 205ft from the soft bed, and bottom chromatogram is at depth 204.5ft from the hard bed.86

Figure 45. Paleorenieratane/Isorenieratane ratio vs. Pr/Ph ratio illustrating reducing conditions of the Speake Ranch samples defined by the concentration and distribution of carotenoids.....86

Figure 46. GC-MS chromatogram showing the distribution of aryl isoprenoids in the aromatic fraction at the summed m/z 133+134. 2,3,6-trimethyl substituted aryl isoprenoids (**XXII**) are indicated by the letter b, and the 3,4,5-trimethyl substituted aryl isoprenoids (**XXIII**) are indicated by the letter a.....88

Figure 47. Depth plots of biomarker parameters as indicator for water structure and chemistry in the Woodford Shale at Speake Ranch. Pr/Ph indicating the redox state of the Woodford paleoenvironment, AIR and C₁₈ Aryl Isoprenoid signify the H₂S presence within the photic zone as well as the stability of the PZA, and the C₂₇/C₂₉ used as a correlation to the effects of the organic matter input source.....91

Figure 48. Fragmentogram of C₃₀ tetracyclic polyprenoid (**XII**) on mass spectra 259. SR-192a is a hard bed at depth 192 ft, and SR-193b is a soft bed at 193.5 ft.....93

Figure 49. Variation in the TPP screened at m/z 259 along with its correlation to gammacerane Index, C₃₀Hopane/C₂₇ $\alpha\alpha\alpha$ S+R sterane, C₂₆/C₂₅ TT, Ts/Tm to determine intervals that illustrate the level of restriction in the water column of the Woodford depositional environment. Highlighted intervals indicate intervals when the environment of deposition for the Woodford Shale at Speake ranch was highly restricted.....94

Figure 50. GC-MS chromatogram monitored for the variation in the dibenzothiophenes (**XVI**) at m/z 184+198+212. The m/z 184 is used to identify the dibenzothiophene, m/z 198 is used to identify the methyl dibenzothiophene, and m/z 212 is used to identify the dimethyl dibenzothiophene.....96

Figure 51. GC-MS chromatogram displaying the distribution of the phenanthrenes (XV) series observed at summed m/z 178+192+206. The m/z 178 is used to identify the phenanthrene, m/z 192 is used to identify the methylphenanthrenes, and m/z 206 is used to identify the dimethylphenanthrenes.....97

Figure 52. The Woodford samples from Speake Ranch show that the major lithology of the source rock is lacustrine/ marine shale of low Pr/Ph and DBT/Phen values. There are several of the hard bed intervals that indicate sulfate poor lacustrine environment (modified from Hughes et al., 1995).....98

Figure 53. Correlation of redox conditions (Pr/Ph, C₂₈ BNH/C₃₀hopane, and C₂₈ BNH/norhopane), presence of sulfur in water column (DBT/PHEN), and water column stratification (gammacerane), to the abundance of organic matter (TOC wt%) of the Woodford Shale from Speake Ranch. Gray intervals indicate the soft beds, and white intervals indicate the hard beds.99

Figure 54. Depth plots of the parameters defining the source of organic matter and its correlation to the Gamma Ray. Yellow highlighted intervals are the chosen samples for high resolution analysis with TOC values ~11%, and red highlighted intervals are chosen samples for low TOC ~3%.....104

Figure 55. Organic geochemical parameters to define the anoxia, eutrophication, and organic matter input to determine the Frasnian – Famennian extinction boundary in the Woodford Shale of the Ardmore Basin in Oklahoma. Highlighted intervals signify the pulses leading up to the F-F.....111

LIST OF TABLES

Table 1. Geochemical screening parameters defined by Peters and Cassa (1994) and Tissot and Welte (1984) for Rock-Eval pyrolysis and Leco-TOC.....	34
Table 2. Bulk geochemical data of the Woodford Shale from Speake Ranch, including S1, S2, S3, HI, OI, Tmax, S1/TOC, and Pr/Ph Pr/Ph.....	53
Table 3. Peak identification of the steranes of sample SR-223a at depth 223ft within the Upper Woodford of Speake Ranch.....	56
Table 4. Sterane and terpane biomarker proxies to determine organic matter source. Empty fields are due to the lack of maltene from extraction.....	61
Table 5. Peak identification of the terpanes at m/z 191 fragmentogram.....	73
Table 6. Geochemical parameters defined to determine redox conditions of the Woodford Shale from Speake Ranch. Empty intervals are due to the lack of maltene from extraction.....	84
Table 7. Peak Identification for the 2,3,6- and 3,4,5 trimethyl substitution for the aryl isoprenoid chromatogram at m/z 133-134 in Figure 48 (TMB: trimethylbenzenes)	89
Table 8. Biomarker proxies for water structure and chemistry in the Woodford Shale at Speake Ranch. Pr/Ph, HHI, and C ₃₅ /C ₃₄ HH indicating the redox state of the Woodford paleoenvironment, AIR and C ₁₈ Aryl Isoprenoid signify the H ₂ S presence within the photic zone as well as the stability of the PZA, and the C ₂₇ /C ₂₉ steranes used as a correlation to the effects of the organic matter input source.....	90
Table 9. Variation in the TPP screened at m/z 259 along with its correlation to gammacerane Index, C ₃₀ Hopane / C ₂₇ Sterane $\alpha\alpha\alpha R + \alpha\alpha\alpha S$, C ₂₆ TT/ C ₂₅ , Ts/Tm to determine intervals that illustrate the level of restriction in the water column of the Woodford depositional environment. DBT/Phen is used to determine the availability of H ₂ S in the anoxic water column.....	95
Table 10. Defining parameter for DBT/Phen with Pr/Ph outputs classified into 4 zones with 4 distinct environments and its associated lithology.....	99

Table 11. Source Rock evaluation high resolution analysis of similar high TOC values distributed throughout the 40ft interval. Lighter green tables indicating Middle Woodford data.....101

Table 12. Organic matter source high resolution analysis of similar high TOC values distributed throughout the 40ft interval to distinguish variability. Lighter green tables indicating Middle Woodford data.....103

Table 13. Main elements analyzed through XRF and their significance in chemostratigraphic interpretations (Galvis, 2017; compiled in Turner, 2016).....103

Table 14. Redox condition high resolution analysis of similar high TOC values distributed throughout the 40ft interval to distinguish variability. Lighter green tables indicating Middle Woodford data.....105

Table 15. Lacustrine vs. Marine source high resolution analysis of similar high TOC values distributed throughout the 40ft interval to distinguish variability. Lighter green tables indicating Middle Woodford data, and white intervals indicate Upper Woodford.....106

ABSTRACT

The Devonian-Early Mississippian Woodford Shale underlying the subsurface of Carter and Murray Counties in the Ardmore Basin, Oklahoma, USA, has attracted growing interest as an unconventional reservoir. Heterogeneity has always been assumed within samples collected from different locations, while uniformity is often assumed in a stratigraphic sequence of the shale both in chemical and physical properties. However, the Woodford Shale is composed of characteristically different layers, a soft bed comprising of higher TOC, higher ductility and clay, as well as a hard layer that is lower in TOC, higher in brittleness and in silica content which greatly contributes to the variation in biomarker distributions. The bulk of the interval shows pristane/n-C₁₇ vs. phytane/n-C₁₈ ratios, C₂₇/C₂₉ sterane ratios, diasterane/sterane ratios, and Ts/Tm ratios indicating a reduced, marine depositional environment, low in maturity.

The variations between the soft and hard beds are responsible for the variability of the biomarkers rather than solely depth. These variations can be seen within the C₃₀ hopanes that show higher values within the harder beds relative to the higher TOC softer beds. Samples have been taken at 6" intervals over a 40ft. outcrop of the Woodford shale to investigate variability in organic facies, source input, and depositional environment conditions.

Shale samples have been characterized by Rock-Eval to determine TOC and hydrocarbon potential to identify variations of biomarkers in TOC rich intervals and TOC lean intervals. Additionally, shale extracts were processed by gas chromatography (GC), gas chromatography-mass spectrometry (GC-MS) and GC-MS-MS to acquire biomarker traces that aid in the construction of paleoenvironmental conditions. Furthermore, the Frasnian-Famennian mass extinction which occurred at the Late Devonian is reflected to have occurred within this interval based on significant changes in the geochemical data. Variations in the biomarker distributions

signify the heterogeneity of the shale over this 40ft interval, which in turn will yield fundamental information related to fine differences that affect reservoir quality in exploration and production of unconventional reservoirs.

CHAPTER I

1. Introduction

1.1 The Woodford Shale of Oklahoma

Fossil fuels have been central to energy resources, relying on hydrocarbon properties to fulfill energy needed to power everyday life. Fossil fuels have become the most sought after and effective source to power energy for life on Earth. It is the vital component to natural gas, oil, and coal for which researchers and industries are endlessly exploring today. The fame of oil and gas rose to fruition when the first oil well was drilled on August 27, 1859 near Titusville in northwestern Pennsylvania (Binet et al., 2002). Today, oil and natural gas have become the most important sources of energy and the engine to modern society, energizing the industry, heating homes, providing fuel for vehicles and all modes of mobile transportation. The increasing necessity for the utilization of hydrocarbons has allowed for the progression and advancement in technology for efficiency and improvement to enhance refineries and transportation of materials. According to Parra et al. (2013) development of shale plays has risen exponentially, and nearly 1,000,000 total wells have already been drilled in the United States according to U.S. Energy Information Administration (2019). Hydrocarbons are the product of continuous generation and accumulation following thermal degradation of biologically derived organic matter deposited in a sedimentary environment (Mulik and Erdman, 1963). The quality and quantity of the organic matter may vary laterally and vertically depending on the process of sedimentation, environmental conditions upon deposition, and the processes that occur post-deposition (diagenesis/thermal alteration). The organic rich-sediments in oil-forming basins are referred to as source rocks and reflect the process of sedimentation over geologic time (Moldowan et al., 1985). According to Peters and Cassa (1994), there are three criterias to consider sediments as “generative source rocks” and these

depend on quantity (amount of organic matter), quality (type of organic matter), and thermal maturity (extent of burial and heating).

The Woodford Shale has risen to fame as the most important and productive hydrocarbon source rock in Oklahoma as well as being the source to the majority of the state's hydrocarbon reserves (Slatt and Rodriguez, 2012; Philp and deGarmo, 2020). Galvis et al. (2018) noted the Woodford Shale, Late Devonian-Early Mississippian in age, has excellent source/reservoir rock properties, which enabled optimal production of oil and gas. Moreover, the Woodford Shale has unconventional reservoir properties that many researchers are continuing to explore and uncover. Unlike the typical conventional reservoirs, unconventional shale reservoirs require hydraulic stimulations to generate commercial rates of hydrocarbons (Temraz et al., 2016). According to Hammes et al. (2013) and Soliman et al. (2015) unconventional shale reservoirs, which include tight-gas sandstone, as well as gas and oil shales, are reservoirs that essentially require additional special recovery operations. Therefore, the inherently complex process of expulsion in unconventional shale reservoirs gives way to the accumulation of significant volumes of oil and gas (Comer, 2008). The major questions for scientists are related to the process of organic material incorporation and preservation into the sediments. In addition, it is appropriate to understand the depositional conditions and settings conducive for the organic matter to be converted into the desired petroleum components (Dembicki Jr., 2017). The mystery of its unconventional properties and the exploration of the Woodford Shale has led to a series of questions that inspired this research.

The approach of this thesis research is to undertake a very high resolution organic geochemical analysis of mudrocks (shales) within a small interval of interbedded siliceous, clay-shale, and chert of the Woodford group. The geochemical data would be integrated with the

geological facets of sequence stratigraphy to uncover further knowledge of the depositional environmental processes within the Ardmore Basin that created the Woodford Shale. The goal is to determine and reconstruct processes that occurred upon deposition in the Ardmore Basin that yield the fine variabilities found in biomarkers. This is to correlate relationships between the current stratigraphic model, and biomarker distributions. The outcome of this research is the provision of fine-scale depositional processes and environmental condition changes that impact large-scale changes seen in the shales today.

1.2 Biomarkers

This research explores and investigates the realm of biomarkers in organic geochemistry. Biomarkers relay the story of the environment in which the sediments were deposited and the organisms that thrived during the Late Devonian – Early Mississippian. Biomarkers are compounds derived from precursors present in living organisms that once thrived (Connan, 1981). Biological markers help scientists determine the environmental conditions during the deposition of sediments, the burial conditions in diagenesis, the thermal maturation the sediments experienced during catagenesis, the degree of biodegradation, and the nature of the source materials of the sediments (Eganhouse, 1997; Philp and deGarmo, 2020). The resulting information that biomarkers provide are helpful tools to correlate with sequence stratigraphy to build on the story of sediment deposition and processes occurring to the organic matter during and after deposition. Exploring biomarkers has been one of the leading geologic methods in exploration, development, and production for oil and gas industries as well as environmental industries (Dahl et al., 1994). Biomarkers mostly retain the molecular structure that they inherit from their biological source (Pratt et al., 1992). Although, the biomarkers do experience alteration and biodegradation during

early diagenesis and catagenesis, this does not eradicate the source signature. The resilience of the carbon-based molecule structure within biomarkers provide geochemists with evidence of the contribution from either bacterial, algal, vascular plant, or animal sources that had accumulated in the sediments. Therefore, the varying geochemical output properties reflect the source input variations and the thermal alteration processes that occur post deposition (Moldowan et al., 1985). Organic matter can be found in two forms which are insoluble kerogen, and soluble bitumen where most of the biomarkers have been found to reside.

For biomarkers to become the effective and reliable indicators that they are today, they require optimal preservation conditions. Optimal preservation of organic matter upon and after deposition depend upon an environment that is anoxic (Volkman, 1988). This will commonly lead to organic-rich, oil-prone petroleum source rocks (Peters et al., 2005). According to Pratt et al. (1992), there are 3 stages for desired organic matter preservation: the first stage of preservation is restriction from oxidation and remineralization, followed by the prevention of destruction caused by both aerobic and anaerobic microbial process (Pratt et al., 1992; Romero and Philp, 2012) and lastly, the organic matter must retain its structure throughout the burial process (diagenesis) (Pratt et al., 1992). Therefore, the controls for optimal organic matter preservation are oxygen content within the water column, the biological productivity or the organisms thriving in the environment, water circulation/stratification, as well as sedimentation rate (Demaison and Moore, 1980). Furthermore, Kirkland et al. (1992) considered anoxic bottom-water conditions and limited water circulation to be the factors that inhibited aerobic microbial activity, which contributed to the enhanced preservation of the Woodford Shale. Different reducing conditions with varying Eh levels affect the biomarker precursor and their product pathways, which need to be taken into consideration (Moldowan et al., 1985).

1.3 Regional Geology

Devonian-Early Mississippian black shales have a complex depositional history reflecting a broad range of fundamental earth processes, such as paleoclimate, paleogeography, eustasy, and tectonism (Ettensohn, 1992). The Earth was in a greenhouse state during the Devonian and the warm climate provided a platform for high productivity. Tectonic activities have played a significant role in the evolution of black shale deposition as it provides the framework for the formation of restricted basins, favorable for organic-rich mud deposition (Klemme and Ulmishek, 1991; Ettensohn, 1997). With an overwhelming rate of subsidence over sedimentation, the sea floor became restricted, allowing for the water column to become stratified and dysoxic to anoxic (Ettensohn, 1992). Oklahoma is home to three major provinces that are the products of Early Paleozoic tectonic activities, namely the Oklahoma Basin, the Southern Oklahoma Aulacogen, and the Ouachita trough (Philp and deGarmo, 2020). The area of interest in this study is the Woodford Shale outcrop located within the Ardmore Basin of Oklahoma (Figure 1; Ham et al., 1964).

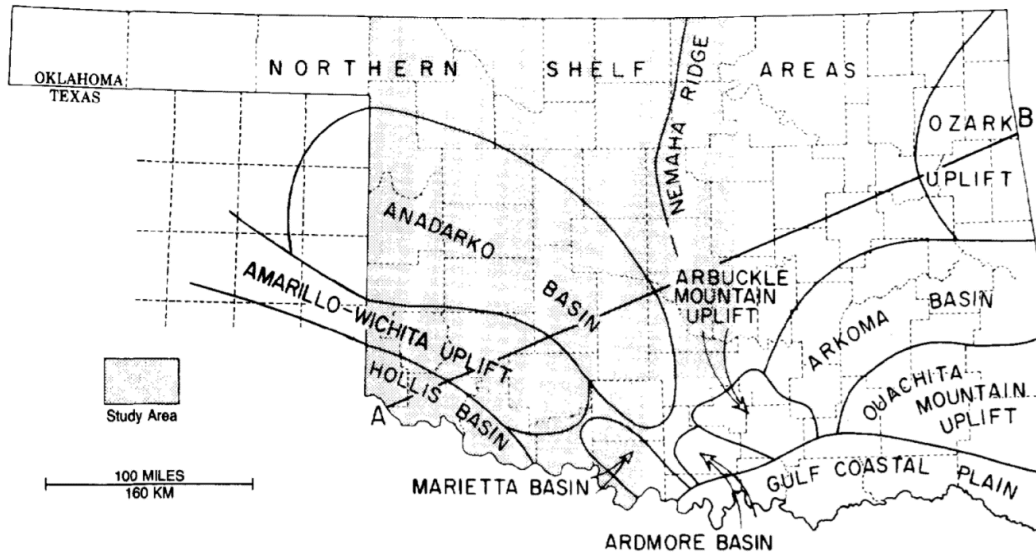


Figure 1. Major geologic provinces of Oklahoma encasing the Southern Oklahoma Aulacogen that comprises the Anadarko, Marietta, and Ardmore Basin (Ham et al., 1964).

The Ardmore Basin is a fault-bounded northwest depression of Pennsylvanian age in South Central Oklahoma (Granath, 1989). The Southern Oklahoma Aulacogen (SOA) is a major depocenter for the accumulation of the Woodford shale, due to an extensional failure in the form of a three-arm rift; SOA arose from the failed arm of the continental lithosphere extension which formed a NW-SE trending trough (Figure 2; Hoffman et al., 1974; Allen 2000; Brueske et al., 2016). The SOA is comprised of the Anadarko, Marietta, and Ardmore Basin (Figure 1; Ham et al., 1964). From the Cambrian to Early Devonian, shales, limestones, and sandstones were deposited within the mega-graben, that was a product of the failed arm of the SOA (Carlucci et al., 2014). After this period of deposition, and approaching the end of the Devonian, the Acadian Orogeny occurred, and eroded sediments that led to the deposition of the Woodford, Sycamore, Caney, and Springer formations well into the Early Pennsylvanian (Allen, 2000). Following this event, the Wichita Orogeny caused a major pulse of deformation, uplifting the Criner Hills 16,000ft above sea level. Then erosion of these structures provided sediments to be deposited into

the Ardmore and Marietta Basin throughout the Late Mississippian (Figure 3; Allen, 2000). Further structural deformation occurred as the Arbuckle Orogeny caused the folding of the Caddo anticline and the Arbuckle anticlines (Figure 4; Northcutt and Campbell, 1995; Allen, 2000). The Ardmore Basin was mostly affected by tectonic activities in the Late Mississippian – Pennsylvanian. However, processes of sedimentation began starting from the Cambrian to Late Devonian. The phases of these events are illustrated in Figure 3 (Hoffman et al., 1974). The Late Devonian to Early Mississippian Woodford Shale was deposited over a span of 33 million years in the Ardmore Basin within Oklahoma, Central USA, and reflects a multiple history of deformation and deposition (Figure 5; Ham et al., 1973; Paxton et al., 2006; Galvis et al., 2018).

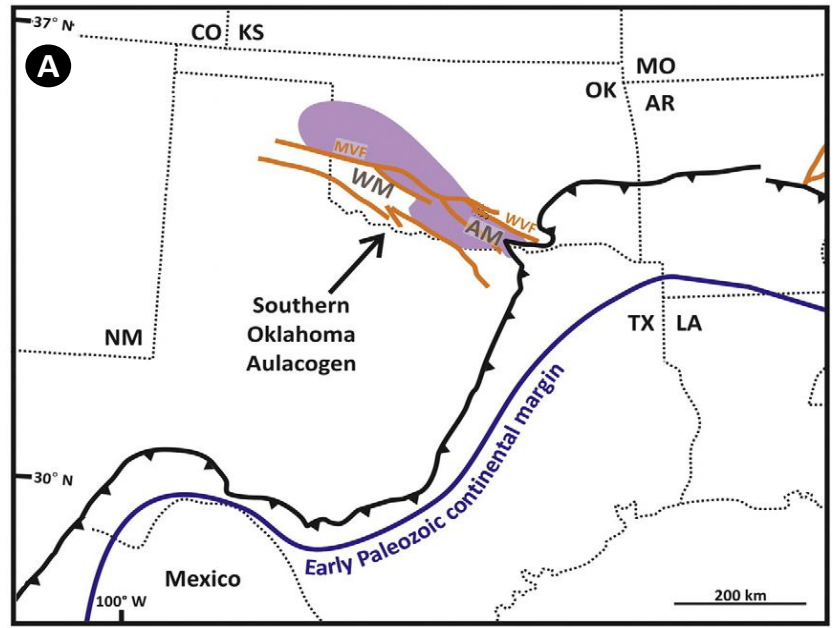


Figure 2. Map of Oklahoma and the tectonic activities during the early Paleozoic showing the Southern Oklahoma Aulacogen (Allen, 2000; Brueske et al., 2016). Two of the arms of the three-arm rift joined to form the Early Paleozoic continental margin, while the third arm formed the SOA. CO: Colorado; OK: Oklahoma; MO: Missouri; AR; Arkansas; LA: Louisiana; TX: Texas; NM: New Mexico; WM: Wichita Mountains, AM; Arbuckle Mountains; WVF: Washita Valley Fault; MVF: Mountain View Fault.

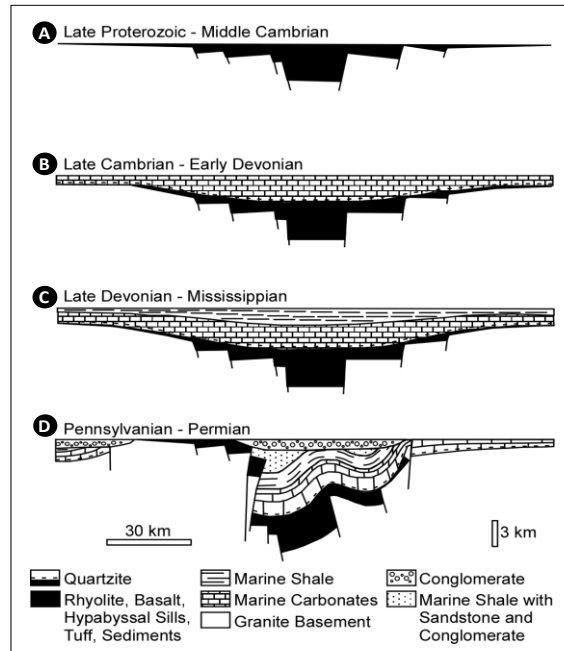


Figure 3. The tectonic events that occurred from the Cambrian until the Permian to illustrate the basinal history of the Ardmore Basin in Oklahoma (Hoffman et al., 1974).

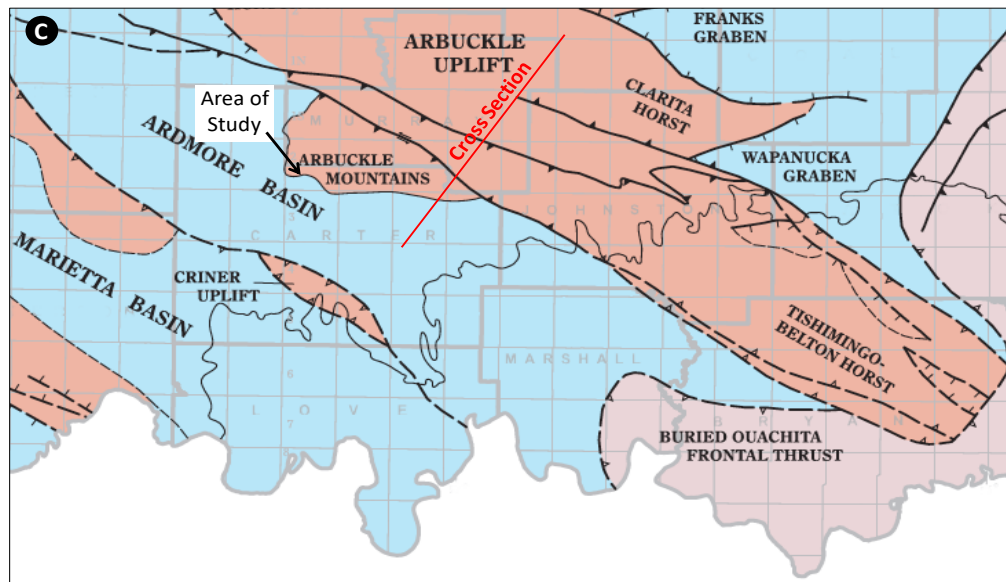


Figure 4. Tectonic map illustrating the location of the study within the Ardmore Basin at the southern flank of the Arbuckle Mountains (Northcutt and Campbell, 1995).

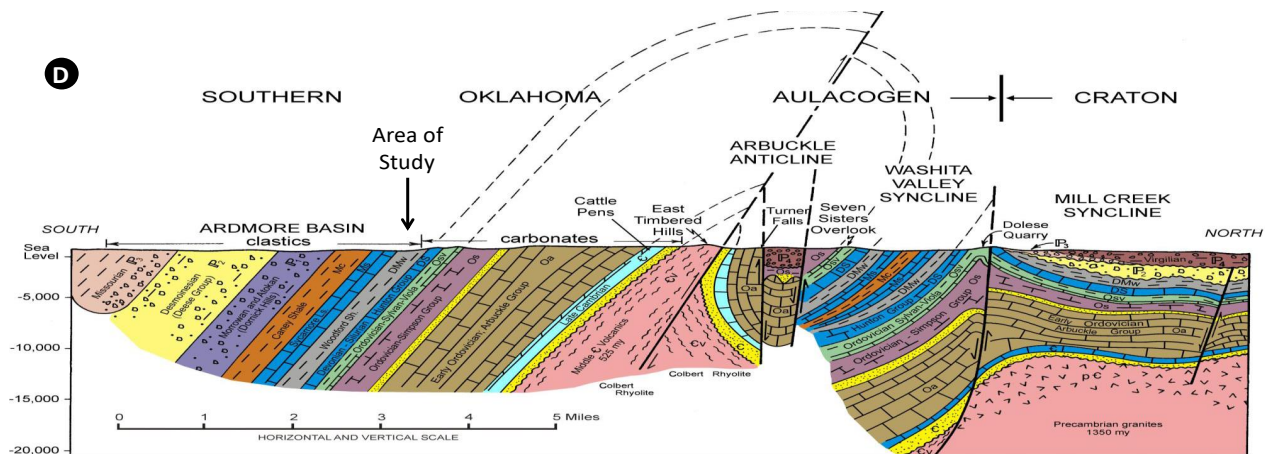


Figure 5. Cross-section across the Southern Oklahoma Aulacogen including the Woodford Shale in the Ardmore Basin. (Ham et al., 1973).

1.4 Paleogeography and climate

Understanding the variability within the sediment input also assists in the understanding of the global framework that sets the stage for erosional and depositional processes that have occurred. During the early Cambrian, marine limestones, sandstones, and shales were deposited into the SOA, over a broad epeiric sea, the Oklahoma Basin (Carlucci et al., 2014). Then, sea level experienced a eustatic drop that exposed the Devonian carbonate platform and created extensive incised valleys and karst topography on the North American Craton. The first stage of eustatic sea level fall provided the platform for the Woodford Shale to be deposited in a restricted marine stratified and dysoxic to anoxic environment throughout the Devonian (Ettensohn, 1992).

Marine transgressions overwhelmed the North American midcontinent craton during the Late Devonian times as shown in Figure 6. The rising sea level filled the NW-SE trending trough (that is deeper from the SE and shallows towards the N), which allowed for favorable accumulation

of organic matter (Galvis et al., 2018). Therefore, the Woodford shale was deposited on a highly time-transgressive 2nd order sea level cycle as the Oklahoma shelf subsided and the Kaskaskia Sea lapped onto the Laurussian Craton (Figure 6; Kvale and Bynum, 2014; Philp and deGarmo, 2020). The Middle Woodford was deposited as a Transgressive System Tract (TST) which graded upwards into the Upper Woodford Highstand System Tract (HST; Romero and Philp, 2008; Philp and deGarmo, 2020). Though the Woodford Shale was deposited during a 2nd order sea level cycle, a superimposed 3rd order sequence stratigraphic parasequence developed as part of the Devonian Sea level curve (Figure 7a ; Slatt and Rodriguez, 2012; Philp and deGarmo, 2020). While this occurred, the maximum flooding surface and underlying Woodford allowed for the deposition of organic rich fine-grained sediments. Interestingly, the Late Devonian was also marked by the expansion of vascular land plants that may have increased chemical weathering and caused runoff of land-plant nutrients into the open marine setting (Algeo and Scheckler, 1998). This is a significant event that affected the organic matter input introduced into the basin. It will be discussed in detail in the following chapters.

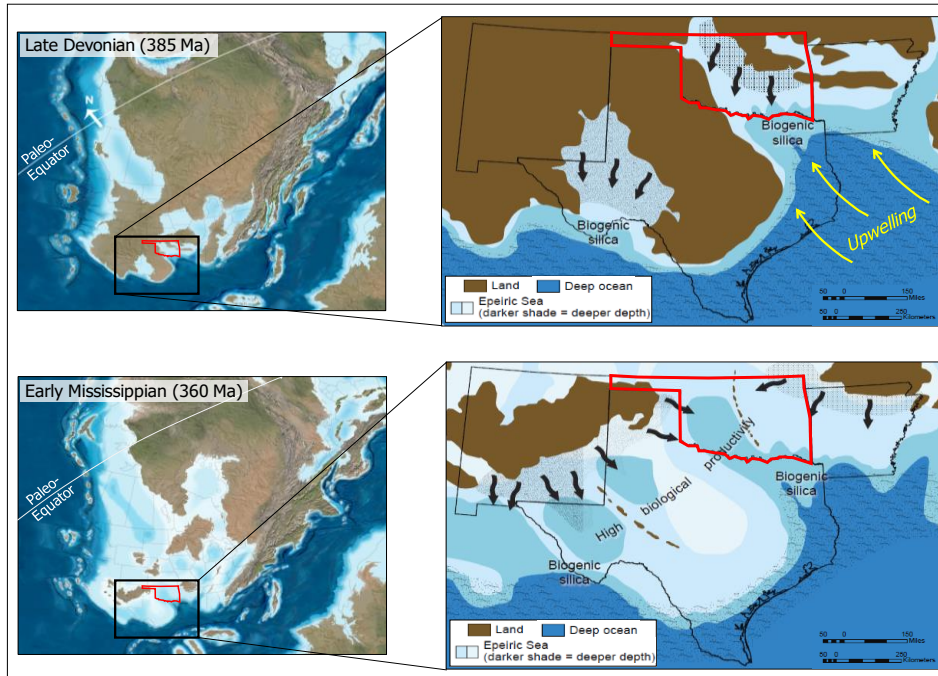


Figure 6. Paleogeography of the mid-continent North America within the Late Devonian and Early Mississippian illustrating the marine transgression that overwhelmed the Oklahoma region (Robinson and Kirschbaum, 1995; modified from Comer, 2008; Blakey, 2011; and illustrated by Galvis, 2017).

Percival et al. (2019) determined that the Late Devonian (383-359Ma) was a time marked by numerous environmental and biotic crises, which included one of the Big Five mass extinction events, namely the Frasnian-Famennian extinction. There was widespread development of marine anoxia recorded by the appearance of organic-rich laminated shales in the stratigraphic record (Buggisch and Joachimski, 2006). There were two anoxic episodes during the Late Frasnian, which are widely known as the Lower Kellwasser and the Upper Kellwasser. There were many factors that affected the climate during the Late Devonian, including extra-terrestrial impacts, large scale volcanic activity potentially linked to the Viluy Traps in Siberia, orogenic uplifts and erosions, as

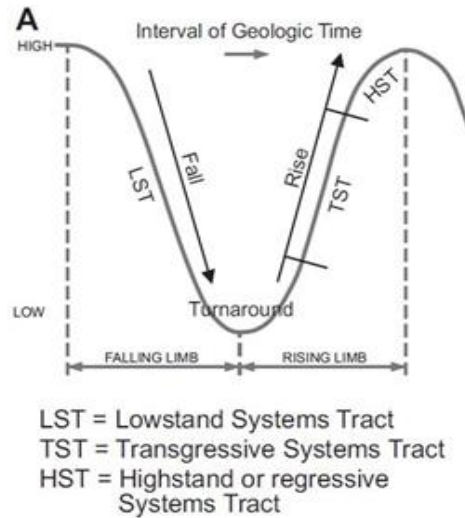
well as the expansion of vascular-rooted terrigenous flora (Wang, 1992; Algeo et al., 1995; Algeo and Scheckler, 1998).

1.5 Sequence Stratigraphy and the Woodford Shale

The Woodford Shale in the Ardmore Basin is among the few complete sections in which all its members (Upper Woodford, Middle Woodford, and Lower Woodford) are exposed and preserved in outcrop at the Speake Ranch location (Galvis et al., 2018). The sequence stratigraphic model is highly correlative to other existing North American Devonian black shales that exhibit these unconventional features, such as the Antrim Shale (Michigan Basin), Ohio Shale (Appalachian basin), New Albany Shale (Illinois Basin), Bakken Shale (Williston Basin), and Exshaw Formation (Western Canada Basin) (Comer, 2008). The Woodford shale has widely been discussed as a formation that is generally deposited in an open marine environment (Slatt and Rodriguez, 2012; Galvis et al., 2018). Moreover, the deposition of the Woodford Shale is highly dependent and controlled by factors such as eustatic sea level fluctuations among many other factors. The cyclic fluctuations in eustatic sea level has caused variability in topographic relief, karsting, periodic subaerial exposure, and subterranean collapse which produced significant local depressions as show in Figure 7b. As sea level periodically drops at Lowstand System Tracts (left falling curve on the Sea Level Curve on Figure 7a), the carbonate platform experienced a periodic subaerial exposure that carved the depressions/minibasins (Slatt and Rodriguez, 2012). The combination of minibasins and sea level fluctuation provides the foundation of variability in sediment influx and organic matter accumulations both vertically as well as laterally, therefore resulting in stratigraphic variability. During a Transgressive System Tract, the rising of the seas

allowed for circulation, deposition of organic rich sediments, and oxygenation of these depressions. Then, in the incoming Highstand System Tract as sea level regressed, the oxygenated waters oxidized the land or marine derived organic matter and allowed for the deposition of fine sediments poor in organic matter. The Lower Woodford and Middle Woodford were primarily deposited during a Transgressive System Tract, with a massive organic rich condensed section and a maximum flooding surface. The ideal preservation of organic matter, where total organic carbon is seen at a maximum, is at a time of Lowstand System Tract, when oxygenation circulation was poor, and the basin was restricted (Figure 8). Biomarkers are important tools in reconstructing the paleoenvironment as they retain conditions of the environment that include levels of oxygenation and eutrophication, in which determine the resulting water depth fluctuation (Philp, and Degarmo, 2020). Specifically, considering the Eh and pH conditions of anoxic environments are important to consider, as they change with varying oxygenation levels. This is caused by their dependency of bacterially mediated sulfate reduction resulting from varying levels of anoxia that may have occurred (Moldowan et al., 1985). Therefore, the key stratigraphic feature of the Woodford shale is the variation of high TOC values that are found in mini-basin topographic lows. Ensuing tectonic events from the Cambrian to the Permian shaped the topography of the N. American mid-continent and created the platform for accumulation of organic rich sediments in restricted basins. Therefore, topography is the control for the variability we see in the lithofacies of the Woodford formation.

a.)



b.)

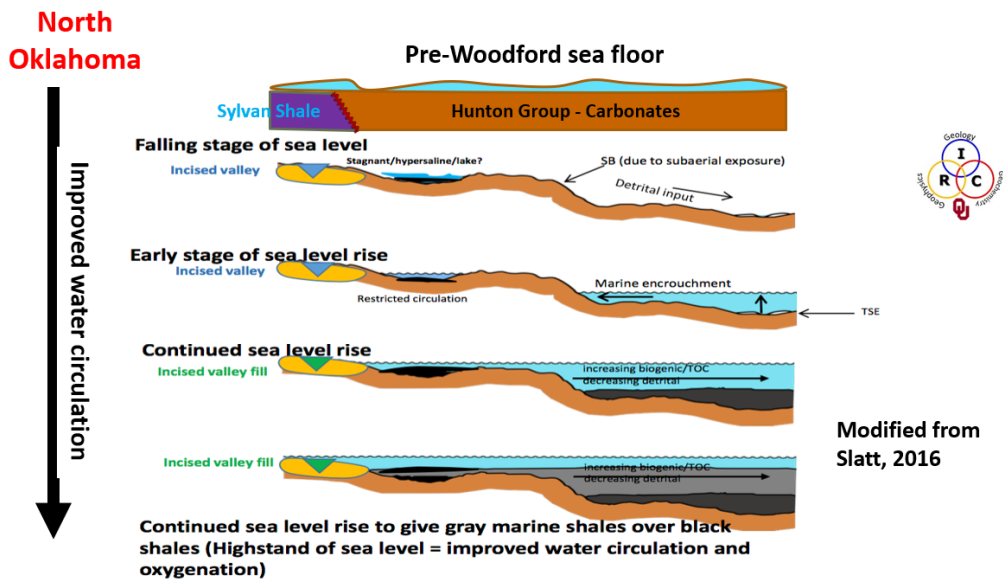


Figure 7(a). Sea Level curve displaying relative positions during a Highstand System Tract, Transgressive System Tract, and Lowstand System Tract; and **(b).** model of the sea level fluctuation stages relative to the depositional and erosional process (Slatt et al., 2016; Slatt and Rodriguez, 2012).

The Woodford Shale is comprised of 13 identified lithofacies and divided into three members which are the Upper Woodford (UW), Middle Woodford (MW), and Lower Woodford

(LW) (Galvis et al., 2018). For the purpose of this research, the division of the members has been classified by their lithologic attributes (Slatt et al., 2012). The geologic provinces in Oklahoma feature a range of geologic formations, ranging from shallow water carbonate platform to clastic abyssal plains, that contain variability within each sequence stratigraphy and reflect different depositional environments (Figure 8; Comer, 2008). There is a consistent alternation of brittle (hard) and ductile (soft) layers throughout the Middle and Upper Woodford. The hard layers are siliciclastic rich sourced from biogenic radiolaria, while the soft layers are clay rich and are the most organic rich intervals (Galvis et al., 2018). The application of this hard-soft couplet to the industry is very helpful as the beds are stratigraphically targeted for drilling. The ductile layer target is the oil zone and the source rock generating the desired hydrocarbons, whereas the brittle zone is the reservoir (Slatt, 2013). This trend has been recognized to be the hard-soft couplet (Slatt et al., 2012).

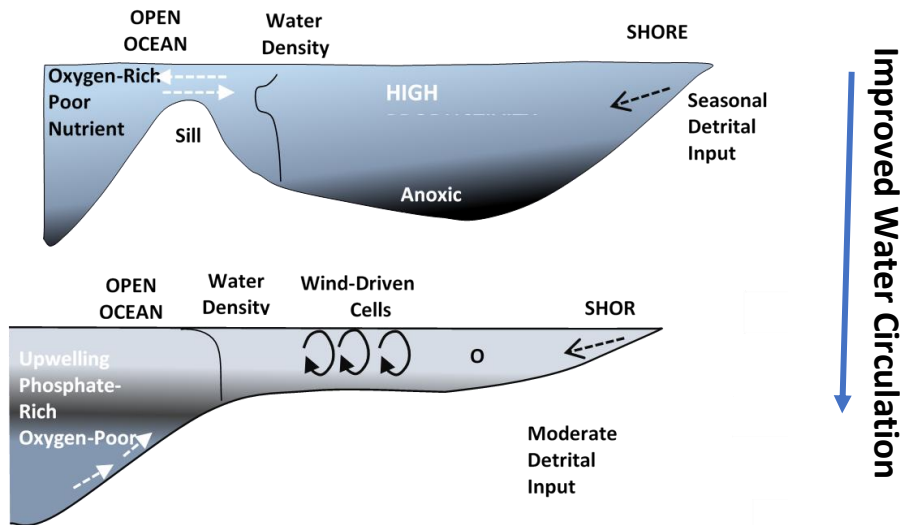


Figure 8. Model of water stratification, and anoxic environment within the minibasins for the Woodford Shale in the Ardmore Basin, Oklahoma.

1.6 Objectives

There is rising interest in the Late Devonian Woodford Shale to many researchers and the oil and gas industry as a prolific unconventional reservoir and a highly generative source rock. Multiple processes that occurred during deposition, such as cycles of sea level changes, the expansion of rooted vascular plants, climate changes and atmospheric composition changes, directly affected the influx of nutrients to the sediments deposited in the Late Devonian Woodford Shale and contributed to the variabilities seen in the formation (Philp and DeGarmo, 2020). Many studies have been accomplished over sedimentological analysis, stratigraphic description, structure analysis, and seismic analysis locally, but a high-resolution geochemical study over the section, which specifically encases one of the ‘Big Five’ global extinction events (Frasnian-Famennian time), is uncommon. The high-resolution analysis is hypothesized to yield significant variability that can help determine reservoir quality and production.

Galvis et al. (2018) presented a detailed rock-based and stratigraphic documentation of the entire Woodford Shale outcrop from the Speake Ranch, Oklahoma, for his M.S. thesis. He identified the Woodford shale to be a transgressive section composed of three different claystones, black argillaceous shale, two types of siliceous shales, siliceous dolomitic shale, two types of limestones and mudstones, as well as two distinct types of cherts (Galvis, 2017). The seven main lithofacies of the 13 identified have high frequency of vertical interbedding of hard (chert) and soft (siliceous, clay-shale) beds within the Middle and Upper members, due in part to the sea level changes (Galvis et al., 2018).

1.7 Purpose of study

- I. The purpose of the study is to conduct a high resolution organic geochemical investigation understanding the effect of depositional processes, lithofacies, and stratigraphy on the distribution of biomarkers of the Late Devonian – Early Mississippian Woodford Shale.
- II. Integrate geochemical analysis into the sequence stratigraphic framework of the Woodford Shale established by Galvis (Portilla, 2018).
- III. Compare and determine minor variabilities (if any) of the samples throughout the 40ft section of the Woodford Shale from the Speake Ranch. Recognize to what degree the complex depositional architecture would control the distribution of various organic compounds.
- IV. Identify the Frasnian-Famennian extinction boundary within the section based upon organic geochemistry.

CHAPTER II

2. METHODOLOGY

2.1 *Study Area and Sample Location*

All the samples analyzed for this research were obtained from Dr. Roger Slatt's core laboratory in Sarkey's Energy Center at the University of Oklahoma campus. These samples were collected from an exposed outcrop at the Speake Ranch within the Ardmore Basin, located between the Carter and Murray County of Oklahoma as shown in Figure 9 (Cardott, 2012; Galvis, 2017). This specific location lies on the southwestern end of the Arbuckle mountains (Galvis et al., 2018). This private quarry on the Speake Ranch, with the geographic coordinates 34°22'40.36" N and 97°20'17.26" W, has the complete, but exposed, sections of the Woodford Formation; making it one of the few preserved outcrops to exist in South Central Oklahoma. The exposed sections span to 335ft of true stratigraphic thickness that comprise the Upper Woodford, Middle Woodford, and Lower Woodford as well as the basal and upper contact with Hunton Group and Sycamore formation respectively. Due to the unconformity boundary of the Hunton, the Woodford Shale across Oklahoma can vary in thickness from 350 to 400ft, displaying the inverse relationship between the Woodford and the Hunton that highlights the effect of paleotopography on the distribution of thicknesses and consequently lithofacies (Ham, 1973; Fay, 1989; Galvis et al., 2018).

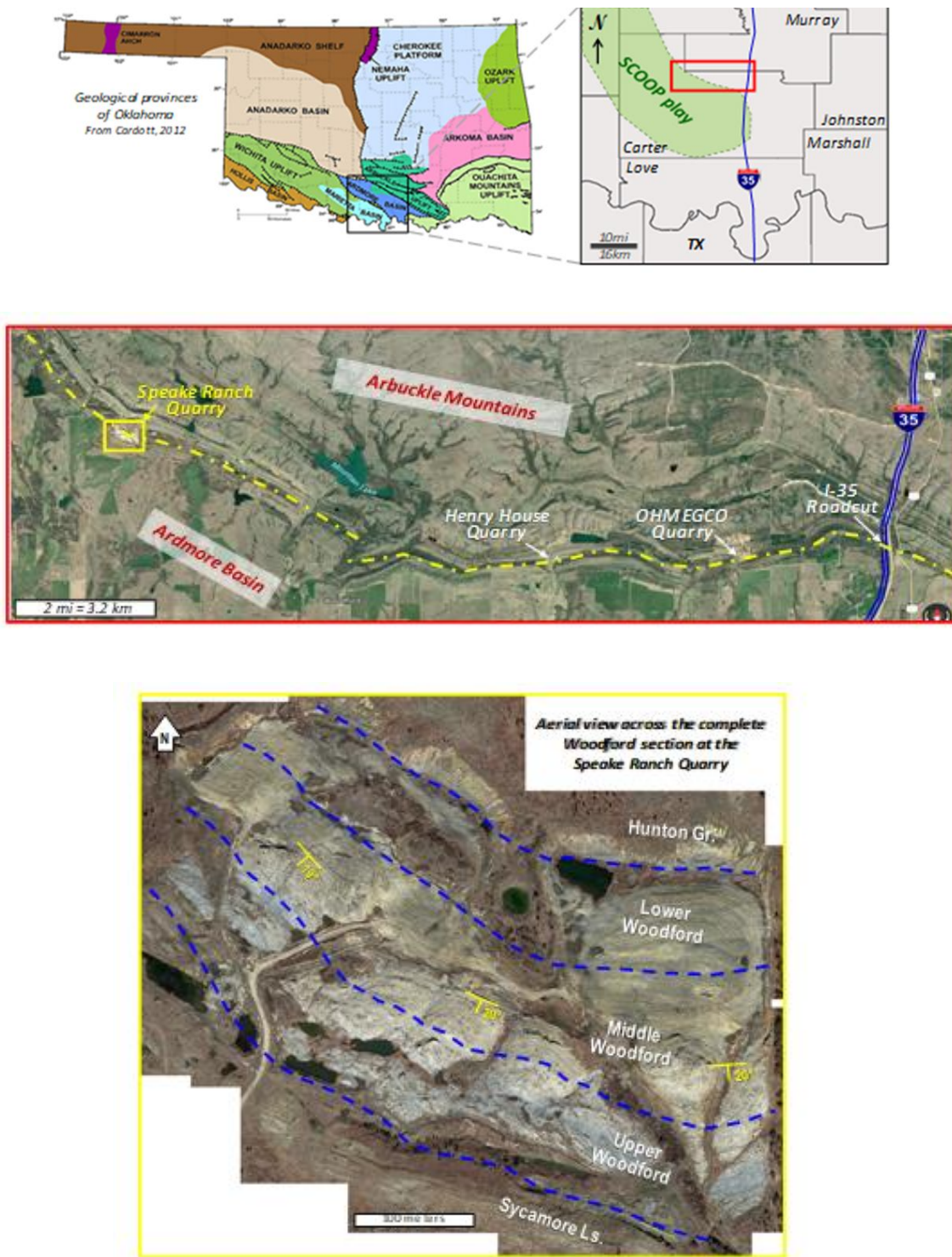


Figure 9. Top figure is location of Ardmore Basin in Oklahoma between the Carter and Murray county which is included in the SCOOP play. Middle figure is the location of Speake Ranch Quarry just west off of I-35 in Southern Oklahoma. Bottom figure is the exposed Speake Ranch Outcrop displaying the complete section of the Woodford Formation including the underlying Hunton Formation, and the overlying Sycamore Formation (Cardott, 2012; Galvis, 2017).

2.2 *Lithofacies Classification and discussion*

The Woodford Shale is comprised of 13 identified lithofacies and divided into three members, which are the Upper Woodford (UW), Middle Woodford (MW), and Lower Woodford (LW) (Galvis et al., 2018). The Woodford members were divided and classified based on its lithologic attributes (Slatt and Rodriguez, 2012). The Lower Woodford is predominantly a black-gray fissile, siliceous/carbonaceous shale, with silicified logs (Molinares, 2013). The Middle Woodford is a dominant pyritic, black shale characterized by the highest Gamma Ray output in response to high TOC (Molinares, 2013). The Upper Woodford is primarily quartzose, phosphatic, gray-black shale dominated by phosphate lenses and pyrite nodules (Molinares, 2013). Within each member lies more variability in the lithofacies and lithologic characteristics as shown in Figure 10. At a finer scale, the Upper and Middle Woodford exhibit intervals of interbedded chert and fissile shale, causing frequent high-low cyclicity within the Gamma Ray log as shown in Figure 10 (Slatt and Rodriguez, 2012; Galvis, 2017). The oscillation of the Gamma Ray throughout the Woodford shale has been recognized as the soft and hard couplet correlating to its lithofacies characteristics (Figure 10; Galvis, 2017).

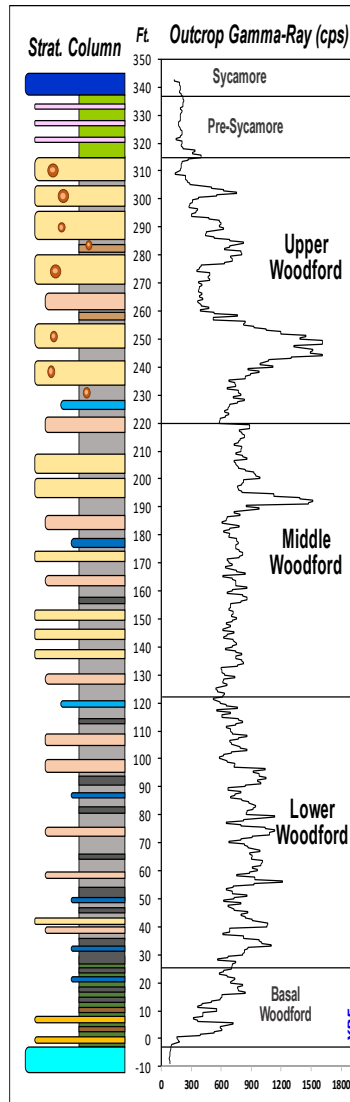


Figure 10. Stratigraphic column and outcrop Gamma Ray depth log of the Woodford Shale from Speake Ranch. The colors of the lithofacies correlate to those in Figure 11. The Upper Woodford is overwhelmed with phosphate concretions within the chert lithofacies indicated by the red circles (Galvis, 2017).

The soft layer is higher in ductility, as it is dominated by abundant clay content, which contains both detrital and authigenic quartz. The soft layers are the intervals with the highest TOC values (Slatt and Rodriguez, 2012). Detrital quartz is often found near continents, along shelf (especially the northwestern shelf of the Anadarko Basin), and basin depocenters where bottom water turbidity flows converge (Comer, 2008). Meanwhile, the hard layers are higher in brittleness

caused by the diagenetically-recrystallized radiolarians and have relatively lower TOC values (Slatt and Rodriguez, 2012). There is a clear trend that shows the ratio of hard to soft beds, which increases upward in the Upper Woodford beginning from the Middle Woodford as more siliclastic facies are introduced into the section. The 13 lithofacies identified can be divided into two major lithologic features which can be further subdivided into various shales and claystones. Brown claystone, green claystone, green silty claystone, black argillaceous shale, black siliceous shale, brown siliceous shale, and siliceous dolomitic shale fall under the soft bed intervals that are spread throughout the Woodford Formation (Figure 11; Galvis, 2017; Galvis et al., 2018). The second major features that fall under the indurated, blocky bed intervals are comprised of crystalline limestone, micritic limestone, dolomitic limestone, siliceous mudstone, black chert, and non-organic chert (Figure 11; Galvis, 2017; Galvis et al., 2018). The 13 identified lithofacies are divided into seven major lithofacies of claystones, shales, limestones, mudstones, and chert as described below (Figure 11).

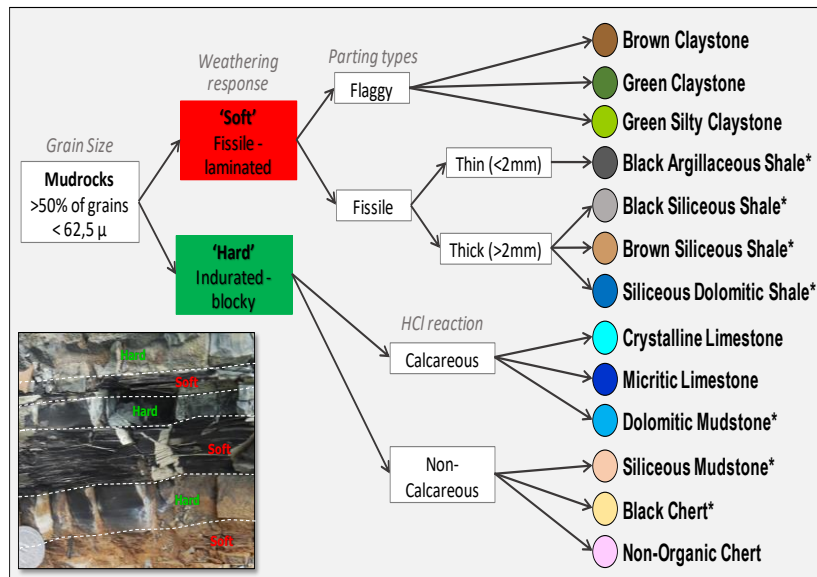


Figure 11. The 13 identified lithofacies within the Woodford Shale of South Central Oklahoma distinguished between the soft and hard layers (Galvis, 2017).

2.2.1 *Argillaceous Shales*

The argillaceous shale is a member of the soft bed containing the most clay content and is one of the most fissile lithofacies (Galvis, 2017). These layers are found to be predominantly black with high TOC values compared to other lithofacies (Galvis, 2017).

2.2.2 *Siliceous Shales*

The siliceous shales are among the soft lithofacies that are the most quartz-rich (Galvis, 2017). These lithofacies are predominantly black and gray, but brown siliceous shales are often found interbedded within the Upper Woodford. These intervals are typically slightly indurated and are composed of microcrystalline quartz, clay minerals, and *Tasmanites* (Galvis, 2017). The gray/black siliceous shales exhibit thicker parting layering among all the other softer lithofacies throughout all the members of the Woodford Shale.

2.2.3 *Brown Siliceous Shales*

The brown siliceous shale is a member of the soft fissile-laminated layer. This lithofacies dominates the Upper and Middle Woodford interlayering between the brittle black chert. The total organic carbon within this layer ranges from 3-12wt% (Galvis, 2017).

2.2.4 *Siliceous-Dolomitic Shales*

The siliceous dolomitic shale is one of the less frequent of the soft lithofacies with moderate quartz and clay content (Galvis, 2017). This interval has TOC values ranging from 8-14wt% and is often found in the Lower and Middle Woodford.

2.2.5 *Siliceous Mudstones*

The siliceous mudstone is among the few lithofacies that contain well-preserved and silicified radiolarians and *Tasmanites*. This lithofacies of the ductile layer member dominates throughout all three members of the Woodford (UW, MW, and LW). Its total organic carbon ranges from 3-8% and falls under the relatively lower organic content abundance (Galvis, 2017).

2.2.6 *Cherts*

The black chert layer is among the most dominant and abundant silica-rich lithofacies of the hard interval members with quartz richness reaching from 87 to 100% (Galvis, 2017). Its brittle characteristic is owed due to the replacement of radiolaria by chalcedony quartz and pyrite (Galvis, 2017). These intervals are found in increasingly thick partitions approaching the Upper Woodford from the Lower Woodford. Its increase in abundance is related to the opening of the ocean and is often found along continental margins or distal areas of cratonic basins such as the Ardmore Basin, Marietta Basin, and Anadarko Basin (Comer, 2008).

2.2.7 *Dolomitic Mudstone*

Dolomitic mudstone is a member of the hard lithofacies that is less frequent among the others in this lithofacies group. It has very high calcareous content with low TOC values less than 4 wt% (Galvis, 2017).

2.3 *Experimental*

2.3.1 *Rock-Eval Pyrolysis and Leco – TOC*

Five hundred thirty-six outcrop samples from the Woodford outcrop at the Speake Ranch within the Ardmore Basin located between the Carter and Murray counties of Oklahoma were collected at approximately 6” intervals. As far as possible, the samples were collected below the weathering zone, although with extensive network of microfractures that had developed over time, this was not always possible. Aliquots (3-4g) of each sample were subjected to Rock-Eval analysis to obtain TOC, HI, OI, S₁, S₂, S₃ values at GeoMark. A TOC value of >1 wt% is indicative of a good petroleum potential rock and the Woodford Shale ranges from 0.05 to 33.9wt% (Peters and Cassa, 1994). The purpose of this research is to consider the relatively high and low TOC values into the correlation of geochemical data variations.

2.3.2 *Laboratory Experimental Procedures*

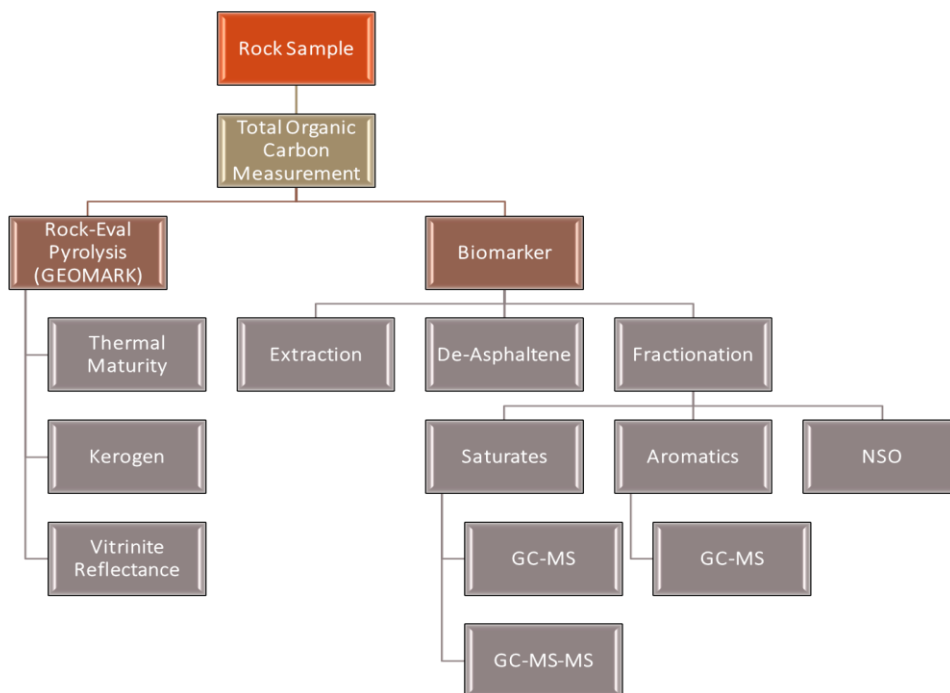
2.3.2.1 *Preliminary Samples Preparation*

A total of 40 samples of Speake Ranch outcrop were collected from Dr. Roger Slatt’s core lab in Sarkey’s Energy Center at the University of Oklahoma. In this study, the samples included both the soft and hard beds of the Upper Woodford and Middle Woodford at 190ft-230ft (Fig. 4). This interval is of interest since it is thought to straddle the Frasnian-Famennian (F-F) boundary. An aim of this study is to determine whether this F-F boundary could be recognized by a high-resolution biomarker investigation. Each sample was crushed to powder with a porcelain mortar and pestle and sieved through a US Standard mesh No. 25. The resulting powder material was then stored in glass jars to be used for extraction and fractionation procedures.

2.3.2.2 *Extraction of Organic Matter*

Approximately 50g of the rock powder were placed in a Soxhlet extraction system, which consisted of the Soxhlet device, thimble, and glass wool to extract the organic constituents of the powdered shale using 350-400ml mixture of methanol (CH₃OH) and dichloromethane (CH₂Cl₂) (1:1). The mixture of methanol and dichloromethane provided an efficient extraction method since it utilized solvents of different polarity. The bitumen is diluted in a less polar solvent (DCM) and a more polar solvent (MeOH) to enhance the expansion of clays and allow for the access to the organic compounds residing within the rock sample (Brassell et al., 1992). Within the Soxhlet apparatus, extraction solvent vaporizes from the 500ml round-bottom flask up through the side arm of the apparatus, condenses at the top, and drips down into the thimble containing the powdered sample, before it finally returns to the round-bottom flask through a siphon. This cycle of mildly hot solvent running through the samples was repeated over a span of 24 hours, to extract the maximum amount of organic matter from the crushed rock samples. The resulting solvent containing the extract was concentrated with a rotary evaporator, prior to transfer to a 4ml vial. This process workflow is illustrated in Figure 12 (a).

(a).



(b).

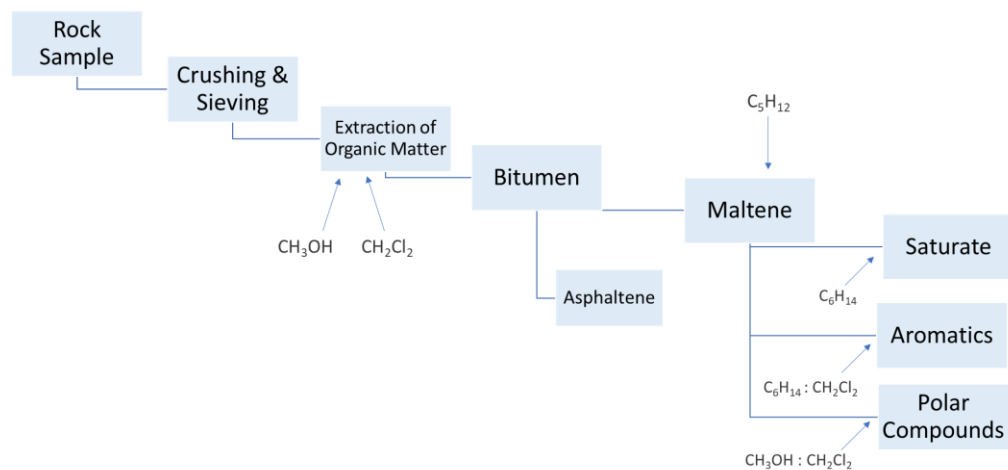


Figure 12(a). Process workflow of sample processing of the Woodford Shale for organic biomarker analysis; **(b).** Enhanced process workflow of sample processing of the Woodford Shale for organic biomarker analysis displaying the detailed fractionation process.

2.3.2.3 *De-Asphalting Process – Bitumen Fractionation*

A known weight of bitumen (approximately 100mg) was transferred into a 50ml centrifuge tube and excess n-pentane (C_5H_{12}) was added to precipitate the asphaltenes. The bitumen solution was placed in a freezer for approximately 15 hours to ensure complete precipitation of the asphaltenes. Next, the mixture was centrifuged and the maltene solution in the pentane was decanted into a 250ml round bottom flask as described below. The asphaltene precipitate was dissolved in DCM and transferred to a 4ml vial, dried, and quantified.

2.3.2.4 *Maltene Fractionation*

The pentane containing the dissolved maltene fraction was transferred from the 50ml centrifuge tube into a 250ml round-bottom flask and the excess solvent removed using the rotary evaporator. The maltenes were fractionated into saturates, aromatics, and polar NSO constituents using a 50ml glass column packed with a small amount of glass wool and 8.5g of activated alumina (Al_2O_3), which had been rinsed using n-hexane (C_6H_{14}). The extended workflow of the extraction and fractionation procedure can be found in Figure 12(b). The saturate fraction was eluted with 16ml of n-hexane (C_6H_{14}). The aromatic fraction was eluted using 25ml of a (7:3) mixture of n-hexane (C_6H_{14}) and dichloromethane (CH_2Cl_2). Finally, the polar resins were eluted using 25ml (1:1) of a mixture of dichloromethane (CH_2Cl_2) and methanol (CH_3OH). The saturate and aromatic fractions were screened by GC, and selected sample fractions were then analyzed by GC-MS for biomarker distributions.. Only 37 of the samples were able to be fractionated and screened due to low extract.

2.3.2.5 *Gas Chromatography*

All 37 samples were diluted in a 4ml vial using n-hexane to prepare for the GC and GC-MS analyses. Gas chromatography has widely been used as a separation tool of complex mixtures, by volatilizing organic compounds at high temperatures. An Agilent Technologies 6890 GC was used to screen all the samples. The GC was equipped with a splitless capillary injection system and a 60m J& W Scientific DB-1 122-0162 fused silica column (0.250mm i.d. and 0.2 μ m liquid film coating). The GC was programmed at an initial temperature of 40°C to be held until 1.5-minute post sample injection, where it is followed by a gradual temperature rise of 4°C/min. The temperature is programmed to reach 310°C and be held constant for 24 minutes until method completion. The diluted sample (1 μ L) is introduced into the GC inlet, volatilized, and transferred to the GC column by a Helium gas carrier at a flow rate of 1.4ml/min. The GC column then separates the compounds based on factors such as polarity, shape, stereochemistry, volatility and size. The purpose of the temperature ramp is to further enhance volatilization and separation for the larger molecules. Though, extreme high temperature was avoided as it would cause premature degradation of the samples and affect the resulting data outcome. As the constituents elute from the column, they pass through a flame ionization detector (FID) where they are combusted and ionized, and a signal is recorded relative to their abundance. The more volatile components elute first, and are the earliest peaks in the chromatograms, as shown in Figure 13 (Brassell et al., 1992; Philp, 2000).

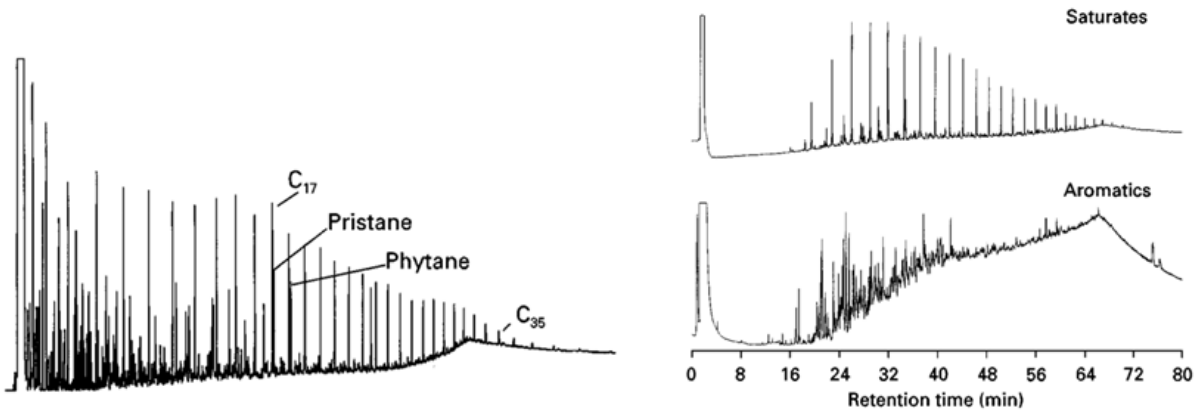


Figure 13. Gas chromatograms displaying the distribution and separation of the n-alkanes. Upper right chromatogram shows the saturate and aromatic fractions (Philp, 2000).

2.3.2.6 Gas Chromatography – Mass Spectrometry

Thirty-seven of the saturate and aromatic fractions were diluted in dichloromethane to a concentration of 4mg/ml and injected with C₂₇-deuterated cholestane (107ppm concentration) used as a standard. An Agilent Technologies 7890A GC was used to screen all the samples with a splitless capillary injection system and a 60m J & W Scientific DB-5MS 122-5562 fused silica column coupled with an Agilent Technologies 5975 XL Mass Selective Detector. Just like the GC, the GC-MS is programmed at an initial temperature of 40°C for 1.5min post sample injection, then it is gradually increased to a temperature of 315°C where it is held constant for 50 minutes. Single-ion monitoring or multiple ion detection was utilized to assess the distribution and concentration

of the hydrocarbons residing within the samples. The coupling of a gas chromatograph to a mass spectrometer helps to determine and identify more complex molecules such as biomarkers that tend to show at relatively low concentrations (Philp, 2000). Unlike the GC, which is specifically characterized by retention times and abundances, the GC-MS aids in the identification of molecules and is most helpful for biomarker analysis (Brassell et al., 1992).

CHAPTER III

3. Results and Discussion

3.1 *Geochemical Screening*

Rock-Eval pyrolysis coupled with TOC measurements have widely been used for source rock characterization (Dahl et al., 2004). Rock samples are introduced to an atmosphere of inert nitrogen and heated to produce organic products. A flame ionization detector is incorporated to detect the compounds emitted from the rock to be utilized as parameters that characterize the source rock. Essentially, Rock-Eval pyrolysis is the volatilization of hydrocarbons residing in the potential source rock (Peters, 1986). The amount of hydrocarbons, CO and CO₂ released are measured to determine quantity, type, and thermal maturity of potential source rocks. Rock-Eval pyrolysis alone is insufficient in examining source rock characterization, as it only quantifies the TOC, petroleum potential, and dominant kerogen type (Demaison and Moore, 1980; Cooper and Barnard, 1984; Isaksen and Ledje, 2001). Throughout the heating process, the temperature programmed pyrolysis detects 5 peaks with increasing temperature that records the degradation of the organic matter in the rocks (Figure 14; Pepper and Corvie, 1995; McCarthy et al., 2011). S₁ is the first peak detected and represents the free hydrocarbons. The free hydrocarbons represent the bitumen in the sample generated in the subsurface that are released during the first stage of heating (Peters, 1986). S₂ represents the hydrocarbons generated by thermal breakdown of kerogen in the source rock at second stage of heating, which reflects the hydrocarbon potential (Peters, 1986). T_{max} is the peak pyrolysis temperature of S₂ at which maximum hydrocarbons are generated. Knowing the T_{max} value reached during S₂ is important to reveal the history of the rock and the thermal alteration the rock has experienced. S₃ is derived from the evolution of CO₂ during thermal cracking of kerogen measured by a thermal conductivity detection. This is followed by S₄,

representing the oxidation of residual organic carbon that is separated into CO and CO₂ components (McCarthy et al., 2011). The very last peak of pyrolysis is the S₅, referring to the carbon dioxide resulted from the decomposition of carbonate material (McCarthy et al., 2011). Table 1 displays the geochemical screening parameters used in this research as defined by Peters and Cassa (1994) and McCarthy et al. (2011).

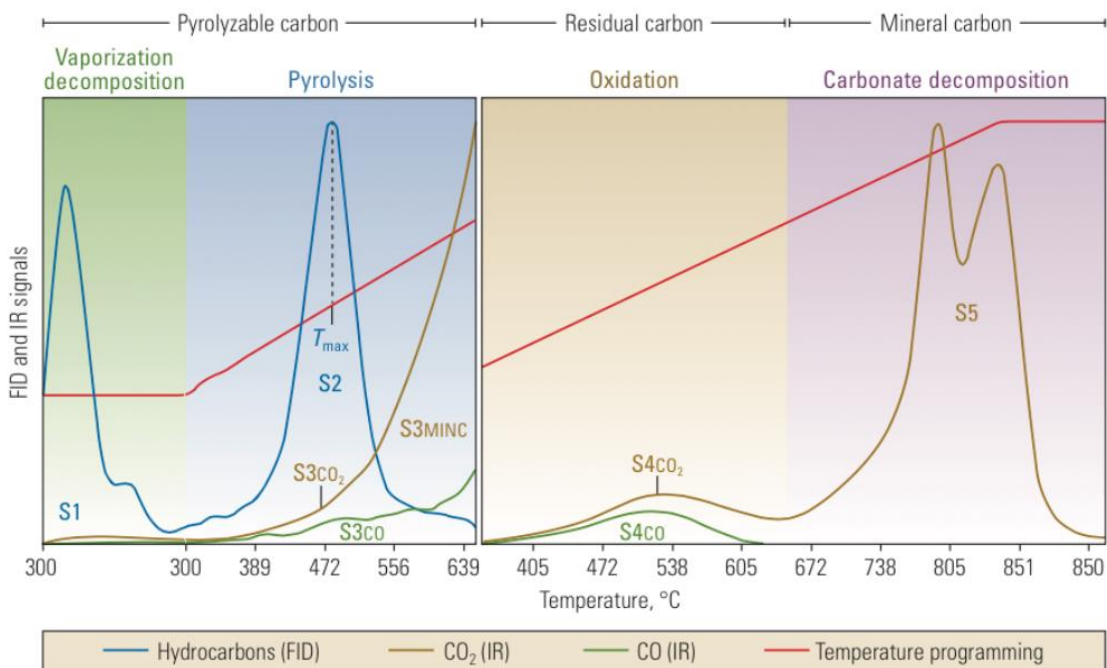


Figure 14. Programmed temperature of Rock-Eval 6 pyrolysis displaying the resulting products and heat signatures (McCarthy et al., 2011).

The petroleum-generating potential of the source rock is directly dependent on volume, organic richness and thermal maturity. Combining the pyrolysis measurements provides information on the potential of petroleum generation, kerogen type, and maturity, which are important for source rock characterization. It is also important to note that with increasing temperature during pyrolysis, abundant expulsion of hydrocarbons results, and the reactive

kerogen is consequently consumed, which will decrease the TOC wt% and hydrogen, therefore resulting in a decrease of S₂. In addition, a decrease in S₂ and hydrogen content is also caused by a process of hydrocarbon adsorption onto the clay minerals of the samples, that are converted to non-volatile char and light materials (Katz, 1983; Peters, 1986; Dahl et al., 2004). The mineral matrix plays a significant role on S₂ pyrolysis yield, and associated T_{max} value. The T_{max} represents the temperature of maximum hydrocarbon generation (S₂). Therefore, abrupt changes in lithology within the sequence, such as the hard and soft lithofacies of Speake Ranch samples, will cause changes in the T_{max} values (Dahl et al., 2004).

Parameter	Definition	Units
TOC	Total Organic Carbon	Wt%
S1	Free Hydrocarbon released at 300°C	mg HC/ g rock
S2	Residual Hydrocarbon	mg HC/ g rock
S3	Evolution of CO ₂ during thermal cracking	Mg CO ₂ / g rock
Tmax	Hydrocarbons generated during S2	°C
HI	Hydrogen Index, quantified hydrocarbons from S2 (HI = S2*100/TOC)	mg HC/g TOC
OI	Oxygen Index, quantified Carbon Dioxide from S3	mg HC/g TOC

Table 1. Geochemical screening parameters defined by Peters and Cassa (1994) and Tissot and Welte (1984) for Rock-Eval pyrolysis and Leco-TOC.

3.2 Organic Richness

Evaluation of organic richness through Rock-Eval pyrolysis includes a quantifiable organic carbon assessment. According to Peters (1986) what constitutes an optimal source rock generative potential is a TOC wt% greater than 2% coupled with S_1 values greater than 2 mg HC/g rock and S_2 values greater than 10 mg HC/g rock. All the members of the Woodford Shale formation from Speake Ranch are abundant in TOC with values ranging from 0.05 to 33.9 wt% (Galvis, 2017). The Lower Woodford displays the highest organic rich interval, owing to its clay rich composition (Figure 15; Galvis, 2017). Kennedy et al. (2014) found that there is a direct relationship between the high surface area of detrital clay minerals with organic carbon, which indicates that abundance of clay provides for an extended preservation capability of organic matter. This property aligns with the characteristics of the Woodford Shale. The Middle Woodford and Upper Woodford from Speake Ranch have TOC values ranging from 0.62% to 15.90%. This classifies the Woodford Shale from Speake Ranch to be an excellent potential source rock.

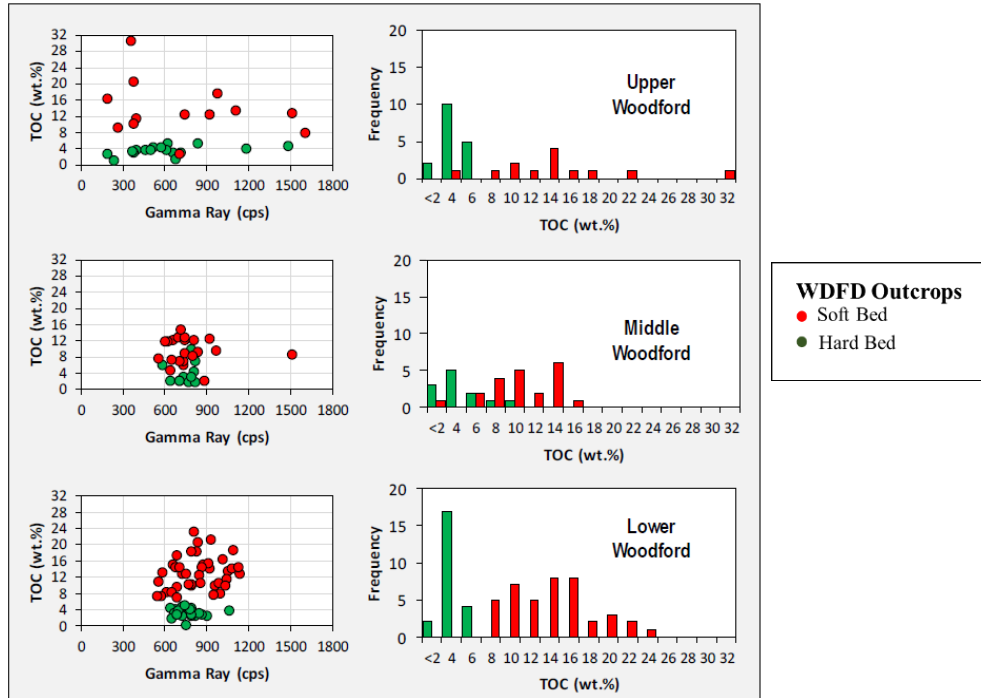


Figure 15. TOC abundance distribution across all the Woodford members from Speake Ranch studied by Galvis (2017). The Lower Woodford displays the most organic rich intervals within the soft lithofacies intervals. The Middle Woodford shows nearly equivalent ratio of hard to soft lithofacies. The Upper Woodford has the lowest average TOC values and a higher hard to soft lithofacies ratio. The TOC and Gamma Ray plots illustrate that high TOC is not always correlative to high Gamma Ray response. The higher Gamma Ray plots may be an effect of the radioactive component, phosphatic particles (Galvis, 2017).

There is an apparent variability throughout the Speake Ranch interval seen in Figure 16 correlating with Gamma Ray, which has been described as the soft and hard couplet by Slatt and Rodriguez (2012). It is clearly illustrated that the hardness depth-log oscillation is correlative to the variations of the TOC, defining the hard-soft bed couplet (Figure 16). The average TOC wt% shows a clear and common trend of decreasing values towards the Upper Woodford from the Lower Woodford. However, a resulting high TOC wt% (5-35%) in the Upper Woodford may be a result of possible migrated hydrocarbons (Torres, 2020). The frequency of the TOC fluctuations within the 40ft sequence may be a product of geochemical and sedimentological effects of water column anoxia (Kennedy and Wagner, 2011). There is a covariance between TOC wt% and

lithofacies earlier discovered by Galvis (2017), where the quartz-rich brittle layers have a negative correlation to TOC wt% richness whilst the clay-rich ductile beds have a positive relationship with organic matter abundance (Figure 17). Significant fluctuations of TOC wt% can be found at very small scales, especially in the studied 40ft interval, where TOC values are observed to have jumped from 5.19 (hard bed) to 12.9 (soft bed) wt% within just 1ft. It is hypothesized that regardless of the location of the sample within the 40ft interval, similar rock lithofacies from the middle or upper of the section will have similar TOC wt% abundances (discussed in Chapter IV). Clay minerals are initially formed in soils prior to erosion and transportation to continental margins, then climate and continental processes alter their mineralogy and affect their preservation capacity (Kennedy and Wagner, 2011). In contrast, the lower TOC contents are commonly found within beds containing cherts resulting in dilution of organics caused by syn-deposition of biogenic silica (Roberts and Mitterer, 1992; Galvis, 2017). Throughout this research the defining term to identify TOC abundance will be dependent on the brittle-ductile (hard-soft bed) couplet; where the soft bed intervals that occur at every foot have relatively higher TOC wt%. In each foot of the Speake Ranch intervals, the average bed thicknesses per rock type were measured in order to estimate the soft-to-hard ratio, relating the cumulative thickness of soft beds over the cumulative thickness of hard beds per each foot (Galvis, 2017). One foot of Speake Ranch interval may be made of 50/50 of hard and soft, however there are still several combinations where the alternation of soft and hard beds stack to accommodate the 50/50 within that foot.

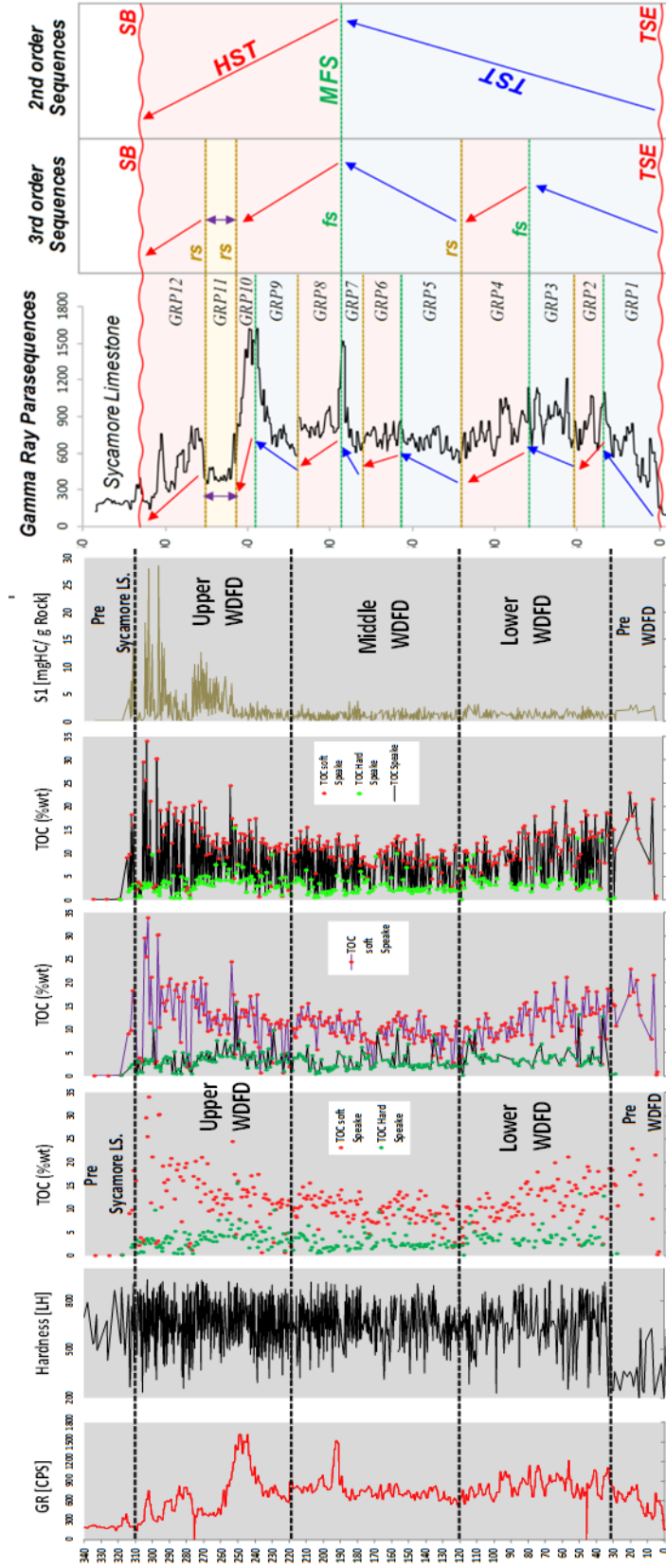


Figure 16. Depth Plots of Gamma-Ray, TOC%, S₁, and XRF-Hardness data for the 536 Speake Ranch samples (Galvis, 2017).

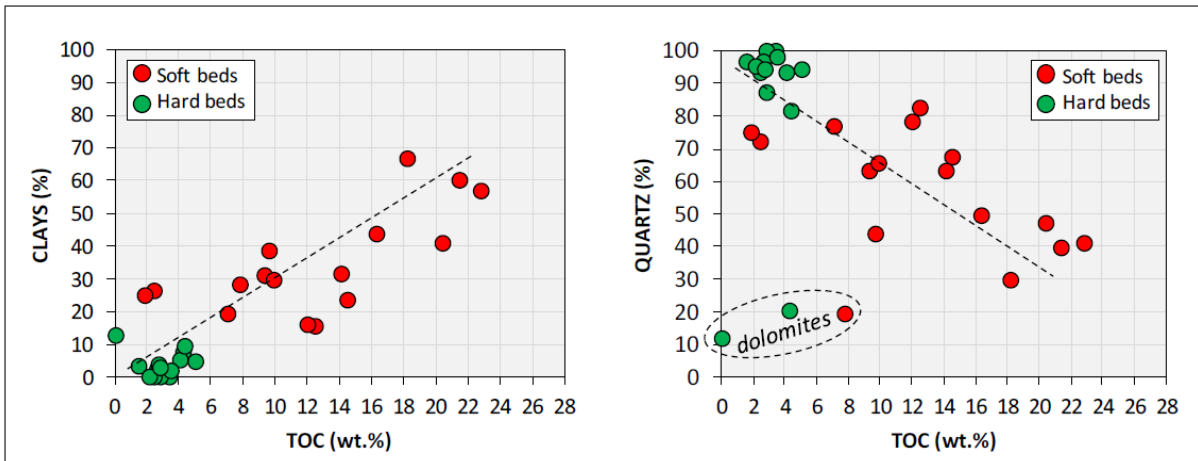


Figure 17. Soft vs. hard relationship with TOC. The softer bed intervals have positive correlations with increasing TOC, while the hard lithofacies intervals have negative correlations with TOC (Galvis, 2017). Hard bed lithofacies are enriched in quartz content and depleted in clay content, while the soft bed lithofacies are enriched in clay content. The outlier symbols of the hard bed and soft beds with significantly low quartz content, may be an indication of dolomites.

These relatively lower TOC values which are found within the brittle beds, may be a product of the predominant regressive 3rd order hemicycles (Molinares, 2013). As sea level regressed the water column shallows and introduces oxygen to bottom waters through vertical mixing. This produces turbulence in sediments that caused disturbances to the anoxia of bottom water sediments ideal for organic matter preservation (Figure 18). In support of Molinares (2013), Philp and DeGarmo (2020) interpreted that lower TOC values are the results of paleoweathering from subaerial exposure as a consequence of sea level regression during climate transition from Late Devonian to Early Mississippian time. Kennedy and Wagner (2011) have suggested that bioturbated intervals, yield lower organic carbon values due to remineralization and removal of organic carbon on sediment surface by oxygenation, which could also apply to the Speake Ranch samples. Considering the above-mentioned possibilities, it is likely that the lower TOC intervals of the Woodford Shale from Speake Ranch resulted from loss of conditions necessary for organic

matter preservation. These conditions include subaerial exposure, turbulence, and disruption of the anoxic water columns. The sequence stratigraphy mentioned in earlier chapters explained that the ratio of the hard to soft lithology increases towards the Upper Woodford from the Middle Woodford, leading to a higher frequency of lower TOC values toward the Upper Woodford. Furthermore, the Si/Al record provides additional support for the association of clay minerals with organic matter, indicating that there is an increase of clay minerals, relative to quartz, in each interval with relatively higher TOC values (Figure 19). The presence of clay-rich composition not only provides favorable conditions for carbon preservation, but it also reflects climatic conditions and sea level fluctuations of the environment relating to marine carbon deposition and burial, which is explored in this research (Kennedy and Wagner, 2011). The bulk geochemical parameters earlier defined such as TOC, HI, OI, Si/Al, maturity, and GR are shown in Figure 19.

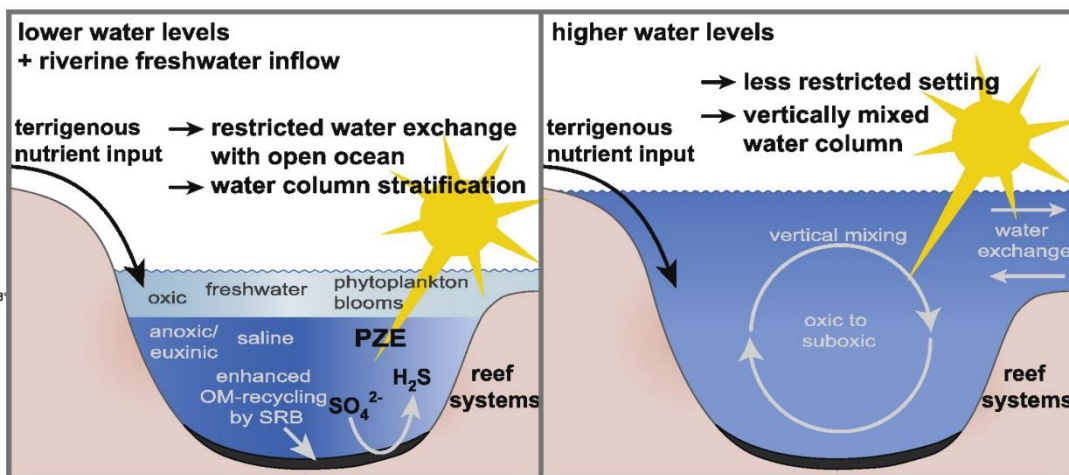


Figure 18. Model of depositional environment and water column for both higher water levels and lower water levels. Higher water levels cause vertical mixing of the water column and introduces oxygen to the system. Lower water levels cause a restricted water column accompanied with stratification (Tulipani et al., 2013).

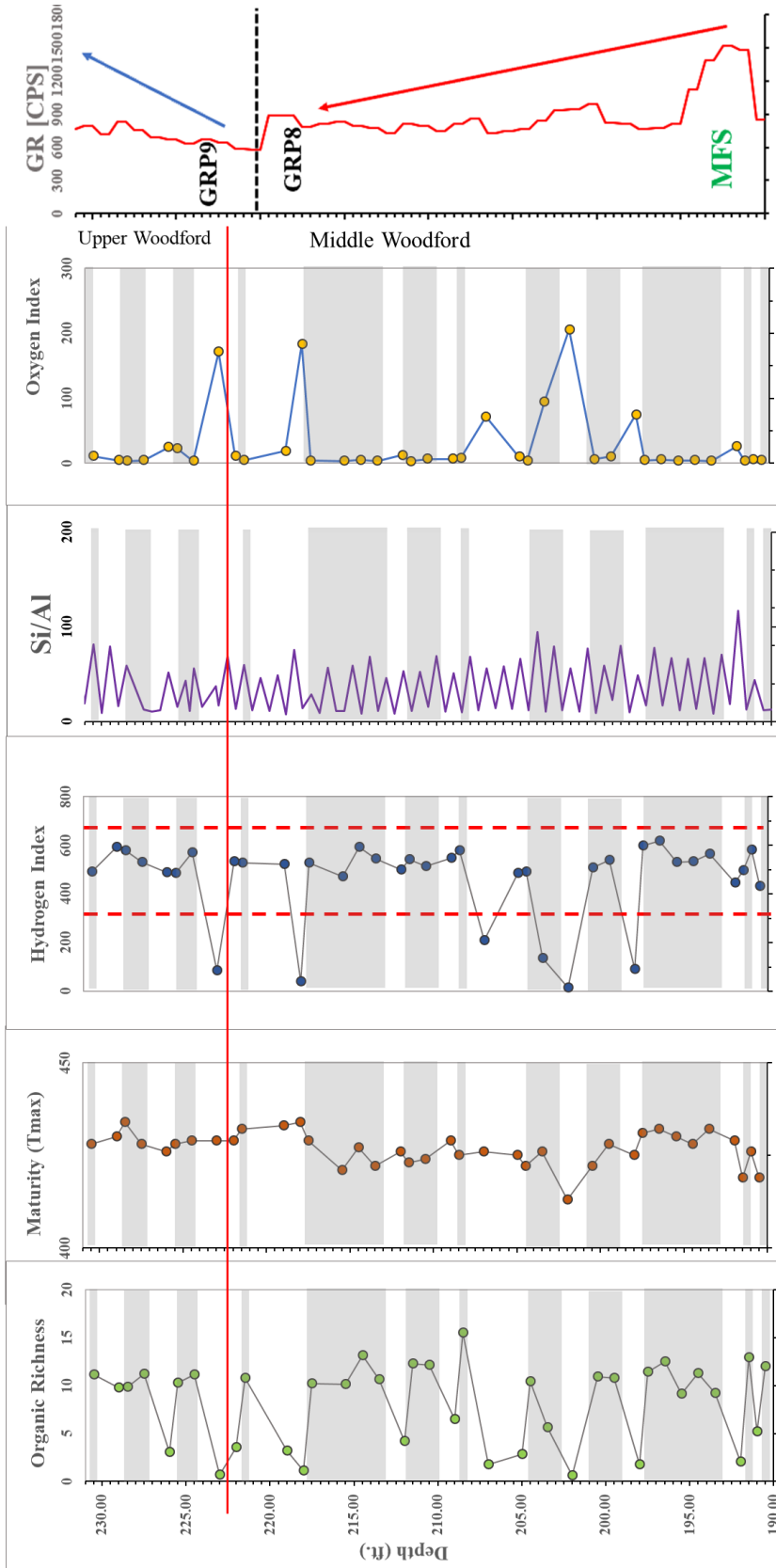


Figure 19. Depth Plots of defined parameters from Rock-Eval pyrolysis and Leco TOC. (Organic richness: TOC wt%, maturity: T_{max} , Hydrogen Index: $S_2/TOC*100$, Oxygen Index: $S_3/TOC*100$, and Si/Al) The grey intervals signify the soft bed intervals while the white intervals indicate hard beds.

3.3 Organic Matter Type

Kerogen maceral composition, which include liptinite, amorphinite, vitrinite, and inertinite, have been utilized for source rock evaluation. Liptinite macerals such as alginite, sporinite, cutinite, and resinite, are dominant within Type I kerogens and are oil producing (Dahl et al., 2004). Amorphinite macerals are insoluble macerals common in Type II Kerogen and are the most oil prolific. Vitrinite macerals originate from woody plant tissue and are predominantly found in Type III kerogens (Dahl et al., 2004). Finally, inertinite macerals are dominant within Type IV kerogen profile which generate little or no petroleum (McCarthy et al., 2011). The plot of the Hydrogen Index vs. T_{max} identified the Woodford Shale to be primarily a Type II kerogen with several members plotting as Type III (Figure 20). Further description of kerogen type characterization will be explained in the next section.

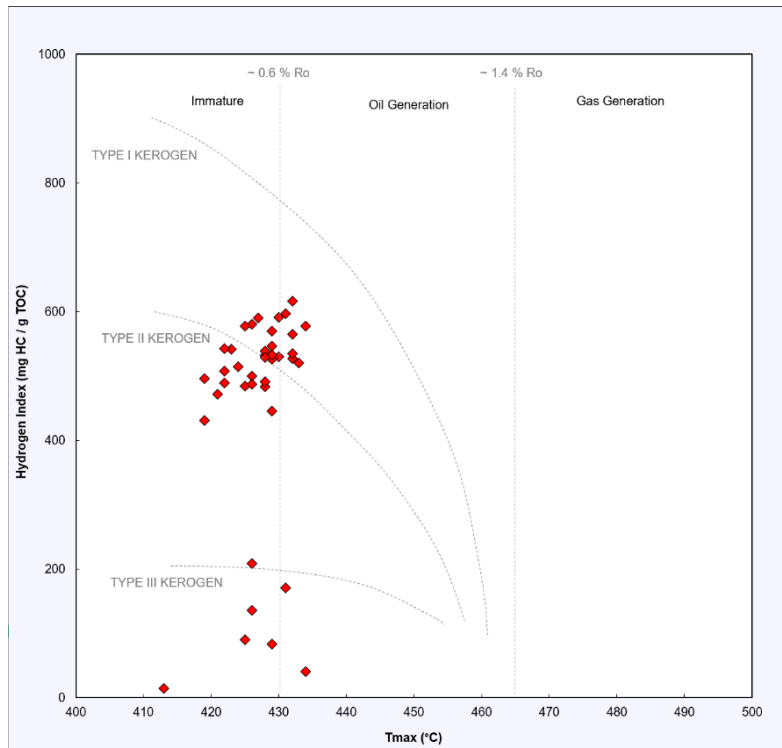


Figure 20. Kerogen classification and maturity assessment utilizing T_{max} vs. Hydrogen Index (HI) parameter plot useful in aiding primary interpretation of source rock analysis. The Speake Ranch samples are primarily a Type II kerogen with several samples plotting as Type III.

3.4 Kerogen Type

Kerogen is the high molecular weight insoluble organic residue in which can generate hydrocarbons during pyrolysis or maturation. Kerogen can be classified into four types, depending on Hydrogen Index (HI) and Oxygen Index (OI) values. The pseudo van Krevelen plot has widely been used to define the 4 types of kerogen to determine its compositional variances and organic matter types (Figure 21; Tissot et al., 1974). The HI is quantified by normalizing S₂ peak to TOC multiplied by 100 which will result in the quantified hydrocarbons from S₂ relative to TOC measured in mg HC/g TOC (McCarthy et al., 2011; Dahl et al., 2014). The OI is quantified from S₃ relative to TOC which measures the quantified carbon dioxide measured in mg CO₂/g TOC (McCarthy et al., 2011). The following sections will discuss the use of biomarkers to identify the influx of organic material and processes that occurred during deposition. Both influx of organic material and processes that occur upon deposition affect the molecular characteristics of the organic material within the sample, thus controlling the generation of petroleum (Hsu et al., 2003). Source rock quality and richness (HI and S₂) have been observed to generally decrease with depth and follow the trends of the Gamma Ray log intensity (Dahl et al., 2004). However, this trend is not clearly visible in the 40ft section of the Woodford Shale from Speake Ranch characterized in this study (Figure 19). Additionally, TOC alone is not an accurate measurement of hydrocarbon generation within the sediment (Dembicki, 2009). Knowing the amount of carbons and hydrogens present, as well as the maturity of the source rock, is required to determine a more accurate quantification of hydrocarbon generation.

Type I kerogen is highly oil prone and possibly gas prone as well, yielding a high HI value and a low OI value (Peters, 1986). Type II kerogen will generate both oil and gas and is characterized by decreasing OI values while initial HI remains nearly constant (McCarthy et al.,

2011). Type III kerogen has low HI values and high OI values and is very prone to generate gas and maybe some oil (Peters, 1986). Many of the Upper and Middle Woodford Shale samples plot as Type I and Type II mixed kerogen, reflecting samples that are in the early oil generative window and sourced from a marine environment (Figure 21). Furthermore, the HI values for the Speake Ranch samples range from 25 to 577 mg HC/g TOC along with OI values that range from 3 to 194 mg CO₂ /g TOC.

The HI values of Speake Ranch have a majority of its samples varying between 400–600 mg HC/g TOC. This interval is indicative of oil generative quality from a marine source based on the parameters define by Peters and Cassa (1994). Nearly all the samples of the Upper Woodford and Middle Woodford from the Speake Ranch plot within the 400-600 mg HC/g TOC interval. However, there are outliers present within the section, displaying values below 200 mg HC/g TOC which are often associated with dilution of the TOC by sediment input from a terrigenous source (Figure 19 and Figure 21). The majority of these outliers can be found distributed within the Middle Woodford of this study. Several of Speake Ranch samples in Figure 21 also display a Type III and IV kerogen, which may be a direct effect of organic matter source input and/or thermal maturation. These distributions are primarily found within the Middle Woodford, and at the boundary of the Upper Woodford and Middle Woodford (Figure 19).

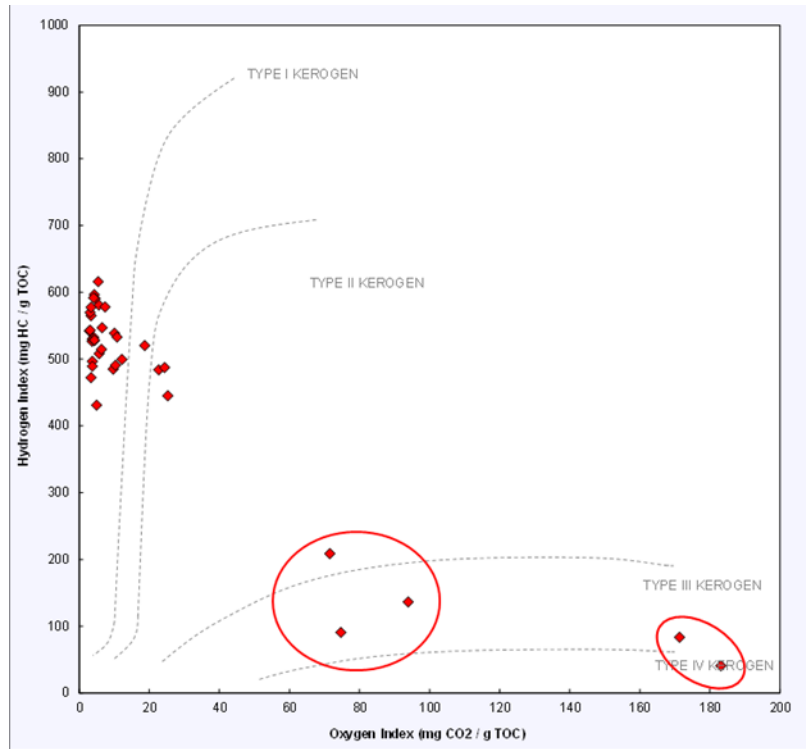


Figure 21. Pseudo van Krevelen type kerogen type plot plotting the HI vs. the OI to assess the kerogen type of the Woodford samples from Speake Ranch. 40 of the studied samples indicate a Type I and Type II kerogen. Outlier sample points within the circles are most likely to a result from organic matter source input.

3.5 Thermal Maturity from Rock-Eval

Thermal maturity can be determined from a combination of vitrinite reflectance, T_{max} , S_1 , and S_2 ratios. There are 3 stages of maturation which include diagenesis, catagenesis, and metagenesis. Diagenesis is the thermally immature phase, where the physical, chemical, and biological transformations occur prior to burial or with increasing thermal gradient while still retaining the molecular structure of the compounds (Peters and Cassa, 1994). Catagenesis is the mature and post mature stage comprising the oil window which is the interval for oil and gas production. It also consists of the wet gas zone containing less than 98% of methane, owing to the light hydrocarbons resulting from cracking (Peters and Cassa, 1994). Finally, metagenesis is the post mature stage/phase which comprises the dry gas zone with more than 98% of methane (Peters

and Cassa, 1994). Maturation pathways help decipher the level of thermal stress the samples in this study have experienced.

Based on the T_{max} values, the Woodford Shale from Speake Ranch is predominantly immature with values ranging from 419 to 434° C, averaging at 426° C. Based on the values proposed by Peters (1986) this constitutes an overall immature source rock characteristic (<435° C). Furthermore, the maximum T_{max} value (434° C) indicates that the Speake Ranch samples are within the early oil window. In a 40 ft interval we would not expect any variations in thermal maturity as earlier defined. However, Figure 22 shows slight variations possibly attributed to the mineral composition within the interval. The variations in the T_{max} do not coincide with oscillations in the TOC values, suggesting that any variabilities within the T_{max} value are not only a reflection of organic matter, but also an effect of weathering. It is insufficient to rely on T_{max} for the evaluation of maturity as errors are likely to be associated due to the changing mineralogical effects within the 40ft sequence. The sulfur-carbon bonds in comparison to the carbon-carbon bonds require a lower bond-breaking temperature, which results in lowering of oil generation by ~30°C (McCarthy et al., 2011). Thus, presence of sulfur within the lithofacies may lower the T_{max} . The characterization of maturity supported by vitrinite reflectance is necessary. The vitrinite reflectance can be calculated using T_{max} derived from Rock-Eval data [$\%Rc=(0.0180*T_{max}-7.16)$] (Jarvie, 1991; Wust et al., 2013). These samples result in values ranging from 0.27 to 0.65%Rc with a mean at 0.53%Rc indicating a relatively low maturity. The average value closely coincides with the mean from direct petrographic measurements of vitrinite reflectance (0.60%Ro) provided by Cardott (2017; written communication to Galvis, 2017) in Figure 23. This was taken over 40 measurements at random within a single depth, varying from 0.49-0.72%Ro. However, Galvis (2017) calculated an average over the entirety of Woodford Shale to be at 0.79%Rc making it

higher than the average calculated for the interval in this study. The discrepancy may be attributed to his measurements over the 536 samples from Speake Ranch vs. the 37 (Upper Woodford and Middle Woodford) samples analyzed in this research. Additionally, lower thermal maturity values discovered in Speake Ranch may be attributed to tectonic uplift of the Arbuckle Mountains during the Pennsylvanian (Ham et al., 1973; Galvis, 2017). The following sections will utilize biomarker parameters to further determine the conclusion that there are slight thermal maturity variations within Speake Ranch samples.

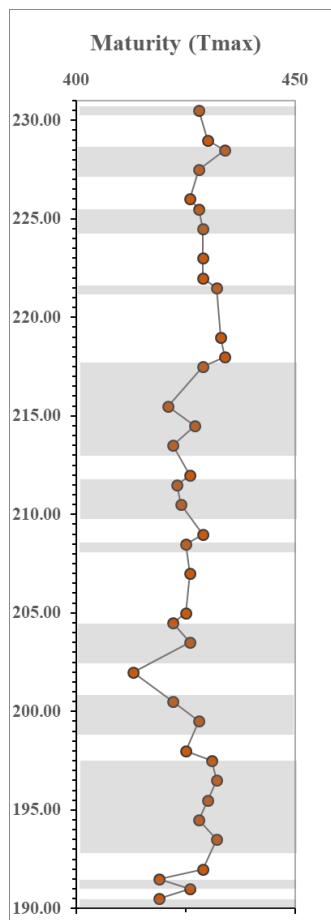


Figure 22. Depth plot of T_{max} showing variations within the 40ft sequence. There is little to no variation in the distribution of the maturity parameter, which justifies suggesting that thermal alteration is not a factor contributing to observed biomarker variations. Gray intervals indicate soft bed lithofacies, while white intervals indicate hard beds.

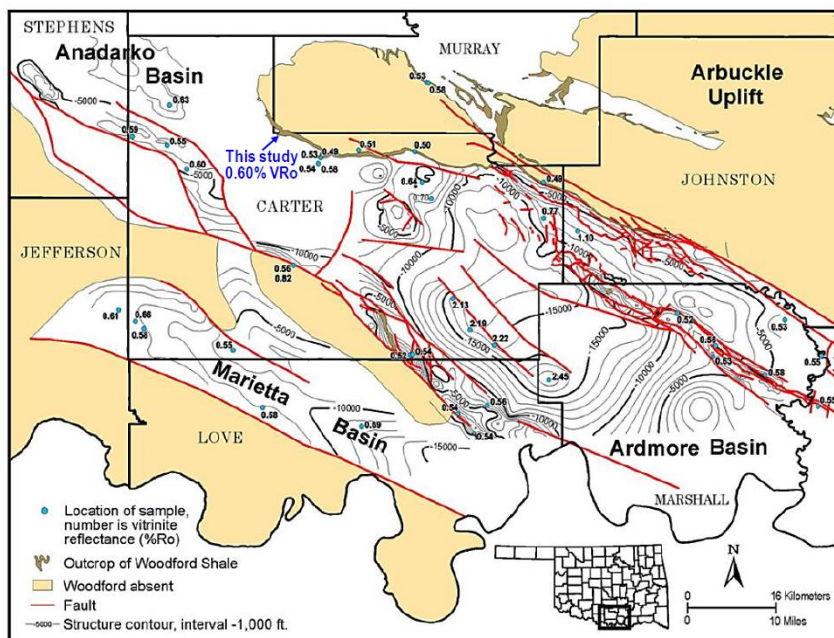


Figure 23. Distribution of vitrinite reflectance in South Central Oklahoma. Petrographic vitrinite reflectance of Speake Ranch ranges from immature to early oil window, with a mean of 0.60% Ro (Cardott, 2012; Galvis, 2017).

3.6 Gas Chromatography

As proposed in previous research, biomarker analysis is useful in determining fluctuating levels of anoxia upon deposition and organic matter source (Connock, 2015; Jones, 2017; Galvis, 2017; and Torres, 2020). This research explores the biomarker families used to identify changing organic matter sources and processes occurring within the paleoenvironment. These biomarkers include the n-alkanes, steranes, terpanes, diasteranes, tetracyclic polyprenoids, aryl isoprenoids, alkyl-naphthalenes, and alkylphenanthrenes screened on the GC-FID and GC-MS. The analysis of these biomarker families will take into account their relationships with depth, maturity, biodegradation and lithology.

3.6.1 *n*-Alkane distribution

The *n*-alkanes are found within the saturate fractions of source rock extracts and crude oils screened by the GC. They are specifically useful as a tool for correlation and organic matter evaluation (Peters et al., 2005). The *n*-alkanes derive from lipids within living organisms, such as higher-order plants (odd-carbon-numbered *n*-alkanes, specifically *n*-C₂₇, *n*-C₂₉, and *n*-C₃₀ or algae which are illustrated in the lower carbon number homologs (Eglinton and Hamilton, 1967; Smith, 1968). The Woodford Shale samples from Speake Ranch have experienced one of the earliest levels of biodegradation, which is the preferential removal of the *n*-alkanes, and isoprenoids (Volkman et al., 1984). Based on several chromatograms, there is a slight odd-even predominance between the *n*-C₁₅ – *n*-C₁₇ (**I**; See Appendix II for compound structure) which are typically attributed to algal/cyanobacteria origin as shown in Figure 24 (Han et al., 1967; Grice et al., 1996). Higher carbon number alkanes that maximize at *n*-C₂₉ with an odd-even predominance are known to be indicative of higher plant input (Eglinton et al., 1962; Grice et al., 1996). However, the preferential removal of the *n*-alkanes in the Speake Ranch samples make it hard to discern any *n*-alkane trend which may lead to misinterpretations. Thus, additional supporting biomarker analysis is essential to further specify the organic matter source.

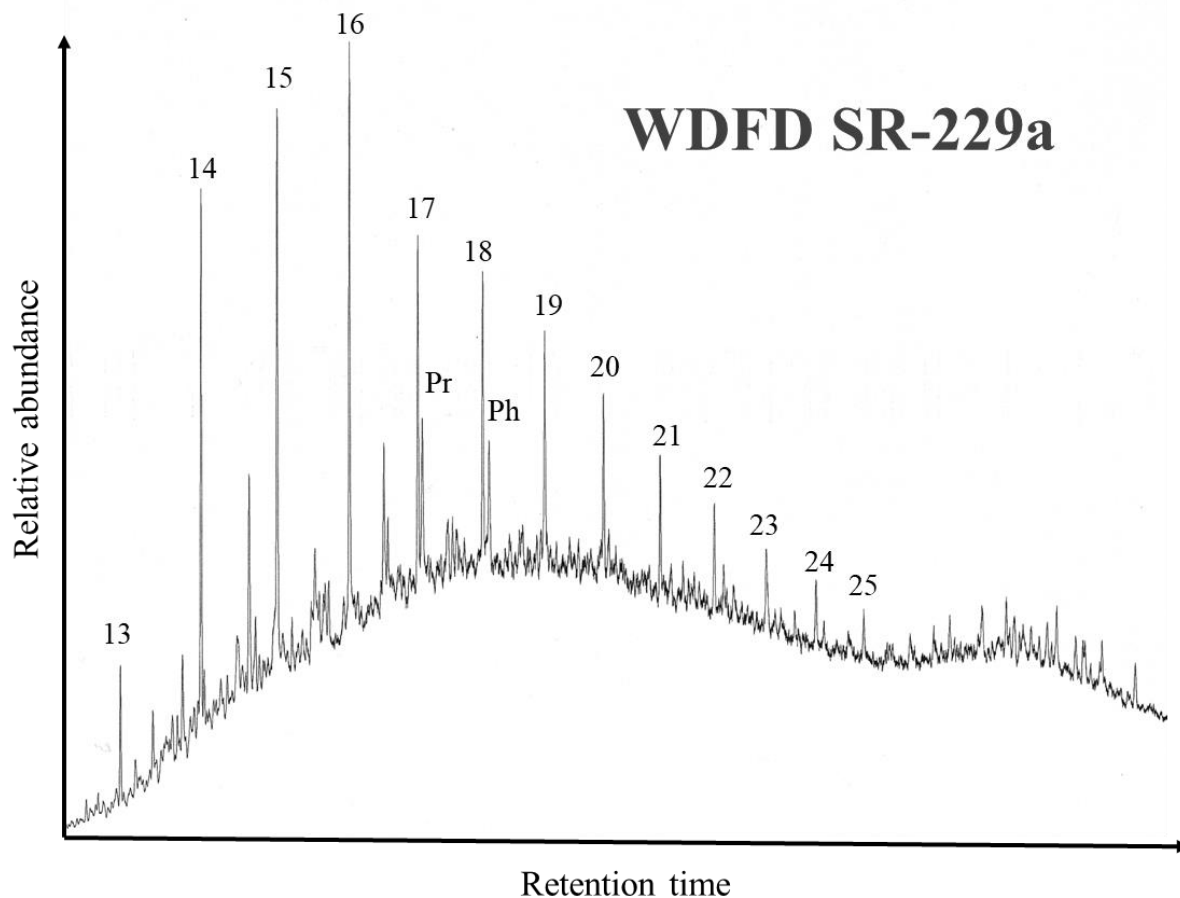


Figure 24. Gas chromatogram of the saturate fraction from the extract of the sample at a depth of 229.0 ft from the Woodford Shale at Speake Ranch.

3.6.2 *Pristane and Phytane*

The acyclic isoprenoid hydrocarbons pristane and phytane are determined by GC. In immature sediments, the pristane (Pr; **II** see Appendix II for compound structure) and phytane (Ph; **III**) reflect the oxidation fluctuations of the phytyl side chain of chlorophyll a and b in phototrophic organisms (Brooks et al., 1969; Powell and McKirdy, 1973; Goosens et al., 1984; Grice et al., 1996). Accordingly, differences in pristane/phytane (Pr/Ph) ratio reflect the level of anoxia within

the water column. Connock (2015) classified that the Upper Woodford was deposited in a dysoxic-suboxic environment whilst the Middle Woodford was deposited in a predominantly anoxic environment as indicated by the Pr/Ph values (Table 2). Similarly, the Woodford Shale from Speake Ranch shares the same characteristics as those classified by Connock (2015). Using the pristane/n-C₁₇ vs. the phytane/n-C₁₈ plot, Speake Ranch samples display values below 1 for both parameters indicating low maturity samples deposited under reducing conditions, with an input of mixed organic matter (Figure 25). These data agree with the identified depositional environment framework of the Woodford Shale present in Late Devonian-Early Mississippian as previously reported by Romero and Philp (2012). The outliers of the hard bed intervals with a Pr/Ph values >1 in Figure 25 are possibly a product of biodegradation effects rather than depositional environmental conditions. However, apparent variations in the Pr/Ph within the depth log shown in Figure 26, follow variations in lithology (tracking the relative TOC wt % abundance of soft and hard beds). This suggests that although the Woodford Shale was deposited predominantly in an anoxic environment, there were periodic oxic to sub-oxic disturbances (Figure 26). It is insufficient to determine organic matter source and nature of depositional environment from Pr/Ph alone. Lower Pr/Ph ratios do not necessarily indicate reducing environments but may also be an effect of lithology and maturity (Marynowski et al., 2000).

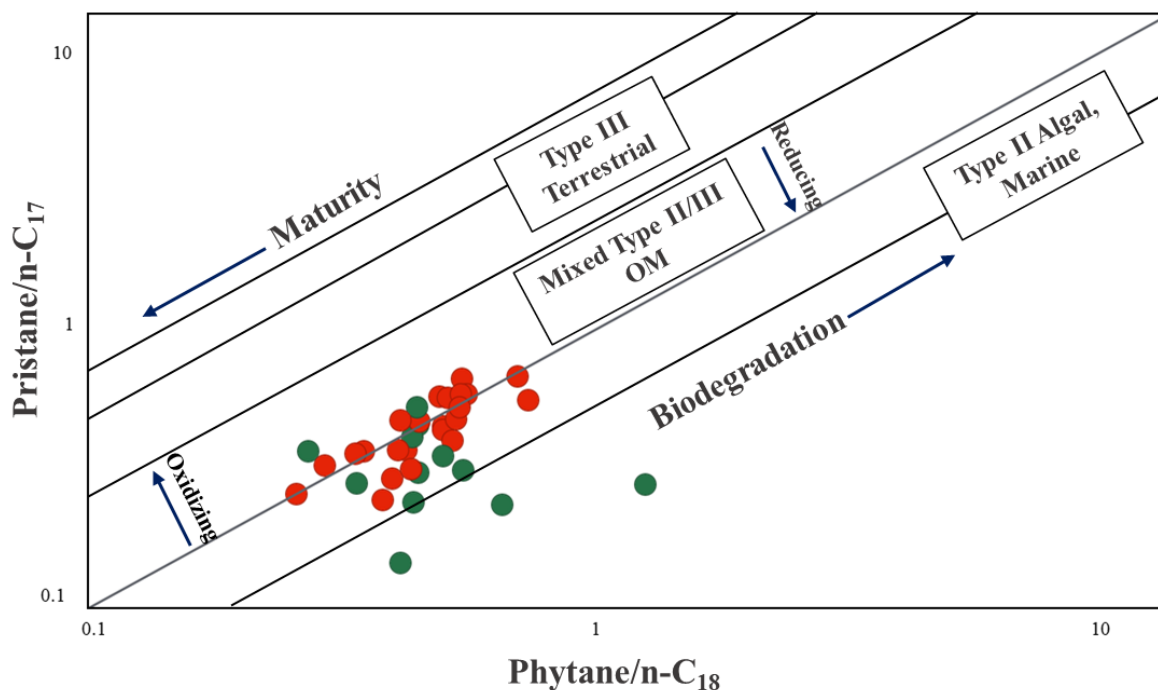


Figure 25. Pr/n-C₁₇ vs. Ph/n-C₁₈ illustrating the redox conditions for the Woodford Shale from the Speake Ranch. All the studied source rock samples illustrate a Type II and Type II/III kerogen of marine and marine-terrestrial mixed organic matter deposited within a reducing environment. The red symbols indicate soft bed lithofacies, while green symbols indicate hard bed lithofacies.

It is expected that lower Pr/Ph values would coincide with high TOC wt% and the data from the Speake Ranch samples confirm that a positive correlation is present (Figure 26). Significant elevated shifts of Pr/Ph coincide with intervals of lower TOC wt%, owing to an oxic environment that caused poor preservation of organic matter. For more accurate evaluation of the relationship between organic carbon preservation and anoxia, more redox evaluator parameters were also utilized in this research.

Sample	Depth (ft.)	Lithology	TOC (wt%)	S1 (mg HC/g)	S2 (mg HC/g)	S3 (mg CO2/g)	Tmax (°C)	HI	OI	S1/TOC	Pr/Ph
SR-190b	190.5	Soft	12	1.55	51.68	0.59	419	430.67	4.92	15.50	0.76
SR-191a	191	Hard	5.19	0.5	30.14	0.29	426	580.73	5.59	15.09	0.75
SR-191b	191.5	Soft	12.9	1.75	64.02	0.48	419	496.28	3.72	15.58	0.66
SR-192a	192	Hard	2.02	0.24	8.99	0.51	429	445.05	25.25	11.16	1.05
SR-193b	193.5	Soft	9.22	1.08	52.06	0.31	432	564.64	3.36	17.11	0.64
SR-194b	194.5	Soft	11.3	1.33	60.15	0.46	428	532.30	4.07	14.95	0.80
SR-195b	195.5	Soft	9.13	1.12	48.39	0.34	430	530.01	3.72	20.36	0.94
SR-196b	196.5	Soft	12.5	1.82	77	0.68	432	616.00	5.44	19.37	0.92
SR-197b	197.5	Soft	11.4	1.95	68.01	0.49	431	596.58	4.30	18.80	1.10
SR-198a	198	Hard	1.78	0.09	1.61	1.33	425	90.45	74.72	16.85	0.78
SR-199b	199.5	Soft	10.8	1.39	58.15	1.09	428	538.43	10.09	21.52	0.71
SR-200b	200.5	Soft	10.9	1.19	55.37	0.62	422	507.98	5.69	6.19	0.63
SR-202a	202	Hard	0.618	0.06	0.09	1.27	413	14.56	205.50	13.53	-
SR-203b	203.5	Soft	5.59	0.3	7.61	5.25	426	136.14	93.92	10.99	-
SR-204b	204.5	Soft	10.4	0.99	50.86	0.39	422	489.04	3.75	14.27	0.73
SR-205a	205	Hard	2.79	0.26	13.52	0.27	425	484.59	9.68	13.30	0.78
SR-207a	207	Hard	1.72	0.15	3.59	1.23	426	208.72	71.51	18.18	1.55
SR-208b	208.5	Soft	15.5	2.32	89.58	1.14	425	577.94	7.35	11.79	0.84
SR-209a	209	Hard	6.46	0.86	35.32	0.42	429	546.75	6.50	11.40	1.15
SR-210b	210.5	Soft	12.1	1.38	62.24	0.77	424	514.38	6.36	13.31	0.85
SR-211b	211.5	Soft	12.3	1.45	66.65	0.36	423	541.87	2.93	14.97	0.76
SR-212a	212	Hard	4.18	0.76	20.88	0.51	426	499.52	12.20	8.72	1.65
SR-213b	213.5	Soft	10.6	1.41	57.56	0.33	422	543.02	3.11	9.32	0.69
SR-214b	214.5	Soft	13.1	1.87	77.36	0.6	427	590.53	4.58	9.52	0.93
SR-215b	215.5	Soft	10.1	1.11	47.68	0.34	421	472.08	3.37	5.37	0.77
SR-217b	217.5	Soft	10.2	1.38	53.69	0.37	429	526.37	3.63	9.71	0.75
SR-218a	218	Hard	1.13	0.07	0.46	2.07	434	40.71	183.19	10.92	-
SR-219a	219	Hard	3.16	0.68	16.44	0.59	433	520.25	18.67	12.87	1.28
SR-221b	221.5	Soft	10.8	1.82	56.96	0.46	432	527.41	4.26	5.06	0.75
SR-222a	222	Hard	3.51	0.66	18.7	0.38	429	532.76	10.83	17.11	1.33
SR-223a	223	Hard	0.671	0.13	0.56	1.15	429	83.46	171.39	14.56	2.56
SR-224b	224.5	Soft	11.1	2.26	63.23	0.34	429	569.64	3.06	12.27	0.86
SR-225b	225.5	Soft	10.3	1.54	49.81	2.34	428	483.59	22.72	11.77	0.77
SR-226a	226	Hard	3.04	0.52	14.81	0.74	426	487.17	24.34	11.71	2.13
SR-227b	227.5	Soft	11.2	1.25	59.2	0.48	428	528.57	4.29	11.88	0.77
SR-228b	228.5	Soft	9.82	1.53	56.71	0.33	434	577.49	3.36	13.57	0.79
SR-229a	229	Hard	9.74	1.47	57.62	0.4	430	591.58	4.11	9.63	0.66
SR-230b	230.5	Soft	11.1	1.72	54.47	1.15	428	490.72	10.36	12.92	0.72

Table 2. Bulk geochemical data of the Woodford Shale from Speake Ranch, including S1, S2, S3, HI, OI, Tmax, S1/TOC, and Pr/Ph Pr/Ph

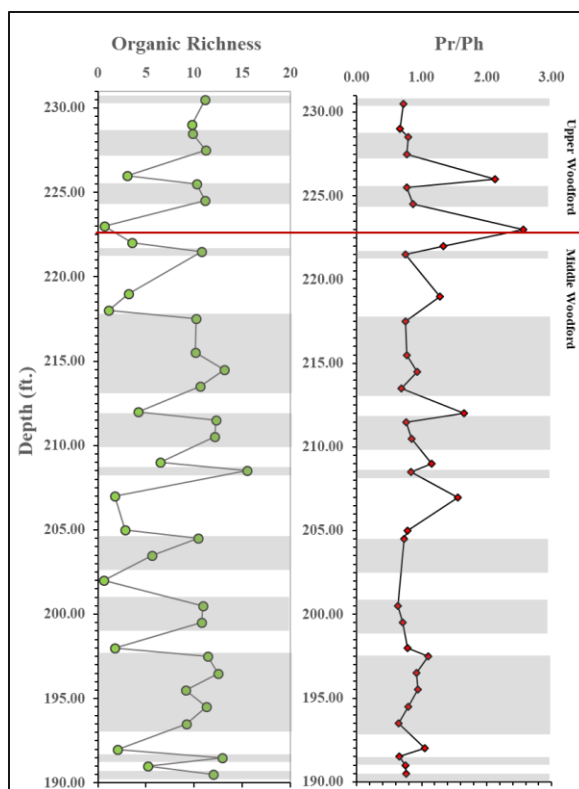


Figure 26. Integration of TOC depth plot and Pr/Ph depth plot generated in this study. Pr/Ph parallels the oscillation of TOC which coincides with the preservation of abundant organic matter within anoxic intervals. Gray intervals indicate soft bed layers, while the white intervals indicate hard bed layers. The red line is the Upper Woodford and Middle Woodford boundary.

More distinctions can be determined between the soft vs. hard of the Pr/Ph values approaching the Upper Woodford, where oxic periods are found to be more frequent (Figure 26). The Pr/Ph values have shown to be consistently anoxic until 205ft, and depths beyond this interval show that the sequence experienced episodes of oxic to sub-oxic disturbances (Figure 26). As TOC-rich intervals have high clay content, it would be expected that these intervals would experience consistently high levels of anoxia (low Pr/Ph). However, the correlation of Pr/Ph vs. C_{27} diasterane/steranes (formulas can be found in Appendix III) show that although clay content stay at nearly consistent values, Pr/Ph values are seen to vary (Figure 27). An elaborated discussion regarding the relationship between clay content, anoxia, and organic richness will follow in the

next sections. Peters et al. (2005) advised that the Pr/Ph in rock and oil samples within the oil-generative window should be used with caution as a correlative tool for depositional redox conditions. As samples of Speake Ranch values fall between 0.8-3, although still reflecting depositional redox conditions, may be influenced by variable source inputs, differing rates of early generation, and variations of thermal maturity (Peters et al., 2005). It is hypothesized in this research that optimal preservation of organic matter results from multiple factors other than anoxia. The highly oscillating TOC must be a result of combined depositional effects, further elaborated in the following sections.

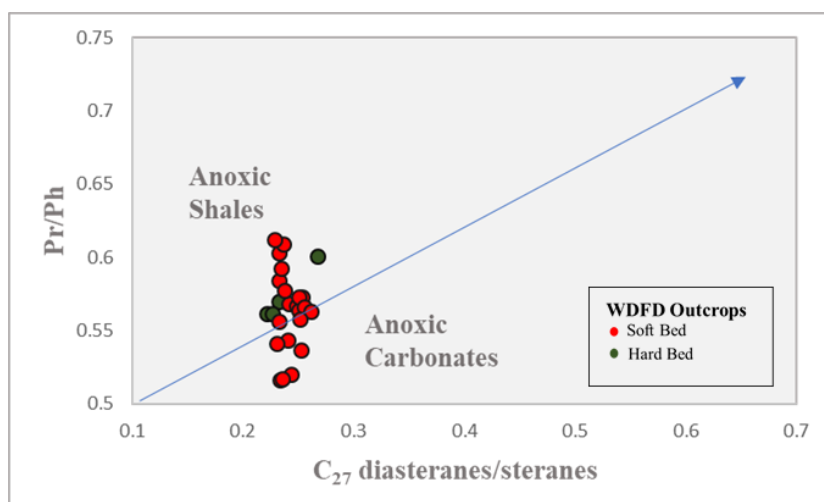


Figure 27. Pr/Ph vs. C₂₇ diasteranes/steranes (Appendix III; modified from Moldowan et al. 1994). The arrow shows the expected direction of thermal maturity effect, which is not considered for these specific samples since they are all of relatively low-maturity rocks. The diagram shows that Pr/Ph varies as clay content stays nearly consistent.

3.6.3 Steranes

Steranes are derived from the precursor steroid molecules (sterols) which contain 27, 28, 29, and 30 carbon atoms and are present in both higher plants and algae (Waples and Machihara, 1990). Steranes can have various conformations, in which the stereochemistry can change according to the level of thermal stress experienced. During diagenesis, these precursor molecules

are converted into a more stable saturate hydrocarbon biomarkers (Grantham, and Wakefield, 1987; Waples and Machihara, 1990). The thermal stability of steranes is lower than that of hopanes in both free and bound fractions due to their differing chemical structures and incorporation into the kerogen (Wu and Geng, 2016). The sterane family has proved to be reliable in the definition of organic matter source, lithology, maturation, biodegradation, and depositional environment conditions used in this research. Sterane distributions are monitored by the GC-MS using the characteristic ion at m/z 217 (Figure 28; Table 3).

Peak No.	Compound	Peak No.	Compound
1	Diapregthane	16	5 α 14 β 17 β 20R Ergostane + 24-Ethyl-13 α 17 β -Diacholestane 20R (C ₂₉)
2	Homopregthane	17	5 α 14 β 17 β Ergostane 20S
3	13 β 17 α Diacholestane 20S (C ₂₇)	18	5 α 14 α 17 α Ergostane 20R
4	13 β 17 α Diacholestane 20R (C ₂₇)	19	5 α 14 α 17 α Stigmastane 20S
5	13 α 17 β Diacholestane 20S (C ₂₇)	20	5 α 14 β 17 β Stigmastane 20R
6	13 α 17 β Diacholestane 20R (C ₂₇)	21	5 α 14 β 17 β Stigmastane 20S
7	24-Methyl-13 β 17 α Diacholestane 20S (C ₂₈)	22	5 α 14 α 17 α Stigmastane 20R
8	24-Methyl-13 β 17 α Diacholestane 20R (C ₂₈)	23	C ₃₀ 5 α 14 α 17 α 24-n-Propylcholestane 20S
9	5 α 14 α 17 α Cholestane 20S + 24-Methyl-13 α ,17 β -Diacholestane 20S (C ₂₈)	24	C ₃₀ 5 α 14 β 17 β 24-n-Propylcholestane 20R
10	5 α 4 β 17 β 20R Cholestane + 24-Ethyl-13 β ,17 α -Diacholestane 20S (C ₂₉)	25	C ₃₀ 5 α 14 β 17 β 24-n-Propylcholestane 20S
11	5 α 14 β 17 β 20S Cholestane + 24-Methyl-13 α ,17 β Diacholestane 20R (C ₂₈)	26	C ₃₀ 5 α 14 α 17 α 24-n-Propylcholestane 20R
12	5 α 14 α 17 α Cholestane 20R		
13	24-Ethyl-13 β ,17 α -Diacholestane 20R (C ₂₉)		
14	24-Ethyl-13 α ,17 β -Diacholestane 20S (C ₂₉)		
15	5 α 14 α 17 α Ergostane 20S		

Table 3. Peak identification of the steranes of sample SR-223a at depth 223ft within the Upper Woodford of Speake Ranch.

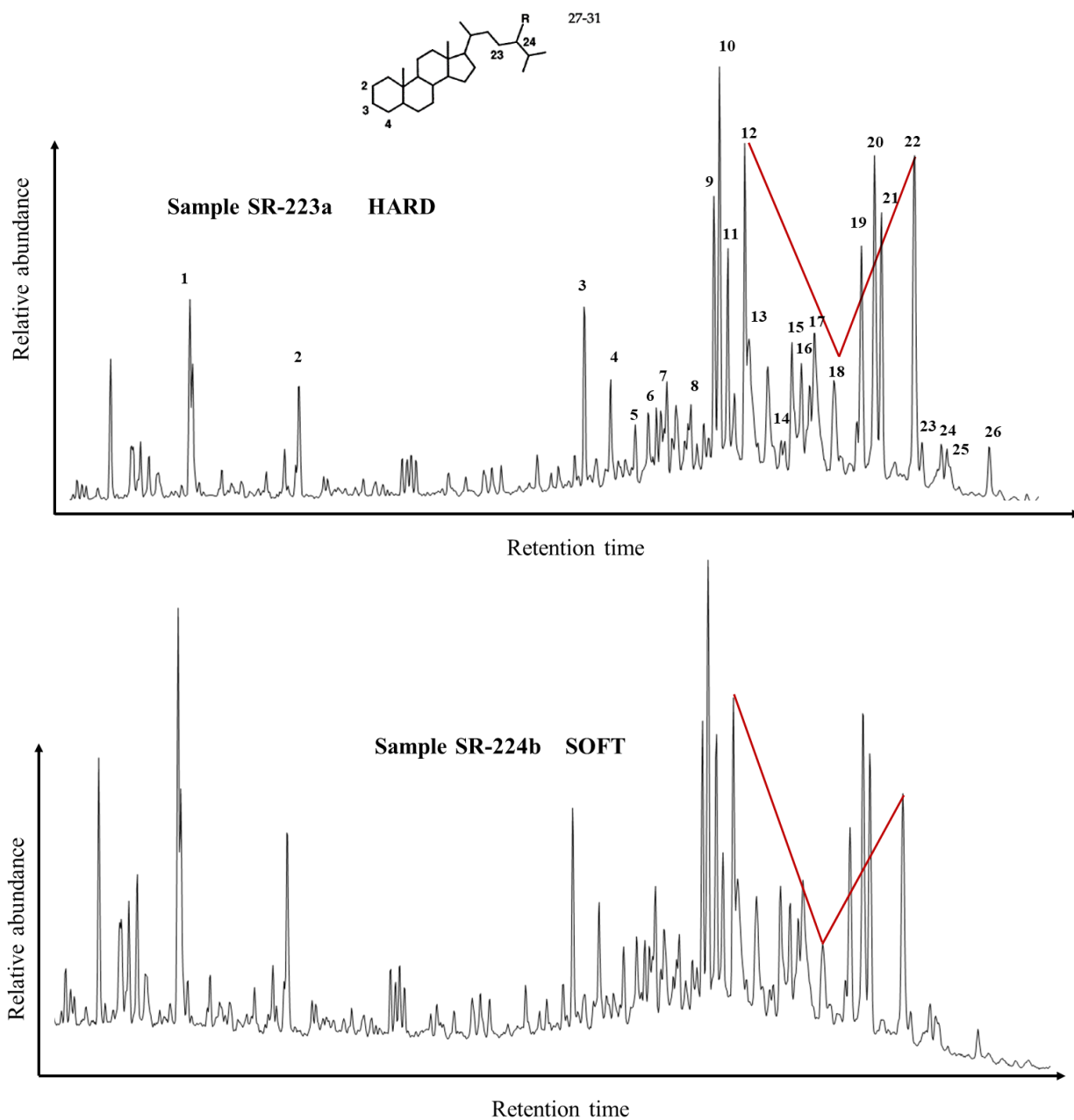
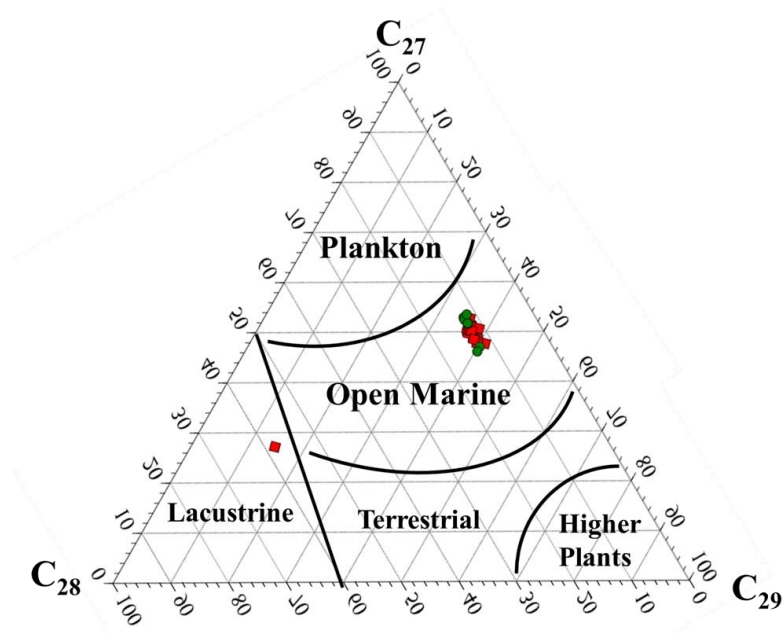


Figure 28. Distribution of the steranes and diasteranes monitored at m/z 217. Molecular structure of sterane from Pratt et al. (1992; IV, V, VI; Appendix II).

3.6.3.1 Organic Matter Source

Regular steranes are useful tools to evaluate and identify the photosynthetic biota (organisms/plants) that could be derived from precursor sources present in marine, terrigenous, or lacustrine environments (Waples and Machihara, 1990). The most common regular steranes used to determine organic matter input include the C₂₇ cholestanes (**IV**) that are abundant within plankton and marine invertebrates, C₂₈ ergostanes (**V**) which are derived from organisms present in lacustrine environments, and the C₂₉ sitostanes (**VI**) derived from land plants. The resulting C₂₇, C₂₈, and C₂₉ steranes acquired from the source rock extracts of Speake Ranch were used to construct a sterane ternary diagram [i.e. % C₂₇ = C₂₇ ααα 20R / (C₂₇ ααα 20R + C₂₈ ααα 20R + C₂₉ ααα 20R); Figure 30]. The steranes from the Speake Ranch cluster very closely to each other and suggest that the samples were deposited in an open marine environment (abundance of C₂₇ relative to C₂₉) with a major source contribution from phytoplankton (Figure 29(a.); modified from Huang and Meinschein, 1979). The modified plot by Moldowan et al. (1985) in Figure 29(b.) illustrate Speake Ranch values plotting below the defined marine shale parameter. As C₂₈ steranes are shown to be present in low abundances within these samples, weathering may have further reduced these abundances. Overall, there are no significant variations found for the distribution of the steranes within the sterane ternary plot, suggesting consistent and invariant influx of organic matter input. However, with higher resolution of biomarker analysis, variations of source input may uncover a principal marine origin with an incorporation of terrigenous input into the system, which is why utilizing the C₂₇ ααα20R/C₂₉ ααα20R steranes for the ratio will reveal the relative proportion of marine vs. terrigenous/algal input (Figure 30).

a.



b.

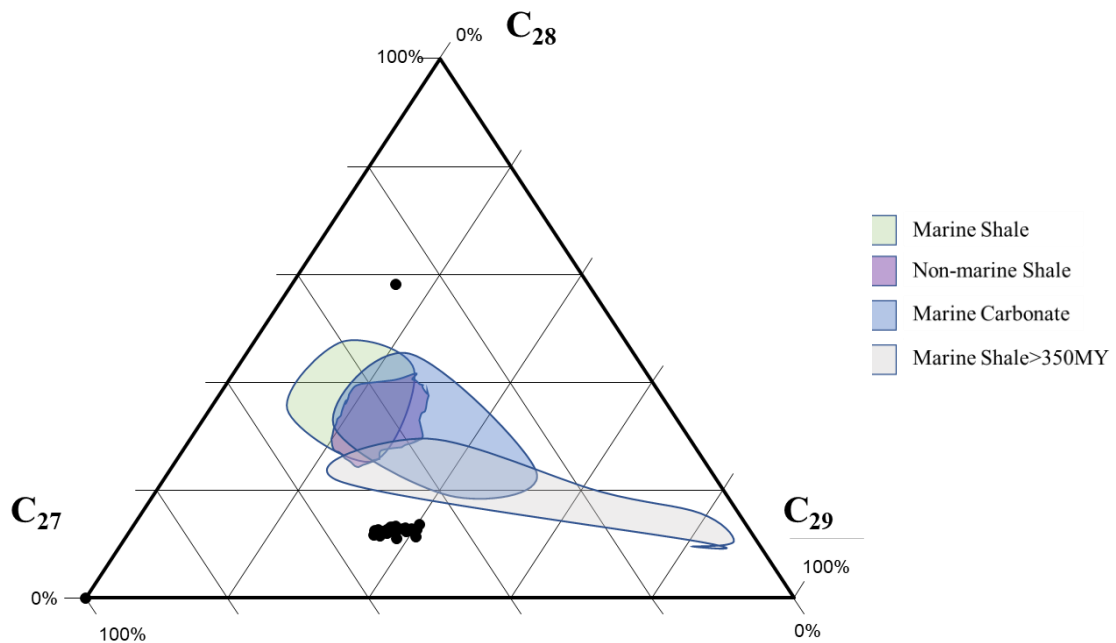


Figure 29(a). Ternary plot of the C₂₇-C₂₈-C₂₉ steranes to indicate organic matter source for the Woodford Shale. Majority of the samples are seen clustering in an abundance of C₂₇ steranes indicating an open marine environment (sterane ternary plot recreated from Huang and Meinschein, 1979); **(b).** distribution determined by Moldowan et al. (1985) for source rocks of varying ages.

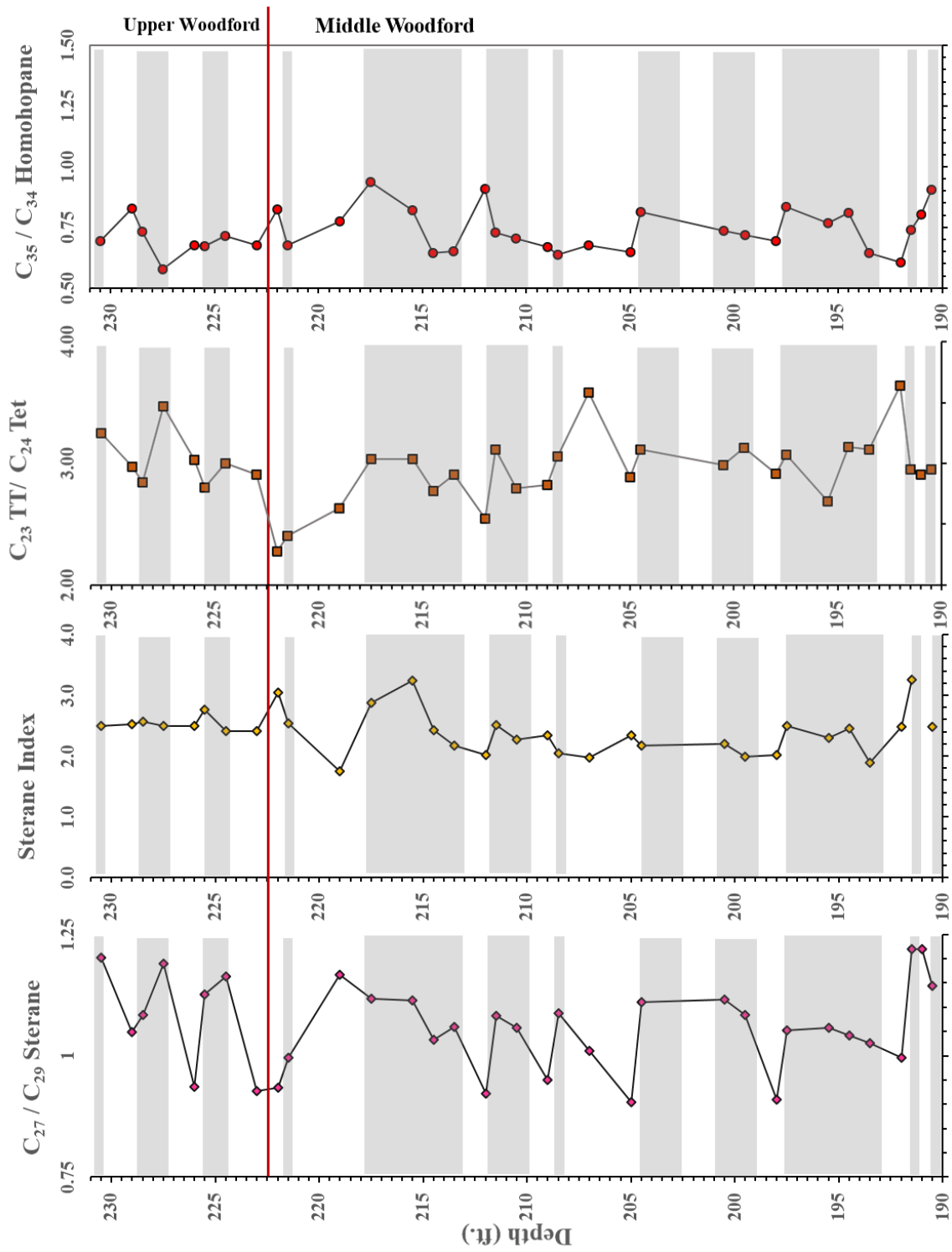


Figure 30. Geochemical logs representing the environmental condition variations that yield the distribution of organic matter source. Gray intervals indicate the soft bed lithofacies.

Sample	Depth (ft.)	Lithology	TOC (wt%)	Pr/Ph	C ₃₀ sterane index	C ₂₇ /C ₂₉ Sterane	C ₂₉ /C ₂₈ Sterane	C ₂₃ T ₁₇ /C ₂₄ Tet	C ₁₉ /C ₂₃ TT	C ₂₈ BNH/C ₃₀ Hopane	C ₂₈ BNH/Norhopane	C ₂₇ diasterane/sterane
SR-190b	190.50	Soft	12.00	0.76	2.48	1.14	0.39	2.95	0.09	0.50	2.18	0.32
SR-191a	191.00	Hard	5.19	0.75	-	1.22	0.39	2.91	0.10	0.53	1.97	0.30
SR-191b	191.50	Soft	12.90	0.66	3.26	1.22	0.39	2.95	0.10	0.52	1.93	0.30
SR-192a	192.00	Hard	2.02	1.05	2.48	1.00	0.40	3.64	0.08	0.29	1.71	0.30
SR-193b	193.50	Soft	9.22	0.64	1.89	1.03	0.40	3.12	0.09	0.39	2.09	0.31
SR-194b	194.50	Soft	11.30	0.80	2.45	1.04	0.41	3.13	0.08	0.34	2.05	0.30
SR-195b	195.50	Soft	9.13	0.94	2.30	1.06	0.39	2.69	0.09	0.42	2.07	0.31
SR-196b	196.50	Soft	12.50	0.92	-	-	-	-	-	-	-	-
SR-197b	197.50	Soft	11.40	1.10	2.49	1.05	0.40	3.07	0.08	0.36	2.08	0.32
SR-198a	198.00	Hard	1.78	0.78	2.02	0.91	0.38	2.91	0.06	0.25	1.65	0.28
SR-199b	199.50	Soft	10.80	0.71	1.98	1.08	0.39	3.13	0.10	0.38	2.07	0.31
SR-200b	200.50	Soft	10.90	0.63	2.20	1.12	0.42	2.98	0.10	0.42	2.07	0.30
SR-202a	202.00	Hard	0.62	-	-	-	-	-	-	-	-	-
SR-203b	203.50	Soft	5.59	-	-	-	-	-	-	-	-	-
SR-204b	204.50	Soft	10.40	0.73	2.17	1.11	0.40	3.12	0.09	0.37	2.03	0.30
SR-205a	205.00	Hard	2.79	0.78	2.34	0.90	0.35	2.88	0.07	0.27	1.72	0.29
SR-207a	207.00	Hard	1.72	1.55	1.97	1.01	0.39	3.58	0.06	0.23	1.34	0.31
SR-208b	208.50	Soft	15.50	0.84	2.04	1.09	0.38	3.06	0.09	0.38	1.94	0.31
SR-209a	209.00	Hard	6.46	1.15	2.34	0.95	0.37	2.82	0.06	0.26	1.67	0.29
SR-210b	210.50	Soft	12.10	0.85	2.26	1.06	0.39	2.80	0.08	0.35	2.02	0.32
SR-211b	211.50	Soft	12.30	0.76	2.51	1.08	0.38	3.11	0.09	0.38	1.93	0.30
SR-212a	212.00	Hard	4.18	1.65	2.01	0.92	0.37	2.55	0.06	0.27	1.62	0.29
SR-213b	213.50	Soft	10.60	0.69	2.16	1.06	0.37	2.90	0.08	0.34	1.94	0.33
SR-214b	214.50	Soft	13.10	0.93	2.43	1.03	0.33	2.77	0.08	0.35	2.02	0.31
SR-215b	215.50	Soft	10.10	0.77	3.24	1.11	0.38	3.04	0.07	0.39	2.18	0.31
SR-217b	217.50	Soft	10.20	0.75	2.88	1.12	0.41	3.03	0.09	0.39	1.92	0.33
SR-218a	218.00	Hard	1.13	-	-	-	-	-	-	-	-	-
SR-219a	219.00	Hard	3.16	1.28	1.74	1.17	1.27	2.63	0.04	0.24	1.59	0.30
SR-221b	221.50	Soft	10.80	0.75	2.53	1.00	0.42	2.40	0.06	0.35	2.17	0.34
SR-222a	222.00	Hard	3.51	1.33	3.04	0.93	0.40	2.27	0.05	0.26	1.54	0.32
SR-223a	223.00	Hard	0.67	2.56	2.41	0.93	0.36	2.91	0.05	0.23	1.47	0.29
SR-224b	224.50	Soft	11.10	0.86	2.42	1.16	0.42	3.00	0.08	0.39	2.28	0.33
SR-225b	225.50	Soft	10.30	0.77	2.76	1.13	0.42	2.80	0.07	0.39	2.25	0.34
SR-226a	226.00	Hard	3.04	2.13	2.50	0.94	0.36	3.03	0.05	0.24	1.47	0.29
SR-227b	227.50	Soft	11.20	0.77	2.49	1.19	0.44	3.47	0.08	0.38	2.13	0.34
SR-228b	228.50	Soft	9.82	0.79	2.56	1.08	0.43	2.84	0.07	0.36	2.11	0.35
SR-229a	229.00	Hard	9.74	0.66	2.52	1.05	0.42	2.97	0.07	0.37	2.21	0.37
SR-230b	230.50	Soft	11.10	0.72	2.49	1.20	0.42	3.25	0.09	0.37	2.23	0.34

Table 4. Sterane and terpane biomarker proxies to determine organic matter source. Empty fields are due to the lack of maltene from extraction.

There is a clear distinction as shown in C_{27}/C_{29} sterane ratio [$C_{27}/C_{29} = C_{27} \alpha\alpha\alpha 20R/C_{29} \alpha\alpha\alpha 20R$ sterane] depth plot of a trend between the soft (gray interval) and the hard (white interval) beds (Figure 30). The C_{27}/C_{29} sterane ratio is often used as a marine organic matter indication when values exceed one (Grantham and Wakefield, 1988). Apart from association with abundant organic matter with the soft lithofacies, the softer beds have also shown to be deposited in a marine environment with an abundance of C_{27} steranes (Figure 31). Conversely, the harder beds generally have C_{27}/C_{29} sterane at values less than 1 (C_{29} steranes abundant) throughout the studied interval, illustrating a relatively higher terrigenous input and a more oxic depositional environment. The ratio that is observed to illustrate values less than 1 are due to a relative increase in the C_{29} sterane, and subsequently a decrease in C_{27} sterane from the measurements of their relative concentrations (Figure 32; $C_{27}/\text{total steranes}$ to $C_{29}/\text{total steranes}$). It is suggested that as the Late Devonian was a time of expanding terrigenous vegetation and higher nutrient input, the resulting fluctuation reflects weathering, widespread anoxia, and eutrophication. According to the sequence stratigraphy more terrigenous input should be naturally observed within the Upper Woodford due to its higher proportion of silica to clay content (Torres, 2020). Therefore, the decrease in clay content in the Upper Woodford signifies an increase of terrigenous source input that dilutes the marine clays, thus reducing the availability of acid sites. The significance of acid sites is that it provides a platform for catalyzing rearrangement of the sterol backbone (van Kaam-Peters et al., 1998). Another possible explanation for the frequent fluctuations between marine and terrigenous input is that as the shoreline retreated, the depositional environment may have become more restricted, which causes CaCO_3 to supersaturate the water column. This resulted in the stimulation of algal blooms from marine ocean water anoxia caused by the Devonian expansion of terrigenous land plants and extensive emission of CO_2 (Philp and DeGarmo, 2020). Furthermore, when the

C_{27}/C_{29} sterane ratio is combined with Pr/Ph ratio, it would appear to suggest that the marine dominated soft beds with high TOC values were deposited in a primarily anoxic condition (Figure 31). Alternatively, the lower TOC intervals of the hard beds were deposited under a more oxidized environment, with a higher input of the C_{29} steranes (Figure 31 highlighted intervals). Using the C_{27}/C_{29} ratio depth plot against Pr/Ph defined from Hossain et al. (2009) can help determine types of organic matter input and the depositional environmental condition as shown in Figure 33. Observed trends in Figure 31, sterane index along with relative abundances in Figure 32, and plot of C_{27}/C_{29} sterane against Pr/Ph (Figure 33) all point toward the same conclusion of the marine/algal source input in an anoxic depositional environment of the Woodford Shale. It is apparent that the relatively lower TOC values are associated with elevated C_{29} sterane abundances within the Upper Woodford and Middle Woodford. However, caution is needed for sediments indicating a terrigenous source environment (showing an abundance of C_{29}) as it is not to confuse such an input from cyanobacteria (green-blue algae) (Boon et al., 1983; Brassell et al., 1988; Telnaes and Cooper, 1991) or chlorophyta (green algae) (Fowler and Douglass, 1987; Waples and Machihara, 1990) which have also been proposed to contribute C_{29} steranes into the sediments. Grantham and Wakefield (1988) have also suggested that C_{29} steranes could result from a contribution of brown algae. Table 4 displays all the values of biomarker parameters evaluating source organic matter input. Intervals without values are due to data limitations from the lack of maltene yield from extraction.

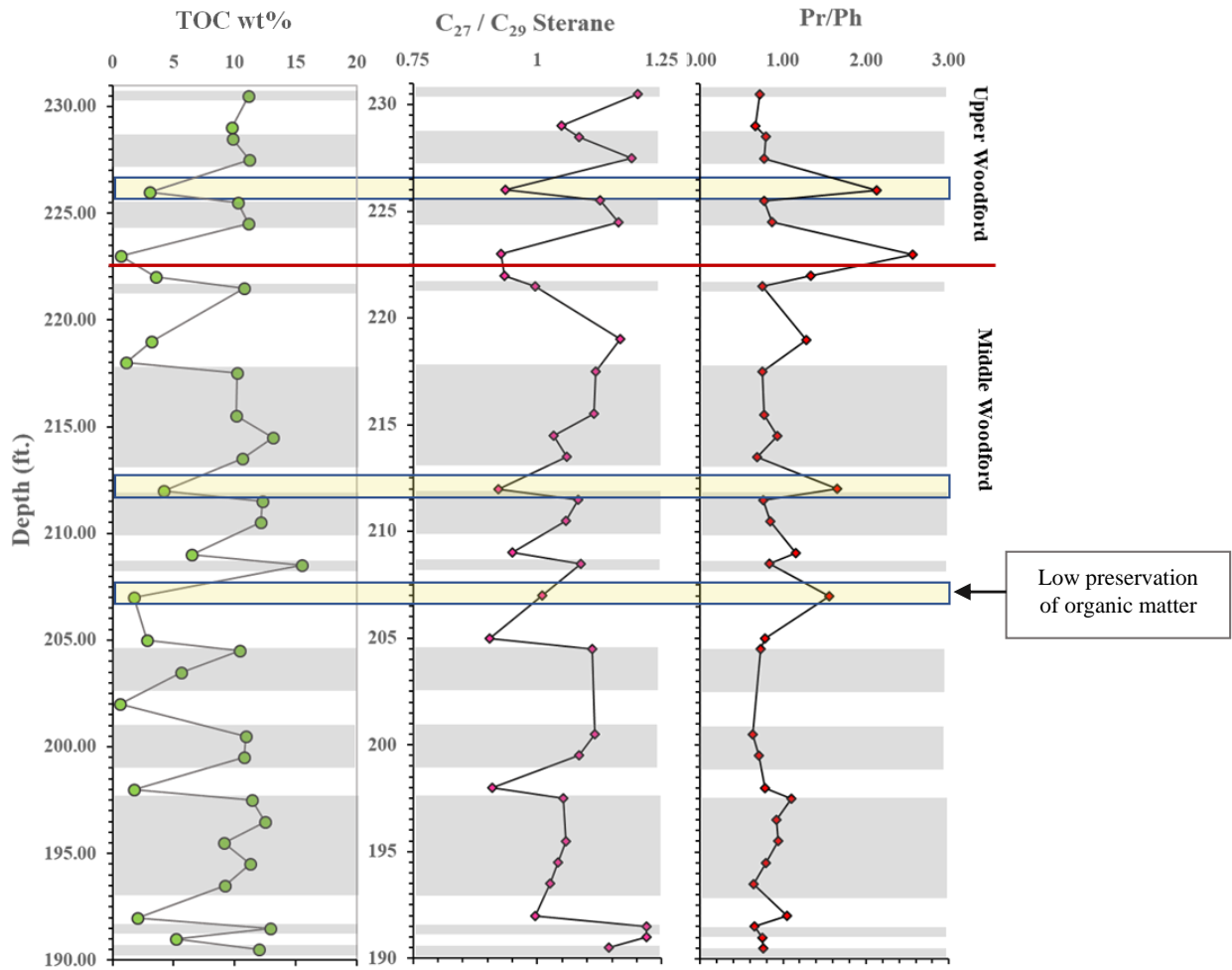


Figure 31. Geochemical logs correlating TOC fluctuations, with the associated marine vs. terrigenous source input (C_{27}/C_{29} sterane), and the role of anoxia (Pr/Ph) in its distribution. Highlighted zones indicate that low preservations of organic matter are associated with high C_{29} input and oxidizing environmental deposition conditions. Gray zones are the soft bed intervals, and the white zones are the hard bed intervals.

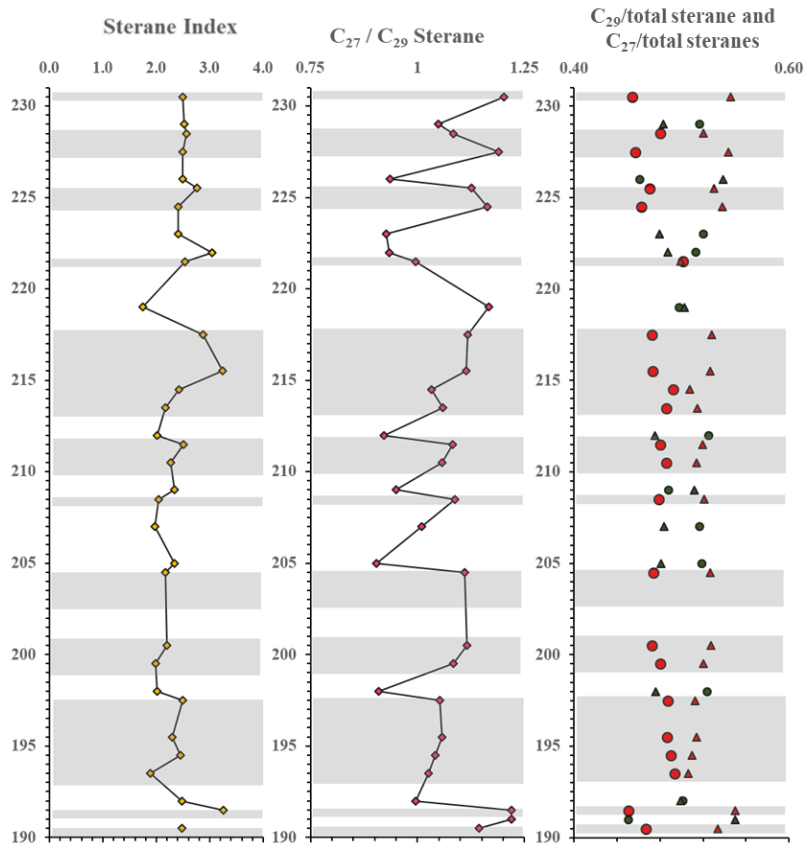


Figure 32. The plot on the right display the relative abundances of C_{27} and C_{29} [C_{27} 14 α ,17 α -+14 β ,17 β -Steranes(20S+20R)/total steranes; C_{29} 14 α ,17 α - +14 β ,17 β -Steranes (20S+20R)/total steranes; **Appendix III**; triangles: C_{27} /total steranes; circles: C_{29} /total steranes]. Decrease in C_{27}/C_{29} steranes coincide with a relative increase in C_{29} steranes.

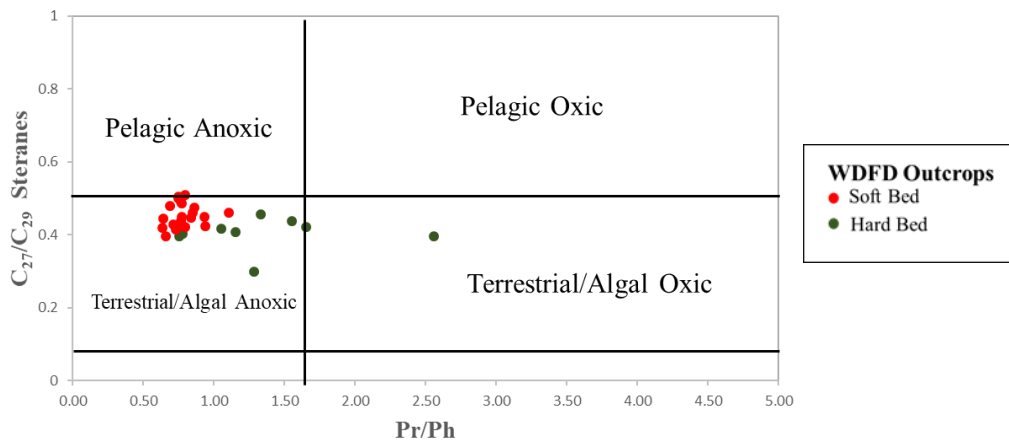


Figure 33. C_{27}/C_{29} steranes vs. Pr/Ph plot characterizing the Woodford Shale from Speake Ranch as algal rich organic matter deposited in an anoxic environment. (modified from Hossain et al., 2009). Samples plotting below 0.55 indicate terrigenous input into the anoxic environment.

The abundance of the C₃₀ steranes (**VII**) in sediments is a strong indication of marine organic matter input (Peters and Moldowan, 1991). The C₃₀ sterane index (Sterane Index: C₃₀/(C₂₇-C₃₀) steranes) has widely been used to discern the amount of marine biotic input (Peters et al., 1986 and Peters et al., 2005). This ratio is suggested to decrease with regression of sea level, as there are less input of marine-sourced organic matter and more of terrigenous-sourced organic matter. The Speake Ranch samples have values ranging from 2.3 - 5.6% averaging at 4.1% (Figure 30 and 32; Table 4). Moldowan et al. (1985), Peters et al. (2005) and Hays et al. (2012) determined that C₃₀ sterane index values >4% are indicative of marine pelagophyte algae, and thus indicating a marine depositional environment. This places majority of the values within the 40ft interval of the Speake Ranch well above that parameter which supports the characterization of marine environment origin. Values plotting below this 4% parameter are most likely due to the elevated C₂₉ sterane (terrigenous input) relative to the C₂₇ sterane values found within the harder lithofacies (Figure 32). Although, as mentioned in the earlier section, the C₂₉ sterane could also be synthesized by green algae (Schwark and Empt, 2006). The C₃₀ sterane index values illustrate an overall marine source input as shown in Figure 32. The C₃₀ sterane index is seen to increase approaching the Upper Woodford, although ironically it has been proposed that the terrigenous input increases prior to the Frasnian-Famennian extinction boundary suggested by Torres (2020) shown in Figure 32. The Frasnian-Famennian (F-F) extinction boundary marks the loss of a wide marine biota, which Torres (2020) has defined to be at 194 to 210 ft. This interpretation was defined by abrupt changes in biomarker parameters. However, a specified interval was unable to be determined by Galvis (2017) and Torres (2020) due to a lack of high resolution biomarker analysis.

A narrow interval in which the F-F boundary is proposed to have occurred will be discussed in Chapter V. It is expected that terrigenous input should overwhelm the Upper Woodford as the

sediments within this endmember were deposited during a Highstand System Tract. As shoreline retreated, erosional events increase with progradation, which introduces terrigenous material into the basin and disturbed the marine productivity, which may contribute to the elevated C₂₉ steranes input (Figure 18).

3.6.3.2 Thermal maturity indicators

The T_{max} and R_c measurements indicated that the Woodford Shale from the Speake Ranch is largely immature throughout the 40ft section. To validate and support the accuracy of the T_{max} and R_c values, several biomarker maturity parameters were also utilized. As discussed earlier, the sterane and hopanes structures will be converted into more stable conformations with increasing levels of thermal stress (Grantham, and Wakefield, 1987; Waples and Machihara, 1990). Reliable assessment of maturity can be determined by utilizing the epimerization of the H atom at C-20 in the S configuration of C₂₉ 5 α ,14 α ,17 α -sterane (VI), specifically for immature to early mature samples (Mackenzie et al., 1980). The 20R configuration in steroid precursors within living organisms, are converted into a mixture of the 20R and 20S configurations with burial and maturation (Requejo et al., 1994). With increasing maturity, the proportion of the 20S increases at the expense of the 20R epimer. Thus, changes in the 20S/(20S+20R) ratio for any of the C₂₇-C₂₈-C₂₉ steranes can be used to evaluate relative maturity levels. The C₂₉ sterane isomers and epimers are generally used for this purpose since all four isomers and epimers are resolved chromatographically (Waples and Machihara, 1990). Seifert and Moldowan (1986) proposed that the isomerization at C-14 and C-17 in the 20S and 20R of the C₂₉ steranes provide for a reliable maturity parameter, $\beta\beta/(\beta\beta+\alpha\alpha)$, which is independent of organic matter source input. An increase

in the $\alpha\beta\beta$ steranes relative to the less stable $\alpha\alpha\alpha$ steranes reaches equilibrium slower than the 20S and 20R, thus making it effective at higher thermal maturity. $C_{29} \beta\beta/(\beta\beta+\alpha\alpha)$ [$C_{29}(14\beta,17\beta$ -Stigmastane (20S+20R)]/[$14\beta,17\beta$ - + $14\alpha,17\alpha$ -Stigmastane (20S+20R))] is a useful and reliable maturity indicator to be incorporated with $C_{29} 20S/(20S+20R)$ [$C_{29} (14\alpha,17\alpha$ -Stigmastane (20S)]/[$14\alpha,17\alpha$ -Stigmastane (20S+20R))]. However, it is also important to note that elevated values of $\beta\beta$ steranes may be a product of reaction to sulfur (ten Haven et al., 1986). Schmid (1986) indicated that heating the $\alpha\alpha\alpha$ cholestane with sulfur gave little isomerization at C-20, however, a substantial amount formed of the $\alpha\beta\beta$ 20R and 20S. The plot of $C_{29} 20S/(20S+20R)$ vs. $C_{29} \beta\beta/(\beta\beta+\alpha\alpha)$ in Figure 34 defined by Peters (1999) have been used as an indicator of organic maturity. The Woodford Shale samples from the Speake Ranch show higher maturity values than indicated for immature characteristics defined by Seifert and Moldowan (1980) in Figure 34. This could possibly reflect migrated hydrocarbons (Torres, 2020) and/or the presence of sulfur upon deposition. The outlier may be due to partial sterane degradation that resulted in increase of the 20S, by selective removal of the 20R epimer by bacteria. Nevertheless, the clustering of the samples in Figure 34 confirms the similar maturity values for all the samples in this study and indicate that maturity is not playing any significant role in variations of any of the biomarker distributions.

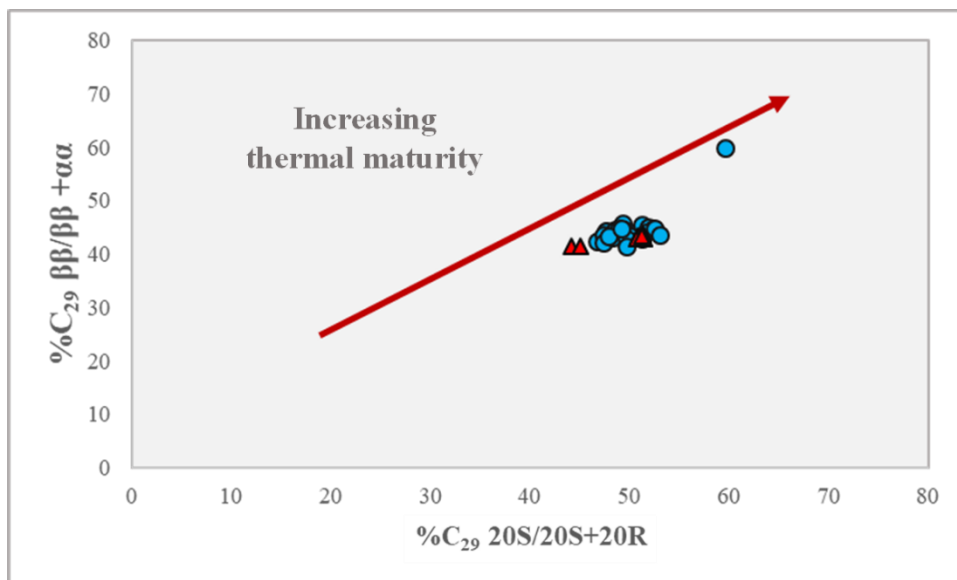


Figure 34. Maturity plot of the 20S/(20S+20R) vs. C₂₉ ββ/ (ββ+ αα) isomers. This plot illustrates clustering of the Woodford Shale samples from Speake Ranch due to their similar levels of maturity. Upper Woodford and Middle Woodford may indicate samples of migrated HC (modified from Peters et al., 1999). Blue circle symbols indicate Middle Woodford and, red triangle symbols indicate Upper Woodford samples. Outlier may be due to partial sterane biodegradation that resulted in increase of the 20S, by selective removal of the 20R epimer by bacteria.

3.6.3.3 Lithology

It was earlier noted that organic matter rich intervals coincide with clay-rich intervals. Therefore, it is expected for those clay-rich intervals to be deposited in a more anoxic environment. The diasteranes have been found to indicate acidic (clay or water chemistry) and oxic conditions during diagenesis (Rubinstein et al. 1975; Sieskind et al., 1979; Moldowan et al., 1985; van Kaam-Peters et al., 1998; Brincat and Abbott, 2001). Acidic sites on clays catalyze sterane conversion to diasteranes during diagenesis (Moldowan et al., 1985; Grantham and Wakefield, 1988). Therefore, diasteranes serve as an indicator of the lithology and oxicity. Moldowan et al. (1985) found that samples from Toarcian shale from southwest Germany, have Pr/Ph values that increase with C₂₇ diasteranes/(diasteranes+steranes) (**VIII**; C₂₇diasterane/sterane). In Speake Ranch, Pr/Ph values significantly vary as C₂₇ diasterane/sterane values stay nearly consistent shown in Figure 27 (formula can be found in Appendix III). However, the Speake Ranch samples in Figure 35 reveal

that approaching the Upper Woodford higher values of clay content determined by C_{27} diasterane/sterane coincide with relatively higher TOC and anoxic environmental condition. Additionally, lower relative clay content indicated by lower C_{27} diasterane/sterane coincides with more oxic conditions starting from 204.5ft within the section. This shows an improved resolution of the relationship between clay abundance and anoxic deposition than the parameter shown in Figure 27.

Mello et al. (1988) noted that the diasterane/sterane ratio using the C_{27} diasteranes and steranes $[(C_{27} (20S+20R \beta\alpha\text{- and } \alpha\beta\text{-Diacholestane})/(20S+20R 5\alpha,14\alpha,17\alpha\text{-Cholestane and } 20S+20R 5\alpha,14\beta,17\beta\text{-Cholestane}))]$ is another correlative tool to distinguish carbonates from siliclastic rocks, whereby a lower diasterane/sterane ratio indicates clay-poor carbonate source rocks (Figure 36). Furthermore, high diasterane concentrations relative to regular steranes are thought to be typical of clay rich source rocks, but they have also been observed in extracts from organic-lean carbonates (Moldowan et al., 1991). van Kaam-Peters et al. (1998) found that the diasterane/sterane ratio does not always correlate directly with clay content as it may be affected by level of oxidation as well. The Speake Ranch samples have low values of diasteranes/steranes ratios below 0.5, ranging between 0.3-0.5, which indicates anoxic carbonate source rocks. Carbonate deposition seems to predominate in the Upper Woodford, illustrating that as the shoreline retreated the depositional environment became increasingly restricted causing supersaturation of the water column by $CaCO_3$. Plots of Pr/Ph vs. diasterane/sterane and C_{27}/C_{29} sterane ratio vs. C_{27}/C_{29} diasterane $[(C_{27}13\beta,17\alpha\text{-Diacholestane } 20R+13\alpha,17\beta\text{-Diacholestane } 20S)/[24\text{-Ethyl-}13\beta,17\alpha\text{-Diacholestane } 20R+-13\alpha,17\beta\text{-Diacholestane } 20S])$ ratio are shown in Figure 36 and both agree on a similar conclusion. The Pr/Ph (0.2-2.5) vs. diasterane/sterane (0.3-0.5) have values indicating anoxic carbonates and C_{27}/C_{29} sterane ratio (0.8-1.3) vs. C_{27}/C_{29}

diasterane ratio (1.61-3.63) indicate mixed marine source input. The plots correspond to a predominantly anoxic carbonate deposition with a mixed input of marine and terrigenous organic matter. Chapter IV discusses the effects of varying levels of anoxia on organic carbon preservation.

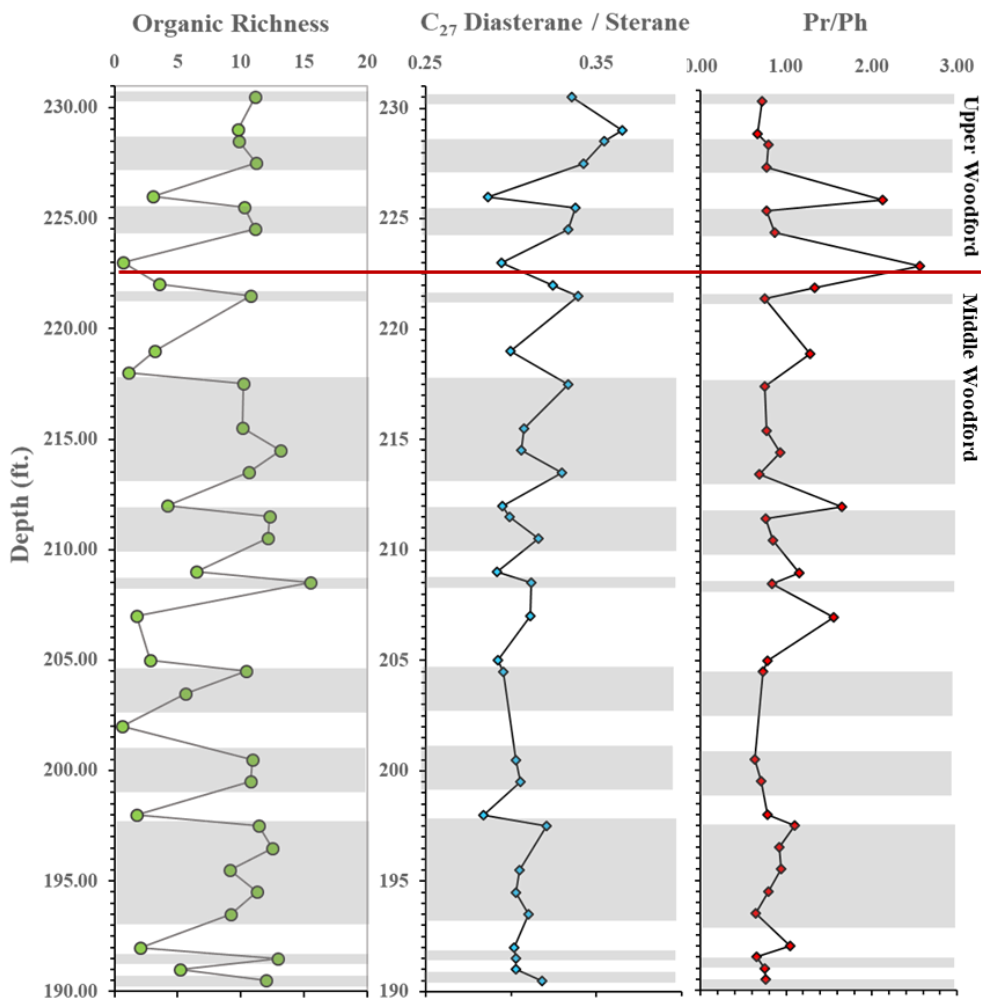


Figure 35. C₂₇ diasterane to non-arranged sterane ratio [C₂₇ 13β,17α-Diacholestane (20S+20R)]/[C₂₇ 14α,17α- + 14β,17β-Cholestane (20S+20R)] as a correlative tool to indicate lithology and level of anoxia. High diasterane values over the regular steranes indicate clay rich intervals, which coincide with the soft beds of the Speake Ranch samples deposited in an anoxic environment, determined by the Pr/Ph ratio.

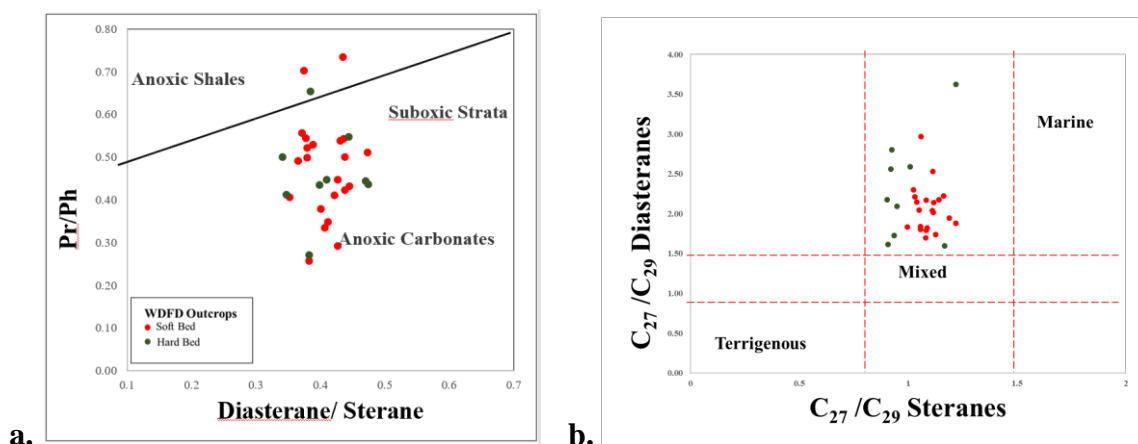


Figure 36 (a). Pr/Ph ratio vs. diasterane/sterane ratio is used to determine the lithology and the extent of anoxia the sediments were deposited (modified from Moldowan et al., 1994) **(b).** C₂₇/C₂₉ sterane ratio vs. C₂₇/C₂₉ diasterane ratio to further support organic matter source influx of predominantly marine with mixed marine (modified from Ghori, 2002). Ratio description are included in the Appendix.

3.6.4 Terpanes

Terpanes are biomarkers derived from bacterial (prokaryotic) membrane lipids (Ourisson et al., 1982; Peters et al., 2005). The dominant bacterial family of terpanes are the hopanoids. The two families that the terpanes are subdivided into are based on the number of rings, where those with 27 to 35 carbons belong to the pentacyclics, often known as the “hopanoid” and “nonhopanoids” (**hopanes; IX**), and the tricyclics and tetracyclic terpanes have 21 to 35 carbon atoms (Waples and Machihara, 1990). The dominant molecular structure of the triterpanes contains 5-rings, where the E-ring contains 5 carbon atoms. Similarly, gammacerane contains the same number of rings but has 6 carbon atoms within the E-ring. Tricyclic terpanes, hopanes and gammacerane are useful for indicating certain depositional environments. A typical terpane distribution is monitored on the GC-MS at m/z 191 as shown in Figure 37 with peak identifications in Table 5.

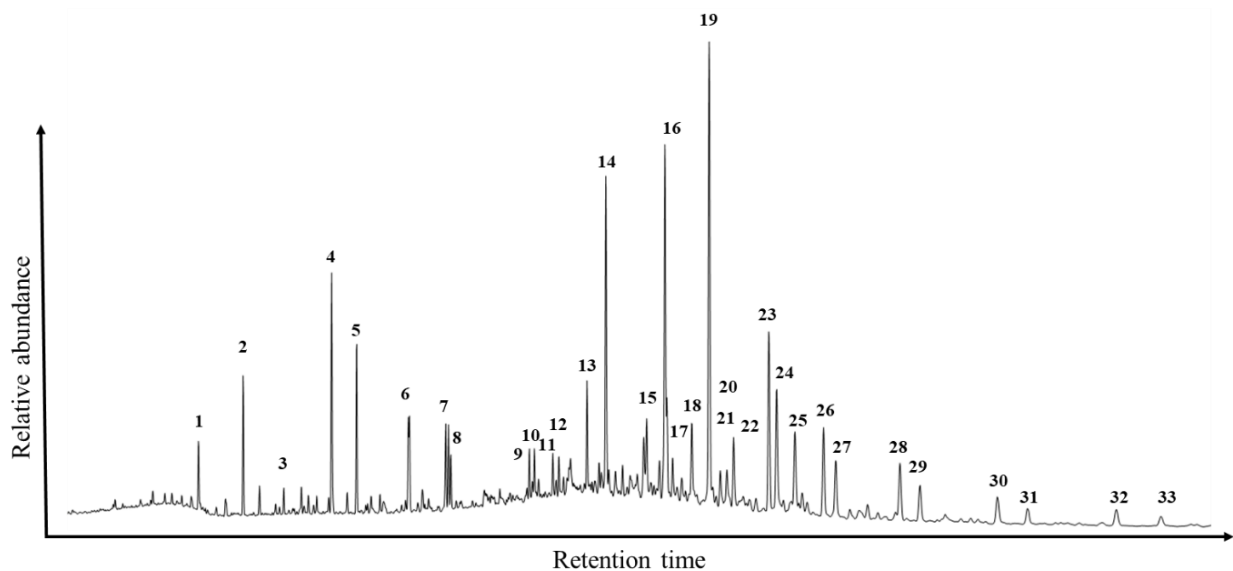


Figure 37. GC-MS chromatogram displaying the distribution of the tricyclic terpanes and hopanes screened at m/z 191. Peaks nomenclature are displayed in Table 5.

Peak No.	Compound	Peak No.	Compound
1	C ₂₀ Tricyclic terpane	19	C ₃₀ Hopane
2	C ₂₁ Tricyclic terpane	20	C ₃₀ Tricyclic terpane
3	C ₂₂ Tricyclic terpane	21	C ₃₁ Tricyclic terpane
4	C ₂₃ Tricyclic terpane	22	Moretane
5	C ₂₄ Tricyclic terpane	23	C ₃₁ Hopane 22S
6	C ₂₅ Tricyclic terpane	24	C ₃₁ Hopane 22R
7	C ₂₄ Tetracyclic terpane	25	Gammacerane
8	C ₂₆ Tricyclic terpane 22S+22R	26	C ₃₂ Hopane 22S
9	C ₂₈ Tricyclic terpane 22S	27	C ₃₂ Hopane 22R
10	C ₂₈ Tricyclic terpane 22R	28	C ₃₃ Hopane 22S
11	C ₂₉ Tricyclic terpane 22S	29	C ₃₃ Hopane 22R
12	C ₂₉ Tricyclic terpane 22R	30	C ₃₄ Hopane 22S
13	Ts	31	C ₃₄ Hopane 22R
14	Tm	32	C ₃₅ Hopane 22S
15	C ₂₈ Bisnorhopane	33	C ₃₅ Hopane 22R
16	C ₂₉ Ts	34	
17	C ₃₀ Diahopane (C ₃₀ D)		
18	C ₂₉ 17 β 21 α Moretane (Normoretane)		

Table 5. Peak identification of the terpanes at m/z 191 fragmentogram.

3.6.4.1 Organic Matter Source

Tricyclic terpanes (**X**) have been found to derive from precursors produced by algae and have been known to occur in small abundances (or absent) in oils and extracts from terrigenous sources (Seifert and Moldowan, 1980; Philp et al., 1992; Peters et al., 2005). Moreover, an abundance of tricyclic terpanes can often be found in immature sediments where the short-chain member of the tricyclic terpanes are believed to be related to bacterial input (Aquino Neto et al., 1986; Chicarelli et al., 1983). Aquino Neto et al. (1992), Simoneit et al. (1993), and Araujo et al. (2018) believe that the source of tricyclic terpanes is associated with samples rich in *Tasmanites* algae, which is highly associated with the Woodford shale from Speake Ranch. *Tasmanites* play a significant role in the production of TOC and biogenic silica, as they contribute to the mechanics of “frackable” intervals for the unconventional play of the Woodford Shale (Slatt, 2013). This further justifies the algal source for the Speake Ranch Woodford samples rather than higher vascular plant input that increased the relative C₂₉ sterane abundance. Araujo et al. (2018) suggested that C₂₃ tricyclic terpanes (C₂₃ TT) are often dominant in marine sourced oils while C₂₄ tetracyclic (C₂₄ Tet) and C₂₀ tricyclic (C₂₀ TT) terpane compounds are found to be more abundant in oils of terrigenous origin. The values of C₂₃ TT/C₂₄ Tet from the Woodford samples are consistently above one, justifying the predominance of marine input. It is also observed that lowering of the C₂₃ TT/C₂₄ Tet coincides with the oxic-suboxic interval indicated by Pr/Ph and C₂₇ diasterane/sterane ratios (Figure 38). However, approaching the Upper Woodford, values can be seen to slightly decrease, most likely as a consequence of the Devonian terrigenous land plant bloom and sea level fluctuation marking the Frasnian-Famennian boundary (Figure 38). Philp et al. (1992) have suggested that tricyclic terpanes were found in oils from a saline lacustrine environment in China, which reflects the function of tricyclic terpanes as salinity parameter. In

addition to a source input indicator, C₂₄ tetracyclic terpanes have been found to occur in highly saline depositional environments within evaporite-carbonate sequences (Connan et al., 1987). The preservation of organic matter in highly saline evaporitic environments is probably due to oxygen depleted waters accompanied by increased salinity and water stratification (Sammy, 1985). However, this does not align to the mudstone lithofacies nature of the Woodford shale, and it is unlikely that the abundance of C₂₄ tetracyclic terpane is associated with carbonate evaporitic environments.

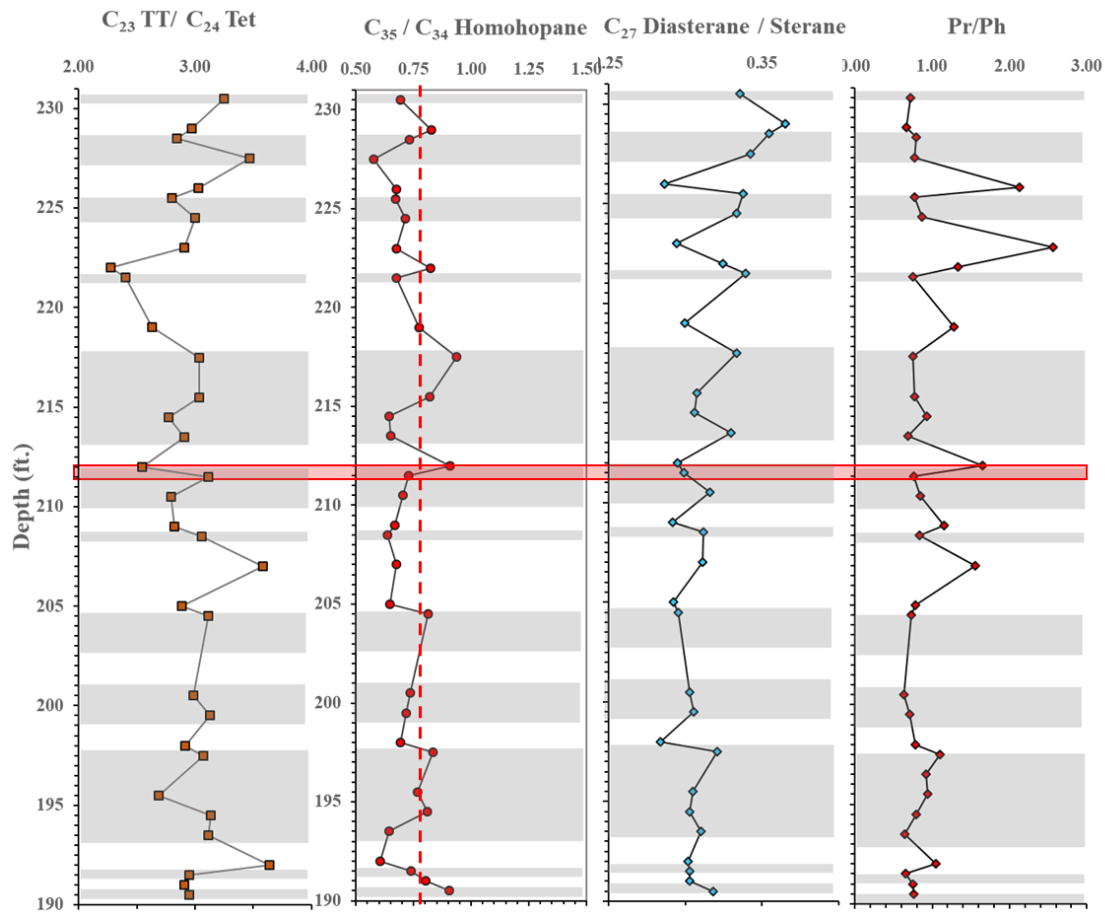


Figure 38. Depth logs of C₂₃ TT/C₂₄ Tet, C₃₅/C₃₄ homohopane, C₂₇ diasterane/sterane and Pr/Ph to correlate origin of organic source matter using terpane parameters and its correlation to anoxia. Highlighted interval show increase in C₂₃ TT/C₂₄ Tet of marine indication along with low values of C₃₅/C₃₄ Homohopane, C₂₇ diasterane/sterane and Pr/Ph parameters reflecting anoxic marine sediments.

3.6.4.2 Depositional Environments

The C₃₅ homohopane index [HHI = C₃₅/Σ(C₃₁- C₃₅) (22S +22R)] is a parameter to evaluate redox conditions especially in marine sediments during diagenesis (Moldowan et al., 1991). High HHI values which indicate relative dominance of C₃₅HH is referred to marine source deposited under anoxic conditions. Low HHI is often associated to prevailing sub-oxic to oxic environment, where preservation of organic matter is low. The Woodford Shale samples from the Speake Ranch have HHI values varying from 5-9% (Table 6). However, the utilization of C₃₅/C₃₄ HH [C₃₅/C₃₄ αβ(22S+22R) HH], in addition to HHI, can further discern and confirm anoxic conditions. The C₃₅/C₃₄ HH has been widely used as a redox indicator as well, due to its sensitivity to oxic conditions, as the C₃₅ HH values are elevated in reducing conditions (Peters et al., 2005). The side chain of the C₃₅ HH rapidly degrades when oxidized and therefore will make C₃₄ HH relatively higher in abundance (Tulipani et al., 2013). Higher C₃₅ homohopane values relative to C₃₁-C₃₅ homohopanes are often associated to marine carbonates or evaporites (Connan et al., 1987; ten Haven et al., 1988; Mello et al., 1988; Clark and Philp, 1989). Additionally, high C₃₅ HH is also a good indicator of highly reducing (low Eh) marine conditions (Peters and Moldowan, 1991). Therefore, the sensitivity of C₃₅/C₃₄ HH ratio to depositional environment and rock lithology makes it a helpful parameter used in this research.

The C₃₅/C₃₄ HH of Speake Ranch samples show values ranging from 0.58-0.91, and according to Peters and Moldowan (1993) and Bishop and Farrimond (1995) the values exceeding 0.8 is indicative of carbonate source rocks (Table 6; Figure 38). The C₃₅/C₃₄ HH can be used in tandem with C₂₉ Ts/C₃₀ diahopane to further identify source facies of Speake Ranch. The correlation between C₃₅/C₃₄ HH against C₂₉ Ts/C₃₀ diahopane is a reliable indicator of lithology, source facies, and level of oxicity. The rearranged hopanes 17α-diahopane (C₃₀ diahopane: C₃₀D)

and 18 α -30-norneohopane (C₂₉Ts) are sensitive to redox conditions (Peters et al., 2005). The oxygen content in the depositional environment can also be evaluated using C₂₉ Ts/C₃₀ D ratio. High values (>1) of C₂₉ Ts/C₃₀ D ratio show shale sediment deposition under oxidizing conditions (Peters and Moldowan, 1993; Peters et al., 2005). The Speake Ranch samples have very low values of the C₂₉ Ts/C₃₀ D ratio (0.07-0.1) in Figure 39. These values are observed to be marine shale deposited in anoxic environmental conditions.

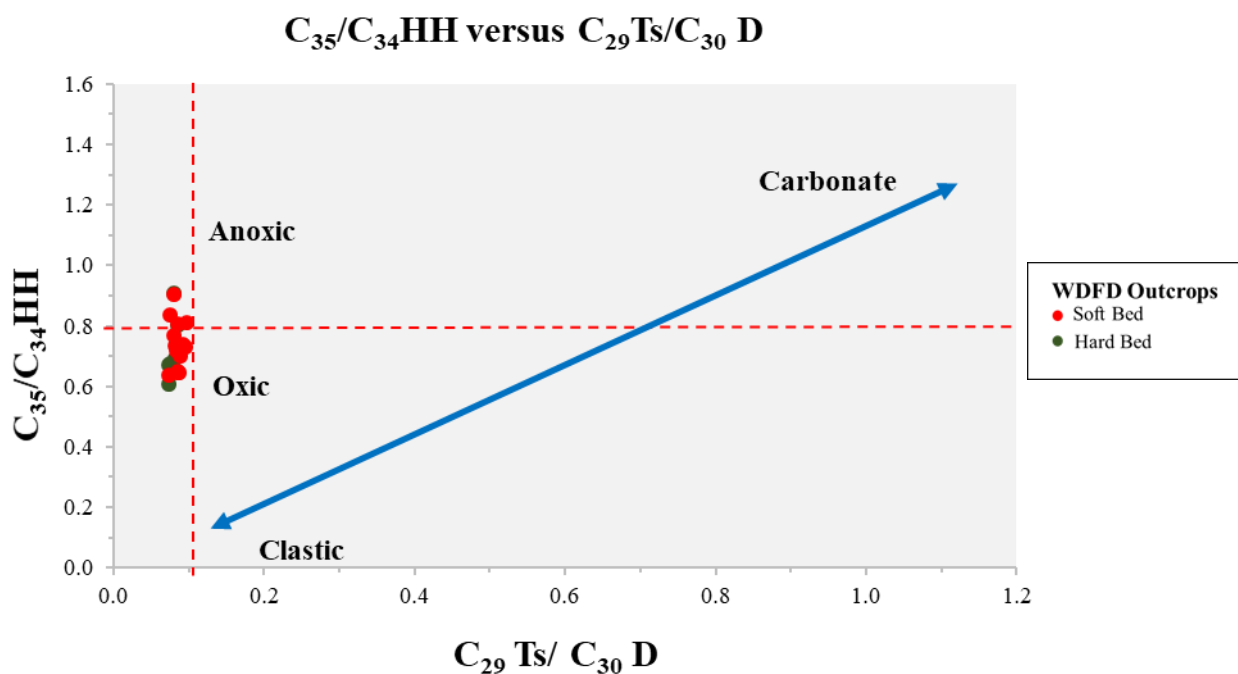


Figure 39. C₃₅/C₃₄ Homohopane vs. C₂₉ Ts/C₃₀ D plot to determine lithology and oxicity level of depositional environment. The Speake Ranch samples were largely deposited in anoxic environment with oxic to sub-oxic disturbances (Zumberge, 2000).

3.6.4.2.1 Ts and Tm

Ts (18 α -22,29,30-trisnorneohopane) and Tm (17 α -22,29,30-trisnorhopane) are a pair of C₂₇ hopanes that are commonly used to identify maturity and anoxia levels of the depositional environment (Waples and Machihara, 1990; El-Sabagh et al., 2018). This is a more reliable

parameter in relation to the sterane biomarkers, as the 20S/(20S+20R) sterane ratio remains in equilibrium after the peak oil generation window, while the Ts and Tm continue to change with increasing thermal maturity. Clear illustration of the consistency in maturity parameter C_{29} 20S/(20S+20R) in Figure 40, shows fluctuating values in Ts/Tm. Values of Ts/Tm in the Speake Ranch samples range from 0.2 to 0.38 in reflection to the immature sediments that are deposited in saline conditions. This agrees with the fact that the organic rich layers are mainly deposited under anoxic environmental conditions with intervals of oxic to sub-oxic that are frequent within such small intervals.

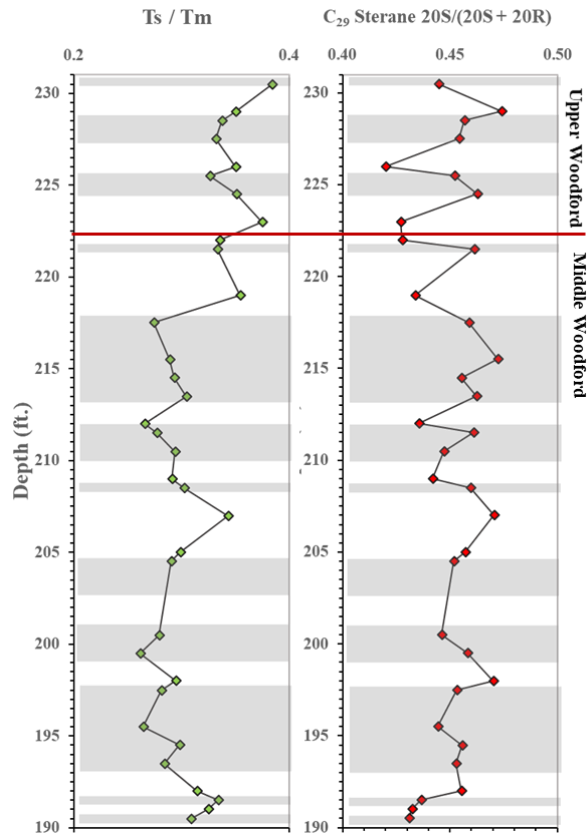


Figure 40. Geochemical logs to determine anoxia proxies (Ts/Tm) of Speake Ranch deposition, and if (at all) output values have been affected by thermal maturation determined using C_{29} sterane 20S/(20S+20R).

Gammacerane (**XI**; **Appendix III**) has been used to assess water column stratification and an aid to identify photic zone anoxia during sediment deposition. Gammacerane (**XI**) is proposed to be derived from tetrahymanol present in bacterivorous ciliates that thrive at the boundary of water salinity differences in the water column (Grantham et al., 1983). Torres (2020) suggested that higher proportions of gammacerane have been found at the base of the Lower Woodford, Middle Woodford, and Upper Woodford of Speake Ranch. This suggests that stratification and water column salinity played a significant role within the sequence transitions. The use of gammacerane index ($GI = G / (G + H)$) parameter has been helpful to determine water column stratification (Sinninghe Damste et al., 1995). The GI of the observed samples plot at values below 0.2 (marker for water salinity and stratification), where the Middle Woodford experienced a gentle decline and moved to a gradual increase within the Upper Woodford (Figure 41). This trend agrees with the discovery made by Torres (2020). The values from GI illustrates a range from 0.12-0.17, showing subtle changes in salinity levels. From the abundance of the gammacerane it appears that saline conditions and density driven water column stratification weakly persisted throughout deposition and periodically euxinia existed as indicated by the presence of aryl isoprenoids discussed below. In the Middle Woodford the depositional conditions were more restricted, possibly resembling a pseudo-lacustrine depositional environment later supported by tetracyclic polyprenoids to be discussed in the following sections. This relationship can be seen in some intervals within Figure 41. Increased water salinity attributes to density stratification and causes a reduction in oxygen content in bottom waters (lower Eh), consequently causing lower Pr/Ph values. A modified plot from Mello et al. (1988) shows that water column stratification does not necessarily covary with varying levels of anoxia (Figure 42). Connock (2015) found similar GI trends in the Woodford Shale from Wyche quarry, and suggested trend of GI is highly correlative

to the C₄₀ aromatic carotenoids (paleorenieratane and isorenieratane) where competition ensued between the potential source organism (bacterial ciliates) and the sulfur-oxidizing chemoautotrophic bacteria.

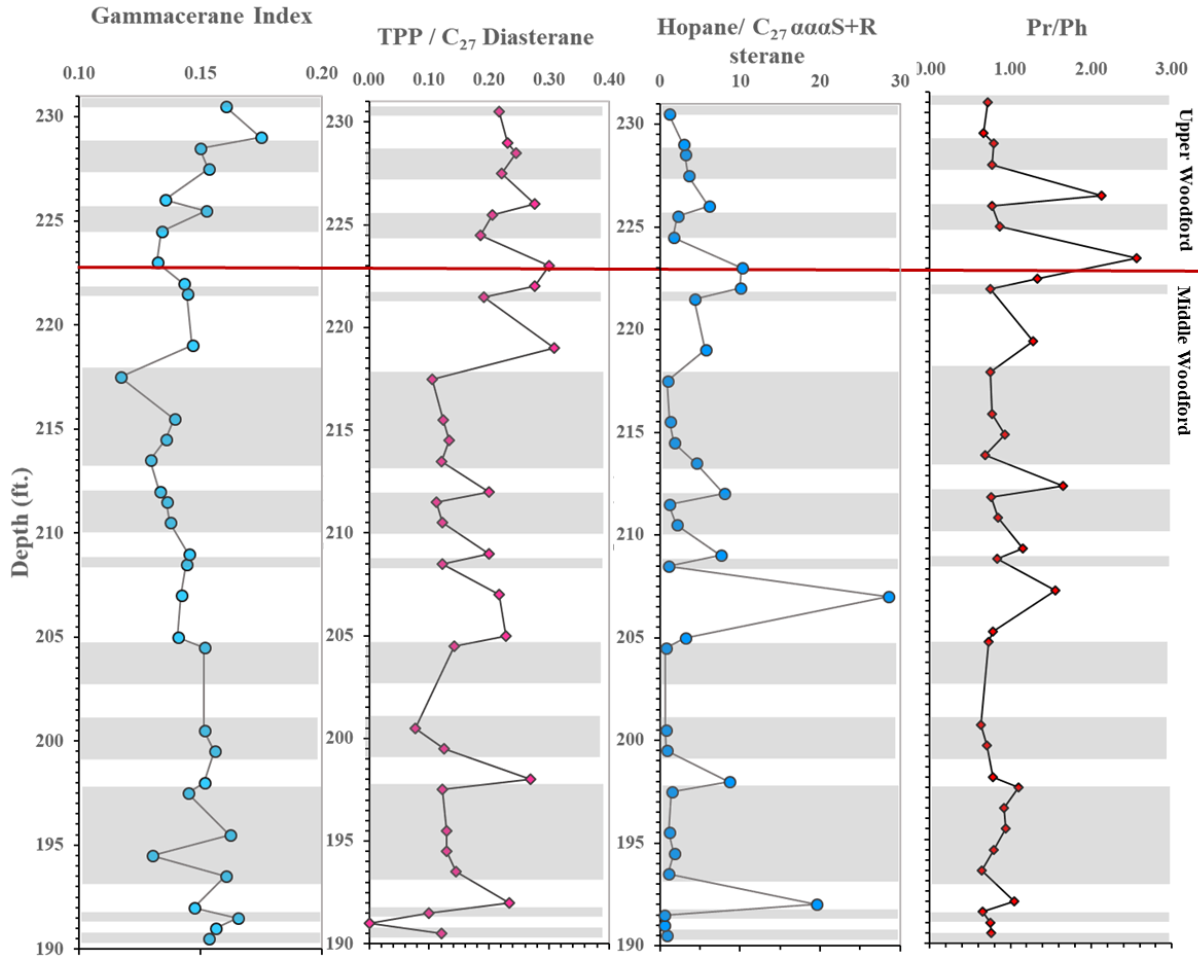


Figure 41. Depth plots for indication of water salinity, water column stratification, and anoxia. GI define the water column stratification, TPP/C₂₇Diasterane and Hopane/C₂₇aaaS+R sterane define the organic matter source, and Pr/Ph defines the water column anoxia. No correlation of the GI to Pr/Ph and organic matter source parameters can be determined.

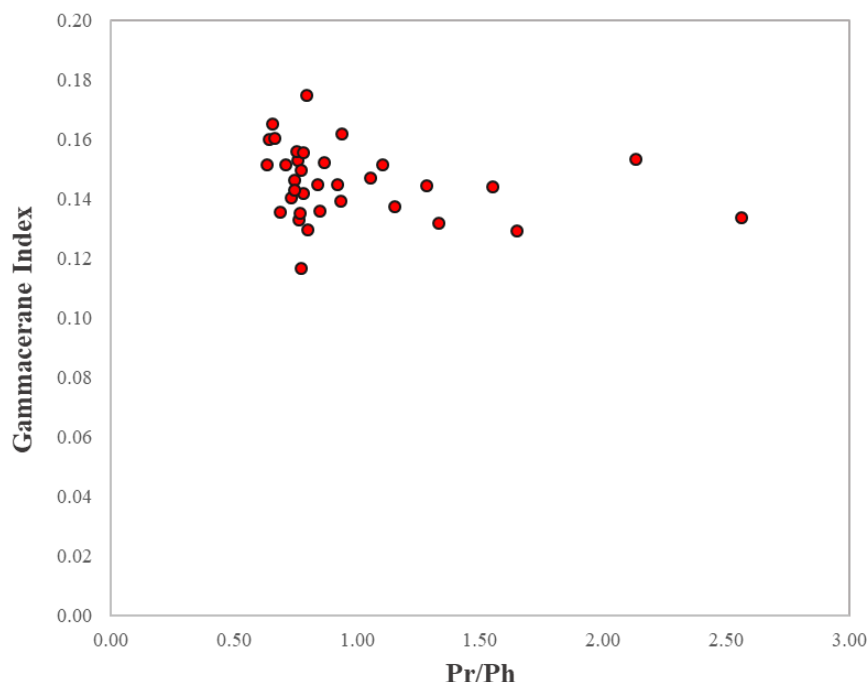


Figure 42. Plot of the relationship between Gammacerane Index and Pr/Ph of the Woodford Shale. There is no direct relationship between Pr/Ph and Gammacerane index, where heightened gammacerane values would yield lower Pr/Ph values (modified from Mello et al., 1988).

The $17\alpha,18\alpha,21\beta$ -28,30-bisnorhopane (**XII**) is one of the three C_{28} hopane stereoisomers first reported in the Monterey Shale by Seifert and Moldowan (1978). Banks et al. (1967) and Grantham et al. (1979) suggested that small concentrations of the 28,30-bisnorhopane (**XII**) in the extract of a pre-Devonian source rock were related to ferns. Therefore, its presence could provide an indication of vascular land plant input within the Speake Ranch samples. However, it was later discovered that 28,30-bisnorhopane (**XII**) may have also been derived from anaerobic bacteria in anoxic depositional environments (Katz, 1983). The latter study is more suitable for the application of this research. It is interpreted that a change in environment from restricted to marine conditions may strongly decrease sulfur oxidizing chemoautotrophic bacterial activity, which controls the abundance of bisnorhopane (Tornabene et al., 1979; Curiale and Odermatt, 1989). Therefore, the abundance of bisnorhopane is a direct reflection of the anoxia and sulfur concentrations within the

water column. Moreover, according to Hughes et al. (1995) the abundance of bisnorhopanes are direct results of sulfur rich environments, making it a possible tool to identify sulfur content for this 40ft interval of the Woodford Shale from Speake Ranch. Mackenzie et al. (1984) measured the bisnorhopane (XII) content relative to the 30-nor-17 α 21 β -hopane (XIII) defined by C₂₈ BNH/C₂₉ norhopane ratio to identify the anoxic levels of the depositional environment in which was used in the Draupne formation in North Sea by Dahl (2004). Additionally, Curiale and Odermatt (1989) also suggested that utilizing the bisnorhopane index (C₂₈ BNH/C₃₀ hopane) would be helpful to determine anoxic conditions. The transition from low or absent bisnorhopane content to higher C₂₈ BNH/C₂₉ norhopane ratios may be a reflection of a change from archipelago setting to a basin deepening setting of widespread marine conditions, just as found at the Draupne Formation in West Greenland (Mackenzie et al., 1984; Miller 1990; Rattey and Hayward, 1993; Dahl, 2004). It is found within Speake Ranch that the C₂₈ BNH/C₂₉ norhopane ratio varies considerably over the 40ft interval and additionally, bisnorhopane abundance covaries with the organic richness. As Curiale et al. (1985) indicated that high bisnorhopane abundance correlates with Pr/Ph. Similarly, the C₂₈ BNH/C₂₉ norhopane ratio of Speake Ranch does coincide with the trend of anoxia determined by the Pr/Ph from its negative correlation shown at 226ft (Upper Woodford), 223ft (Upper Woodford), and 207ft (Middle Woodford) (Figure 43). The majority of relatively lower C₂₈ BNH/C₂₉ norhopane values are found within the softer bed intervals (Table 6). Tornabene et al. (1979) determined from a study that the C₂₈ BNH/C₂₉ norhopane ratio does not co-vary with lithology nor the organic matter quality, but instead is associated with anoxia. A decreasing C₂₈ BNH/C₂₉ norhopane trend reflects the change from restricted to more general marine conditions causing termination or strong reduction of the sulfur oxidizing chemoautotrophic bacterial activity in the water column responsible for controlling the synthesis

of bisnorhopane (Tornabene et al., 1979). A later section within this chapter will discuss the correlation of anoxia as determined by bisnorhopane and Pr/Ph ratios to the amount of sulfur present in the water column determined by dibenzothiophenes.

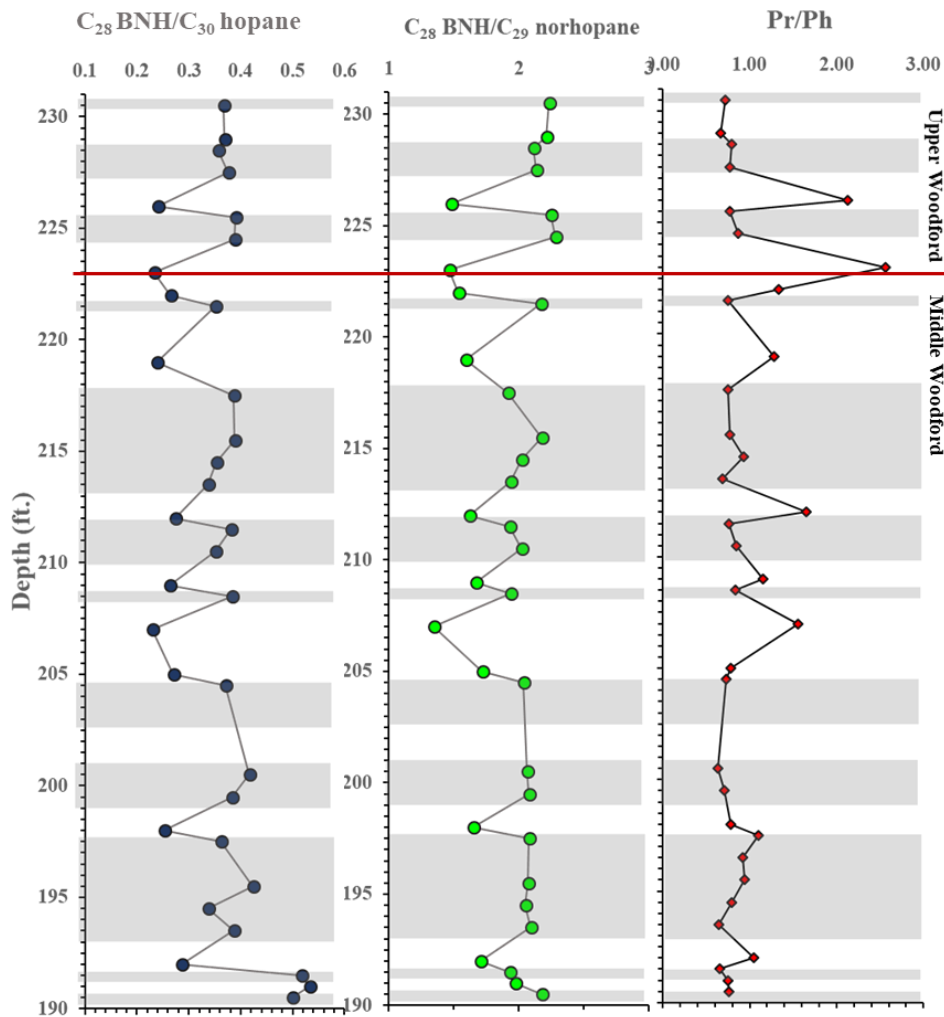


Figure 43. Speake Ranch anoxia proxies utilizing $C_{28} \text{BNH}/C_{30} \text{ hopane}$, $C_{28} \text{BNH}/C_{29} \text{ norhopane}$, and Pr/Ph to observe frequency of anoxia.

Sample	Depth (ft.)	Lithology	TOC (wt%)	Pr/Ph	C ₂₈ BNH/C ₃₀ Hopane	C ₂₈ BNH/Norhopane	C ₂₇ /C ₃₄ HH	HHI	Ts/Tm	C ₃₀ D/C ₂₉ Ts	DBT/PHEN
SR-190b	190.50	Soft	12.00	0.76	0.50	2.18	0.90	8.16	0.31	0.08	0.82
SR-191a	191.00	Hard	5.19	0.75	0.53	1.97	0.80	5.80	0.33	0.09	0.69
SR-191b	191.50	Soft	12.90	0.66	0.52	1.93	0.74	6.96	0.33	0.09	0.87
SR-192a	192.00	Hard	2.02	1.05	0.29	1.71	0.61	5.46	0.31	0.07	0.22
SR-193b	193.50	Soft	9.22	0.64	0.39	2.09	0.64	5.34	0.28	0.09	0.68
SR-194b	194.50	Soft	11.30	0.80	0.34	2.05	0.81	7.02	0.30	0.09	0.59
SR-195b	195.50	Soft	9.13	0.94	0.42	2.07	0.77	6.91	0.26	0.08	0.74
SR-196b	196.50	Soft	12.50	0.92	-	-	-	-	-	-	0.57
SR-197b	197.50	Soft	11.40	1.10	0.36	2.08	0.84	8.53	0.28	0.08	0.56
SR-198a	198.00	Hard	1.78	0.78	0.25	1.65	0.69	7.59	0.29	0.08	0.25
SR-199b	199.50	Soft	10.80	0.71	0.38	2.07	0.72	5.86	0.26	0.08	0.68
SR-200b	200.50	Soft	10.90	0.63	0.42	2.07	0.74	6.39	0.28	0.08	0.70
SR-202a	202.00	Hard	0.62	-	-	-	-	-	-	-	-
SR-203b	203.50	Soft	5.59	-	-	-	-	-	-	-	-
SR-204b	204.50	Soft	10.40	0.73	0.37	2.03	0.81	6.78	0.29	0.10	0.65
SR-205a	205.00	Hard	2.79	0.78	0.27	1.72	0.65	6.76	0.30	0.08	0.49
SR-207a	207.00	Hard	1.72	1.55	0.23	1.34	0.68	6.80	0.34	0.08	-
SR-208b	208.50	Soft	15.50	0.84	0.38	1.94	0.64	5.32	0.30	0.07	0.79
SR-209a	209.00	Hard	6.46	1.15	0.26	1.67	0.67	7.28	0.29	0.07	0.49
SR-210b	210.50	Soft	12.10	0.85	0.35	2.02	0.70	6.37	0.29	0.09	0.85
SR-211b	211.50	Soft	12.30	0.76	0.38	1.93	0.73	6.47	0.28	0.09	0.79
SR-212a	212.00	Hard	4.18	1.65	0.27	1.62	0.91	9.82	0.27	0.08	0.86
SR-213b	213.50	Soft	10.60	0.69	0.34	1.94	0.65	6.15	0.30	0.09	0.95
SR-214b	214.50	Soft	13.10	0.93	0.35	2.02	0.64	6.10	0.29	0.09	0.87
SR-215b	215.50	Soft	10.10	0.77	0.39	2.18	0.82	6.94	0.29	0.08	0.88
SR-217b	217.50	Soft	10.20	0.75	0.39	1.92	0.93	7.02	0.27	0.08	0.95
SR-218a	218.00	Hard	1.13	-	-	-	-	-	-	-	-
SR-219a	219.00	Hard	3.16	1.28	0.24	1.59	0.77	8.40	0.35	0.07	0.39
SR-221b	221.50	Soft	10.80	0.75	0.35	2.17	0.68	6.74	0.33	0.07	0.78
SR-222a	222.00	Hard	3.51	1.33	0.26	1.54	0.82	8.57	0.34	0.08	0.55
SR-223a	223.00	Hard	0.67	2.56	0.23	1.47	0.68	7.22	0.38	0.07	0.32
SR-224b	224.50	Soft	11.10	0.86	0.39	2.28	0.71	6.28	0.35	0.08	0.74
SR-225b	225.50	Soft	10.30	0.77	0.39	2.25	0.67	6.32	0.33	0.08	0.70
SR-226a	226.00	Hard	3.04	2.13	0.24	1.47	0.67	7.12	0.35	0.08	0.38
SR-227b	227.50	Soft	11.20	0.77	0.38	2.13	0.58	6.27	0.33	0.08	0.80
SR-228b	228.50	Soft	9.82	0.79	0.36	2.11	0.73	6.76	0.34	0.08	0.67
SR-229a	229.00	Hard	9.74	0.66	0.37	2.21	0.83	8.19	0.35	0.09	0.57
SR-230b	230.50	Soft	11.10	0.72	0.37	2.23	0.69	7.50	0.38	0.09	0.54

Table 6. Geochemical parameters defined to determine redox conditions of the Woodford Shale from Speake Ranch. Empty intervals are due to the lack of maltene from extraction.

3.6.5 *C₄₀ Aromatic carotenoids and aryl isoprenoid*

Anoxic conditions in marine environments are a product of a depleted supply of oxygen and a lack of water circulation at marine bottom waters due to temperature and density stratification (Koopmans et al., 1996). The zone of oxygen depletion is commonly termed as photic zone euxinia (PZE) which can extend from marine bottom waters into the photic zone as indicated by the presence of the green sulfur bacteria, *Chlorobiaceae*. The green sulfur bacteria is an anoxygenic photosynthetic bacteria that requires the photic zone to be in H₂S waters (Koopmans et al., 1996). According to Koopmans et al. (1996), *Chlorobiaceae* utilizes reverse tricarboxylic acid cycle to fix CO₂. The presence of PZE can be determined by the abundance of C₄₀ diaromatic carotenoids (Grice et al., 1996). The paleorenieratane (**XIV**), isorenieratane (**XV**), and renieratane (**XVI**) are derivatives of the C₄₀ diaromatic carotenoids detected at the mass fragmentogram m/z 133-134 (Figure 44; Table 7). Isorenieratane (**XIX**), a diaromatic carotenoid diagenetic and catagenetic product, correlates with a distinct enrichment in δ¹³C. This provides for the initial evidence of the applicability of isorenieratane and its derivatives, such as aryl isoprenoids, for the implication of photic zone euxinia, which will be utilized in this study. Percival et al. (2019) found that there is a positive correlation between TOC and δ¹³C. Furthermore, samples from Dongcun and Yangdi in China have shown that the δ¹³C closely tracks with oxygenation levels, where the values are at a maximum at the lowering of oxygenation (Joachimski et al., 2002). The paleorenieratane (**XIV**) and the isorenieratane (**XV**) are present at higher concentrations in the Woodford Samples from Speake Ranch (Figure 44). A consistent proportion of higher paleorenieratane to the isorenieratane are consistent throughout the Speake Ranch section despite the lithofacies variations. The proportions of the C₄₀ carotenoid paleorenieratane/isorenierane were plotted against Pr/Ph (Figure 45). This ratio serves as evidence that the carotenoids are affected with varying levels of anoxia. All of the soft bed lithofacies plot in the reducing area, while the

hard beds (yellow symbol) vary within areas defining oxidizing and reducing conditions. Due to data limitation only 13 Speake Ranch samples were able to be observed.

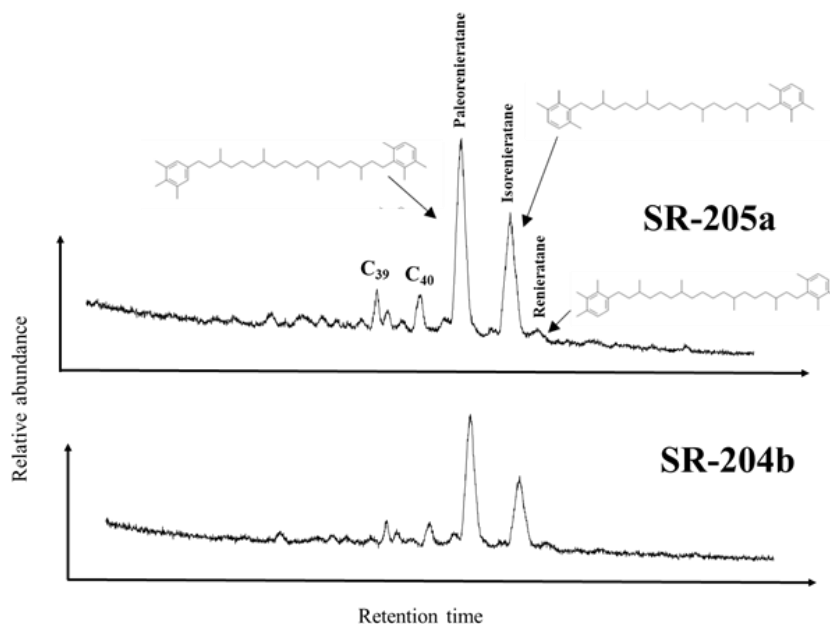


Figure 44. Identification of the C₄₀ carotenoids screened at summed m/z 133+134 at depth 204.5ft within the Middle Woodford. Top chromatogram is at depth 205ft from the soft bed, and bottom chromatogram is at depth 204.5ft from the hard bed.

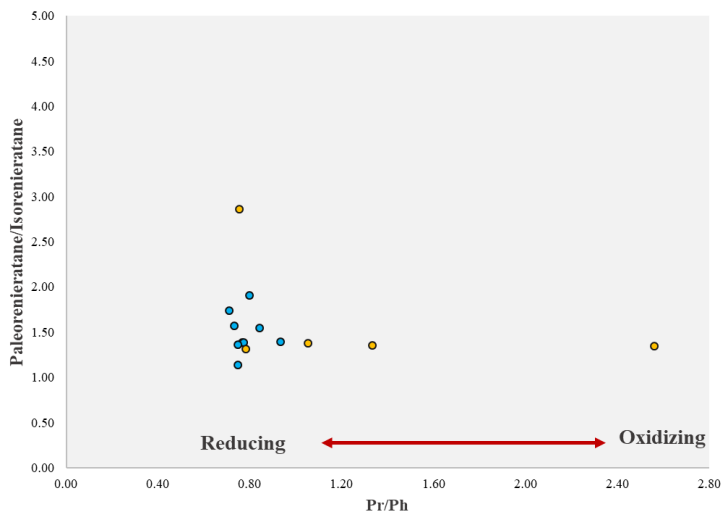


Figure 45. Paleorenieratane/Isorenieratane ratio vs. Pr/Ph ratio illustrating a mainly reducing condition of the Speake Ranch samples defined by the concentration and distribution of carotenoids. However, hard beds (yellow symbols) are seen to vary within areas of oxidation and anoxia.

Aryl isoprenoids are the diagenetic products of aromatic carotenoids, whose formation result from the cleavage of the isorenieratane chain. Koopmans et al. (1996) has stated that there is a broad range of diagenetic and catagenetic derivatives of the diaromatic carotenoid isorenieratane, a pigment of *Chlorobiaceae* found in sedimentary rocks. These aryl isoprenoids are comprised of C₄₀, C₃₃, C₃₂, diaryl isoprenoids, and short-chain aryl isoprenoids. The compounds of interest in addition to paleorenieratanes and isorenieratanes, are the aryl isoprenoids, which are extremely useful in evaluating variability in the persistence of PZE. Distribution of the aryl isoprenoids are found in the mass fragmentogram m/133-134 (Figure 46; Table 7). The assessment of PZE is done through the calculation of the short-chain C₁₃-C₁₇ of the 2,3,6-trimethylated aryl isoprenoids (2,3,6-TMB) (XVII) substitution proportion in relation to the intermediate chain aryl isoprenoid, C₁₈-C₂₂ 2,3,6-trimethylated aryl isoprenoids (3,4,5-TMB) (XVII), to obtain the aryl isoprenoid ratio (AIR). The AIR is helpful to determine the relative amounts of aryl isoprenoids from *Chlorobiaceae* indicated by lower values, whereas higher values will indicate cyanobacteria input (Schwark and Frimmel, 2004). It is known that if there is more of an abundance of the short chain components it is an indication of a more intense aerobic degradation of aryl isoprenoids (Schwark and Frimmel, 2004).

Development of PZE which is the enhancement of anoxia and sulfide within the photic zone of the water column, is additional support to indicate restriction within the basin that may have been caused by early erosional events of the pre-Woodford. Schwark and Frimmel (2004) suggested that the development of a low AIR coupled with low Pr/Ph values within the samples is suggestive of more persistent PZE conditions, while high values of AIR (>3) and Pr/Ph (>1) values indicate short termed episodic PZE. Schwark and Frimmel (2004) concluded that AIRs are never below 0.5 indicating that PZE has always been episodic. The Woodford Shale has shown values

ranging from 0.34-1.18, indicating variable episodic PZE (Figure 47). Additionally, not much variation can be seen within the boundary separating the Middle Woodford and Upper Woodford at Speake Ranch. A distinctive fluctuation is found between 210-220ft which may indicate unstable PZE and may be a time marker of F-F coinciding with the Pr/Ph depth plot.

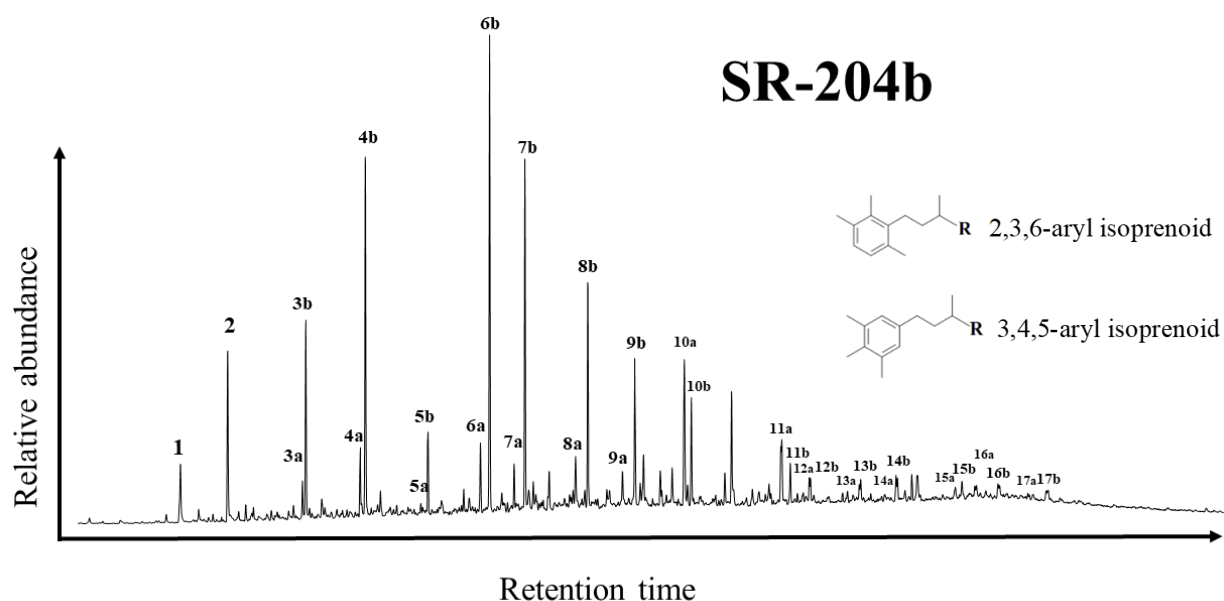


Figure 46. GC-MS chromatogram showing the distribution of aryl isoprenoids in the aromatic fraction at the summed m/z 133+134. 2,3,6-TMB aryl isoprenoids (**XXII**) are indicated by the letter b, and the 3,4,5-TMB (**XXIII**) are indicated by the letter a.

Peak No.	Compound	Peak No.	Compound
1	C ₁₃ TMB	10a	C ₂₂ 3,4,5 TMB
2	C ₁₄ TMB	10b	C ₂₂ 2,3,6 TMB
3a	C ₁₅ 3,4,5 TMB	11a	C ₂₄ 3,4,5 TMB
3b	C ₁₅ 2,3,6 TMB	11b	C ₂₄ 2,3,6 TMB
4a	C ₁₆ 3,4,5 TMB	12a	C ₂₅ 3,4,5 TMB
4b	C ₁₆ 2,3,6 TMB	12b	C ₂₅ 2,3,6 TMB
5a	C ₁₇ 3,4,5 TMB	13a	C ₂₆ 3,4,5 TMB
5b	C ₁₇ 2,3,6 TMB	13b	C ₂₆ 2,3,6 TMB
6a	C ₁₈ 3,4,5 TMB	14a	C ₂₇ 3,4,5 TMB
6b	C ₁₈ 2,3,6 TMB	14b	C ₂₇ 2,3,6 TMB
7a	C ₁₉ 3,4,5 TMB	15a	C ₂₉ 3,4,5 TMB
7b	C ₁₉ 2,3,6 TMB	15b	C ₂₉ 2,3,6 TMB
8a	C ₂₀ 3,4,5 TMB	16a	C ₃₀ 3,4,5 TMB
8b	C ₂₀ 2,3,6 TMB	16b	C ₃₀ 2,3,6 TMB
9a	C ₂₁ 3,4,5 TMB	17a	C ₃₁ 3,4,5 TMB
9b	C ₂₁ 2,3,6 TMB	17b	C ₃₁ 2,3,6 TMB

Table 7. Peak Identification for the 2,3,6- and 3,4,5 trimethyl substitution for the aryl isoprenoid chromatogram at m/z 133-134 in Figure 48.

The distribution and variability of aryl isoprenoid composition is mainly affected by the primary environmental conditions during sediment deposition, burial, as well as diagenesis (Schwark and Frimmel, 2004). This in turn can also reflect the productivity of *Chlorobiaceae*, which could be explained by the extent of anoxia that intruded through the photic zone or to the availability of nutrients (Schwark and Frimmel, 2004). The concentration of *Chlorobiaceae* biomass found in sediment is mainly controlled by the persistence of PZE over a time interval, which is controlled by the “stability of water-column” driven by climate (Schwark and Frimmel, 2004). They also concluded that the high surface productivity and the decomposition of organisms via sulfate-reducing bacteria within the sediments as well as anoxia bottom waters during deposition would lead to an expansion of the euxinic zone.

The C₁₈ aryl isoprenoid ratio was calculated from the proportions of the C₁₈ 2,3,6-trimethyl aryl isoprenoid (XVII) to the C₁₈ 3,4,5-trimethyl substitution (XVIII) to determine redox

conditions of the depositional environment. Relatively low values of C₁₈ AIR plotting below 10 (Figure 47) coincide with low Pr/Ph ratios indicating anoxic waters and presence of H₂S, later confirmed by tetracyclic polyprenoids as well. The instability of C₁₈ aryl isoprenoid ratio parameters is also monitored in the same interval where this behavior is found in the Pr/Ph and AIR (2,3,6/3,4,5-trimethyl-substituted aryl isoprenoid; Formulas can be found in Appendix III). In summary, the Upper and Middle Woodford members from Speake Ranch show evidence for bottom water anoxia including periods of oxic to sub-oxic as indicated by Pr/Ph values, and periodic photic zone euxinia as indicated by the aryl isoprenoid ratio.

Sample	Depth (ft.)	Lithology	TOC (wt%)	Pr/Ph	AIR	C ₁₈ -Aryl Isoprenoid	Gammacerane Index	C ₃₅ /C ₃₄ HH	HHI
SR-190b	190.50	Soft	12.00	0.76	0.84	4.04	0.15	0.90	0.08
SR-191a	191.00	Hard	5.19	0.75	0.75	5.17	0.16	0.80	0.45
SR-191b	191.50	Soft	12.90	0.66	1.12	10.96	0.17	0.74	0.07
SR-192a	192.00	Hard	2.02	1.05	1.15	0.72	0.15	0.61	0.38
SR-193b	193.50	Soft	9.22	0.64	0.83	6.94	0.16	0.64	0.05
SR-194b	194.50	Soft	11.30	0.80	0.60	5.16	0.13	0.81	0.07
SR-195b	195.50	Soft	9.13	0.94	0.62	4.24	0.16	0.77	0.07
SR-196b	196.50	Soft	12.50	0.92	0.56	6.49	-	-	-
SR-197b	197.50	Soft	11.40	1.10	0.57	3.67	0.14	0.84	0.09
SR-198a	198.00	Hard	1.78	0.78	0.52	8.70	0.15	0.69	0.08
SR-199b	199.50	Soft	10.80	0.71	0.72	4.34	0.16	0.72	0.06
SR-200b	200.50	Soft	10.90	0.63	0.78	8.27	0.15	0.74	0.06
SR-204b	204.50	Soft	10.40	0.73	0.68	4.41	0.15	0.81	0.07
SR-205a	205.00	Hard	2.79	0.78	0.59	5.39	0.14	0.65	0.07
SR-207a	207.00	Hard	1.72	1.55	0.34	4.23	0.14	0.68	0.07
SR-208b	208.50	Soft	15.50	0.84	0.83	5.47	0.14	0.64	0.05
SR-209a	209.00	Hard	6.46	1.15	0.85	9.05	0.14	0.67	0.07
SR-210b	210.50	Soft	12.10	0.85	0.95	6.20	0.14	0.70	0.06
SR-211b	211.50	Soft	12.30	0.76	1.55	6.90	0.14	0.73	0.06
SR-212a	212.00	Hard	4.18	1.65	0.34	7.62	0.13	0.91	0.10
SR-213b	213.50	Soft	10.60	0.69	1.06	6.73	0.13	0.65	0.06
SR-214b	214.50	Soft	13.10	0.93	0.56	4.73	0.14	0.64	0.06
SR-215b	215.50	Soft	10.10	0.77	0.78	7.98	0.14	0.82	0.07
SR-217b	217.50	Soft	10.20	0.75	1.26	9.79	0.12	0.93	0.07
SR-219a	219.00	Hard	3.16	1.28	0.17	6.88	0.15	0.77	0.08
SR-221b	221.50	Soft	10.80	0.75	0.62	8.41	0.14	0.68	0.07
SR-222a	222.00	Hard	3.51	1.33	0.46	12.73	0.14	0.82	0.09
SR-223a	223.00	Hard	0.67	2.56	0.40	4.76	0.13	0.68	0.07
SR-224b	224.50	Soft	11.10	0.86	-	-	0.13	0.71	0.06
SR-225b	225.50	Soft	10.30	0.77	0.75	4.91	0.15	0.67	0.06
SR-226a	226.00	Hard	3.04	2.13	0.67	11.54	0.14	0.67	0.07
SR-227b	227.50	Soft	11.20	0.77	0.72	9.27	0.15	0.58	0.06
SR-228b	228.50	Soft	9.82	0.79	0.79	10.75	0.15	0.73	0.07
SR-229a	229.00	Hard	9.74	0.66	0.62	6.93	0.17	0.83	0.08
SR-230b	230.50	Soft	11.10	0.72	1.18	8.41	0.16	0.69	0.08

Table 8. Biomarker proxies for water structure and chemistry in the Woodford Shale at Speake Ranch. Pr/Ph, HHI, and C₃₅/C₃₄ HH indicating the redox state of the Woodford paleoenvironment, AIR and C₁₈ Aryl Isoprenoid signify the H₂S presence within the photic zone as well as the stability of the PZA, and the C₂₇/C₂₉ steranes used as a correlation to the effects of the organic matter input source.

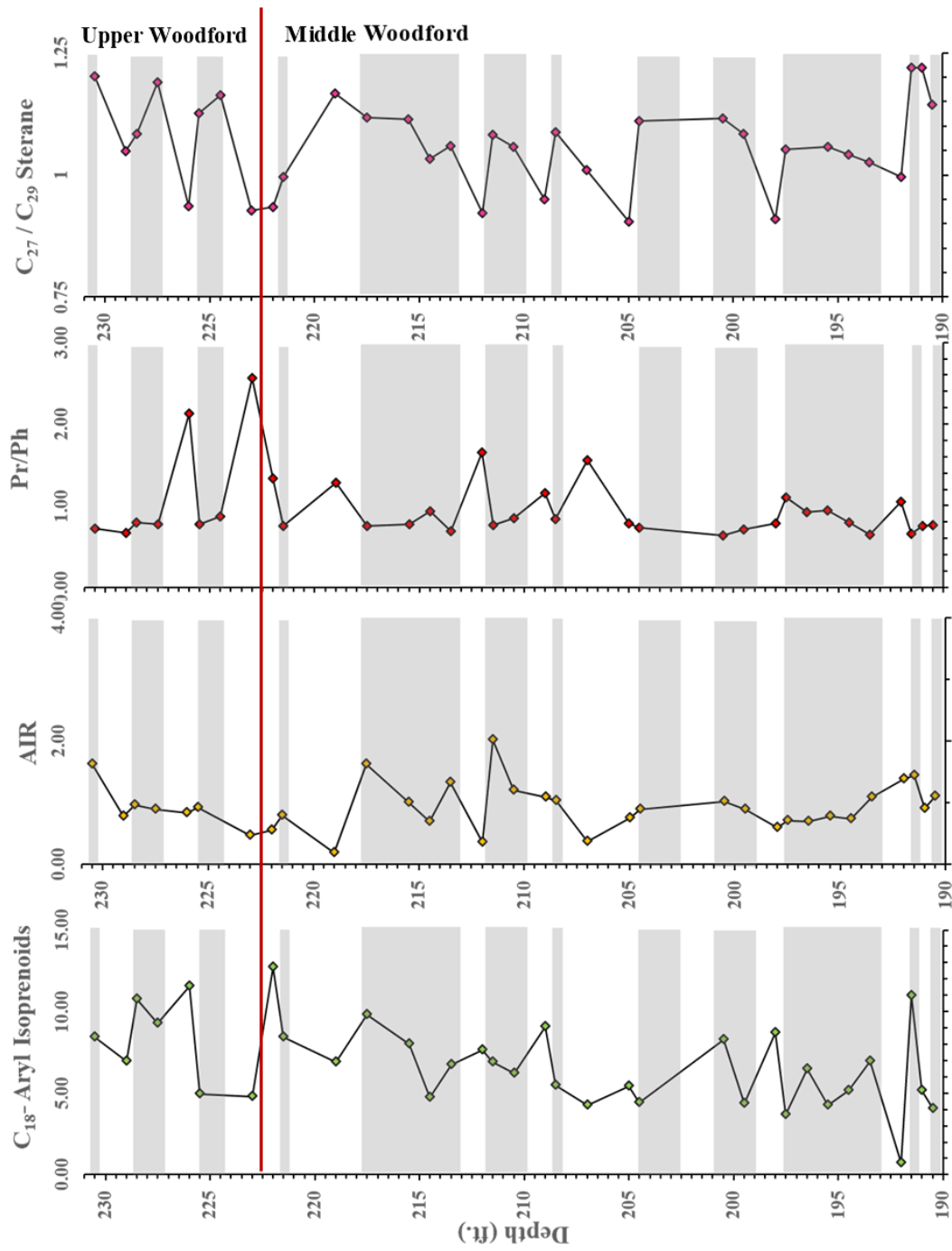


Figure 47. Depth plots of biomarker parameters as indicator for water structure and chemistry in the Woodford Shale at Speake Ranch. Pr/Ph indicating the redox state of the Woodford paleoenvironment, AIR and C₁₈ Aryl Isoprenoid signify the H₂S presence within the photic zone as well as the stability of the PZA, and the C₂₇/C₂₉ used as a correlation to the effects of the organic matter input source.

3.6.6 Tetracyclic Polyrenoids

The C₃₀ tetracyclic polyrenoids (**XIX**) which are detected by GC-MS using the ions at m/z 191 and m/z 259 are highly specific indicators of brackish lacustrine environment and freshwater algae (Holba et al., 2003). They are represented by two peaks that signify the 21S and 21R isomers, suggested to be derived from green algae (*Chlorophyta*) (Figure 48; Li et al., 1996; Poinot et al., 1997; Holba et al., 2003; Araujo et al., 2018). Not only do their abundances indicate lacustrine environment dominance over marine environment, but they also indicate a predominance of fresh-water algal precursor or preferential preservation of saturate hydrocarbons within non-marine conditions (Holba et al., 2000; Araujo et al., 2018). When tetracyclic polyrenoids (TTP) (**XIX**) are correlated with tricyclic terpane ratios [C_{26}/C_{25} TT = C_{26} 13 β ,14 α -tricyclic terpane)/(C₂₅ 13 β ,14 α -tricyclic terpane)] the distinction between marine or lacustrine source rock organic matter is enhanced (Holba et al., 2000). Furthermore, abundance of the pentacyclic terpanes, C₃₀ 17 α ,21 β -hopane (C₃₀ H) identify the significant presence of microbially reworked organisms (Mello et al., 1988; Araujo et al., 2018). The combination of C₂₆/C₂₅ tricyclic terpane (C₂₆/C₂₅ TT), C₃₀ tetracyclic polyrenoid/C₂₇ diasterane (TPP/C₂₇ diasteranes), and, Hopane/C₂₇ $\alpha\alpha\alpha$ (S+R) sterane ratios provide a stronger correlation platform to identify lacustrine vs. marine paleoenvironments. If values are high enough to indicate lacustrine environment, then these parameters may indicate that the marine environment had become so restricted it became pseudo lacustrine. TPP/C₂₇ diasteranes values are well below 0.4, illustrating a marine depositional environment (Casilli et al., 2014; Araujo and Azevedo, 2016). Additionally, based on Figure 49, harder beds tend to illustrate higher TPP C₃₀ values relative to the C₂₇ diasteranes. According to Zumberge et al. (1987), Mello et al. (1988), Casilli et al. (2014), and Araujo et al. (2018) values of high Hopane/C₂₇ $\alpha\alpha\alpha$ (S+R) sterane (>5), high C₂₆/C₂₅ TT (>1) and high TPP/C₂₇ diasterane (>1) are associated with a lacustrine environment, which were found in crude oils from Espirito Santo

Basin, Brazil. While, low Hopane/C₂₇ $\alpha\alpha\alpha$ (S+R) sterane (0.58-3.70), low C₂₆ TT/C₂₅ TT (0.78-0.85) and low TPP/C₂₇ diasterane (0.07-0.24) reflect a marine environment. The values of Speake Ranch samples illustrated in Figure 49 and Table 9 clearly depict that these observed samples have low Hopane/C₂₇ $\alpha\alpha\alpha$ (S+R)sterane with some intervals plotting above 10. TPP/C₂₇ diasteranes ratios range from 0.1 to 3, showing low, but largely varying values. Additionally, the C₂₆/C₂₅ TT have values that are commonly invariant around 1. The highlighted intervals in Figure 49 show that relatively higher Hopane/C₂₇ $\alpha\alpha\alpha$ (S+R) sterane and TPP/C₂₇ diasteranes illustrate the pseudo lacustrine environment. Red highlighted zones are those increased parameters within the Middle Woodford, and the yellow highlighted interval indicates elevated parameter values within the Upper Woodford. In summary, data show that lowest TOC values coincide with all the combined effects of oxicity and no specificity of water stratification, while elevated TOC values can be found to associate with the highest indication of anoxia and elevated gammacerane values.

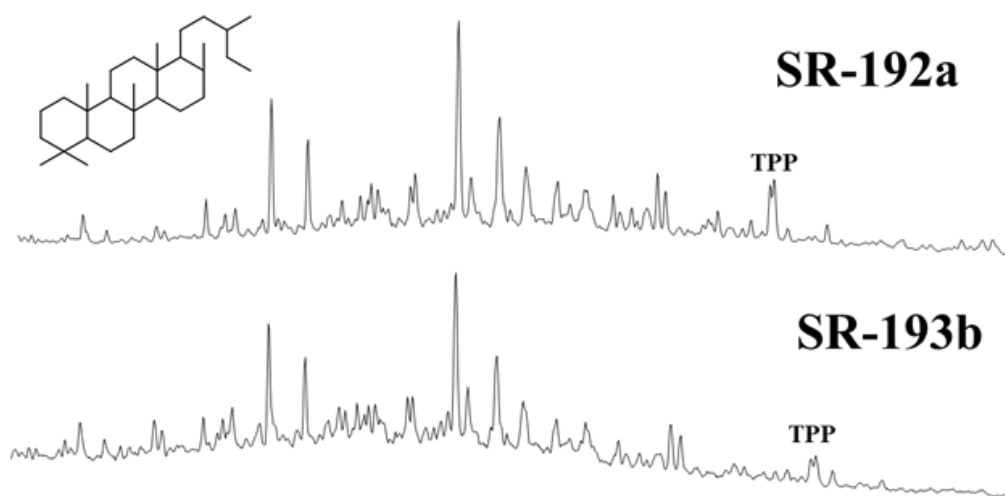


Figure 48. Fragmentogram of C₃₀ tetracyclic polyprenoid (XII) on mass spectra 259. SR-192a is a hard bed at depth 192 ft, and SR-193b is a soft bed at 193.5 ft.

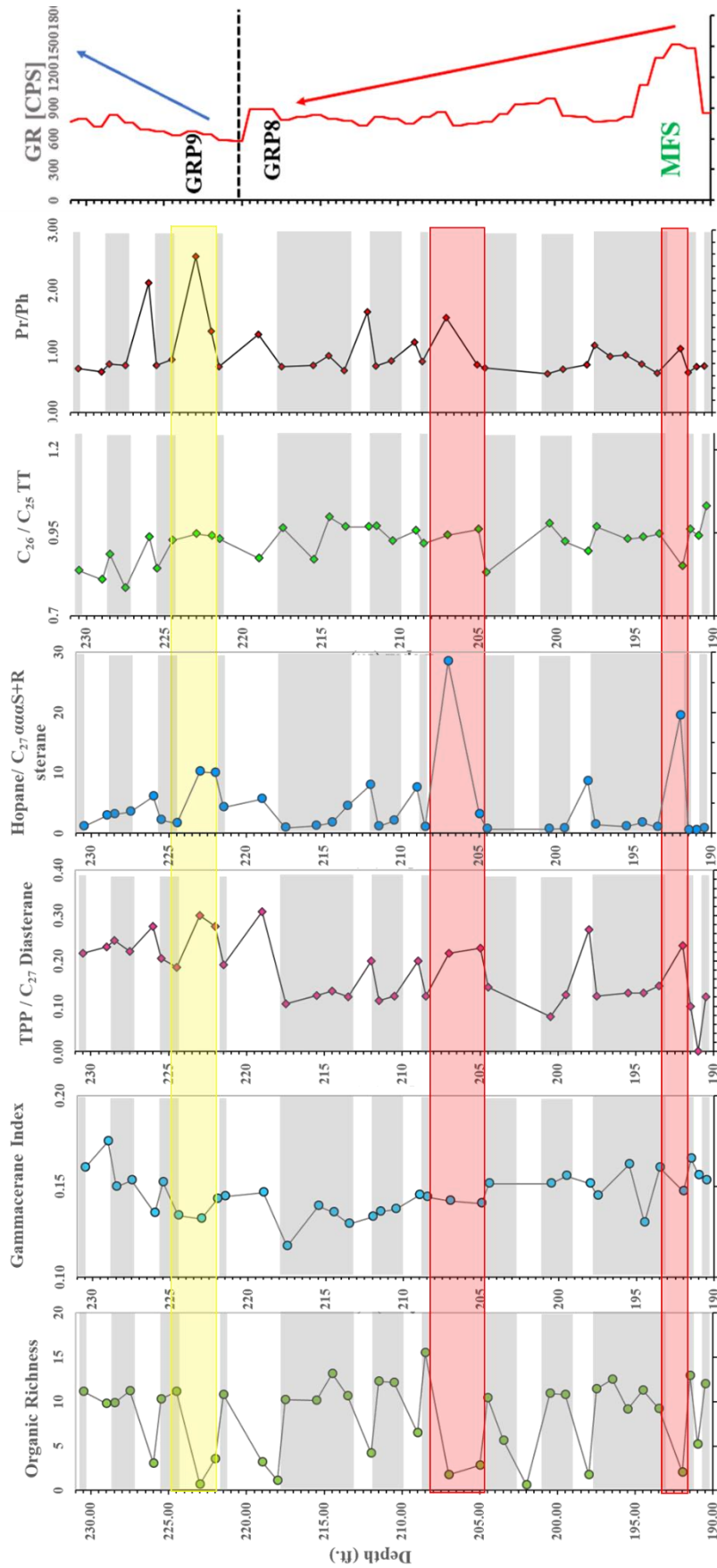


Figure 49. Variation in the TPP screened at m/z 259 along with its correlation to gammacerane Index, C_{30} Hopane/ C_{27} $\alpha\alpha\alpha$ S+R sterane, C_{26} TT/ C_{25} Ts/Tm to determine intervals that illustrate the level of restriction in the water column of the Woodford depositional environment. Highlighted intervals indicate intervals when the environment of deposition for the Woodford Shale at Speake ranch was highly restricted.

Sample	Depth (ft.)	Lithology	TOC (wt%)	Pr/Ph	TPP/C ₂₇ Diasterane	C ₃₀ H/C ₇ αααS+R	C ₂₆ /C ₂₅ TT	GI	DBT/PHEN
SR-190b	190.50	Soft	12.00	0.76	0.12	0.71	1.03	0.15	0.82
SR-191a	191.00	Hard	5.19	0.75	-	0.47	0.94	0.16	0.69
SR-191b	191.50	Soft	12.90	0.66	0.10	0.48	0.96	0.17	0.87
SR-192a	192.00	Hard	2.02	1.05	0.23	19.48	0.85	0.15	0.22
SR-193b	193.50	Soft	9.22	0.64	0.14	0.91	0.95	0.16	0.68
SR-194b	194.50	Soft	11.30	0.80	0.13	1.72	0.94	0.13	0.59
SR-195b	195.50	Soft	9.13	0.94	0.13	1.11	0.93	0.16	0.74
SR-196b	196.50	Soft	12.50	0.92	-	-	-	-	0.57
SR-197b	197.50	Soft	11.40	1.10	0.12	1.34	0.97	0.14	0.56
SR-198a	198.00	Hard	1.78	0.78	0.27	8.60	0.89	0.15	0.25
SR-199b	199.50	Soft	10.80	0.71	0.12	0.75	0.92	0.16	0.68
SR-200b	200.50	Soft	10.90	0.63	0.08	0.61	0.98	0.15	0.70
SR-202a	202.00	Hard	0.62	-	-	-	-	-	-
SR-203b	203.50	Soft	5.59	-	-	-	-	-	-
SR-204b	204.50	Soft	10.40	0.73	0.14	0.60	0.83	0.15	0.65
SR-205a	205.00	Hard	2.79	0.78	0.23	3.04	0.96	0.14	0.49
SR-207a	207.00	Hard	1.72	1.55	0.22	28.45	0.94	0.14	-
SR-208b	208.50	Soft	15.50	0.84	0.12	0.92	0.92	0.14	0.79
SR-209a	209.00	Hard	6.46	1.15	0.20	7.50	0.96	0.14	0.49
SR-210b	210.50	Soft	12.10	0.85	0.12	2.06	0.92	0.14	0.85
SR-211b	211.50	Soft	12.30	0.76	0.11	1.03	0.97	0.14	0.79
SR-212a	212.00	Hard	4.18	1.65	0.20	7.99	0.97	0.13	0.86
SR-213b	213.50	Soft	10.60	0.69	0.12	4.45	0.97	0.13	0.95
SR-214b	214.50	Soft	13.10	0.93	0.13	1.73	1.00	0.14	0.87
SR-215b	215.50	Soft	10.10	0.77	0.12	1.16	0.87	0.14	0.88
SR-217b	217.50	Soft	10.20	0.75	0.11	0.87	0.96	0.12	0.95
SR-218a	218.00	Hard	1.13	-	-	-	-	-	-
SR-219a	219.00	Hard	3.16	1.28	0.31	5.64	0.87	0.15	0.39
SR-221b	221.50	Soft	10.80	0.75	0.19	4.21	0.93	0.14	0.78
SR-222a	222.00	Hard	3.51	1.33	0.28	9.99	0.94	0.14	0.55
SR-223a	223.00	Hard	0.67	2.56	0.30	10.20	0.95	0.13	0.32
SR-224b	224.50	Soft	11.10	0.86	0.19	1.61	0.93	0.13	0.74
SR-225b	225.50	Soft	10.30	0.77	0.21	2.14	0.84	0.15	0.70
SR-226a	226.00	Hard	3.04	2.13	0.28	6.04	0.94	0.14	0.38
SR-227b	227.50	Soft	11.20	0.77	0.22	3.46	0.78	0.15	0.80
SR-228b	228.50	Soft	9.82	0.79	0.24	3.05	0.88	0.15	0.67
SR-229a	229.00	Hard	9.74	0.66	0.23	2.88	0.81	0.17	0.57
SR-230b	230.50	Soft	11.10	0.72	0.22	1.07	0.84	0.16	0.54

Table 9. Variation in the TPP screened at m/z 259 along with its correlation to gammacerane Index, C₃₀Hopane / C₂₇ Sterane αααS + αααS, C₂₆ TT/ C₂₅, Ts/Tm to determine intervals that illustrate the level of restriction in the water column of the Woodford depositional environment. DBT/Phen is used to determine the availability of H₂S in the anoxic water column.

3.6.7 Dibenzothiophene and phenanthrene

Dibenzothiophenes (**XX**) are important sulfur-containing aromatic compounds with two benzene rings connected to a central thiophene ring (Figure 50; Li et al., 2012). This compound is thought to be derived from a thermal reaction between sulfur and the organic matter contained within the sediment producing dibenzothiophene (**XX**). The dibenzothiophene/phenanthrene (DBT/Phen) ratio is often used to assess the presence and abundance of reduced sulfur within the organic matter, primarily hydrogen sulfide (H_2S) and polysulfides (H_2Sn) (Hughes et al., 1995). This is a helpful parameter to indicate anoxia within the depositional environment as sediments must be anoxic for the accumulation of reactive sulfur (Hughes et al., 1995). Dibenzothiophenes are monitored on the GC-MS of the aromatic fraction at m/z 184, 198, and 212 (Figure 50), while the phenanthrenes (**XXI**) are observed at m/z 178, 192, 206 as shown in Figure 51.

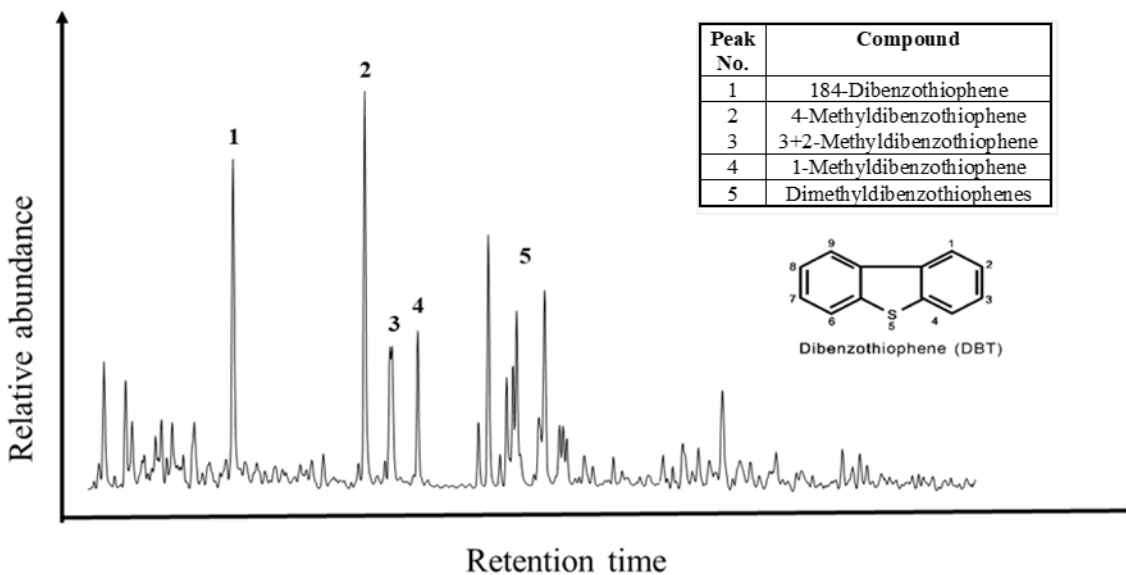


Figure 50. GC-MS chromatogram monitored for the variation in the dibenzothiophenes (**XVI**) at m/z 184+198+212. The m/z 184 is used to identify the dibenzothiophene, m/z 198 is used to identify the methyl dibenzothiophene, and m/z 212 is used to identify the dimethyl dibenzothiophene.

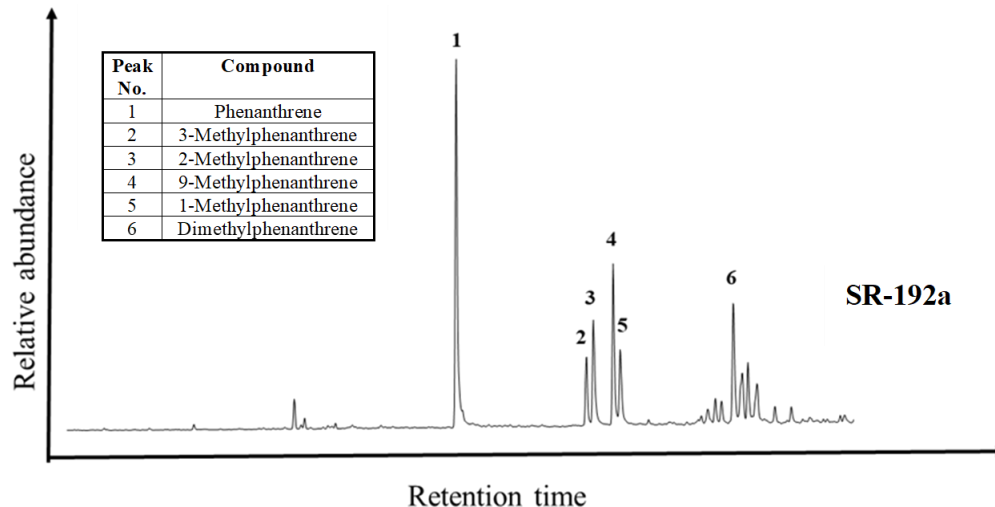


Figure 51. GC-MS chromatogram displaying the distribution of the phenanthrenes (**XV**) series observed at summed m/z 178+192+206. The m/z 178 is used to identify the phenanthrene, m/z 192 is used to identify the methylphenanthrenes, and m/z 206 is used to identify the dimethylphenanthrenes.

According to Hughes et al. (1995) all oils from marine, predominantly carbonate source rocks have (DBT/Phen) ratios >1 and Pr/Ph ratios <1 . Marine siliclastic and fluvial/deltaic source rocks have DBT/Phen ratios <0.5 and Pr/Ph ratios >1 as defined by Hughes et al. (1995). The Woodford has Pr/Ph ratios <3 whereas those generated from nonmarine carbonaceous shales and coals have Pr/Ph ratios >3 as defined in Table 9. Thus, the DBT/Phen ratio alone is a good discriminator of siliclastic vs. nonsiliclastic source rock lithologies. Sediments with the highest DBT/Phen ratios indicate elevated sulfur concentrations. Based on the DBT/Phen vs. Pr/Ph plot, the source rocks can be divided into 4 zones that determine its depositional environment and lithology (Table 10). According to Figure 52, the Speake Ranch samples are mostly of Zone 3 representing sulfide-rich sediments of lacustrine derived environment. However, several of the hard samples plot in the Zone 2, representing thiophene-rich sediments originating from a marine and lacustrine environment. Concentrations of DBT correlated to the organic carbon and clay content of the sediments, suggesting that the clay and organic carbon contents are two prime factors

that are controlling dibenzothiophene levels (Yang, 1998). Changing extents of anoxia (accompanied by changes in the variability of ferric iron) could have made different amounts of elemental sulfur available to the depositional systems corresponding to the two different lithofacies. The combined parameters Pr/Ph, bisnorhopanes, tetracyclic polyprenoids, and gammacerane, with dibenzothiophene to phenanthrene, show evidence that sulfur rich intervals coincide with anoxic intervals as well as water column stratification, that provide a suitable environment for an abundant preservation of organic matter as shown in Figure 53. The highest values of TOC wt% are found within the intervals that show high values of all the mentioned environmental condition.

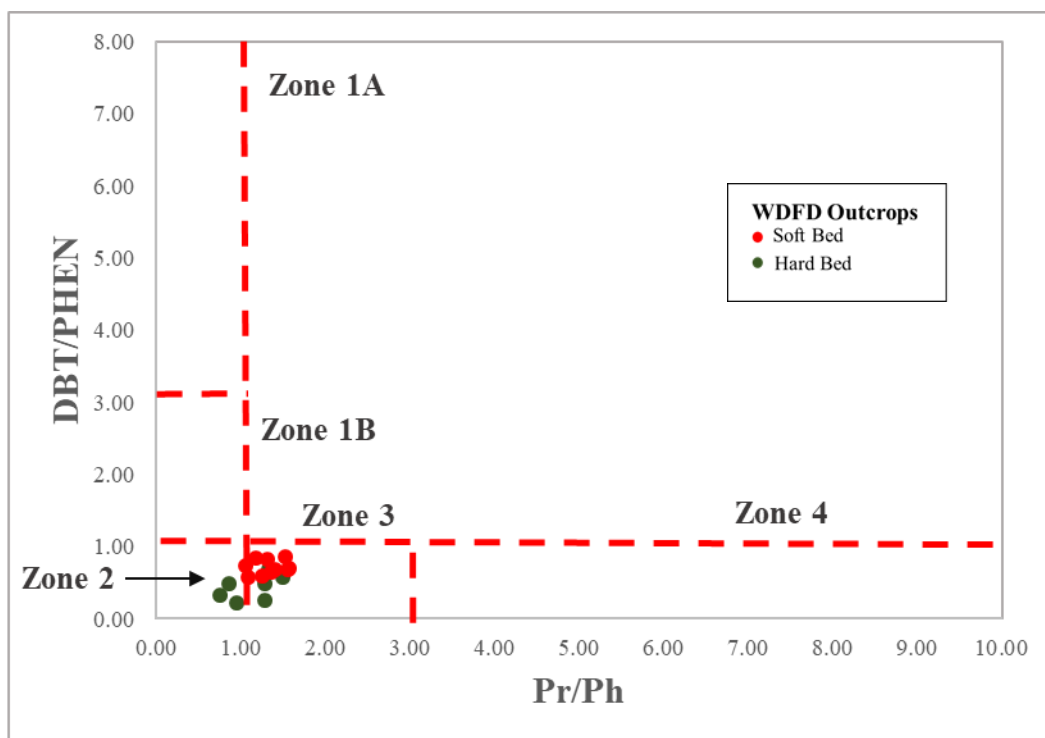


Figure 52. The Woodford samples from Speake Ranch show that the major lithology of the source rock is lacustrine/ marine shale of low Pr/Ph and DBT/Phen values. There are several of the hard bed intervals that indicate sulfate poor lacustrine environment (modified from Hughes et al., 1995).

ZONE	DBT/PHEN	PR/PH	DEPOSITIONAL ENVIRONMENT	LITHOLOGY
1A	> 3	< 1	Marine	Carbonate
1B	1-3	< 1	Marine and Lacustrine (sulfate-rich)	Carbonate and Mixed*
2	< 1	< 1	Lacustrine (sulfate-poor)	Variable
3	< 1	1-3	Marine and Lacustrine	Shale
4	< 1	> 3	Fluvio/Deltaic	Carbonaceous shale and Coal

* Mixed includes marls, argillaceous carbonates and siliceous/phosphatic rocks

Table 10. Defining parameter for DBT/Phen with Pr/Ph outputs classified into 4 zones with 4 distinct environments and its associated lithology.

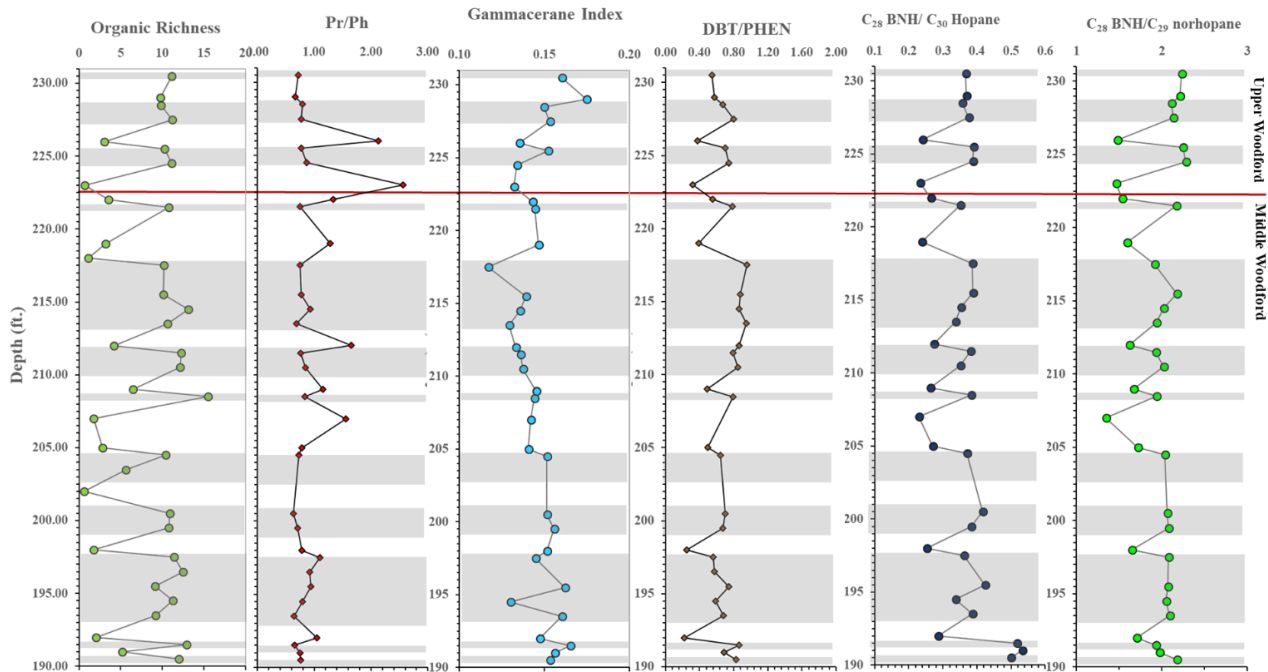


Figure 53. Correlation of redox conditions (Pr/Ph, C_{28} BNH/ C_{30} hopane, and C_{28} BNH/norhopane), presence of sulfur in water column (DBT/PHEN), and water column stratification (gammacerane), to the abundance of organic matter (TOC wt%) of the Woodford Shale from Speake Ranch. Gray intervals indicate the soft beds, and white intervals indicate the hard beds.

CHAPTER IV

4. Discussion

4.1 *High Resolution Analysis of Biomarker Distributions*

As discussed earlier, the Woodford Shale has frequent variations in the organic matter abundance within the Upper and Middle Woodford members. This positive correlation of TOC to the hard-soft bed couplet are controlled by changing lithofacies. The purpose of this research is to determine whether the variations found within the biomarkers are an effect of a compilation of multiple factors that include sea level changes, onset of terrigenous influx, tectonic disturbances, varying levels of anoxia, and marine biota productivity. In prior chapters, the effects of maturity have been eliminated because maturity changes are not expected or observed over a 40ft interval.

For the high-resolution analysis purposes discussed in this section, Speake Ranch samples with similar TOC values were taken at different depths of the 40ft interval. The aim of this chapter is to determine if intervals of similar TOC wt% would yield similar distributions of biomarkers. The chosen samples were 5 samples with relatively higher TOC wt% (11%) and 3 samples with relatively lower TOC wt% (~3%) found at varying depths within the Upper Woodford and Middle Woodford of Speake Ranch (Figure 54). All bulk geochemical source rock evaluation parameters, such as S_1 , S_2 , S_3 , and T_{max} , were consistent throughout the chosen depths (Table 11). Significant variations were seen at depth 230.5 ft (SR-230b, Upper Woodford) for the soft bed group which shows the lowest HI value and highest OI value, possibly signifying a different kerogen type from the other samples, or one that is heavily weathered. Anoxia (based on the Pr/Ph) is consistent within intervals of high TOC. However, the soft bed at 197.5 ft has a higher Pr/Ph value, indicating a more oxic condition as shown in Table 11. In addition to that, SR-205a, of the hard bed group,

shows a Pr/Ph value indicating anoxic water column upon deposition. These two outlier values contradict the hypothesis that organic rich layers are always found in highly reducing environments. However, these values may be affected by weathering, as the Speake Ranch samples were collected from an exposed outcrop.

Sample	Depth (ft.)	Lithology	TOC (wt%)	S ₁ (mg HC/g)	S ₂ (mg HC/g)	S ₃ (mg CO ₂ /g)	T _{max} (°C)	HI	OI	Pr/Ph
SR-230b	230.5	Soft	11.1	1.72	54.47	1.15	428	490.72	10.36	0.72
SR-227b	227.5	Soft	11.2	1.25	59.2	0.48	428	528.57	4.29	0.77
SR-224b	224.5	Soft	11.1	2.26	63.23	0.34	429	569.64	3.06	0.86
SR-197b	197.5	Soft	11.4	1.95	68.01	0.49	431	596.58	4.30	1.10
SR-194b	194.5	Soft	11.3	1.33	60.15	0.46	428	532.30	4.07	0.80
SR-226a	226	Hard	3.04	0.52	14.81	0.74	426	487.17	24.34	2.13
SR-219a	219	Hard	3.16	0.68	16.44	0.59	433	520.25	18.67	1.28
SR-205a	205	Hard	2.79	0.26	13.52	0.27	425	484.59	9.68	0.78

Table 11. High resolution source rock analysis of similar high TOC values distributed throughout the 40ft interval. Lighter green tables indicating Middle Woodford data.

4.1.1 Organic Matter Source

The C₃₀ sterane index is a direct reflection of marine source input (Waples and Machihara, 1990; Fildani et al., 2005). The soft bed group shown in Table 12 has consistent C₂₇/C₂₉ sterane and C₂₈/C₂₉ sterane values, indicating a predominantly marine source input along with a consistent C₃₀ sterane index. The hard bed group shows consistent but contrasting values, except for SR-219a, indicating a higher marine input from C₂₇/C₂₉ steranes and C₂₈/C₂₉ steranes, but a lower C₃₀ sterane index. It is possible that these values were also affected by weathering, as C₃₀ steranes are already found in low concentrations in proportion to the C₂₇-C₂₈-C₂₉ steranes. The TST occur when sea level is rising (representing deposition of Middle Woodford), and the basin becomes flooded with less influx from terrigenous and reworked (inert) organic material. During the HST, more

terrigenous derived and reworked organic material (with lower HI values) comes into the basin (representing deposition of Upper Woodford). However, this can only be assumed for Speake Ranch samples as the 40ft interval only shows a dominating marine source input throughout the Upper and Middle Woodford in most of its soft bed lithofacies. As mentioned in an earlier chapter particulate organic matter in certain marine environments were found to contain C₂₉ steranes which were reasoned to be derived from green algae (chlorophyta), *Prymnesiophycean* algae, as well as cyanobacteria or *Tasmanites algae*, and not from land-plants (Grantham and Wakefield, 1987). From the depth logs of organic matter source input, high values of C₃₀ sterane index plotting beyond 4% are found periodically and correlates with the marine indicating ratios of the C₂₇/C₂₉ steranes in Figure 54. Since all the organic matter source input parameters used in this study point toward a marine source input, it is interesting that we would see differences in the proportion of C₂₉ and C₂₇ steranes. The correlation of low C₃₀ sterane index values with lower C₂₇/C₂₉ sterane, C₂₃ TT/C₂₄ Tet, and C₁₉/C₂₃ TT ratios, may attest to the theory that bioturbated intervals yield lower organic carbon loading onto the sediment surfaces. This process caused remineralization and removal of organic carbon from sediment surface by oxygenation as previously suggested by Kennedy and Wagner (2011). The XRF-data of the Mo/Al ratio help determine whether water column mixing, and oxygenation co-vary with the low marine input intervals. The main elements analyzed by XRF are defined in Table 13. Interestingly, Mo/Al negatively correlates to all the organic matter source input parameters shown in Figure 54. This justifies that a lower marine source input indication and heightened “terrigenous” markers may just be a product of water column oxygenation. As sea level regressed, oxygenation is introduced by water column mixing and weathering of terrigenous sediments by erosion are introduced into the basin.

Sample	Depth (ft.)	Lithology	TOC (wt%)	Pr/Ph	Sterane index	C ₂₇ /C ₂₉ sterane	C ₂₈ /C ₂₉ sterane	C ₂₃ TT/C ₂₄ Tet	C ₁₉ /C ₂₃ TT
SR-230b	230.5	Soft	11.1	0.72	2.49	1.20	0.42	3.25	0.09
SR-227b	227.5	Soft	11.2	0.77	2.49	1.19	0.44	3.47	0.08
SR-224b	224.5	Soft	11.1	0.86	2.42	1.16	0.42	3.00	0.08
SR-197b	197.5	Soft	11.4	1.10	2.49	1.05	0.40	3.07	0.08
SR-194b	194.5	Soft	11.3	0.80	2.45	1.04	0.41	3.13	0.08
SR-226a	226	Hard	3.04	2.13	2.50	0.94	0.36	3.03	0.05
SR-219a	219	Hard	3.16	1.28	1.74	1.17	1.27	2.63	0.04
SR-205a	205	Hard	2.79	0.78	2.34	0.90	0.35	2.88	0.07

Table 12. Organic matter source high resolution analysis of similar high TOC values distributed throughout the 40ft interval to distinguish variability. Lighter green tables indicating Middle Woodford data.

Element	Proxy - Significance
Titanium (Ti)	Continental source and dust input
Zirconium (Zr)	Continental source
Silicon/Aluminum (Si/Al)	Quartz origin (biogenic or detrital)
Aluminum (Al)	Clay contents and feldspar
Potassium (K)	Clay contents and feldspar
Thorium (Th)	Clay contents and feldspar
Calcium (Ca)	Carbonate source and phosphates
Strontium (Sr)	Carbonate source and phosphates
Magnesium (Mg)	Carbonates, dolomitization
Manganese (Mn)	Carbonates, dolomitization
Uranium (U)	Organic matter richness, ?bitumen
Vanadium (V)	Bottom water anoxia, redox sensitive
Molybdenum (Mo)	Bottom water euxinia, redox sensitive
Sulfur (S)	Pyrite, reducing conditions, euxinia
Phosphorous (P)	Phosphate accumulation

Table 13. Main elements analyzed through XRF and their significance in chemostratigraphic interpretations. (Galvis, 2017; compiled in Turner, 2016)

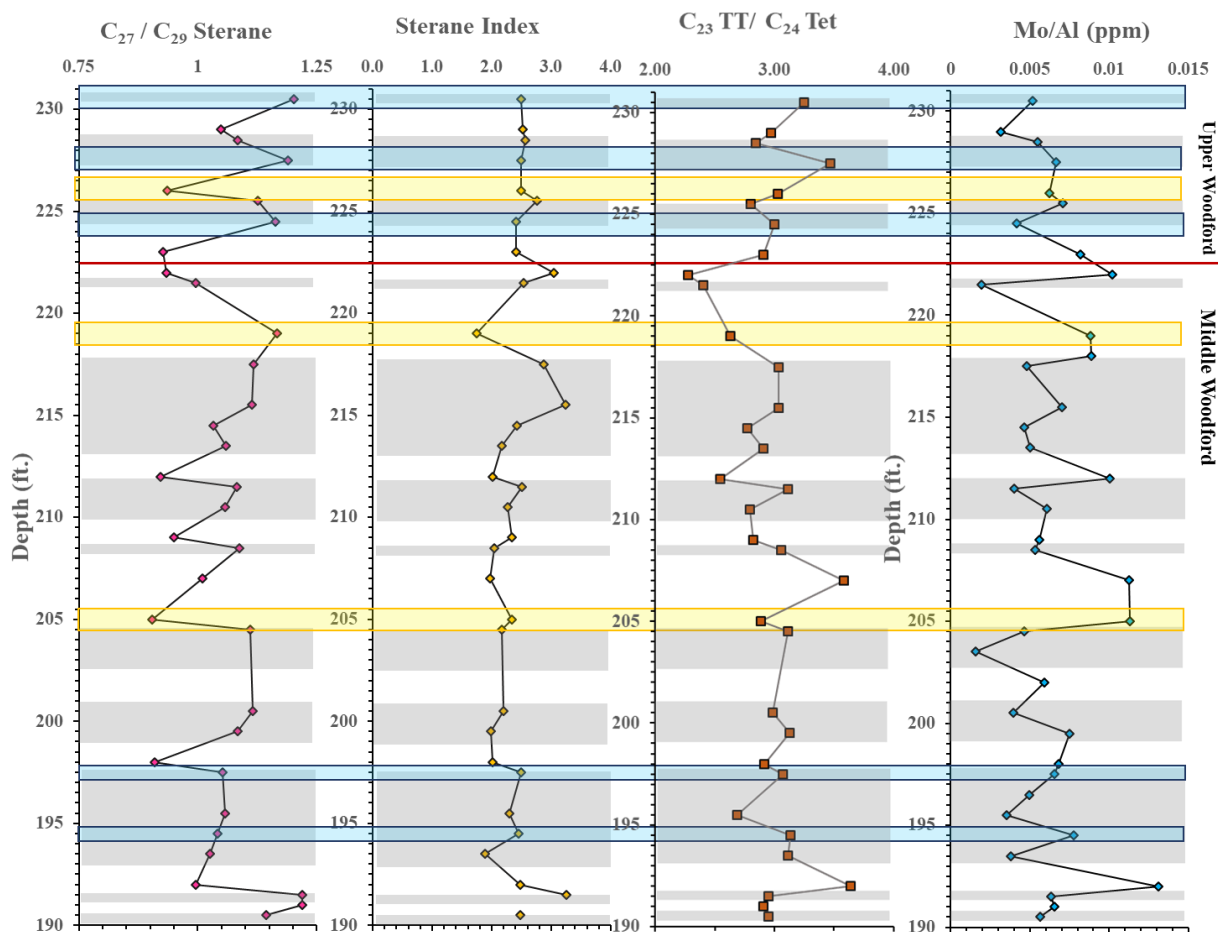


Figure 54. Depth plots of the parameters defining the source of organic matter and its correlation to the Gamma Ray. Yellow highlighted intervals are the chosen samples for high resolution analysis with TOC values ~11%, and red highlighted intervals are chosen samples for low TOC ~3%.

4.1.2 Depositional Environment

The Pr/Ph values analyzed in the prior section suggested that a majority of the hard bed group 3% TOC (wt%) coincide with oxic depositional environment (high Pr/Ph), while high TOCs coincide with anoxic depositional environment (low Pr/Ph and high C_{35}/C_{34} HH). The anoxic intervals within the soft bed group 11% TOC (wt%) are mostly consistent, except for specific disturbances where intervals may have been more restricted in certain periods. Within these

selected intervals in Table 14, the C₂₈ BNH/C₃₀ hopane and the C₂₈ BNH/C₂₉ norhopane ratios show consistency in their values. The values of C₂₈ BNH/C₃₀ hopane and the C₂₈ BNH/C₂₉ norhopane are higher for intervals indicating anoxic water column (Table 14). Changing extents of anoxia (accompanied by changes in the variability of ferric iron) could have made different amounts of elemental sulfur available to the depositional systems corresponding to the two different lithofacies. Thus, the soft bed lithofacies which have been shown to be deposited in a more anoxic environment are enriched with the presence of sulfur by DBT/Phen (Table 15). While, hard bed lithofacies have lower sulfur content.

Sample	Depth (ft.)	Lithology	TOC (wt%)	Pr/Ph	C ₃₅ /C ₃₄ HH	Homohopane Index	Ts/Tm	C ₃₀ D/C ₂₉ Ts	C ₂₈ BNH/C ₃₀ hopane	C ₂₈ BNH/C ₂₉ norhopane
SR-230b	230.5	Soft	11.1	0.72	0.69	0.08	0.38	0.09	0.37	2.23
SR-227b	227.5	Soft	11.2	0.77	0.58	0.06	0.33	0.08	0.38	2.13
SR-224b	224.5	Soft	11.1	0.86	0.71	0.06	0.35	0.08	0.39	2.28
SR-197b	197.5	Soft	11.4	1.10	0.84	0.09	0.28	0.08	0.36	2.08
SR-194b	194.5	Soft	11.3	0.80	0.81	0.07	0.30	0.09	0.34	2.05
SR-226a	226	Hard	3.04	2.13	0.67	0.07	0.35	0.08	0.24	1.47
SR-219a	219	Hard	3.16	1.28	0.77	0.08	0.35	0.07	0.24	1.59
SR-205a	205	Hard	2.79	0.78	0.65	0.07	0.30	0.08	0.27	1.72

Table 14. Redox condition high resolution analysis of similar high TOC values distributed throughout the 40ft interval to distinguish variability. Lighter green tables indicating Middle Woodford data.

4.1.3 Marine vs. Lacustrine

Anoxic intervals could largely be restricted and create a marine environment to become pseudo lacustrine and therefore may contribute to the abundance of TOC. Heightened Hopane/C₂₇ αααS+R values have indicated a lacustrine freshwater organic matter input (Mello et al., 1988; Araujo et al., 2018). The low Hopane/C₂₇ αααS+R ratio value intervals are found within the soft bed group of Speake Ranch (~1-2). In accordance to the trend we have been observing regarding organic matter source input, it is expected that soft bed lithofacies would

have relatively lower Hopane/C₂₇ $\alpha\alpha\alpha$ S+R ratio values. As throughout this study, soft bed lithofacies are found to be enriched in marine source input. A relatively higher Hopane/C₂₇ $\alpha\alpha\alpha$ S+R (3.46) can be found signifying more of a lacustrine freshwater input at SR-227b ft (227.5 ft) shown in Table 15. This outlier does not correlate to the variation of organic matter source input in Table 13 nor the variations in the redox parameters in Table 14. However, this outlier does correlate with an elevated DBT/Phen value and suggests that this value may be affected by the presence of sulfur in the water column. It is clear that the GI is consistent throughout both the hard bed group and soft bed group just as the DBT/Phen values shown in Table 15. From these 8 chosen samples, only one interval can be identified as pseudo lacustrine (SR-205a) in Table 15. Otherwise, there aren't any further and significant value distributions conclusive of lacustrine vs. marine implications within these 8 samples.

Sample	Depth (ft.)	TOC (wt%)	Lithology	Pr/Ph	TPP/C ₂₇ diasterane	Hopane/C ₇ $\alpha\alpha\alpha$ S+R	C ₂₆ /C ₂₅ TT	GI	DBT/Phen
SR-230b	230.5	11.1	Soft	0.72	0.22	1.07	0.84	0.16	0.54
SR-227b	227.5	11.2	Soft	0.77	0.22	3.46	0.78	0.15	0.80
SR-224b	224.5	11.1	Soft	0.86	0.19	1.61	0.93	0.13	0.74
SR-197b	197.5	11.4	Soft	1.10	0.12	1.34	0.97	0.14	0.56
SR-194b	194.5	11.3	Soft	0.80	0.13	1.72	0.94	0.13	0.59
SR-226a	226	3.04	Hard	2.13	0.28	6.04	0.94	0.14	0.38
SR-219a	219	3.16	Hard	1.28	0.31	5.64	0.87	0.15	0.39
SR-205a	205	2.79	Hard	0.78	0.23	3.04	0.96	0.14	0.49

Table 15. Lacustrine vs. Marine source high resolution analysis of similar high TOC values distributed throughout the 40ft interval to distinguish variability. Lighter green intervals indicate Middle Woodford data, and white intervals indicate Upper Woodford.

4.2 Evidence of Frasnian – Famennian Extinction Boundary

The Frasnian-Famennian extinction boundary is marked by the loss of a wide and diverse range of marine biotic organisms, such as brachiopods, rugose corals, coral stromatoporoids, pelagic conodonts, and benthic faunas within the shallow marine settings, similar to most extreme

crises (Tulipani et al., 2015; Ma et al., 2016). This extreme loss of biodiversity within the Devonian time interval came to be known as a “reef gap”, reflecting a transitional cause to the instigation of climate change from Devonian Greenhouse to the Carboniferous Icehouse (Zhang et al. 2019). Percival et al. (2016) suspected that the underlying cause for the loss of marine biodiversity was the widespread of marine anoxia and the consequential high rates of continental weathering, shown through the occurrence and appearance of black organic rich shales within the stratigraphic record. Ma et al. (2016) also believed that it was the combined forces of marine anoxia, continental weathering and the association of multiple volcanic/hydrothermal activities that caused the fluctuating and erratic climate cooling and warming which affected sea level dynamics. According to Wang et al. (2018), the Frasnian-Famennian boundary was marked by a preceding two-phase event called the “Kellwasser Event” and the “Annulata event”, which signified the horizontal pulses leading up to the extinction. The Kellwasser Event is characterized by tectonic processes that include the large-scale volcanic activity associated with the Viluy Traps in Siberia, orogenic uplift, erosion, and the expansion of vascular rooted terrigenous flora (Wang et al., 2018). Alternatively, the Annulata horizon marked a great anoxic event that corresponded with a major marine transgression and global volcanic activity. The Late Devonian was not only recognized as a time marked by severe extinction, but it was also a time of evolution of the terrigenous forests and seed plants, which may have affected the dynamics of the ecosystem (Zhang et al. 2019). All of these processes that have been suspected to cause the wide extinction of marine biodiversity could possibly be traced by organic geochemical biomarker analysis.

The massive loss of marine biota did not occur abruptly, but rather in a transitional progress. Therefore, to identify the Frasnian-Famennian boundary, extreme climatic and environmental shifts need to be identified. This can be done by organic geochemical analysis

through biomarkers to track large shifts in organic matter input. It is possible that the influx of weathered terrigenous organic matter from a Transgression System Tract to a regression of sea level were introduced into the ocean and disturbed the marine organic productivity. Thus, stimulated algal blooms resulted in anoxic water columns and provided the mechanism that led to the end-Frasnian extinction (Philp and DeGarmo, 2020). It is also hypothesized that with such a high-resolution study over the Woodford interval from Speake Ranch, an accurate identification of the F-F boundary can be established. Moldowan et al. (1985) suggested that low values of T_s/T_m are an indication of different organic material which are often related to bacterial and/or terrigenous input. Not much can be deduced for the T_s/T_m of the Speake Ranch, as the ratio values are nearly linear and consistent low as previously discussed in Chapter 3. No significant shifts in organic matter source input can be dictated within the 40ft interval of the Woodford Shale. Biomarkers utilized in this section have been targeted to define signs of euxinia, distinct fluxes of terrigenous input along with algal blooms, and a shift in anoxia.

Previous studies from Nowaczewski (2011), Connock (2015), deGarmo (2015), Jones (2017), and Torres (2020) have made efforts to locate the Frasnian-Famennian (F-F) extinction boundary within the Woodford Shale using geochemical evidence. Nowaczewski (2011) indicated that there are biomarker anomalies which include elevated C_{30} hopanes at the expense of C_{29} hopanes, high abundance of gammacerane, and isorenieratane as markers to determine the F-F boundary. His findings demonstrated that the F-F boundary was a time marked by an increase in marine eukaryotic preservation within a stratified, anoxic marine water column. Connock (2015) and deGarmo (2015) indicated that the F-F boundary is marked by elevated H_2S presence and persistent PZE prior to marine biota loss. The increased nutrients from the PZE conditions and terrigenous blooms cause eutrophication and algal blooms. Moreover, Connock (2015) determined

that the F-F is located within the Middle Woodford at two occurrences of euxinic conditions of the Woodford. Both Over (1992) and Turner (2016) suggested that the F-F boundary to be just below the Middle Woodford and Upper Woodford contact boundary using lithology, chemostratigraphy, and conodont stratigraphy. Jones (2017) also indicated that the F-F boundary to be slightly below the Middle Woodford and Upper Woodford contact boundary as well. More specifically, Torres (2020) indicated that the F-F event to be located between 202ft to 220ft of the Speake Ranch section. The purpose of this research is to mark the exact interval of where this boundary could be located.

Schwark and Frimmel (2004) suggested a crossplot of the Pr/Ph ratio against aryl isoprenoid ratio to better assess the extent and persistence of photic zone anoxia during deposition of Jurassic Possidonian Shale. The distribution indicates the anoxic event coincides with facies changes as a reflection of rapid transgression. Grice et al. (2005) suggested that sulfide toxicity was a driving factor in the extinction and in the protracted recovery. Furthermore, indication of euxinia can be further assessed by the abundance of dibenzothiophene (DBT), where high contents of this compound in parallel to high values of aryl isoprenoids are suggestive of rapid input of terrigenous matter that consumed the oxygen within the water column and caused for further reduction optimal for DBT production (Mizukami et al., 2013). Combining all the geochemical parameters used to assess the paleoenvironment condition of the Ardmore Basin in Oklahoma, it seems that the F-F boundary is not a single bed but a transitional event, where the environment shifts with changing conditions. In agreement to Zhang et al. (2019), the F-F boundary is followed by preceding erratic environmental conditions. These are dictated by 3 intervals shown in Figure 55. The initial drop of GI, C₂₇/C₂₉ sterane, C₂₃/C₂₄ Tet, DBT/Phen, HHI, as well as enhanced Pr/Ph and TPP/C₂₇ diasterane could be a possible mark for the Maximum Flooding Surface (MFS) in

preparation for the F-F at 191-192ft. The MFS has been determined by prior studies by Galvis (2017) and Torres (2020) from their correlation of the Gamma Ray to the Speake Ranch section. However, due to the lack of data prior to MFS, the interval we have discovered as MFS may just be a preceding pulse of environmental instability leading up to the F-F boundary. The following highlighted event upsection is manifested based on the elevated and erratic fluctuation of values in Pr/Ph, HHI, AIR, TPP/C₂₇ diasterane, DBT/Phen, C₂₃TT/C₂₄Tet, and C₂₇/C₂₉ Sterane at 205.5ft to 215ft. Finally, the interval at 218.5ft to 227.5ft has shown significant instability and a transition to elevated and erratic values of Pr/Ph, homohopane index, TPP/C₂₇, GI, and AIR in correlation to a shift to decreasing C₃₅/C₃₄ HH and C₂₃ TT/C₂₄ Tet that serve as a marker of the Frasnian-Famennian boundary (Figure 55).

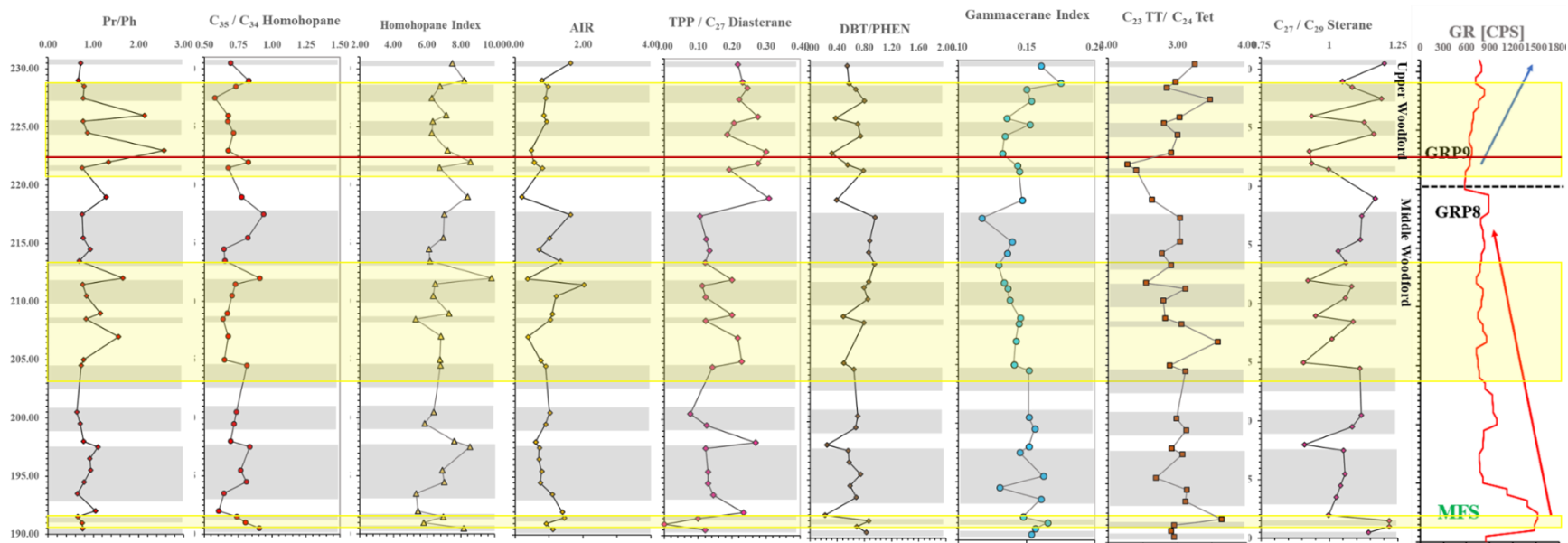


Figure 55. Organic geochemical parameters to define the anoxia, eutrophication, and organic matter input to determine the Frasnian – Famennian extinction boundary in the Woodford Shale of the Ardmore Basin in Oklahoma. Highlighted intervals signify the pulses leading up to the F-F.

Chapter V

5. Conclusion

Previous studies (Galvis, 2017; Torres, 2020) set lithostratigraphy and sequence stratigraphy frameworks for the Woodford Shale in southern Oklahoma at the Speake Ranch. The challenge posed by those two studies was the characterization of the Woodford shale at a smaller scale to observe the geochemical changes within the hard-to-soft cycles. This study is the first to explore a high resolution organic geochemical analysis to understand the effects of depositional processes, lithofacies, and stratigraphy over a 40ft interval.

Throughout the Upper and Middle Woodford, oscillations of soft and hard lithofacies are found at every 6 inches. Soft lithofacies, which are the clay abundant intervals, provide for a better petroleum source rock (high TOC) than the siliceous hard bed lithofacies. Maturity parameters (T_{max} , $C_{29} 20S/(20S+20R)$, and $C_{29} \beta\beta/(\beta\beta+\alpha\alpha)$ steranes) explored in this study show that the Speake Ranch samples are consistently immature. Therefore, variations in the biomarker distributions are independent of thermal alteration. There exist covariances of the lithofacies with biomarker distribution variations, which provide insight concerning the environmental deposition of the Woodford Shale from Speake Ranch. The organic matter source determined by C_{27}/C_{29} sterane, C_{30} sterane index, and $C_{23} TT/C_{24} Tet$, illustrate a predominantly marine source input. Several intervals within the 40ft sequence have shown lower marine source input within the hard bed lithofacies and were thought to be derived from elevated terrigenous input. However, these elevated terrigenous markers identified by C_{29} steranes, and C_{24} tetracyclic terpanes may have been attributed to the input of marine algae (*Tasmanites*) instead. The retreating shoreline causes restriction in the water column causing $CaCO_3$ to supersaturate, thus stimulating algal blooms (Philp and DeGarmo, 2020). Torres (2020) also suggested that upwellings leading to chert

deposition provide nutrient-rich waters, which caused for algal blooms. The result of this study also documented the high-resolution analysis of biomarkers defining redox and euxinia of the depositional environment of the Woodford shale. It is anticipated that high sulfur content in the water column and high levels of anoxia are the optimal environmental conditions for organic matter preservation. Multiple biomarker parameters that are used to evaluate redox conditions, such as Ts/Tm, Pr/Ph, relative concentrations of bisnorhopanes, and homohopanes, illustrate that anoxia prevailed throughout soft bed lithofacies deposition. The combined parameters Pr/Ph, bisnorhopanes, tetracyclic polyprenoids, and gammacerane, with the dibenzothiophene/phenanthrene ratio, show evidence that sulfur rich intervals coincide with anoxic intervals along with providing a suitable environment for abundant preservation of organic matter. The analysis of elevated tetracyclic polyprenoid concentrations combined with tricyclic terpanes, hopanes, steranes, and diasteranes reveal that there may have been three intervals within the Speake Ranch samples that became pseudo lacustrine depositional environments affecting total organic carbon yield.

A closer look into the biomarker distributions does attest to a major input of marine source. However, the analysis from XRF (Mo/Al) has also revealed that the fluctuations found within the organic matter source parameter indicate that bioturbated intervals yield lower organic carbon loading onto the sediment surface. This is due to remineralization and removal of organic carbon by oxygenation. In addition to that theory, mineral composition of the rock, whereby an abundance of clay is present, provides for optimal preservation properties. Therefore, variations in the abundance of organic matter preservation are controlled by varying levels of anoxia, water stratification, and mineral composition.

A combined study of indicators for euxinia, distinct fluxes of terrigenous input along with algal blooms, helped define the extinction of the marine biota during the Late Devonian. This study explored the idea that the F-F extinction boundary was a transitional and gradual event that was preceded by two pulses of extreme conditions that preceded the extinction. No significant and definite shifts could be determined at the high-resolution sampling in this study. However, the events were signified by erratic distribution of the biomarkers within these intervals, indicating an instability of fluxes of organic matter source, anoxia, and euxinia.

In summary, the complex features of the unconventional Woodford Shale from Speake Ranch can be discerned using a high-resolution analysis that help integrate small scale environmental conditions to the sequence stratigraphy. However, the characteristics of the Middle and Upper Woodford members of this study may not reflect the Woodford Shale across Oklahoma, as this section may vary depending on the location. This could possibly be attributed to the enclosed mini-basin fill deposits nature of the section and may only be accurately compared to sections of other areas identified with the same nomenclature and interval thicknesses.

REFERENCES

- Achari, R.G., Shaw, G. and Holleyhead, R. (1973). Identification of ionene and other carotenoid degradation products from the pyrolysis of sporopollenins derived from some pollen exines, a spore coal and the green river shale. *Chemical Geology*, **12**, 229-234.
- Akinlua, A., Torto, N. and Ajayi, T. R. (2007). Oils in the Northwestern Niger Delta: aromatic hydrocarbons content and infrared spectroscopic characterization. *J. Petroleum Geology* **30(1)**, 91-100.
- Alexander, R., Bastow, T. P., Fisher, S. J., Kagi, R. I. (1995). Geosynthesis of organic compounds II. Methylation of phenanthrene and alkylphenanthrenes. *Geochimica et Cosmochimica Acta*, **59**, 4259-4266.
- Algeo, T.J., Berner, R.A., Maynard, J.B. and Scheckler S.E. (1995). Late Devonian oceanic anoxic events and biotic crises. “Rooted” in the Evolution of Vascular Land Plants. *GSA Today* **5**, 45–66.
- Algeo T.J. and Maynard J.B. (1997). Cyclic Sedimentation of Appalachian Devonian and Midcontinent Pennsylvanian Black Shales: Analysis of Ancient Anoxic Marine Systems— A Combined Core and Field Workshop: Joint Meeting of Eastern Section AAPG and The Society for Organic Petrography (TSOP), Lexington, Kentucky. Univ. of Cincinnati, Dept. of Geology, Cincinnati, Ohio, 147.
- Algeo, T.J. and Scheckler S.E. (1998). Terrestrial-marine teleconnections in the Devonian: links between evolution of land plants, weathering processes, and marine anoxic events. *Philosophical Transactions of the Royal Society of London* **353**, 113-30.
- Allen, R.W. (2000). Stratigraphy, mountain building and complex geological structures of the Ardmore Basin. *Oklahoma Geological Society*, Shale Shaker **51**, 10-21.
- Aquino Neto, F. R., Cardoso, J. N., Rodriguez, R. and Trindade A. F. (1986). Evolution of tricyclic alkanes in the Espirito Santo Basin, Brazil. *Geochimica et Cosmochimica Acta* **50**, 2069-2072.
- Araújo, B.Q. and Azevedo D.A. (2016). Uncommon steranes in Brazilian marginal crude oils: dinoflagellate molecular fossils in the Sergipe-Alagoas Basin, Brazil. *Organic Geochemistry* **99**, 38–52.
- Araujo, B. Q., Aquino Neto, F. R. and Azevedo D. A. (2018). Occurrence of extended tetracyclic polyprenoid series in crude oils. *Elsevier Science Organic Geochemistry* **118**, 27-35.

- Banks, H. P., Chaloner, W. G. and Lacey W. S. (1967). Pteridophyta-I. In: *The Fossil Record* (eds W. B. Harland, C. H., Holland, M. R. House, N. F., Huges, A. B. Reynolds, M. J. S. Rudwinck, G. E. Satterthwaite, L. B. H. Tarlo and E. C. (Wiley) Chapter 4. Geological Society of London.
- Bishop A.N. and Farrimond P. (1995). A new method of comparing extended hopane distributions *Organic Geochemistry* **23**, 987-990.
- Blakey, R. (2011). Colorado Plateau Geosystems, Inc., <http://cpgeosystems.com/index.html>, accessed March 3rd, 2014.
- Boon, J. J., Hines, H., Burlingame, A. L., Klok, J., Rijpstra, W. I. C., De Leeuw, J. W., Edmunds, K. E. and Eglinton G. (1983). Organic geochemical studies of Solar Lake laminated cyanobacterial mats. *Advances in Organic Geochemistry 1981* (Eds M. Bjoroy et al.) Wiley, Chichester, 207-277.
- Brassell, S. C. (1992). Biomarkers in Sediments, Sedimentary Rocks and Petroleum: Biological Origins, Geological Fate and Applications. In L. M. Pratt, J. B. Comer, S. C. Brassell, & R. Droppo (Eds.), *Geochemistry of Organic Matter in Sediments and Sedimentary Rocks* **27**, 29-72.
- Brassell, S. C., Meloy, B. J., Fan, S., Sheng, G.-Y. and Fu J. (1988). Biological markers in the assessment of depositional environments: Chinese lacustrine shales and petroleum. In: *Advances in Organic Geochemistry* (Eds L. Mattavelli and L. Novelli) Pergamon Press, Oxford, 31-45.
- Brincat, D. and Abbott, G. (2001). Some aspects of the molecular biogeochemistry of laminated and massive rocks from the Naples Beach Section (Santa Barbara- Ventura Basin). *The Monterey Formation: From Rocks to Molecules*, 140-149.
- Brito, R.J., Slatt, R.M, Ekwunife, I.C. and Turner B.W. (2017). The Woodford Shale in the Marietta Basin (Oklahoma and Texas): Abstract presented at 2017 AAPG Mid- Continent Section Continent Section Meeting, Oklahoma City, Oklahoma, September 30-October 3.
- Brooks, J. D., Gould, K. and Smith J. W. (1969). Isoprenoid hydrocarbons in coal and petroleum. *Nature* **222**, 257-9.
- Brueseke, M., Hobbs, J., Bulen, C., Mertzman, S., Puckett, R., Walker, J. and Feldman J. (2016). Cambrian intermediate-mafic magmatism along the Laurentian margin: Evidence for flood

- basalt volcanism from well cuttings in the Southern Oklahoma Aulacogen (U.S.A.). *LITHOS* **260**, 164-177.
- Buggisch, W. and Joachimski M.M., (2006). Carbon isotope stratigraphy of the Devonian of Central and Southern Europe. *Palaeogeography Palaeoclimatology Palaeoecology* **240**, 68–88.
- Cardott, B. J. (2005). Overview of unconventional energy resources of Oklahoma. In B. J. Cardott, ed., Unconventional energy resources in the southern mid-continent. 2004 Symposium *Oklahoma Geological Survey Circular* **110**, 7-18.
- Cardott, B. J. (2012). Thermal maturity of Woodford Shale gas and oil plays, Oklahoma, USA. *International Journal of Coal Geology* **103**, 109–119.
- Carlucci, J.R., Westrop, S.R., Brett, C.E. and Burkhalter R. (2014). Facies architecture and sequence stratigraphy of the Ordovician Bromide Formation (Oklahoma): a new perspective on a mixed carbonate-siliciclastic ramp. *Facies* **60**, 987-1012.
- Casilli, A., Silva, R.C., Laakia, J., Oliveira, C.J.F., Ferreira, A.A., Loureiro, M.R.B., Azevedo, D.A. and Aquino Neto F.R., (2014). High resolution molecular organic geochemistry assessment of Brazilian lacustrine crude oils. *Organic Geochemistry* **68**, 61–70.
- Chaffee, A. L. and Johns, R.B. (1983). Polycyclic aromatic hydrocarbons in Australian coals: I. Angularly fused pentacyclic tri- and tetraaromatic components of Victorian brown coal. *Geochimica et Cosmochimica Acta*, **47**, 2141-2155.
- Chaffee, A. L. and M.G., and Johns R. B. (1984). Polycyclic aromatic hydrocarbons in Australian coal: II. Novel tetracyclic components from Victorian brown coal. *Geochimica et Cosmochimica Acta*, **48**, 2037-2043.
- Chicarelli, M., I., Aquino Neto, F. R. and Albrecht P. (1983). Preliminary identification of the less stable isomers of the anti-isocopalane in the Irati oil shale. *II Encontro Nacional de Quimica Analitica*, Rio de Janeiro. November 9-11.
- Clayton, J. L. and King, J. D. (1987). Effects of weathering on biological marker and aromatic hydrocarbon composition of organic matter in Phosphoria shale outcrop. *Geochimica et Cosmochimica Acta* **51**, 2153-2157.
- Comer J. B. (2008). Woodford Shale in southern Midcontinent, USA – Transgressive system tract marine source rocks on an arid passive continental margin with persistent ocean upwelling. *American Association of Petroleum Geologists Annual Convention*, San Antonio, Texas. Poster presentation.

- Comer, J.B. (2012). Woodford Shale and the evaporate connection – the significance of aridity and hypersalinity in organic matter productivity and preservation. *Geological Society America Abstracts with Programs* **44(5)**, 6.
- Connan, J. and Dessort, D. (1987). Novel family of hexacyclic hopanoid alkanes occurring in sediments and oils from anoxic paleoenvironments. *Organic Geochemistry* **11**,103–113.
- Connock, G.T. (2015). Paleoenvironmental interpretation of the Woodford Shale, Wyche Farm shale pit, Pontotoc County, Arkoma Basin, Oklahoma with primary focus on water column structure: M.S. thesis, University of Oklahoma, pp. 253.
- Cooper, B.S. and Barnard P.C. (1984). Source rocks and oils of the central and northern North Sea. Demaison, G., Murriss, R.J. (Eds.), *Petroleum Geochemistry and Basin Evaluation*, AAPG Memoir. *American Association of Petroleum Geologists*, Tulsa **35**, 1–14.
- Curiale, J. A. (1986). Origin of solid bitumens, with emphasis on biological marker results. *Organic Geochemistry* **10**, 559-80.
- Curiale, J. A. and Odermatt J. R. (1989). Short-term biomarker variability in the Monterey Formation, Santa Maria Basin. *Organic Geochemistry* **14**, 1-13.
- Dahl, B. (2004). The use of bisnorhopane as a stratigraphic marker in the Oseberg Back Basin, North Viking Graben, Norwegian North Sea. *Organic Geochemistry* **35**, 1551–1571.
- Dahl, J. E., Moldowan, J.M., and Teerman S. C. (1994). Source rock quality determination from oil biomarkers. a new geochemical technique. *American Association of Petroleum Geologists Bulletin* **78**, 1507-26.
- Dahl, B., Bojesen-Koefed, J., Holm, A., Justwan., Rasmussen, E. and Thomsen E. (2004). A new approach to interpreting Rock-Eval S₂ and TOC data for kerogen quality assessment. *Organic Geochemistry*, **35**, 1461-1477.
- DeGarmo, C. D. (2015). Geochemical characterization of the Woodford Shale (Devonian-Mississippian), McAlister Cemetery Quarry, Criner Hills Uplift, Ardmore Basin, Oklahoma: M.S. Thesis, University of Oklahoma, Thesis, pp. 223.
- de Leeuw, J. W., van Bergen, P. F., van Aarssen, B. G. K., Gatellier, J. P. L. A., Sinninghe Damste, J. S. and Collinson, M. E. (1991) Resistant biomacromolecules as major contributors to kerogen. *Philosophical Transactions Royal Society of London B* **333**, 329-337.

- Demaison, G.J. and Moore G.T. (1980). Anoxic environments and oil source bed genesis. *American Association of Petroleum Geologists Bulletin* **64** (8) 1179–1209.
- Dembicki, H. Jr. (2009). Three common source rock evaluation errors made by geologists during prospect or play appraisals. *American Association of Petroleum Geologist Bulletin* **93**, 341-356.
- Dembicki, H. Jr. (2017). Practical Petroleum Geochemistry for Exploration and Production. *Elsevier Science*, pp. 342.
- Eganhouse, R. P. (1997). Molecular Markers in Environmental Geochemistry. *American Chemical Society symposium series*, Washington, DC **671**, 1-20.
- Eglinton, G., Gonzales, A.G., Hamilton, R. J. and Raphael R.A. (1962). Hydrocarbon constituents of the wax coatings of plant leaves: a taxonomic survey *Phytochemistry* **1**, 89-102.
- Eglinton, G. and Hamilton R. J. (1967). Leaf epicuticular waxes. *Science* **156**, 1322-35.
- EIA (2019). US Oil and Gas Wells by Production Rate – U.S. Energy Information Administration (EIA). *US Oil and Gas Wells by Production Rate – U.S. Energy Information Administration (EIA)*. www.eia.gov/petroleum/wells/.
- El- Sabagh, S. M., El-Naggar, A. Y., El Nady, M. M., Ebiad, M. A., Rashad, A.M. and Abdullah E. S. (2018). Distribution of triterpanes and steranes biomarkers as indication of organic matters input and depositional environments of crude oils of oilfields in Gulf of Suez, Egypt. *Egyptian Journal of Petroleum* **27**, 969-977.
- Ettensohn, F.R. (1992). Controls on the origin of the Devonian-Mississippian oil and gas shales, east-central United States. *Fuel* **71**(12), 1487-1492.
- Ettensohn, F.R. (1997). Assembly and dispersal of Pangea: Large-scale tectonic effects on coeval deposition of North American, marine, epicontinental, black shales. *Journal of Geodynamics* **23** (3-4), 287-309.
- Fay, R.O. (1989). Geology of the Arbuckle Mountains along Interstate 35, Carter and Murray Counties, Oklahoma. *Oklahoma Geological Survey Guidebook* **26**, 50.
- Fisher, S. J., Alexander, R., Kagi, R. I. and Oliver, G. A. (1998). Aromatic hydrocarbons as indicators of biodegradation in north Western Australian reservoirs. P.G. Purcell, R.R. Purcell (Eds.), *Sedimentary Basins of Western Australia: West Australian Basins*

- Symposium, Petroleum Exploration Society of Australia, WA Branch, Perth, Australia (1998), pp. 185-194.
- Fowler, M.G. and Douglas A. G. (1987). Saturated hydrocarbon biomarkers in oils of Late Precambrian age from Eastern Siberia. *Organic Geochemistry* **11**, 201-213.
- Galvis, P. H. (2017). Detailed Lithostratigraphic characterization and sequence stratigraphy of a complete Woodford shale outcrop section in southern Oklahoma. M.S. Thesis, pp.169.
- Galvis, P. H., Becerra, D. and Slatt R. (2018). Lithofacies and stratigraphy of a complete Woodford Shale outcrop section in South Central Oklahoma: Geologic considerations for the evaluation of unconventional shale reservoirs. *Interpretation* **6**, SC15–SC27.
- Ghori, K. A. R. (2002). Modelling the hydrocarbon generative history of the Officer Basin, Western Australia. *Petroleum Exploration Society of Australia* **29**, 1-16.
- Gieskes, J.M., Simoneit, B.R.T., Magenheimer, A.J. and Leif, R.N. (1990). Retrograde oxidation of hydrothermal precipitates and petroleum in Escanaba Trough sediments. *Applied Geochemistry* **5**, 93-101.
- Golovko, A. K., Kontorovich, A. E., Pevnia, G. S. and Fursenko, E. A. (2014). Composition and distribution of alkylnaphthalenes in West Siberian oils. *Russian Geology and Geophysics*, **55(5-6)**, 737-744.
- Goosens H., de Leeuw, J. W., Schenck, P. A., and Brassell S. C. (1984). Tocopherols as likely precursors of pristane in sediments and crude oils. *Nature* **312**, 440-442.
- Granath, J. W. (1989). Structural evolution of the Ardmore Basin, Oklahoma: Progressive deformation in the foreland of the Ouachita collision. *American Geophysical Union*, **8(5)**, 1015-1036
- Grantham P. J., Posthuma J. and DeGroot K. (1980). Variation and significance of the C27 and C28 triterpane content of a North Sea core and various North Sea crude oils. *Advances in Organic Geochemistry*, 675-683.
- Grantham P. J., Posthuma J. and Baak A. (1983). Triterpanes in a number of Far-Eastern crude oils. *Advances in Organic Geochemistry*, 675-683.
- Grantham, P. J. and Wakefield L. L. (1987). Variations in the sterane carbon number distributions of marine source rock derived crude oils through geologic time. *Organic Geochemistry* **12** (1), 61-73.

- Grice K., Schaeffer P., Schwark L. and Maxwell J. R. (1996). Molecular indicators of palaeoenvironmental conditions in an immature Permian shale (Kupferschiefer, Lower Rhine Basin, north-west Germany) from free and S-bound lipids. *Organic Geochemistry* **25**,131–147.
- Grice, K., Backhouse, J., Alexander, R., Marshall, N. and Logan G.A. (2005). Correlating terrestrial signatures from biomarker distributions, $\delta^{13}C$, and palynology in fluvio-deltaic deposits from NW Australia (Triassic-Jurassic). *Organic Geochemistry* **36**, 1347-1358.
- Ham, W.E., Denison, R.E. and Merritt C.A., (1964). Basement rocks and structural evolution of southern Oklahoma. *Oklahoma Geological Survey Bulletin* **95**, 1-302.
- Ham, W. and Stitt James H. (1969). *Regional geology of the Arbuckle Mountains, Oklahoma* [by William E. Ham. With contributions by James H. Stitt [and others] (Guidebook (Oklahoma Geological Survey); 17). Norman: University of Oklahoma.
- Ham, W.E. (1973). Regional geology of the Arbuckle Mountains, Oklahoma. *Oklahoma Geological Survey Special Publication* **73-3**, 61.
- Hammes, Krause and Mutti (2013). Unconventional Reservoir Potential of the Upper Permian Zechstein Group: a slope to basin sequence stratigraphic and sedimentological evaluation of carbonates and organic-rich mudrocks, Northern Germany. *Environmental Earth Sciences* **70(8)**, 3797-3816.
- Han, J., McCarthy, E. D., Van Hoesen, W., Calvin, M. and Bradley W. H. (1967). A preliminary report on the distribution of aliphatic hydrocarbons in algae, in bacteria and in a recent lake sediment. In: *Organic geochemical studies II* **59**, 29-33.
- Hays, L.E., Beatty, T., Henderson, C.M., Love, G.D. and Summons R.E. (2007). Evidence for photic zone euxinia through the end-Permian mass extinction in the Panthalassic Ocean (Peace River Basin, Western Canada). *Paleoworld* **16 (1-3)**, 39-50.
- Hays, L. E., Grice K., Foster. C. B. and Summons R. E. (2012). Biomarker and isotopic trends in a Permian-Triassic sedimentary section at Kap Stosch, Greenland. *Organic Geochemistry* **43**, 67-82.
- Hoffman, P., Dewey, J. F. and Burke K. (1974). Aulacogens and their genetic relation to geosynclines, with a Proterozoic example from Great Slave Lake, Canada. Modern and ancient geosynclinal sedimentation: *Society of Economic Paleontologists and Mineralogists Special Publication* **19**, 38-55.

- Holba, A.G., Tegelaar, E., Ellis, L., Singletary, M.S. and Albrecht P. (2000). Tetracyclic polyprenoids: indicators of freshwater (lacustrine) algal input. *Geology* **28**, 251–254.
- Holba, A.G., Dzou, L.I., Wood, G.D., Ellis, L., Adam, P., Schaeffer, P., Albrecht, P., Greene, T. and Hughes W.B. (2003). Application of tetracyclic polyprenoids as indicators of input from fresh-brackish water environments. *Organic Geochemistry* **34**, 441–469.
- Hossain, Z. M., Sampei, Y., and Roser B. P. (2009). Characterization of organic matter and depositional environment of Tertiary mudstones from the Sylhet Basin, Bangladesh. *Organic Geochemistry* **40**, 743–754.
- Hsu, C. Walters, C., Isaksen, G., Schaps, M. and Peters K. (2003). Biomarker Analysis in Petroleum Exploration. 10.1007/978-1-4419-9212-3_9.
- Huang, W.Y. and Meinschein W.G. (1979). Sterols as ecological indicators. *Geochimica et Cosmochimica Acta* **43**, 739-745.
- Hughes, W. B., Holba, A. G. and Dzou L. I. P. (1995). The ratios of dibenzothiophene to phenanthrene and pristane to phytane as indicator of depositional environment and lithology of petroleum source rocks. *Geochimica et Cosmochimica Acta* **59**(17), 3581-3598.
- Hussler, G., Connan, J. and Albrecht, P. (1984). Novel families of tetra- and hexacyclic hopanoids predominant in carbonate rocks and crude oils. *Oxford: Pergamon Pres.* **6**, pp. 39.
- Isaksen, G.H. and Ledje, H. (2001). Source rock quality and hydrocarbon migration pathways within the Greater Utsira High Area, Viking Graben, Norwegian North Sea. *American Association of Petroleum Geologists Bulletin* **85** (5), 861–883.
- Jarvie, D. M. (1991). Factors affection Rock-Eval derived kinetic parameters. *Chemical Geology* **93**, 79-99.
- Jiang, C., Alexander, R., Kagi, R. and Murray, A. P. (1998). Polycyclic aromatic hydrocarbons in ancient sediments and their relationship to paleoclimate. *Organic Geochemistry*, **29**, 1721-1735.
- Joachimski, M., Pancost, R., Freeman, K., Ostertag-Henning, C. and Buggisch W. (2002). Carbon isotope geochemistry of the Frasnian–famennian transition. *Paleogeography, Paleoclimatology, Paleoecology*, **181**, 91-109.
- Johnson, K.S. (2008). Geologic History of Oklahoma. *Oklahoma Geological Survey: Educational Publication* **9**, 2-9.

- Jones, L.C. (2017). An integrated analysis of sequence stratigraphy, petroleum geochemistry, and Devonian mass extinction events in the Woodford Shale, southern Oklahoma. M.Sc. thesis manuscript, The University of Oklahoma, pp.198.
- Katz, B.J. (1983). Limitations of Rock-Eval pyrolysis for typing of organic matter. *Organic Geochemistry* **4**, 195–199.
- Kennedy, M. and Wagner T. (2011). Clay mineral continental amplifier for marine carbon sequestration in a greenhouse ocean. *Proceedings of the National Academy of Sciences of the United States of America* **108(24)**, 9776-9781.
- Kennedy, M. J., Lohr, S. C., Fraser, S. A. and Baruch E. T. (2014). Direct evidence for organic carbon preservation as clay-organic nanocomposites in a Devonian black shale; from deposition to diagenesis. *Earth and Planetary Science Letters*, **388**, 59-70.
- Killops, S.D., and Killops, V.J., 2005. Introduction to organic geochemistry. 2nd Edition, Blackwell Science Publishing Limited, pp. 393.
- Kirkland D. W., Denison R. E., Summers D. M. and Gormly J. R. (1992). Geology and organic geochemistry of the Woodford Shale in the Criner Hills and western Arbuckle Mountains, Oklahoma. In Johnson K. S. and Cardott B. J. (eds.) Source rocks in the Southern Midcontinent, 1990 symposium. *Oklahoma Geological Survey Circular* **93**, 38-69.
- Klemme, H. and Ulmishek, G. (1991). Effective Petroleum Source Rocks of the World: Stratigraphic Distribution and Controlling Depositional Factors. *American Association of Petroleum Geologists Bulletin* **75**, 1809-1851.
- Koopmans M. P., Köster J., Van Kaam-Peters H. M. E., Kenig F., Schouten S., Hartgers W. a., De Leeuw J. W. and Sinninghe Damsté J. S. (1996). Diagenetic and catagenetic products of isorenieratene: Molecular indicators for photic zone anoxia. *Geochimica et Cosmochimica Acta* **60**, 4467–4496.
- Krystyniak, A.M., (2005). Outcrop-based gamma-ray characterization of the Woodford Shale of south-central Oklahoma. M.S. thesis, Oklahoma State University, pp. 160.
- Kvale, E and Bynum J. (2014), Regional Upwelling During Late Devonian Woodford Deposition in Oklahoma and Its Influence on Hydrocarbon Production and Well Completion. Woodford Shale Forum: Lecture conducted from AAPG.

- Li, M., Riediger, C.L., Fowler, M.G., Snowdon, L.R. and Abrajano Jr. T.A. (1996). Unusual polycyclic alkanes in Lower Cretaceous Ostracode sediments and related oils of the Western Canada Sedimentary Basin. *Organic Geochemistry* **25**, 199–209.
- Li, M., Wang, T., Zhong, N., Zhang, W., Sadik, A. and Li H. (2013). Ternary diagram of fluorenes, dibenzothiophenes and dibenzofurans: Indicating depositional environment of crude oil source rocks. *Energy Exploration & Exploitation* **31**, 569-588.
- Ma, X., Gong, Y., Chen, D., Racki, G., Chen, X. and Liao W. (2016). The Late Devonian Frasnian–Famennian Event in South China — Patterns and causes of extinctions, sea level changes, and isotope variations. *Palaeogeography, Palaeoclimatology, Palaeoecology* **448**, 224-244.
- Mackenzie, A. S. (1984). Application of biological markers in petroleum geochemistry. *In: Advances in Petroleum Geochemistry* **1**, 115-214.
- Mackenzie, A. S., Patience, R. L., Maxwell, J. J., Vandenbroucke, M. and Durand B. (1980). Molecular parameters of maturation in the Toarcian shales, Paris Basin, France- I. Changes in the configuration of acyclic isoprenoid alkanes, steranes, and triterpanes. *Geochimica et Cosmochimica Acta* **44**, 1709-1721.
- Marynowski, L., Narkiewicz, M., and Grelowski C. (2000). Biomarkers as environmental indicators in a carbonate complex, examples from the Middle Devonian, the Holy Cross Mountains, Poland. *Sedimentary Geology* **137**, 187–212.
- Marynowski, L. and Filipiak, P. (2007). Water column euxinia and wildfire evidence during the deposition of the Upper Famennian Hangenberg event horizon from the Holy Cross Mountains (Central Poland). *Geology Magazine* **144**, 569-595.
- Marynowski, L. and Wyszormirski, P. (2008). Organic geochemical evidences of early diagenetic oxidation of the terrestrial organic matter during the Triassic arid and semi arid climatic conditions. *Applied Geochemistry* **23**, 2612-2618.
- Marynowski, L., Rakociński, M., Borcuch, E., Kremer, B., Schubert, B. A. and Jahren A. H. (2011). Molecular and petrographic indicators of redox conditions and bacterial communities after the F/F mass extinction (Kowala, Holy Cross Mountains, Poland). *Palaeogeography, Palaeoclimatology, Palaeoecology* **306**, 1–14.
- McCarthy, K., Niemann, M., Palmowski, D., Peters, K., and Stankiewicz, A. (2011). Basic Petroleum Geochemistry for Source Rock Evaluation. *Oilfield Review* **23 (2)**, 32- 43.

- Mello, M.R., Gaglianone, P.C., Brassel, S.C. and Maxwell J.R. (1988). Geochemical and biological marker assessment of depositional environments using Brazilian offshore oils. *Marine and Petroleum Geology* **5**, 205-23.
- Mello, M.R., Telnaes, N., Gaglianone, P.C., Chicarelli, M.I., Brassel, S.C. and Maxwell J.R. (1988). Organic geochemical characterization of depositional paleoenvironments of source rocks and oils in Brazilian marginal basins. *Organic Geochemistry* **13**, 31–45.
- Miceli-Romero, A. and Philp R.P. (2012). Organic geochemistry of the Woodford Shale, southeastern Oklahoma: How variable can shales be? *American Association of Petroleum Geology Bulletin* **96**, 493-517.
- Miller, R. (1990). A paleogeographic approach to the Kimmeridge clay formation. Huc, A. (Ed.), Deposition of Organic Facies. AAPG Studies in Geology #30. *The American Association of Petroleum Geologists*, Tulsa, 13-26.
- Mizukami, T., Kaiho, K. and Oba M. (2013). Significant changes in land vegetation and oceanic redox across the Cretaceous/Paleogene boundary. *Palaeogeography, Palaeoclimatology, Palaeoecology* **369**, 41-47.
- Moldowan, J. M., Seifert W. F., Arnold E. and Clardy J. (1984). Structure proof and significance of stereoisomeric 28,30-bisnorhopanes in petroleum and petroleum source rocks. *Geochimica et Cosmochimica Acta* **48**,1651-1661.
- Moldowan, J. M., Seifert W. K. and Gallegos E. J. (1985). Relationship between petroleum composition and depositional environment of petroleum source rocks. *American Association of Petroleum Geologists Bulletin* **69**, 1255-1268.
- Moldowan, J. M., Sundararaman, P. and Schoell M. (1986). Sensitivity of biomarker properties to depositional environment and/or source input in the Lower Toarcian of S.W. Germany. *Organic Geochemistry* **10**, 915-926
- Moldowan J. M., Fago F. J., Carlson R. M. K., Young D. C., Duvne G., Clardy J., Schoell M., Pillinger C. T. and Watt D. S. (1991). Rearranged hopanes in sediments and petroleum. *Geochimica et Cosmochimica Acta* **55**, 3333–3353.
- Moldowan J.M. and McCaffrey M. A. (1995). A novel microbial hydrocarbon degradation pathway revealed by hopane demethylation in a petroleum reservoir. *Geochimica et Cosmochimica Acta* **59**, 1891-1894.

- Moldowan, J., Dahl, J., Zinniker, D. and Barbanti S. (2015). Underutilized advanced geochemical technologies for oil and gas exploration and production-1. The diamondoids. *Journal of Petroleum Science and Engineering*, **126**, 87-96.
- Molinares, C. (2013). Stratigraphy and palynomorphs composition of the Woodford Shale in the Wyche Farm Shale Pit, Pontotoc County, Oklahoma. University of Oklahoma M.S. Thesis, pp. 102.
- Mulik, J. and Erdman, J. (1963). Genesis of Hydrocarbons of Low Molecular Weight in Organic-Rich Aquatic Systems. *Science* **141(3583)**, 806-807.
- Northcutt, R., Campbell, Jock A and Oklahoma Geological Survey. (1995). Geologic provinces of Oklahoma. In: *Transactions of the 1995 American Association of Petroleum Geologists Mid-Continent Section Meeting*. compiled by Robert A. Northcutt and Jock A. Campbell. (Open-file report (Oklahoma Geological Survey), 5-95.
- Nowaczewski, V. (2011). Biomarker and paleontological investigations of the Late Devonian extinctions, Woodford Shale, southern Oklahoma. M.Sc. thesis manuscript, University of Kansas, pp. 96.
- Ogala, J. E. and Akaegbobi, M. I. (2014). Using aromatic biological markers as a tool for assessing thermal maturity of source rocks in the Campano-Maastrichtian Mamu Formation, southeastern Nigeria. *Earth Sciences Research Journal: Petroleum Geology*, **18**, 51-62.
- Ourisson G. and Albrecht P. (1992). Hopanoids: 1. Geohopanoids: The most abundant natural products on Earth? *Accounts of Chemical Research* **25**, 398-402.
- Over, D.J., (2002). The Frasnian/Famennian boundary in central and eastern United States. *Palaeogeography, Palaeoclimatology, Palaeoecology* **181**, 153-169.
- Parra, P. A., Rubio, N., Ramirez, C., Guerra, B. D. V., Exler, V. A., Campos, I. R. and Garcia M. (2013). Unconventional reservoir Development in Mexico: Lessons Learned from the First Exploratory Wells. doi:10.2118/164545-MS.
- Paxton S.T., Cruse, A.M. and Krystyniak A.M. (2006). Fingerprints of Global Sea-level Change Revealed in Upper Devonian/Lower Mississippian Woodford Shale of South-central Oklahoma. *American Association of Petroleum Geologists Search and Discovery Article #4021*.
- Paxton, S.T. and Cardott B.J. (2008). Oklahoma gas shales field trip, October 21 & 23, 2008: Oklahoma Geological Survey Open File Report **2**, 110.

- Pepper, A.S. and Corvi P.J. (1995). Simple kinetic models of petroleum formation. Part I: oil and gas generation from kerogen. *Marine Petroleum Geology* **12** (3), 291–319.
- Percival, L., Selby, D., Bond, D., Rakociński, M., Racki, G., Marynowski, L. and Föllmi, K. (2019). Pulses of enhanced continental weathering associated with multiple Late Devonian climate perturbations: Evidence from osmium-isotope compositions. *Palaeogeography, Palaeoclimatology, Palaeoecology* **524**, 240-249.
- Peters K. E. (1986). Guidelines for Evaluating Petroleum Source Rock Using Programmed Pyrolysis. *American Association of Petroleum Geologists Bulletin* **70**, 318–329.
- Peters K. E. and Moldowan J. M. (1991). Effects of source, thermal maturity, and biodegradation on the distribution and isomerization of homohopanes in petroleum. *Organic Geochemistry* **17**, 47–61.
- Peters, K. E., Kontorovich, A. E. and Moldowan, J. M. (1993). Geochemistry of selected oils and rocks from the central portion of the West Siberian Basin, Russia. *American Association of Petroleum Geologists Bulletin* **77**, 863-87.
- Peters K.E. and Cassa M. R. (1994). Applied source rock geochemistry. *American Association of Petroleum Geologists Memoir* **60**, 93-117.
- Peters, K. E., Fraser, T.H., Amris, W., Rustanto, B. and Hermanto, E. (1999). Geochemistry of crude oils from eastern Indonesia. *American Association of Petroleum Geologists Bulletin* **83**, 1403.
- Peters K. E., Walters, C. C. and Moldowan, J. M. (2005). *The biomarker guide, Volume 2: biomarkers and isotopes in petroleum exploration and earth history*. Second Edition, Cambridge University Press. USA, 1155.
- Philp, R.P. (2000). Geochemical analysis: Gas Chromatography and GC-MS. In *Encyclopedia of Separation Science*, 2948-2959.
- Philp, R.P., Chen, J.H., Fu, J.M., and Sheng, G.Y. (1992). A geochemical investigation of crude oils and source rocks from Biyang Basin, China. *Organic Geochemistry* **18**, 933-945.
- Philp, R. P. and DeGarmo, C. (2020). Geochemical characterization of the Devonian-Mississippian Woodford Shale from the McAlister Cemetery Quarry, Criner Hills Uplift, Ardmore Basin, Oklahoma. *Marine and Petroleum Geology*, **112**, 1-21.

- Poinsot, J., Schneckenburger, P., Adam, P., Schaeffer, P., Trendel, J. and Albrecht, P., (1997). Novel polycyclic polyprenoid sulfides in sediments. *Chemical Communications* **22**, 2191–2192.
- Powell, T. G. and McKirdy, D. M. (1973). Relationship between ratio of pristane to phytane, crude oil composition and geological environment in Australia. *Nature* **243**, 37-9.
- Pratt, L. M., Comer, J. B. and Brassell S. C. (1992). Geochemistry of Organic Matter in Sediments and Sedimentary Rocks. *SEPM (Society for Sedimentary Geology)*, **93(1)**, 150-151.
- Radke, M., Welte, D. H., and Willsch, H. (1991). Distribution of alkylated aromatic hydrocarbons and dbt in rocks of the Upper Rhine Graben. *Chemical Geology* **93**, 325-341.
- Rathey, R. P. and Hayward, A.B., (1993). Sequence stratigraphy of a failed rift system: the Middle Jurassic to Early Cretaceous evolution of the Central and Northern North Sea. Parker, J. R. (Ed.), *Petroleum Geology of North West Europe*, Proceedings of the fourth Conference 215-249.
- Requejo, A.G., Wielchowsky, C. C., Klosterman, M. J., and Sassen, R. (1994). Geochemical characterization of lithofacies and organic facies in Cretaceous organic-rich rocks from Trinidad, East Venezuela Basin. *Organic Geochemistry* **22**, 441-459.
- Roberts, C.T., and Mitterer, R.M., (1992). Laminated black shale-bedded chert cyclicity in the Woodford Formation, southern Oklahoma, in K.S. Johnson and B.J. Cardott, eds., *Source rocks in the southern Midcontinent, 1990 symposium: Oklahoma Geologic Society Circular* **93**, 330-336.
- Robinson, L.N. and Kirschbaum, M.A. (1995). Paleogeography of the Late Cretaceous of the Western Interior of middle North America – coal distribution and sediment accumulation. *USGS Professional Paper* **1561**, 1-115.
- Romero, A. M. (2008). Geochemical characterization of the Woodford Shale, Central and Southeastern Oklahoma. University of Oklahoma M.S. Thesis, pp. 289.
- Romero, A. M. and Philp R. P. (2012). Organic geochemistry of the Woodford Shale, southeastern Oklahoma: How variable can shales be? *American Association of Petroleum Geologists Bulletin* **96**, 493–517.
- Rubinstein, I., Sieskind, O. and Albrecht, P. (1975). Rearranged steranes in a shale: occurrence and simulated formation. *Journal of Chemical Society, Perkin Transaction*, **I**, 1833-6.

- Sammy, N. (1985). Biological systems in northern Australia solar salt and fields. In: Schreiber, B.C., Harner, L., eds., 6th International Symposium on Salt. Salt Institute, Alexandria, Virginia 1, 207-215.
- Schmid, J. C. (1986). Marqueurs biologiques soufres dans les petroles. Ph.D. thesis, University of Strausbourg, Strasbourg, France, pp. 262.
- Schwark, L. and Frimmel. (2004). Chemostratigraphy of the Posidonia Black Shale, SW-Germany: II. Assessment of extent and persistence of photic-zone anoxia using aryl isoprenoid distributions. *Chemical Geology* **206(3)**, 231-248.
- Schwark, L. and Empt, P. (2006). Sterane biomarkers as indicators of palaeozoic algal evolution and extinction events. *Palaeogeography, Palaeoclimatology, Palaeoecology* **240**, 225–236.
- Seifert, W. K. and Moldowan, J. M. (1979). The effect of biodegradation on steranes and terpanes in crude oils. *Geochimica et Cosmochimica Acta* **43**, 111-126.
- Serna-Bernal, A. (2013). Geological Characterization of the Woodford Shale, McAlister Cemetary Quarry, Criner Hills, Ardmore Basin, Oklahoma. M.S. Thesis, The University of Oklahoma, pp. 141.
- Sieskind, O., Joly, G. and Albrecht, P. (1979). Simulation of the geochemical transformation of sterols: superacid effects of clay minerals. *Geochimica et Cosmochimica Acta*, **43**, 1675-9.
- Simoneit, B. R. T., Schoell, M., Dias, R.F. and Aquino Neto, F. R., (1993). Unusual carbon isotope compositions of biomarker hydrocarbons in a Permian tasmanite. *Geochimica et Cosmochimica Acta* **57**, 4205-4211.
- Sinninghe Damsté, J., Keely, B., Betts, S., Baas, M., Maxwell, J. and De Leeuw, J. (1993). Variations in abundances and distributions of isoprenoid chromans and long-chain alkylbenzenes in sediments of the Mulhouse Basin: A molecular sedimentary record of palaeosalinity. *Organic Geochemistry* **20(8)**, 1201-1215.
- Sinninghe Damste, J. S., Kenig, F., Koopmans, M., P., Koster, J., Schouten, S., Hays, J. M. and de Leeuw, J. W. (1995). Evidence for gammacerane as an indicator of water column stratification. *Geochimica et Cosmochimica Acta* **59(9)** 1895-1900.

- Slatt, R.M. (2013). Paleotopographic and Depositional Environment Control on ‘Sweet Spot’ Locations in Some Unconventional Resource Shales. Presented at Houston Geological Society.
- Slatt, R.M., (2013). Sequence stratigraphy of the Woodford Shale and application to drilling and production: AAPG Search and Discovery Article #50792, Oral presentation AAPG Woodford Shale Forum, Oklahoma City, April 11, 2013.
- Slatt, R.M., (2016). Institute of Reservoir Characterization (IRC), Woodford-Mississippian consortium, phase III technical report. The University of Oklahoma, 202.
- Slatt, R. M. and Rodriguez, N. D. (2012). Comparative sequence stratigraphy and organic geochemistry of gas shales: Commonality or coincidence? *Journal of Natural Gas Science and Engineering* **8**, 68–84.
- Smith, H.M. (1968). Qualitative and quantitative aspects of crude oil composition. *US Bureau of Mines Bulletin* **642**, 1-136.
- Speczik, S., Bechtel, A., Sun, Y. Z., and Puttman, W. (1995). A stable isotope and organic geochemical study of the relationship between the Antracosia shale and Kupferschiefer mineralization (SE Poland). *Chemical Geology* **123**, 133-151.
- Soliman, A., Abdelfattah, M. and Ahmed Yassin, M. (2015). Unconventional Reservoir: Definitions, Types and Egypt’s Potential. 10.13140/RG.2.1.3846.0880.
- Strachan, M.G., Alexander, R., and Kagi, R.I., 1988. Trimethylnaphthalenes in crude oils and sediments: Effects of source and maturity. *Geochimica et Cosmochimica Acta*, **52**, 1255-1264.
- Suneson, N. H., C. Ibrahim., K. Dennis., S. Roberts., T. Michael., R. M. Slatt and Stone, C. G. (2005). Stratigraphic and structural evolution of the Ouachita Mountains and Arkoma Basin, southeastern Oklahoma and west-central Arkansas: applications to petroleum exploration. *Oklahoma Geological Survey Guidebook* **34**, 128-134.
- Telanes, N. and Cooper, B. S. (1991). Oil-source rock correlation using biological marker, Norwegian continental shelf. *Marine and Petroleum Geology* **8**, 302-310.
- Temraz, M., Mousa, D. and Lofty, M. (2016). Evaluation of the Shale Beds within ALam El bueib formation as an unconventional reservoir, Western Desert, Egypt. *Journal of Petroleum Exploration and Production Technology* **8(1)**, 43-49.
- ten Haven H. L., Leeuw J. W., Peakman T. M. and Maxwell J. R. (1986). Anomalies in steroid and hopanoid maturity indices. *Geochimica et Cosmochimica Acta* **50**, 853-855.

- Ten Haven, H. L., de Leeuw, J. W., Sinninghe Damste J. S., Schenck P.A., Palmer, S. E. and Zumberge, J. E. (1988). Application of biological markers in the recognition of paleohypersaline environments. *Lacustrine Petroleum Source Rocks* **40**, 123-130.
- Tissot, B., Durand, B., Espitalie, J. and Combaz, A., (1974). Influence of nature and diagenesis of organic matter in the formation of petroleum. *American Association of Petroleum Geologists Bulletin* **58(3)**, 499-506
- Tissot, B. P. and Welte D. H. (1984). *Petroleum Formation and Occurrence*. Springer-Verlag, New York, 540.
- Tornabene, T. G., Langworth, T. A., Holzer, G. and Oro, J. (1979). Squalenes, phytanes and other isoprenoid as major neutral lipids of methanogenic and thermoacidophilic "archaeobacteria". *Journal of Molecular Evolution* **13**, 73-83.
- Torres-Parrada, E. J. (2020). Woodford Shale enclosed mini-basin fill on the Hunton Pale Shelf. A depositional model for unconventional resource shales. Phd manuscript pp. 362.
- Treanton, J.A. (2014). Outcrop-derived chemostratigraphy of the Woodford Shale, Murray County, Oklahoma. M.S. thesis, The University of Oklahoma, pp.83.
- Tulipani, S., Grice, K., Greenwood, P., Haines, P. W., Summons, R. E., Bottcher, M. E., Foster, C. B., Woltering, M. and Playton T. (2013). Changes in palaeoenvironmental conditions in Late Devonian reef systems from the Canning Basin, WA: a biomarker and stable isotope approach. *Wabs 2013*, 1.
- Tulipani, S., Grice, K., Greenwood, P., Haines, P., Sauer, P., Schimmelmann, A. and Schwark, L. (2015). Changes of palaeoenvironmental conditions recorded in Late Devonian reef systems from the Canning Basin, Western Australia: A biomarker and stable isotope approach. *Gondwana Research* **28(4)**, 1500-1515.
- Turner, B.J., (2016). Utilization of Chemostratigraphic Proxies For Generating And Refining Sequence Stratigraphic Frameworks in Mudrocks and Shales, Ph.D dissertation, University of Oklahoma, 135.
- Turner, B.W., J.A. Tréanton and R.M. Slatt, (2016). The use of chemostratigraphy to refine ambiguous sequence stratigraphic correlations in marine mudrocks. An example from the Woodford Shale, Oklahoma, USA: London, *Journal of the Geological Society* **173 (5)**, 854-868.

- Van Kaam-Peters, H. M. E., Köster, J., Van Der Gaast, S. J., Dekker, M., De Leeuw, J. W. and Sinninghe Damsté J. S. (1998). The effect of clay minerals on diasterane/sterane ratios. *Geochimica Cosmochimica Acta* **62**, 2923–2929.
- van Krevelen, D. W. (1984). Organic geochemistry—old and new. *Organic Geochemistry* **6**, 1–10.
- Volkman, J. K. (1986). A review of sterol markers for marine and terrigenous organic matter. *Organic Geochemistry* **9**, 83-99.
- Volkman, J. K. (1984). Biodegradation of aromatic hydrocarbons in crude oils from Barrow Sub-basin of Western Australia. *Organic Geochemistry* **6**, 619-632.
- Volkman, J. K. (1988). Biological marker compounds as indicators of the depositional environments of petroleum source rocks. *Lacustrine Petroleum Source Rocks* (A. J. Fleet, K. Kelts, and M. R. Talbot, eds.), Blackwell, London, 103-22.
- Wang, K. (1992). Glassy microspherules (microtektites) from an Upper Devonian limestone. *Science*, **256**, 1547–1550.
- Wang, G., Goodfellow and Drouse (1996). Carbon and sulfur isotope anomalies across the Frasnian-Famennian extinction boundary, Alberta, Canada. *Geology* **24**(2), 187.
- Wang, X., Liu, S., Wang, Z., Chen, D. and Zhang, L. (2018). Zinc and strontium isotope evidence for climate cooling and constraints on the Frasnian-Famennian (~372 Ma) mass extinction. *Palaeogeography, Palaeoclimatology, Palaeoecology* **498**, 68-82.
- Waples, D. W. and Machihara, T. (1990). Application of sterane and triterpane biomarkers in petroleum exploration. *Bulletin of Canadian Petroleum Geology* **38**(3), 357-380.
- Wu, L. and Geng, A. (2016). Differences in the thermal evolution of hopanes and steranes in free and bound fractions. *Organic Geochemistry* **101**, 38-48.
- Wust, R. A. J., Nassichuk, B. R., Brezovski, R., Hackley, P. C. and Willment, N. (2013). Vitrinite reflectance versus pyrolysis Tmax data: Assessing thermal maturity in shale plays with special reference to the Duvernay shale play of the Western Canadian Sedimentary Basin, Alberta, Canada. *Society of Petroleum Engineers Conference*. doi:10.2118/167031-MS.

- Xu, B., Gu, Z., Wang, Chengyuan, H., Qingzhen, H., Jingtai, L. and Qiang, Lu, Y. (2012). Carbon isotopic evidence for the associations of decreasing atmospheric CO₂ level with the Frasnian-Famennian mass extinction. *Journal of Geophysical Research: Biogeosciences*, v. **117**(G1).
- Yang, G. P., Liu, X. L. and Zhang, J. W. (1998). Distribution of dibenzothiophene in the sediments of the South China Sea. *Environment Pollution* **101** (3), 405-414.
- Youngblood, W. W. and Blumer, M. (1975). Polycyclic aromatic hydrocarbons in the environment: homologous series in soils and recent marine sediments. *Geochimica et Cosmochimica Acta* **39**, 1303-1314.
- Zeng, Y., Fu, X., Zeng, S., Du, G., Chen, J., Zhang, Q., Zhang, Y. and Yao, Y. (2011). Organic Geochemical Characteristics of the Bilong Co. Oil Shale (China): Implications for Paleoenvironment and Petroleum Prospects. *Oil Shale* **28** (3), 398-414.
- Zhang, X., Joachimski, M., Over, D., Kunyuan, M., Cheng, Huang. and Yiming, G. (2019). Late Devonian carbon isotope chemostratigraphy: A new record from the offshore facies of South China. *Global and Planetary Change*. 182. 103024.
- Zumberge, J.E. (1987). Prediction of source rock characteristics based on terpane biomarkers in crude oils: a multivariate statistical approach. *Geochimica et Cosmochimica Acta* **51**, 1625–1637.

Appendix I: Naphthalenes and Phenanthrenes

Naphthalenes and phenanthrenes are among the most common aromatic hydrocarbons in crude oils and can be used to determine thermal maturity of oils and extracts. When the relative abundance of 1,2,7-trimethylnaphthalene (**14**) predominates over the 1,2,5-trimethylnaphthalene (TMN; **17**), this is an indication of early oil window or immature extract (Strachan et al., 1988; Akinlua et al., 2007; Philp and DeGarmo, 2020). The Speake Ranch samples illustrate that the 1,2,7-TMN predominates over the 1,2,5-TMN throughout the Middle Woodford. However, in the Upper Woodford abundance of 1,2,7-TMN is observed to significantly decrease, while 1,2,5-TMN predominates. This clearly suggests that the Middle Woodford is immature, while the Upper Woodford experiences higher thermal maturity. The 1,2,5-TMN and the 1,2,7-TMN are suggested to originate from constituents of angiosperms, such as the β -amyrin (Strachan et al., 1988; Ogala and Akegbobi, 2014). Furthermore, these compounds can form as diagenetic products of oleanane-type triterpenoids (Chaffee and Johns, 1982; Chaffee et al., 1984; Ogala and Akegbobi, 2014). Golovko et al. (2014) indicated that the alkylated naphthalenes are less resistant to thermal alteration than the phenanthrenes and their alkylated derivatives. The thermal alterations of the methylnaphthalenes (MN) and dimethylnaphthalenes (DMN) occur upon removal of the n-alkanes (Fisher et al., 1998; Peters et al., 2005). Additionally, the trimethylphenanthrenes are altered during removal of isoprenoids, while tetramethylphenanthrenes remain unaltered until steranes are significantly depleted (Fisher et al., 1998; Peters et al., 2005). Naphthalenes and the alkylated naphthalenes were screened on the GC-MS at m/z 128, 142, 156, 170, 184, 198, 212, 226 (Figure 1; Table 1). Alkylated naphthalenes are not only a product of different genesis and different deposition ages, but they are also the products of alteration from varying organic matter sources. The effect of sedimentation environment and influence of catagenesis cause a secondary conversion of the

alkylnaphthalenes into more stable molecules with substituents in the β -positions (Ogala and Akaegbobi, 2014; Golovko et al., 2014). Therefore, the relative changes in β - and α -isomers of the alkylnaphthalenes have been used to indicate thermal maturity as well. The stable 2-ethyl,3-methylnaphthalene ($\beta\beta$) relative to the less stable 1-ethyl,2-methylnaphthalene ($\alpha\beta$) ($\beta\beta/\alpha\beta$ -ethyl-methylnaphthalene) is largely enhanced throughout the samples of Speake Ranch, and is also seen to frequently oscillate (Figure 2). This indicates that secondary conversions of the alkylnaphthalenes to the more stable β -positions had resulted, and therefore illustrates an increase in the degree of rock transformation.

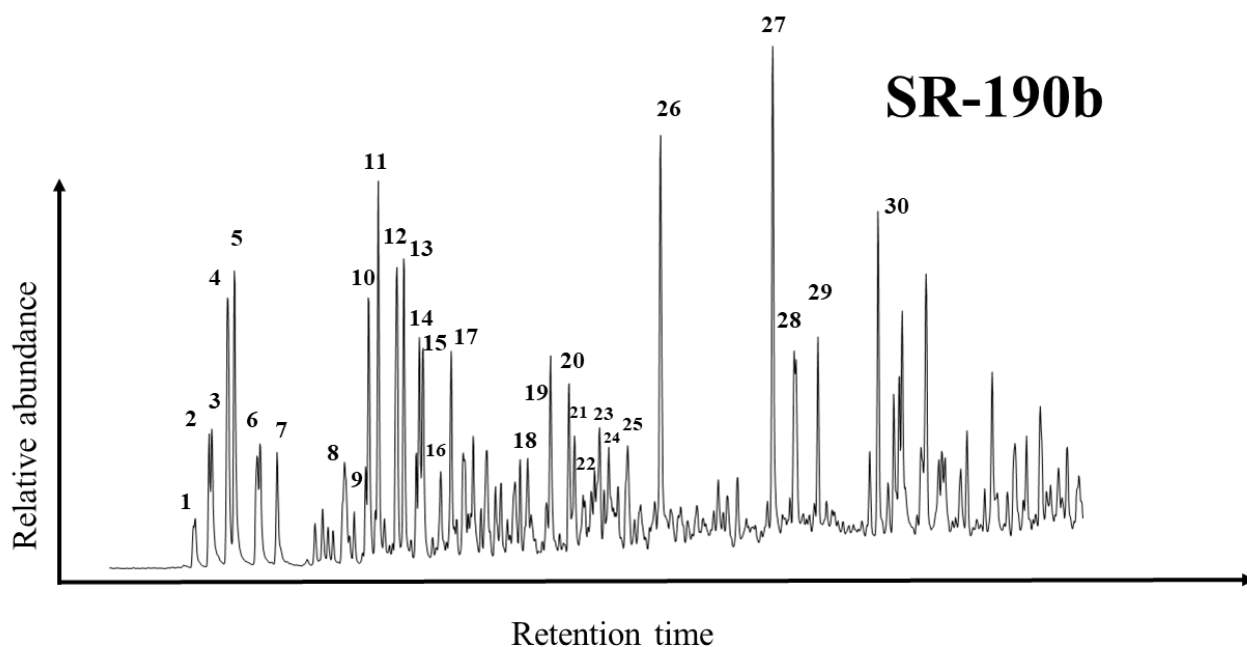


Figure 1. Distribution of the naphthalenes and the alkylated naphthalenes screened on the GC-MS at m/z 128, 142, 156, 170, 184, 198, 212, 226.

Peak No.	Compound	Peak No.	Compound
1	1-Ethyl-naphthalene	16	1,2,4-Trimethylnaphthalene
2	2,6-Dimethylnaphthalene	17	1,2,5-Trimethylnaphthalene
3	2,7-Dimethylnaphthalene	18	1,3,5,7-Tetramethylnaphthalene
4	1,3+1,7-Dimethylnaphthalene	19	1,3,6,7-Tetramethylnaphthalene
5	1,6-Dimethylnaphthalene	20	1,2,4,7-Tetramethylnaphthalene
6	1,5-Dimethylnaphthalene	21	1,2,5,7-Tetramethylnaphthalene
7	1,2-Dimethylnaphthalene	22	2,3,6,7-Tetramethylnaphthalene
8	2-Ethyl,3-methylnaphthalene ($\beta\beta$)	23	1,2,6,7-Tetramethylnaphthalene
9	1-Ethyl,2-methylnaphthalene ($\alpha\beta$)	24	1,2,3,6-Tetramethylnaphthalene
10	1,3,7-Trimethylnaphthalene	25	1,2,5,6-Tetramethylnaphthalene
11	1,3,6-Trimethylnaphthalene	26	Dibenzothiophene
12	1,4,6-+1,3,5-Trimethylnaphthalene	27	4-Methyldibenzothiophene
13	2,3,6-Trimethylnaphthalene	28	3-+2-Methyldibenzothiophene
14	1,2,7-Trimethylnaphthalene	29	1-Methyldibenzothiophene
15	1,4,7+1,2,7-Trimethylnaphthalene	30	Dimethyldibenzothiophene

Table 1. Peak identifications for m/z 128, 1492, 156, 170, 184, 198, 212, 226 of naphthalenes and alkylnaphthalenes.

The naphthalene and its alkylated derivatives have also been used as a proxy for biodegradation. The level of biodegradation experienced can be seen using DBR [DBR=1,6-dimethylnaphthalene (**5**)/1,5-dimethylnaphthalene (**6**)], TBR [TBR= 1,3,6-trimethylnaphthalene (**11**)/1,2,4-trimethylnaphthalene (**16**)], and TeBR [TeBR= 1,3,6,7-tetramethylnaphthalene (**19**)/1,3,5,7-tetramethylnaphthalene (**18**)] ratios developed by Fisher et al. (1998). The reduction of the ratio values should indicate rising levels of biodegradation according to Fisher et al. (1998). There is an apparent oscillation from 190-194ft across DBR, TBR, and TeBR depth plots, whereby lower values are found within the harder beds, and relatively higher values are observed at the softer beds of Speake Ranch (Figure 2). The reduction of the DBR, TBR and TeBR values within the harder beds (190-194ft) suggests that these intervals experienced relatively higher levels of biodegradation than their overlying and underlying softer beds. This confirms the earlier finding

that utilized the XRF data of Mo/Al to determine weathering, where hard bed lithofacies experienced higher level of weathering. The DBR, TBR, and TeBR show an interesting trend whereby at the contact of the Upper and Middle Woodford, a significant shift is found. Values are seen to shift to lower values in DBR and TBR within the Upper Woodford, while values in TeBR experienced an elevated shift. The decreasing shift in values for DBR and TBR indicate that significant level of biodegradation occurred in the Upper Woodford.

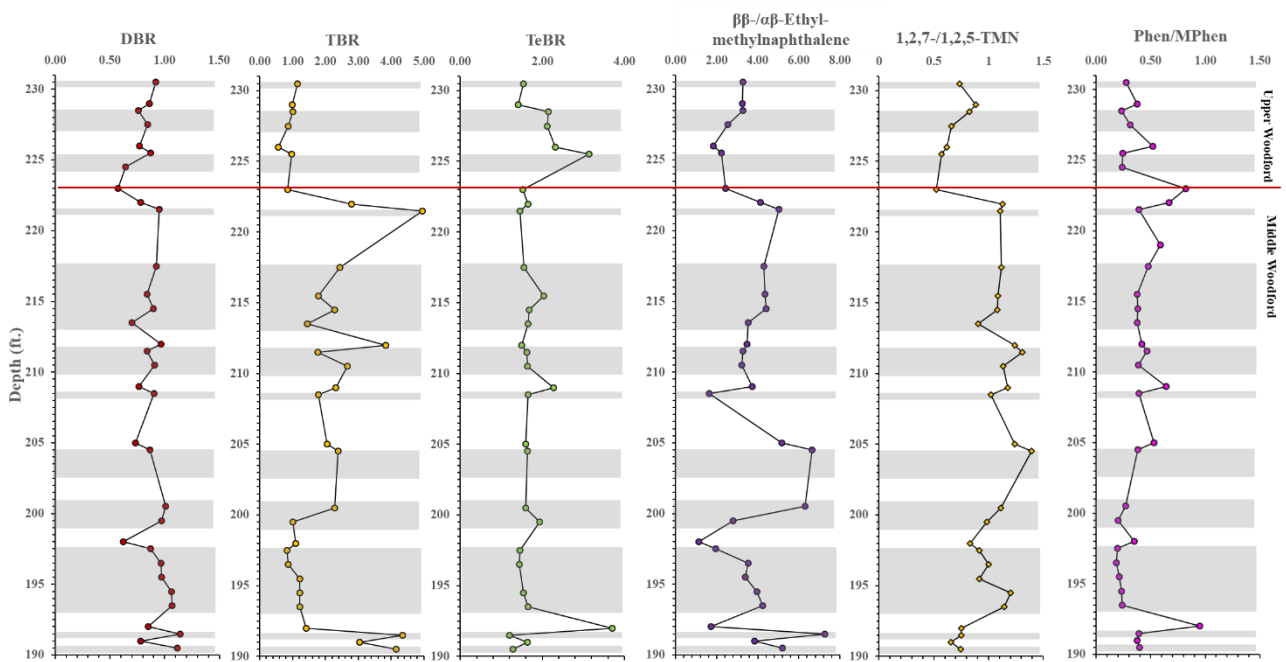


Figure 2. Depth plots of the biodegradation parameters utilizing the alkylated naphthalenes. DBR, TBR, TeBR, MNR, $\beta\beta$ -/ $\alpha\beta$ -ethyl-methylnaphthalene ratio and 1,2,7/1,2,5-TMN.

It was earlier discussed that relative concentrations of the alkylnaphthalenes generally reflect the presence of gymnosperms and terrigenous input into the system. Resins of higher plants, bryophytes, containing cadalene carbon skeleton convert to DMN and TMN with catagenetic effects, thus substitutions of the alkylnaphthalenes also make a reliable indicator of terrigenous input (de Leeuw et al., 1991). Golovko et al. (2014) suggested that marine organic matter derived oils are dominated by DMN over the MN, TMN, and naphthalenes. Additionally, he also suggested that a predominance of TMN over DMN, MN, and naphthalenes is found within continental oils, suggesting terrigenous source matter input (Golovko et al., 2014). The ternary plot of DMN-TMN-TeMN, reveal that the Speake Ranch is depleted with the DMN concentration, and has relatively higher values of TMN and TeMN (Figure 3). This suggests a predominant terrigenous source input. However, this does not align to the organic matter source finding that we utilized using sterane and terpane biomarkers. These values had possibly experienced alteration from weathering as well as the removal of n-alkanes as previously discussed.

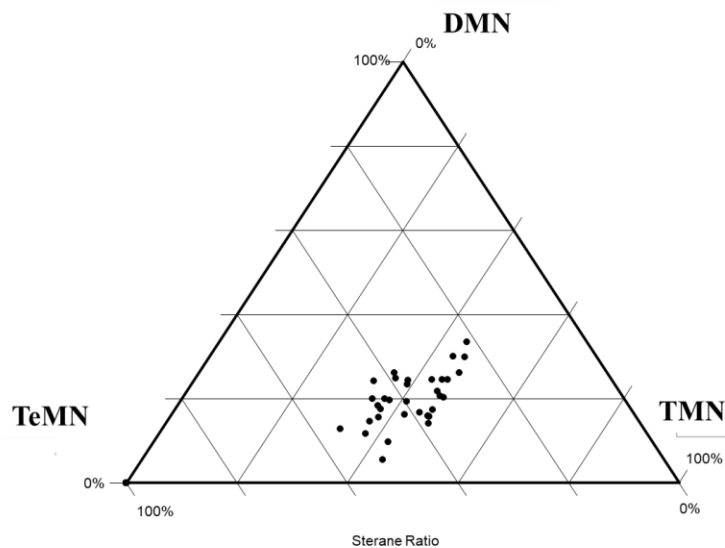


Figure 3. Ternary plot of DMN, TMN, and TeMN to determine relative concentrations of the alkylated derivatives of the naphthalenes.

Phenanthrenes behave in a similar manner to the naphthalenes with increasing alkylation. Though, they are more resistant to biodegradation than alkyl naphthalenes (Philp and deGarmo, 2020). The abundance of phenanthrenes over the alkyl derivatives, methylphenanthrenes, is suggested to be attributed to pyrolysis and combustion derived PAH illustrating a source from natural fires (Youngblood and Blumer, 1975). The distribution of the phenanthrenes and their alkylated derivatives are screened on the GC-MS at m/z 178, 192, 206, 220, 234 (Figure 4). Therefore, phenanthrene/methylphenanthrene (phenanthrene/3-+2-+9-+1-methylphenanthrene) ratio has widely been used as a parameter to evaluate level of weathering (Radke et al., 1987). It is suggested that with increasing oxidation within the system, the phenanthrenes are thought to be more stable than their methylated derivatives (Clayton and King, 1987; Gieskes et al., 1990; Speczik et al., 1995; Marynowski and Wyszomirski, 2008). Thus, an increase in the phenanthrene/methylphenanthrene ratio is an indication of weathering, possibly a modern surface weathering from sea level regression or paleoweathering. An overall increase towards Upper Woodford at Speake Ranch does suggest that weathering was enhanced approaching the Upper Woodford (Figure 2). However, the phenanthrene/methylphenanthrene illustrates a shift to depletion in values in the Upper Woodford and this is possibly due to the predominating methylphenanthrene reflecting paleoweathering. An important factor to note is that the effect of paleoweathering by enhanced concentration of methylphenanthrene may be accurate if the mechanism of its generation is controlled by sedimentary methylation (Alexander et al., 1995; Jiang et al., 1998).

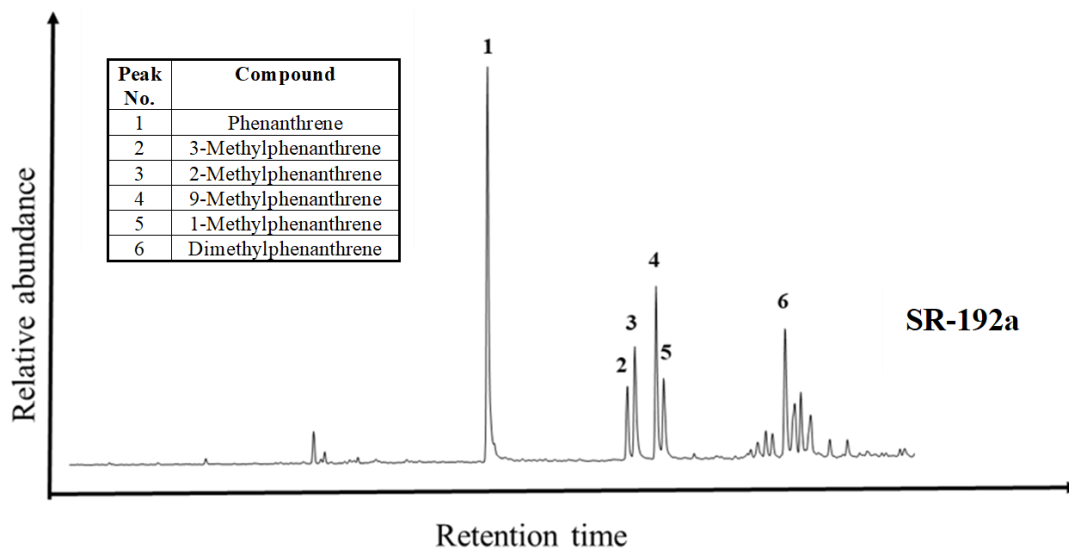
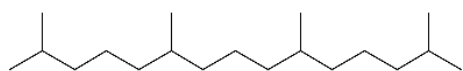


Figure 4. Phenanthrene and methylphenanthrene distribution screened on the GC-MS at m/z 178, 192, 206, 220, 234.

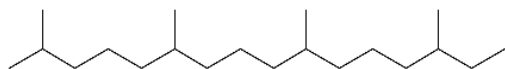
Appendix II: Compound Structures



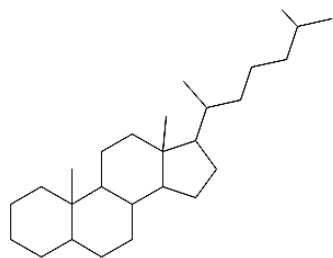
I: C₁₇ n-Alkane



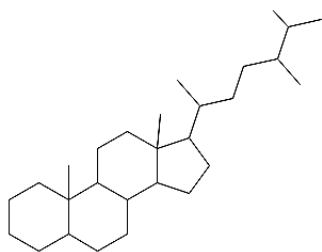
II: Pristane



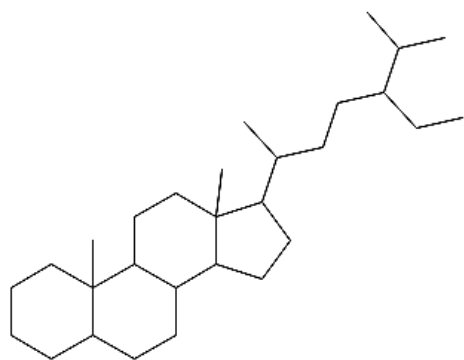
III: Phytane



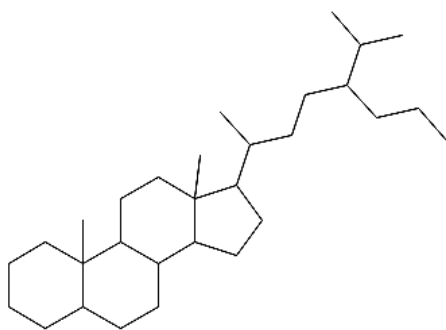
IV: C₂₇ Sterane



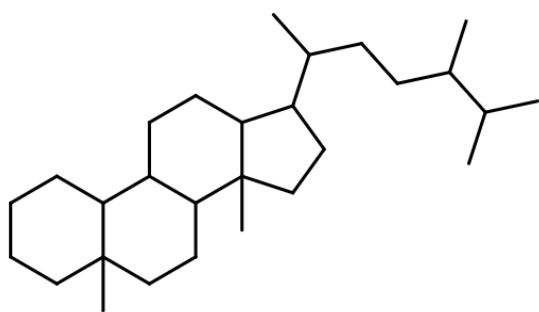
V: C₂₈ Sterane



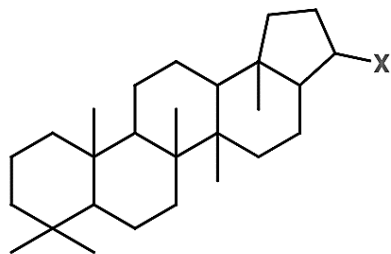
VI: C₂₉ Sterane



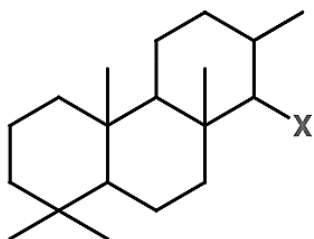
VII: C₃₀ Sterane



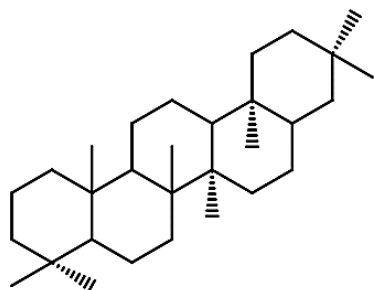
VIII: C₂₇ Diasterane



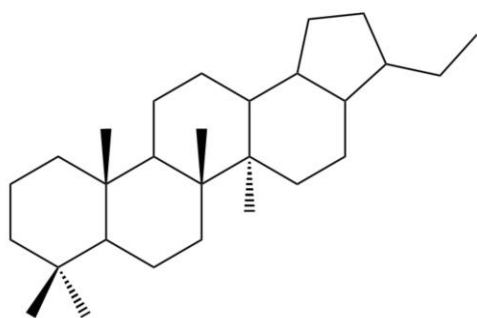
IX: Hopane



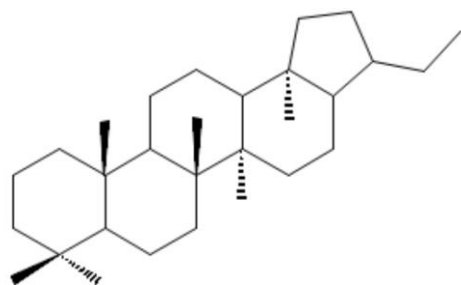
X: Tricyclic Terpane



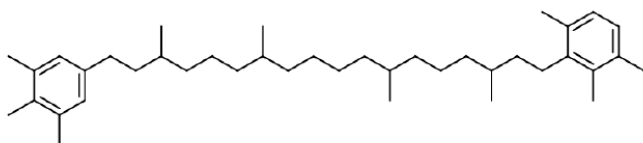
XI: Gammacerane



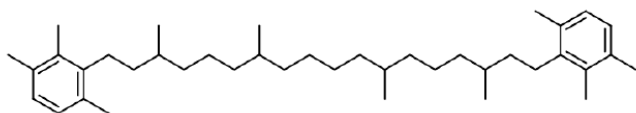
XII: C₂₈ Bisnorhopane



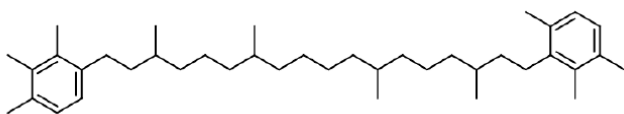
XIII: C₂₉ Norhopane



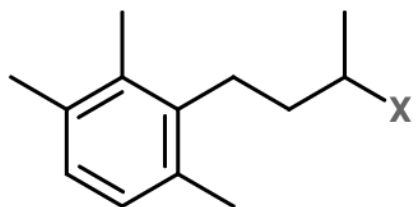
XIV: Paleorenieratane



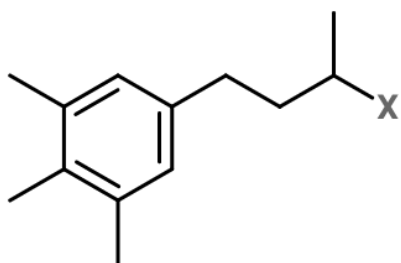
XV: Isorenieratane



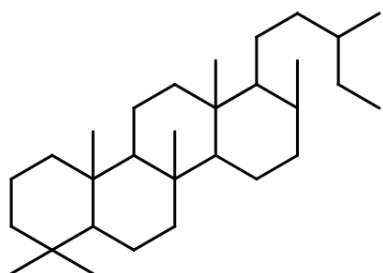
XVI: Renieratane



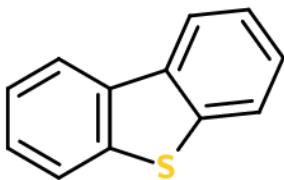
XVII: 2,3,6-TMB



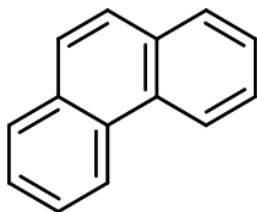
XVIII: 3,4,5-TMB



XIX: Tetracyclic Polyprenoid (C₃₀)



XX: Dibenzothiophene



XXI: Phenanthrene

XIII: Tetracyclic Polyprenoid (C₃₀)

Appendix III: Abbreviations and formulas for calculation of geochemical biomarkers

Maturity Parameters	Formula
$C_{29} 20S / (20S + 20R)$	$C_{29} [14\alpha, 17\alpha\text{-Stigmastane (20S)}] / [14\alpha, 17\alpha\text{-Stigmastane (20S+20R)}]$
$C_{29} \beta\beta / (\beta\beta + \alpha\alpha)$	$C_{29} [14\beta, 17\beta\text{-Stigmastane (20S+20R)}] / [14\beta, 17\beta\text{-} + 14\alpha, 17\alpha\text{-Stigmastane (20S+20R)}]$

Organic Matter Source	Formula
$C_{27}\%$, $C_{28}\%$, $C_{29}\%$	$C_{27}, C_{28}, C_{29} [C_{27} = C_{27} \alpha\alpha\alpha 20R / (C_{27} \alpha\alpha\alpha 20R + C_{28} \alpha\alpha\alpha 20R + C_{29} \alpha\alpha\alpha 20R \text{ Steranes})]$
C_{27}/C_{29} Steranes	$(C_{27} \alpha\alpha\alpha (S+R) + C_{27} \alpha\beta\beta (S+R)) / (C_{29} \alpha\alpha\alpha (S+R) + C_{29} \alpha\beta\beta (S+R))$
Sterane Index	$C_{30} / (C_{27}-C_{30}) = [C_{30} 14\alpha, 17\alpha\text{-} + 14\beta, 17\beta \text{ Steranes (20S+20R)}] / \Sigma C_{27}, C_{28}, C_{29}, C_{30} [14\alpha, 17\alpha\text{-} + 14\beta, 17\beta \text{ Steranes (20S+20R)}]$
$C_{23} TT / C_{24} Tet$	$C_{23} \text{ Tricyclic terpane} / C_{24} \text{ Tetracyclic terpane}$
$C_{26}/C_{25} TT$	$C_{26}/C_{25} \text{ Tricyclic terpanes}$
$C_{30} \text{ Hopane} / C_{27} \text{ Diasterane}$	$C_{30} \text{ Hopane} / C_{27} 13\beta, 17\alpha\text{-Diacholestane}$
$C_{30} \text{ TPP} / C_{27} \text{ Diasterane}$	$C_{30} \text{ Tetracyclic Polyprenoid} / C_{27} 13\beta, 17\alpha\text{-Diacholestane}$
$C_{27}/\text{total steranes}$	$(C_{27} \alpha\alpha\alpha (S+R) + C_{27} \alpha\beta\beta (S+R)) / (C_{27}\text{-}C_{30} \text{ Steranes})$

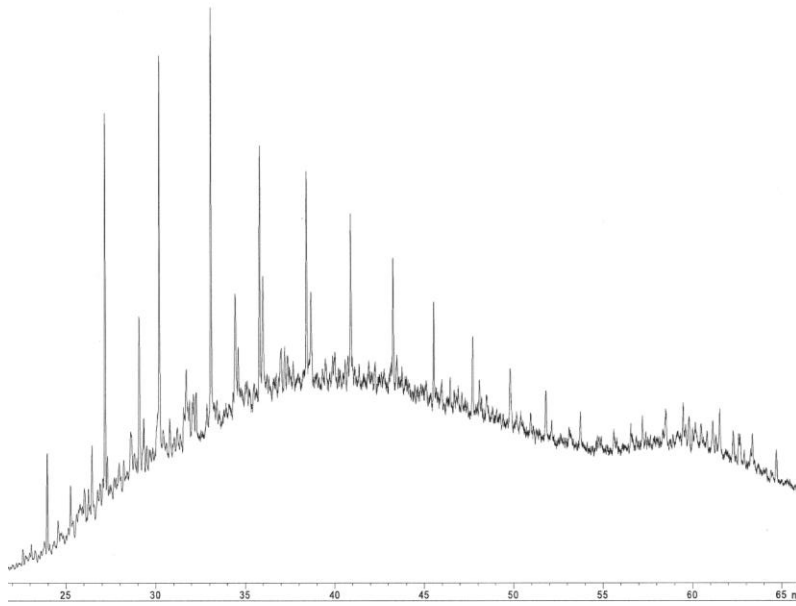
Environmental Indicators	Formula
$C_{35}/C_{34} HH$	$C_{35} 17\alpha, 21\beta\text{-Pentakishomohopane (22S+22R)} / C_{34} 17\alpha, 21\beta\text{-Tetrakishomohopane (22S+22R)}$
Homohopane Index (%)	$C_{35} / (C_{31} - C_{35}) = C_{35} 17\alpha, 21\beta\text{-Pentakishomohopane (22S+22R)} / [C_{31} + C_{32} + C_{33} + C_{34} + C_{35} 17\alpha, 21\beta\text{-Homohopanes (22S+22R)}]$
AIR	$(C_{13}\text{-}C_{17}) / (C_{18}\text{-}C_{22}) 2,3,6\text{-Trimethyl substituted aryl isoprenoids}$
Gammacerane Index	$\text{Gammacerane} / C_{30} \text{ Hopane}$
Pr/Ph	$C_{19} \text{ Pristane} / C_{20} \text{ Phytane}$
Ts/Tm	$18\alpha\text{-}22, 29, 30\text{-Trisnorneohopane} / 17\alpha\text{-}22, 29, 30\text{-Trisnorhopane}$
$C_{30} \text{ Diahopane} / C_{29} Ts$	$C_{30} 17\alpha \text{ Diahopane} / C_{29} Ts$
$C_{28} \text{ BNH} / C_{30} \text{ Hopane}$	$C_{28} \text{ Bisnorhopane} / C_{30} \text{ Hopane}$
$C_{28} \text{ BNH} / C_{29} \text{ Norhopane}$	$C_{28} \text{ Bisnorhopane} / C_{29} \text{ Hopane}$
$C_{18}\text{-Aryl isoprenoid}$	$C_{18} 2,3,6\text{-Trimethyl substituted aryl isoprenoids} / C_{18} 3,4,5\text{-Trimethyl substituted aryl isoprenoids}$

Lithology Proxies	Formula
C ₂₇ Dia/Sterane	[C ₂₇ 13β,17α-Diacholestane (20S+20R)]/[C ₂₇ 14α,17α- + 14β,17β-Cholestane (20S+20R)]
Diasterane/Steranes	[C ₂₇ 13β,17α- + 13α,17β-Diacholestane (20S+20R)]/[C ₂₇ 14α,17α- + 14β,17β-Cholestane (20S+20R)]
C ₂₇ /C ₂₉ diasteranes	[C ₂₇ 13β,17α-Diacholestane 20R + 13α,17β-Diacholestane 20S]/[24-Ethyl-13β,17α-Diacholestane 20R + -13α,17β-Diacholestane 20S]

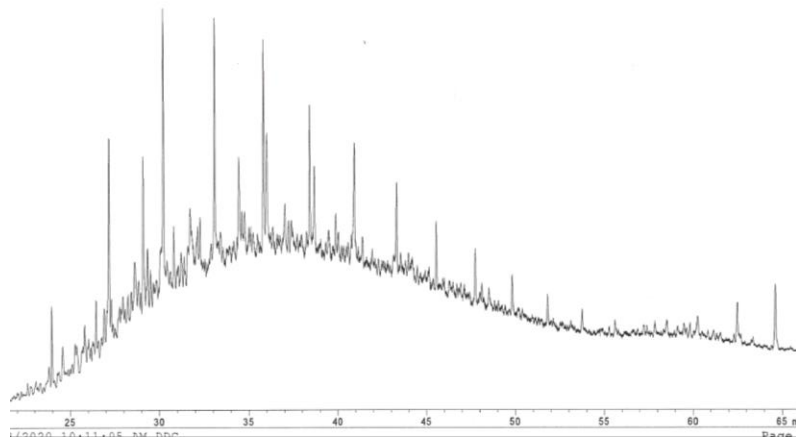
APPENDIX IV

GC-Chromatograms

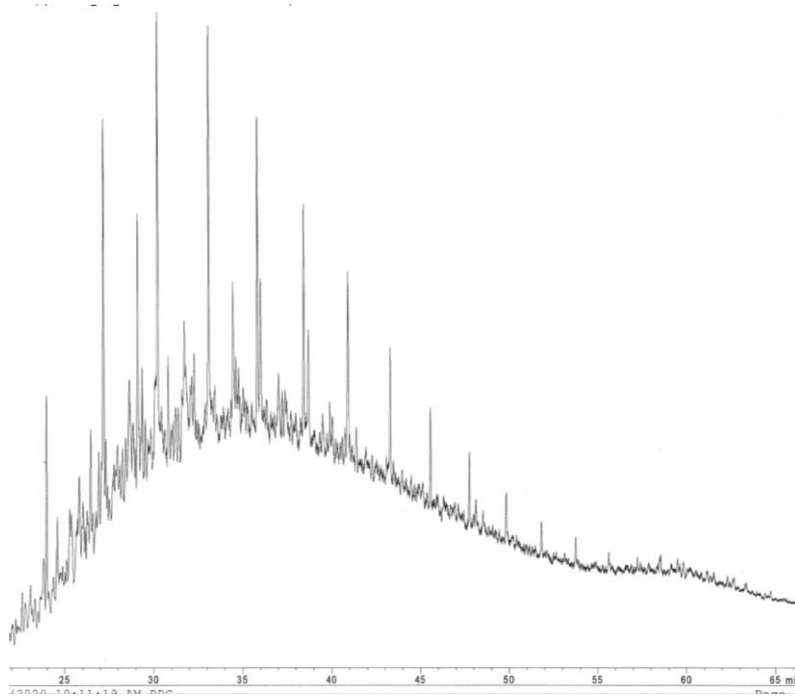
TAP759



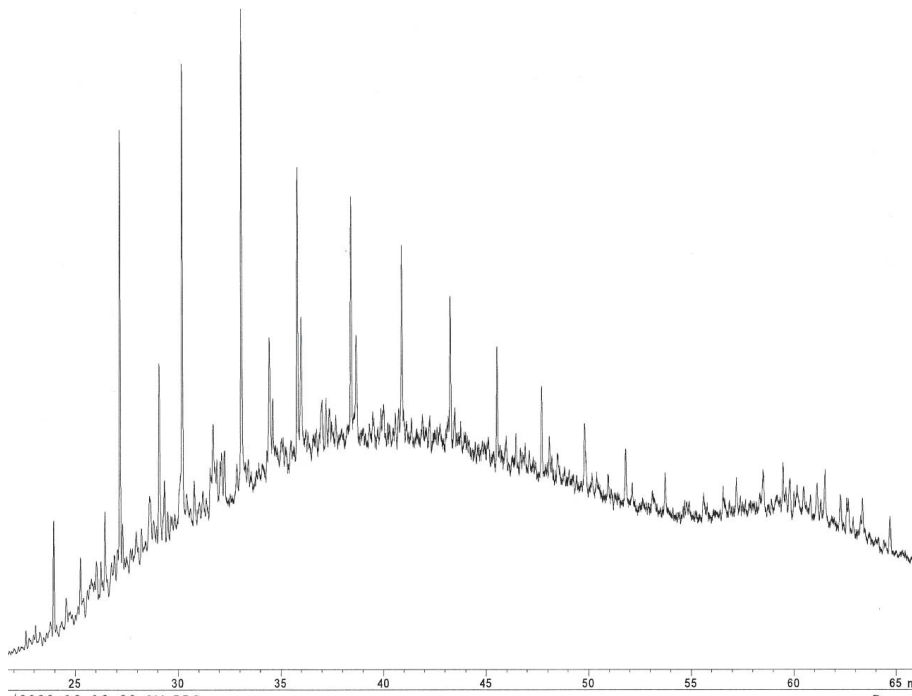
TAP751



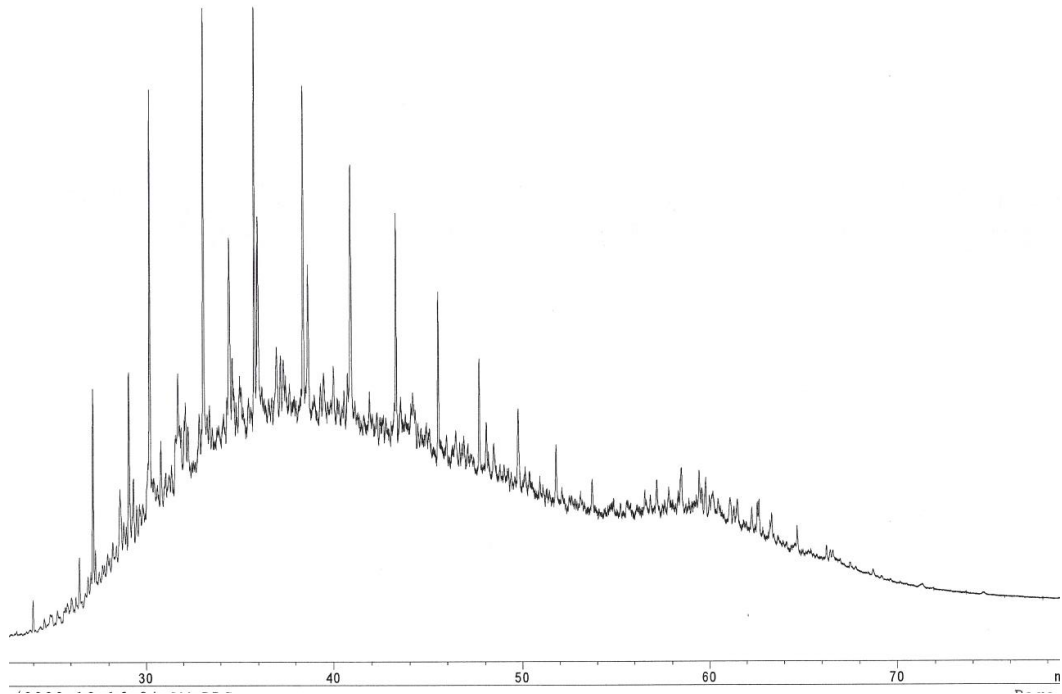
TAP752



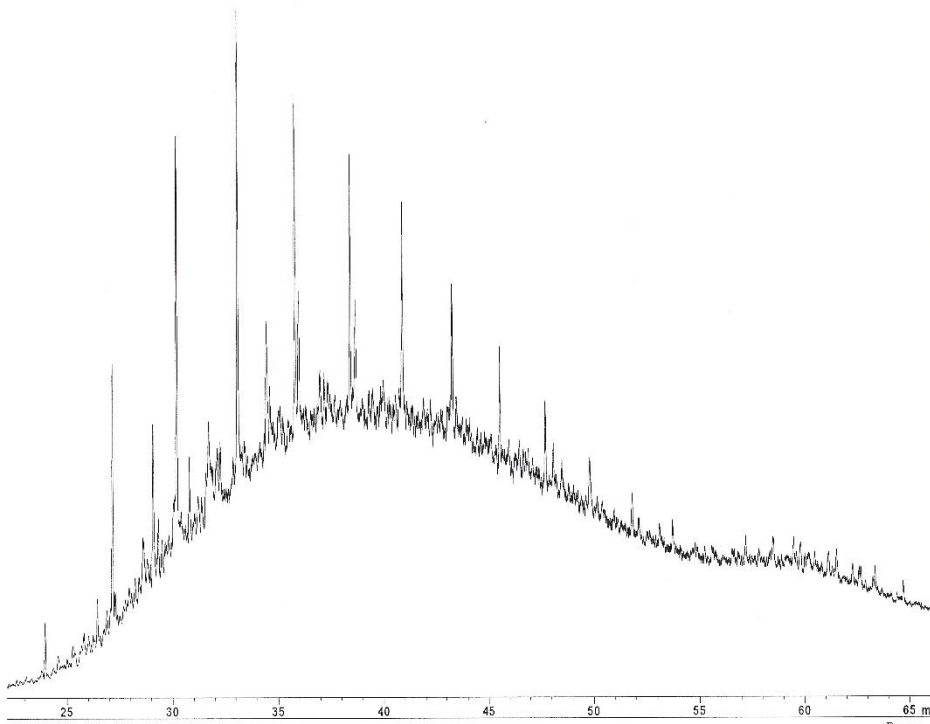
TAP759



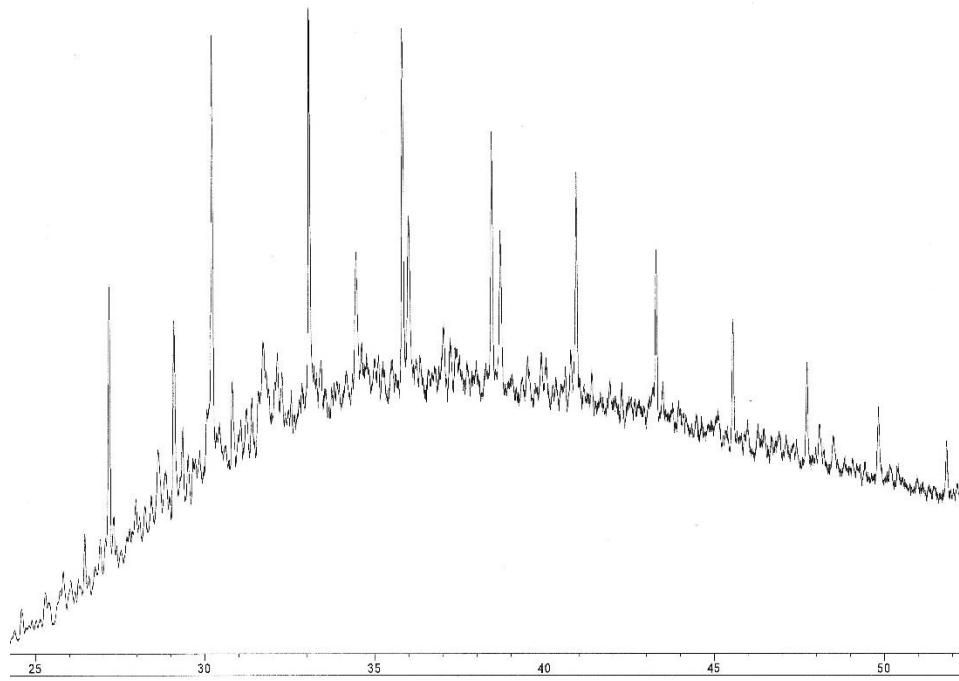
TAP766



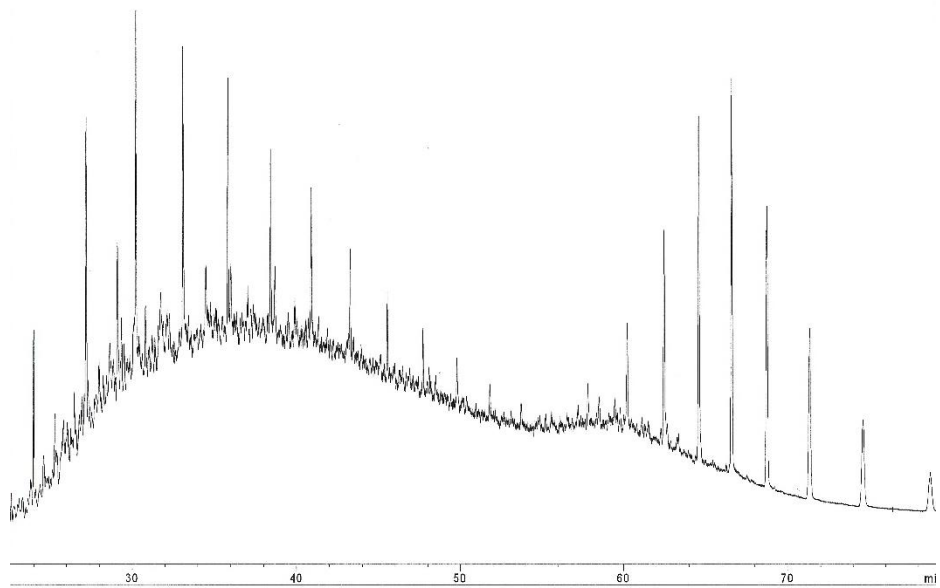
TAP758



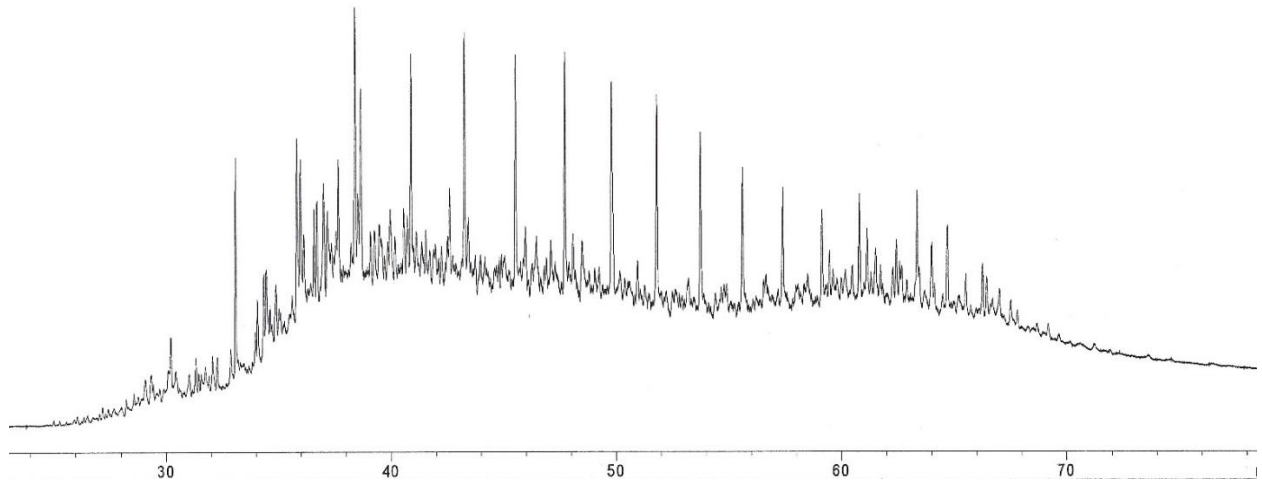
TAP760



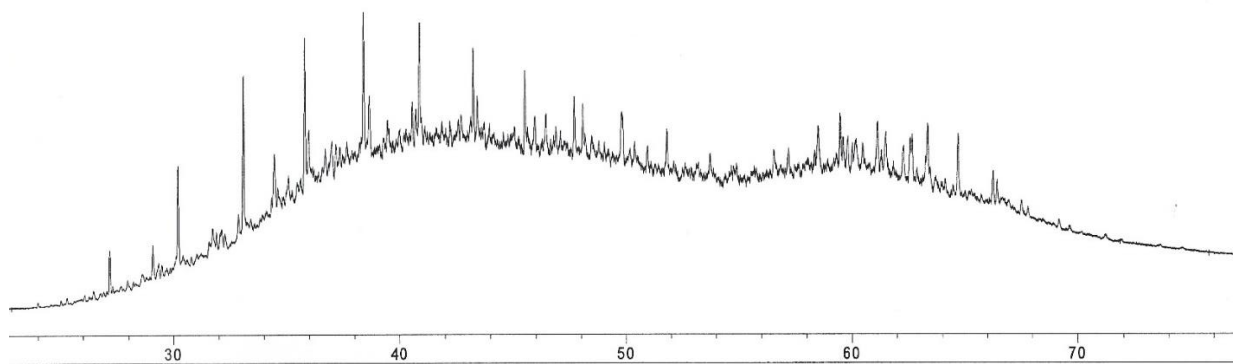
TAP 761



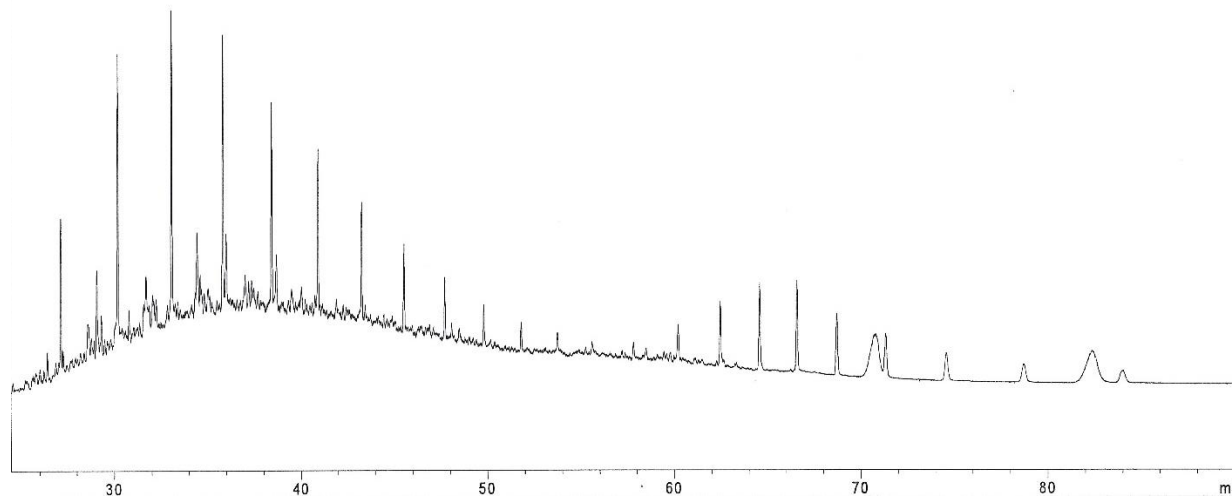
TAP765



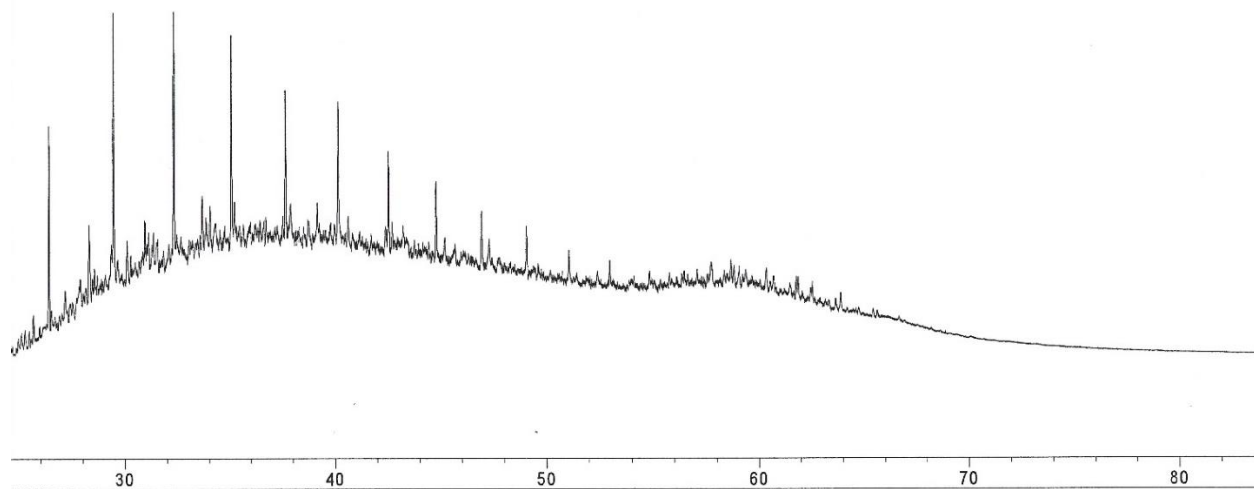
TAP767



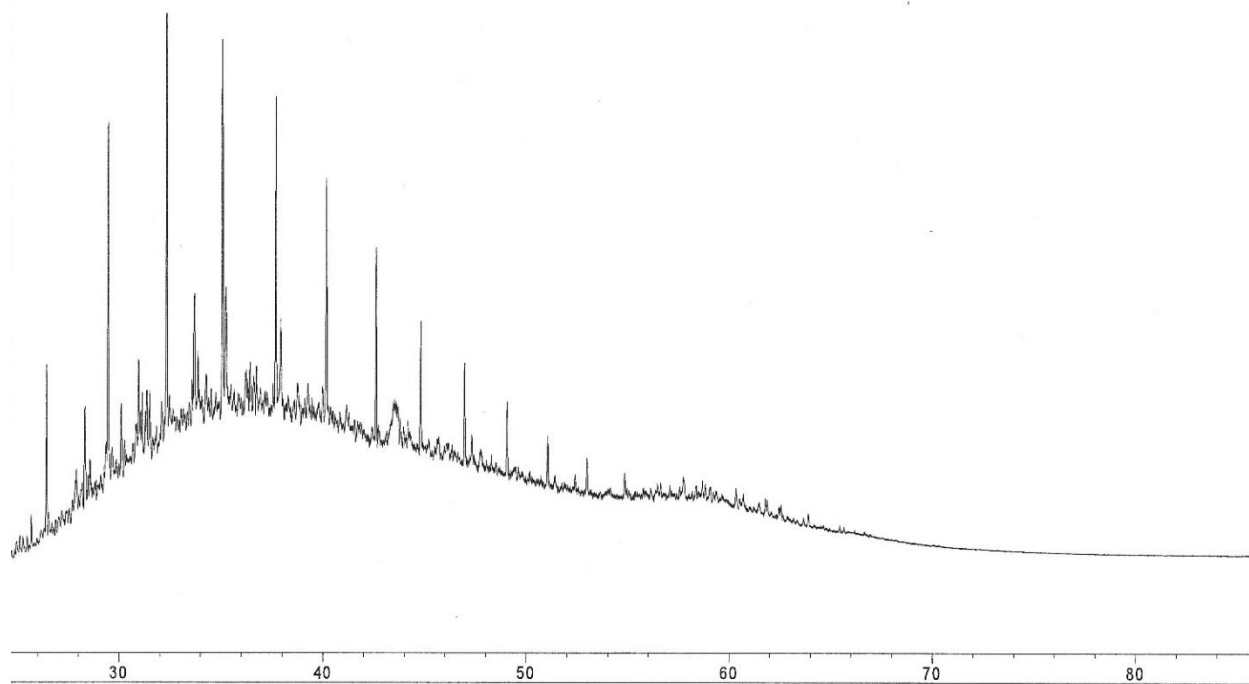
TAP769



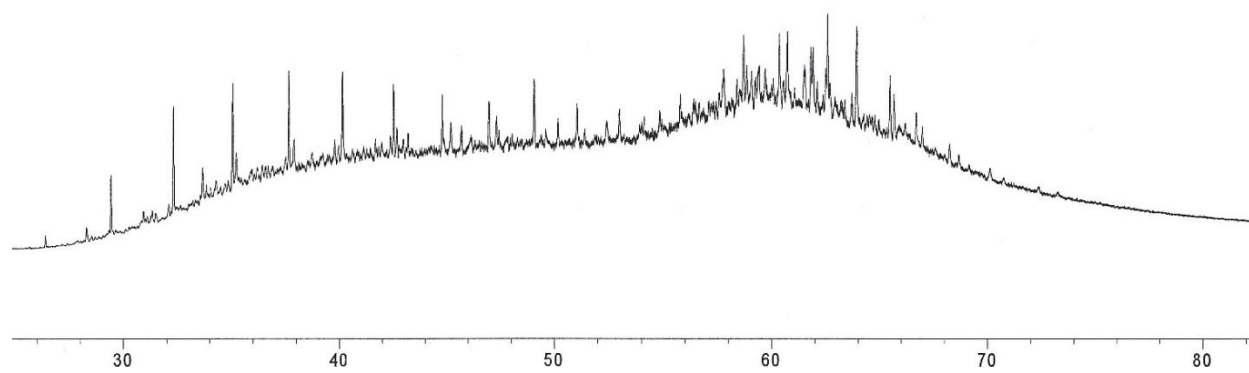
TAP 826



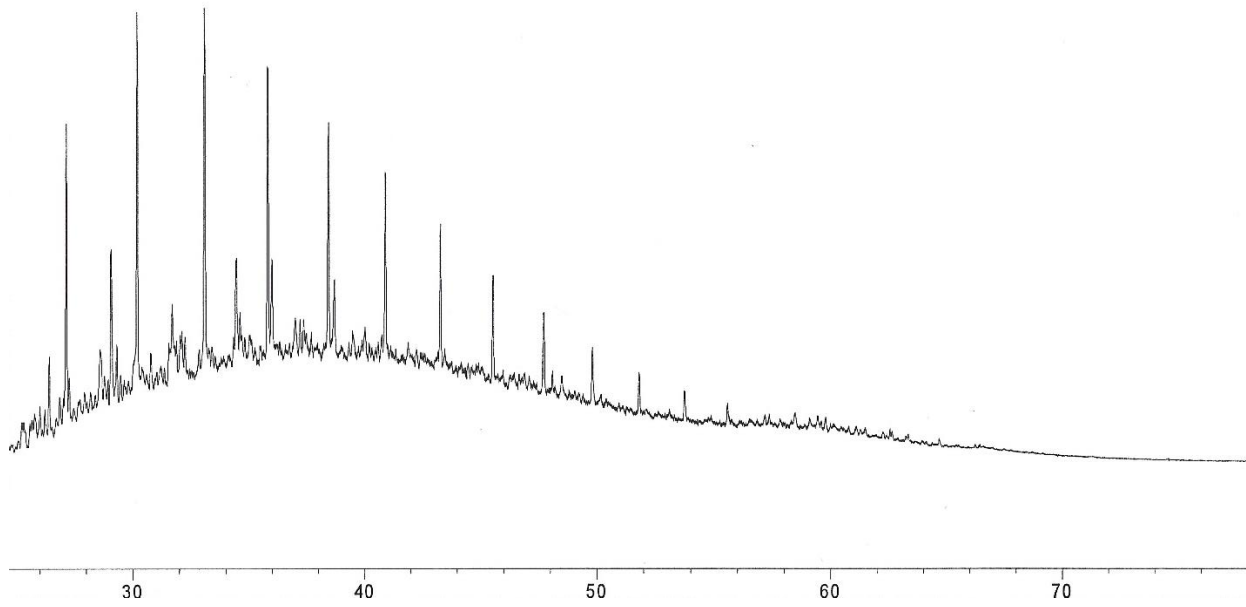
TAP827



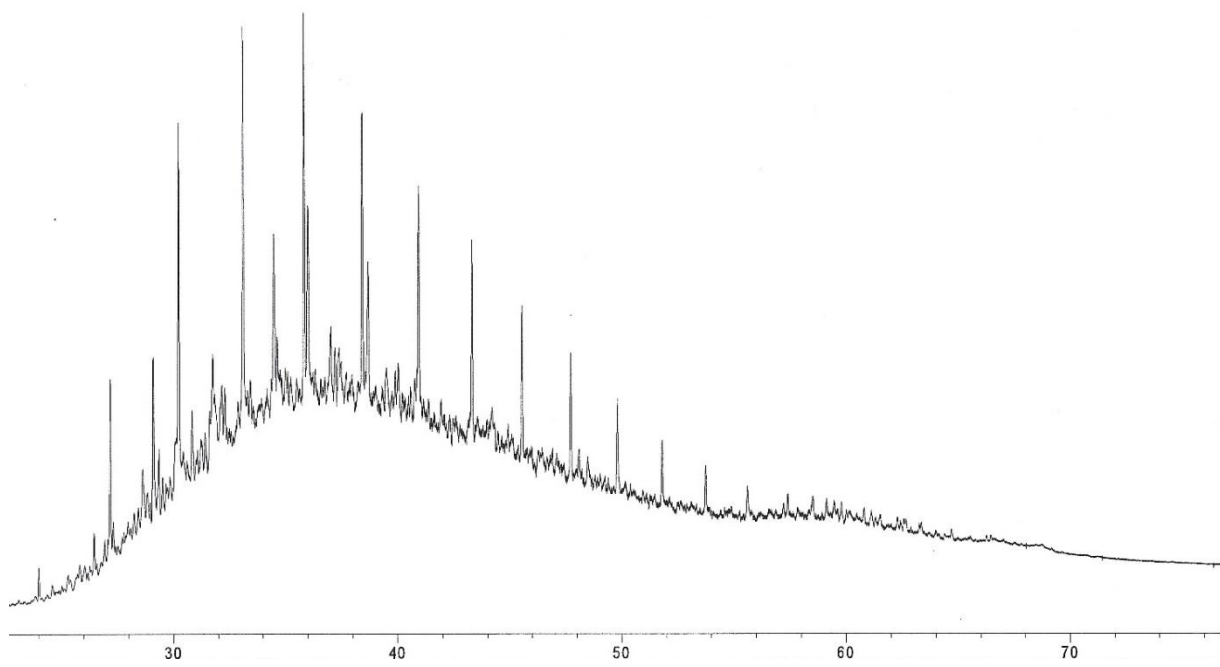
TAP828



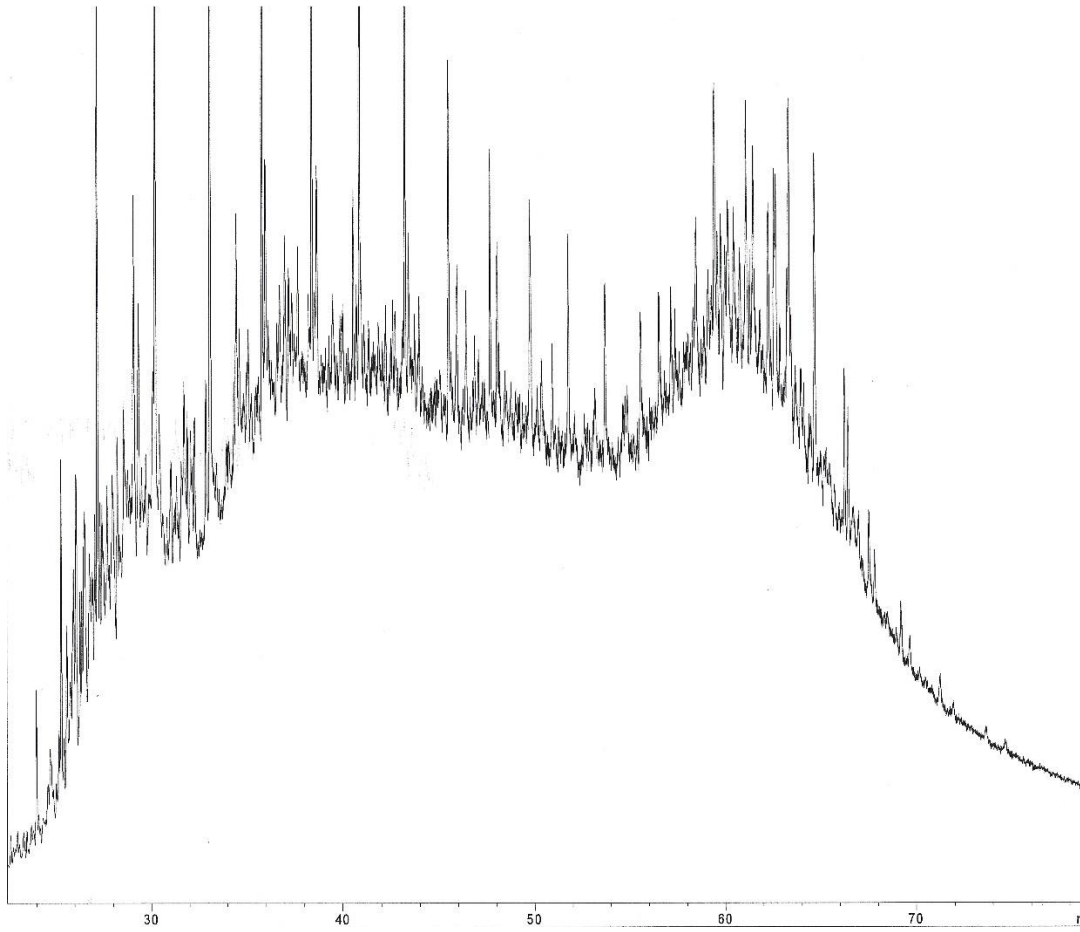
TAP 772



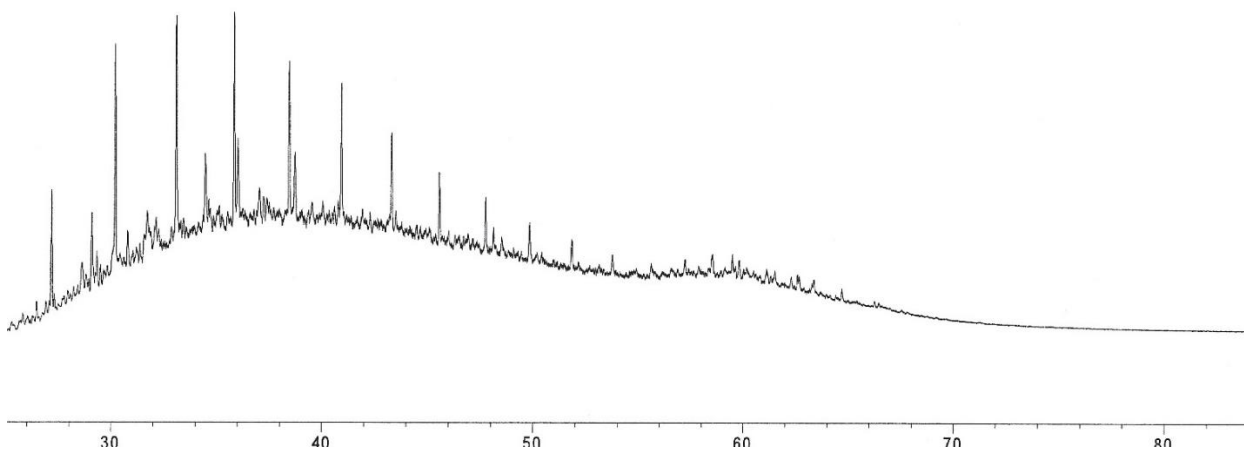
TAP763



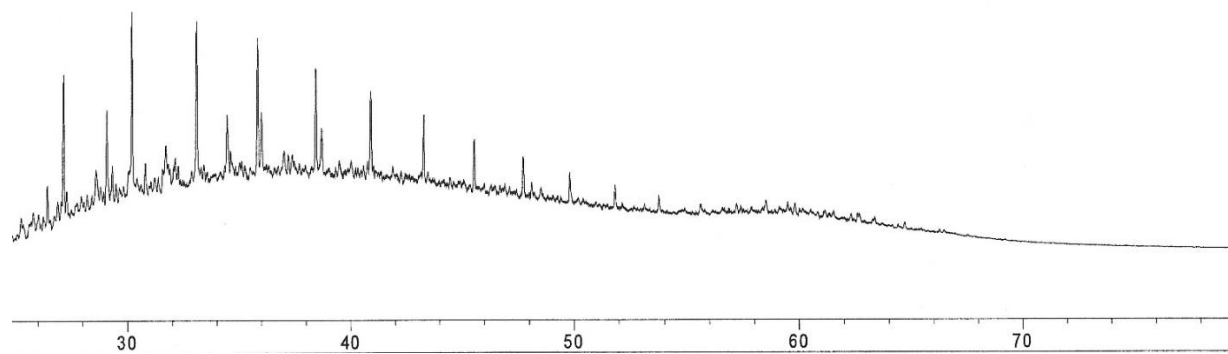
TAP764



TAP722

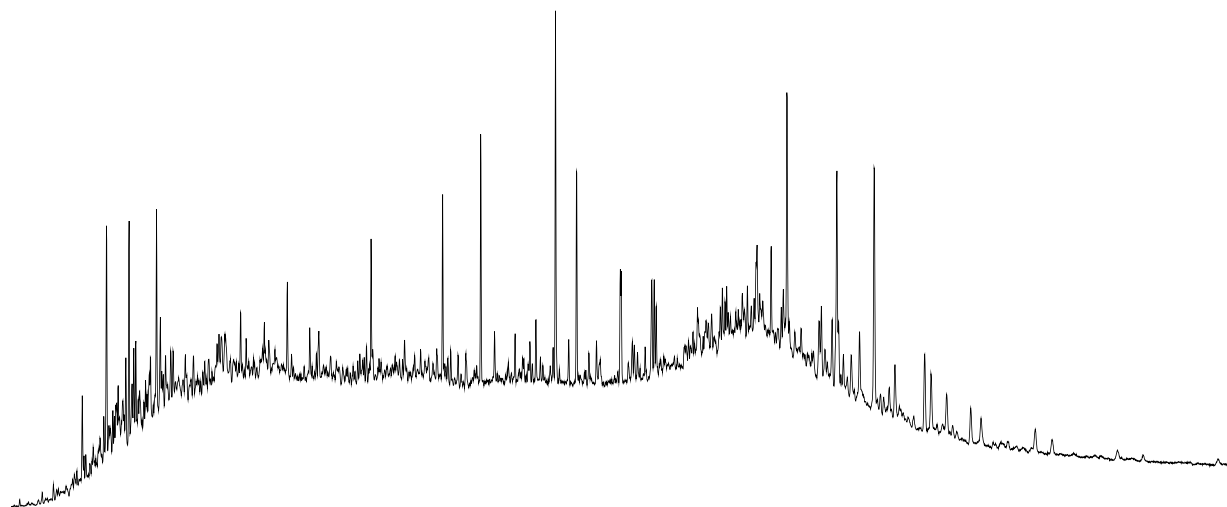


TAP724

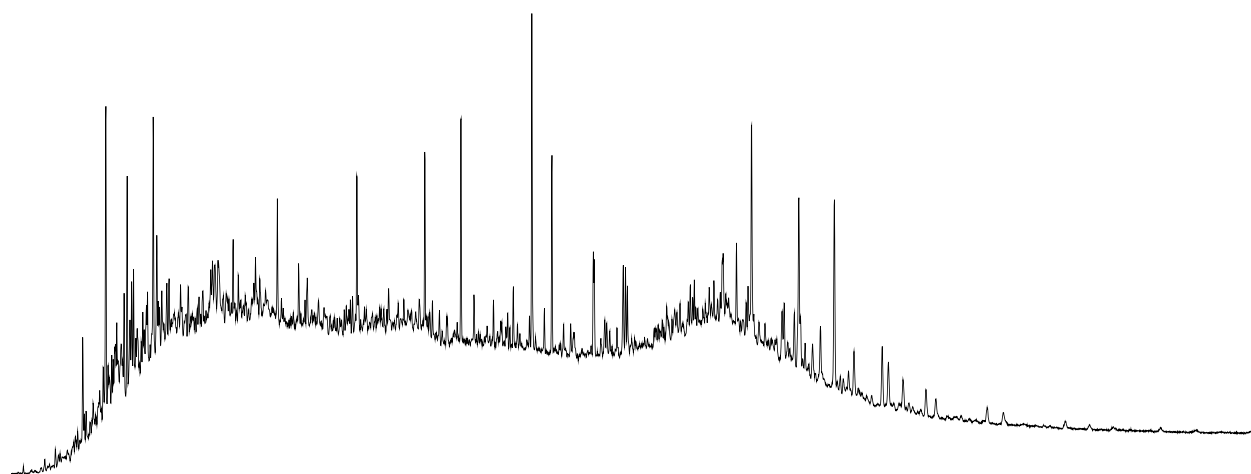


SATURATES M/Z 191

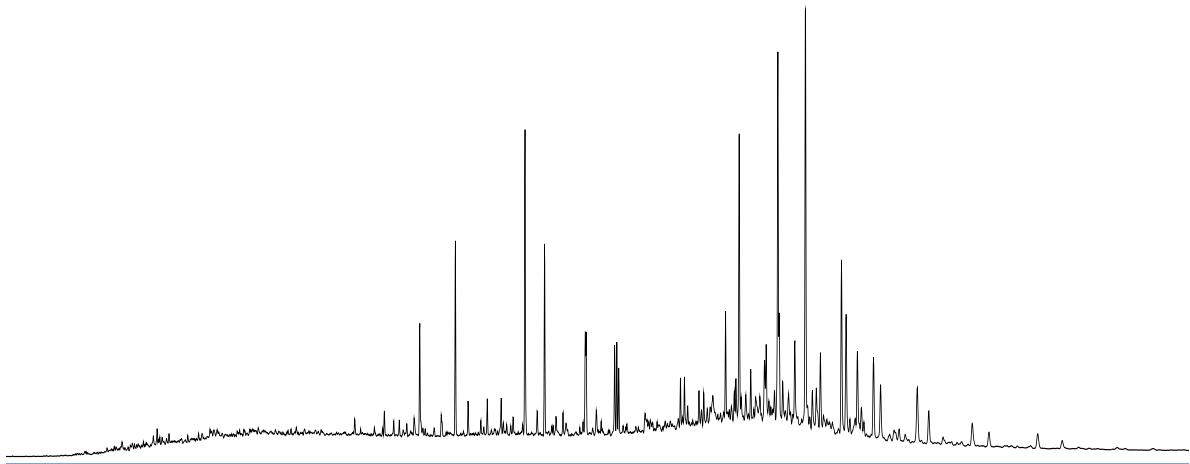
SR-190b



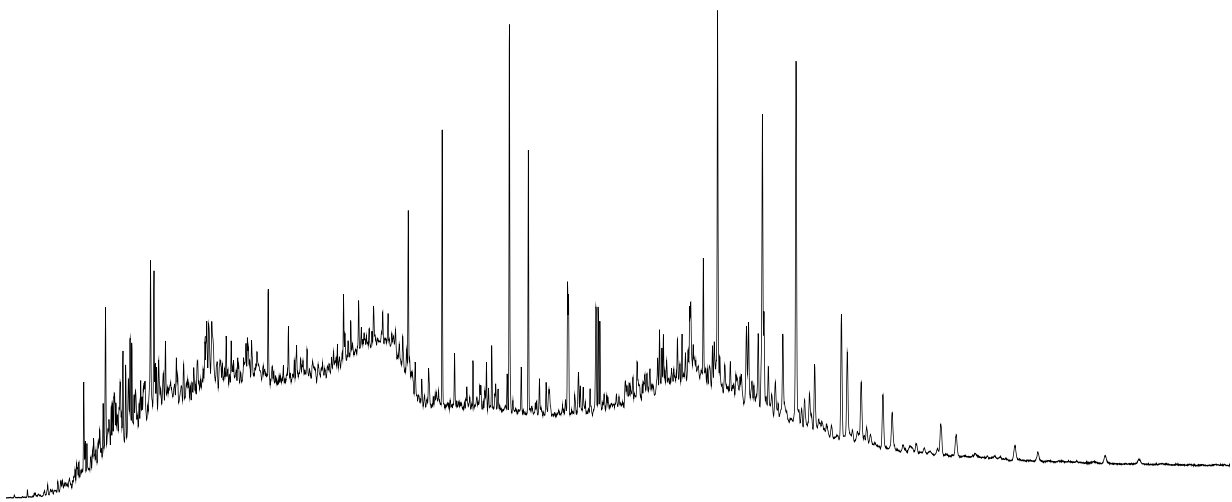
SR-191b



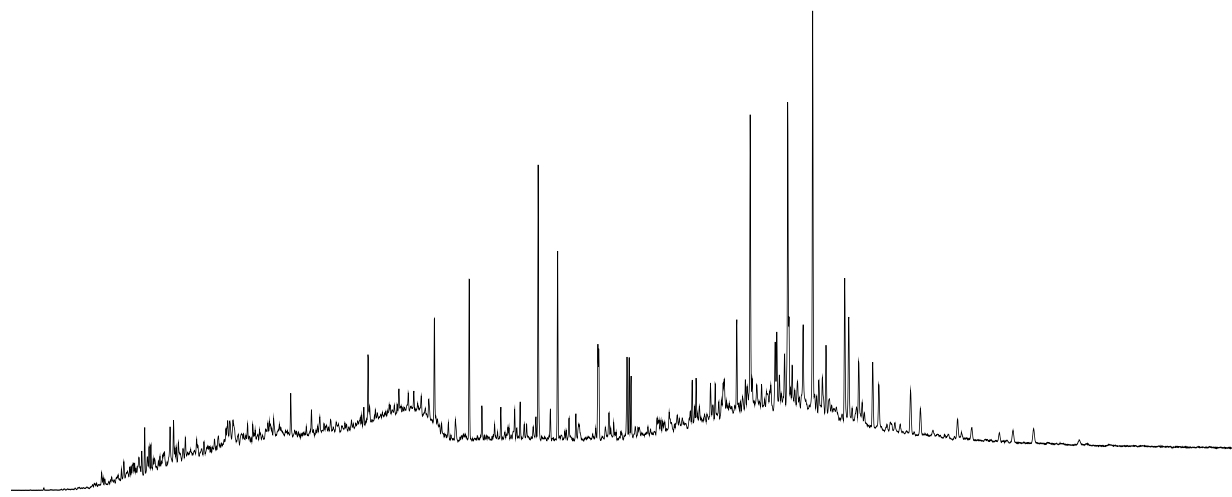
SR-192a



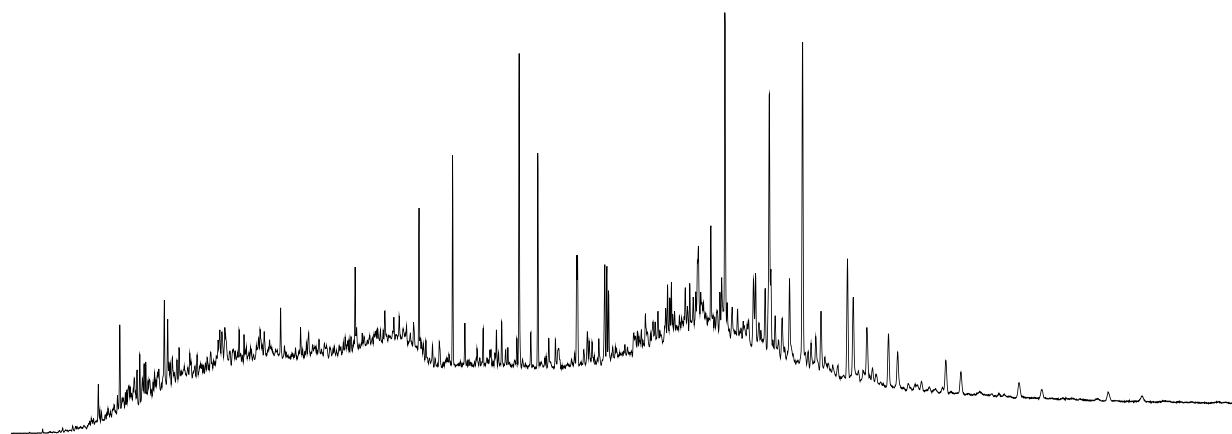
SR-193b



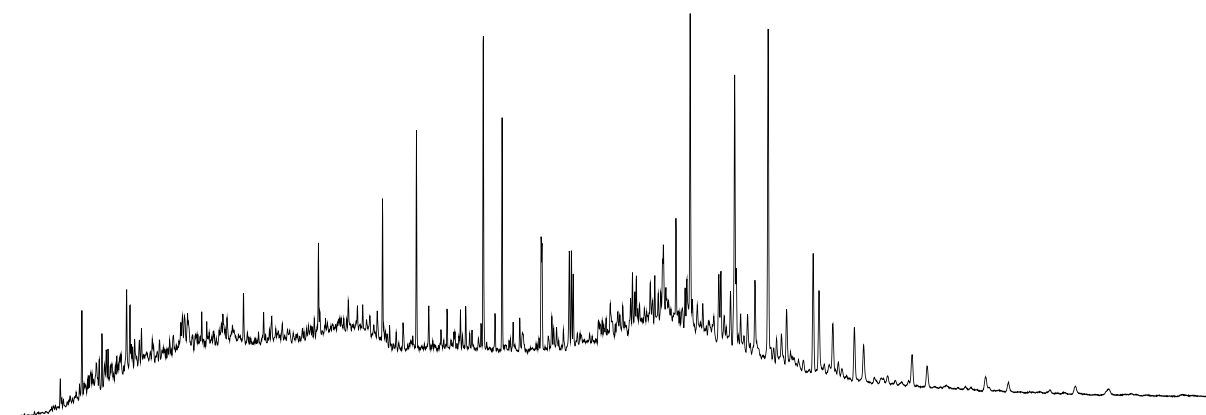
SR-194b



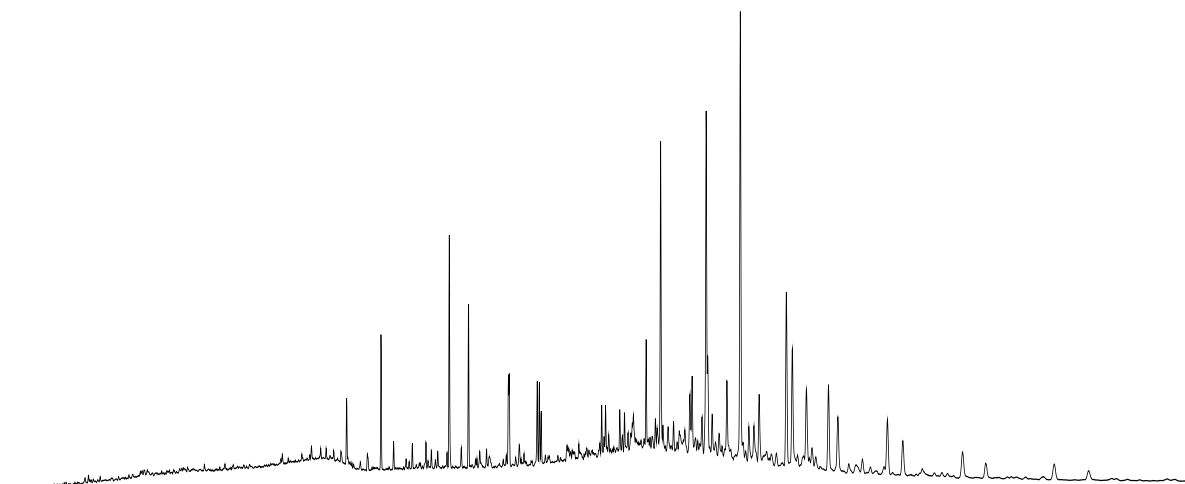
SR-195b



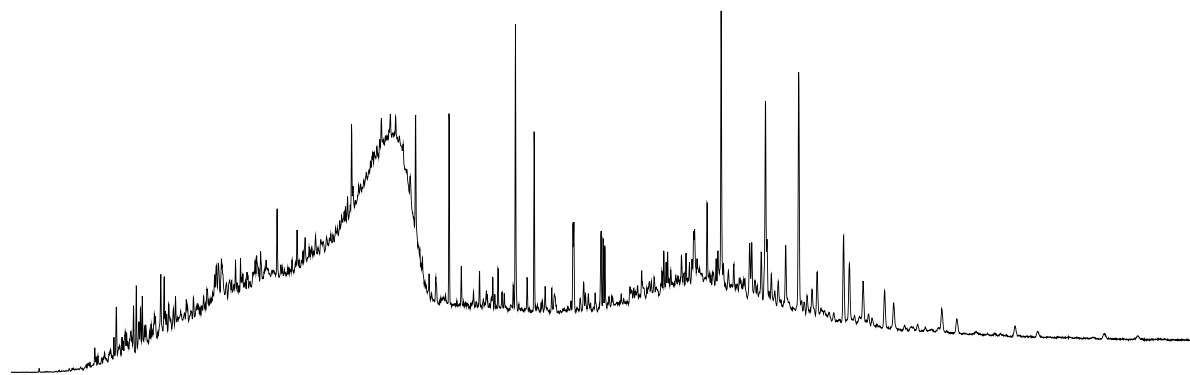
SR-197b



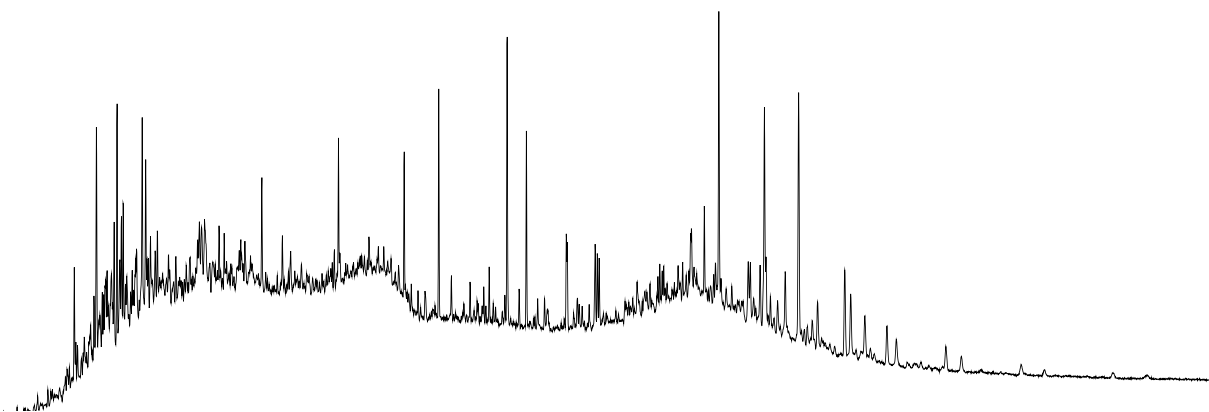
SR-198a



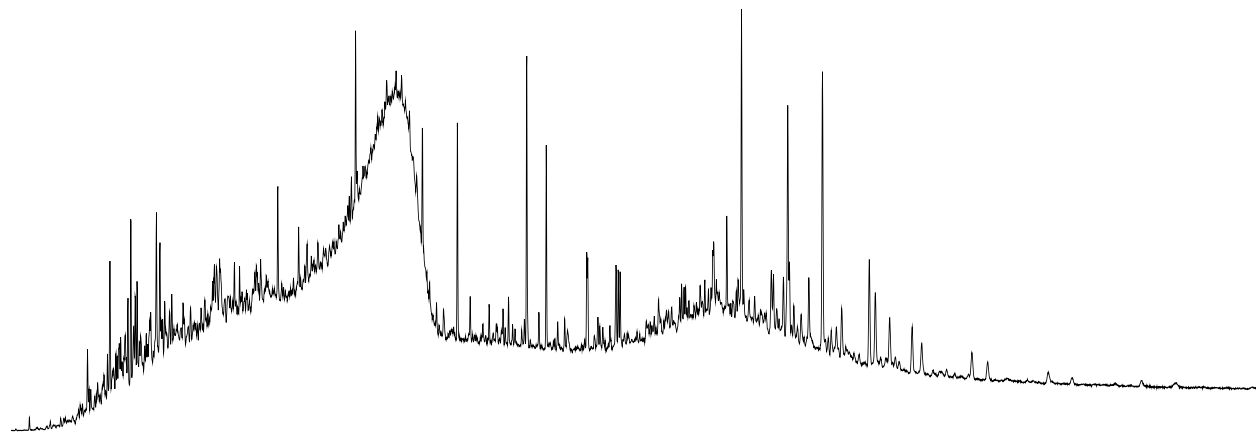
SR-199b



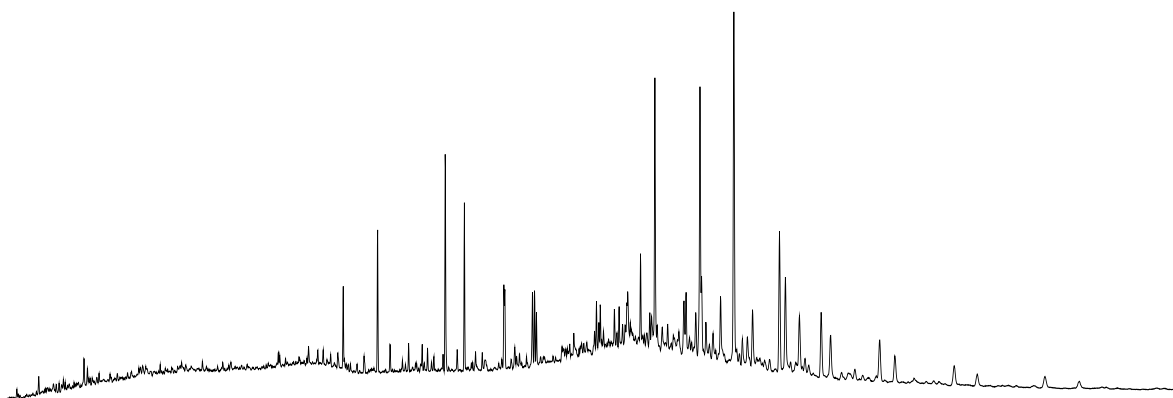
SR-200b



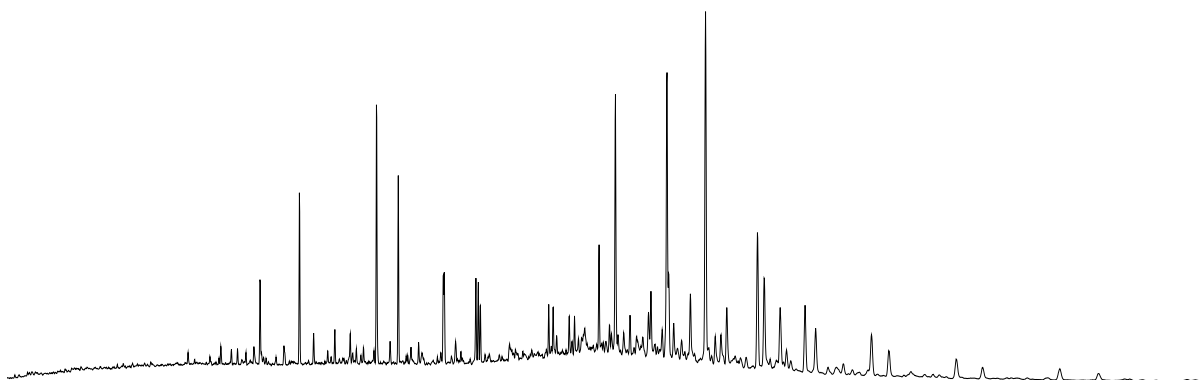
SR-204b



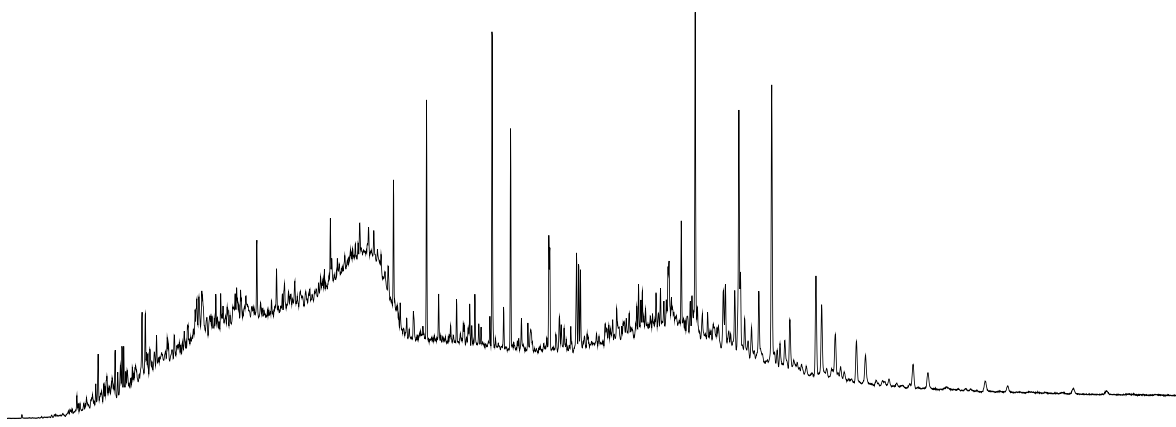
SR-205a



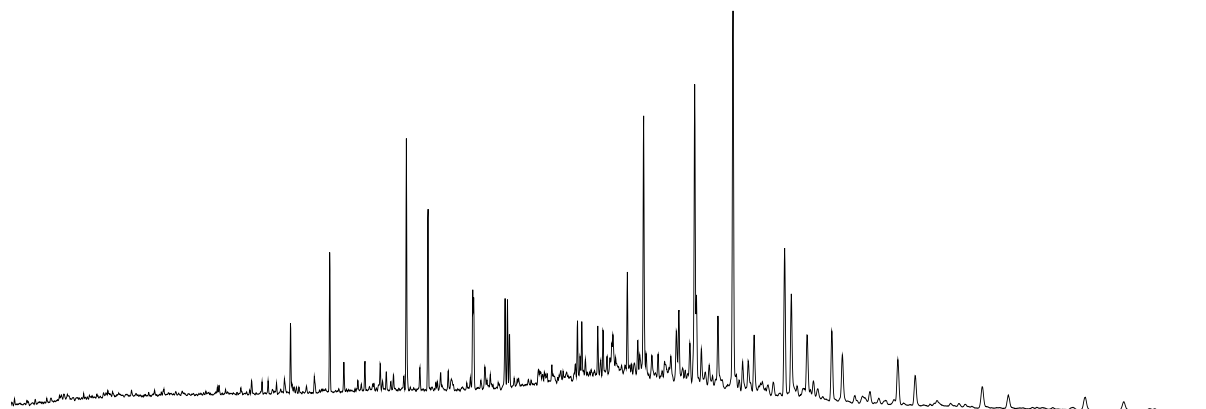
SR-207a



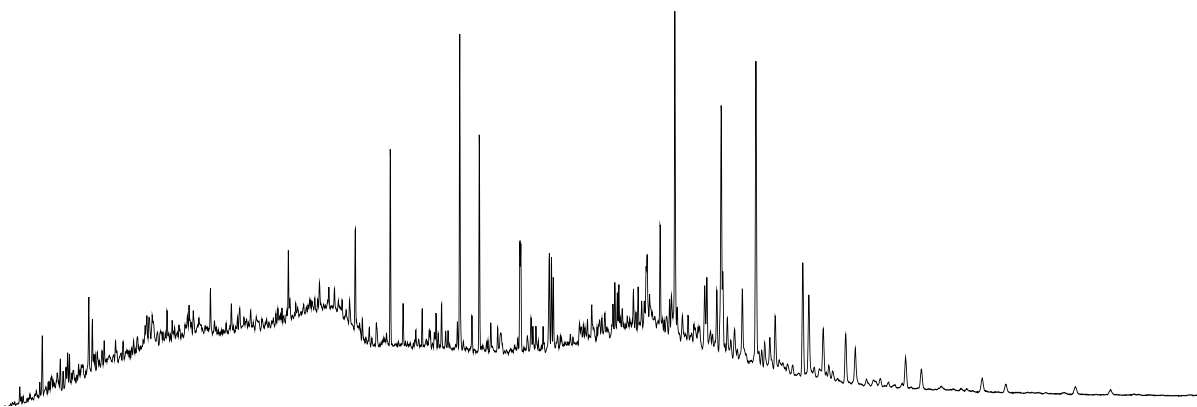
SR-208b



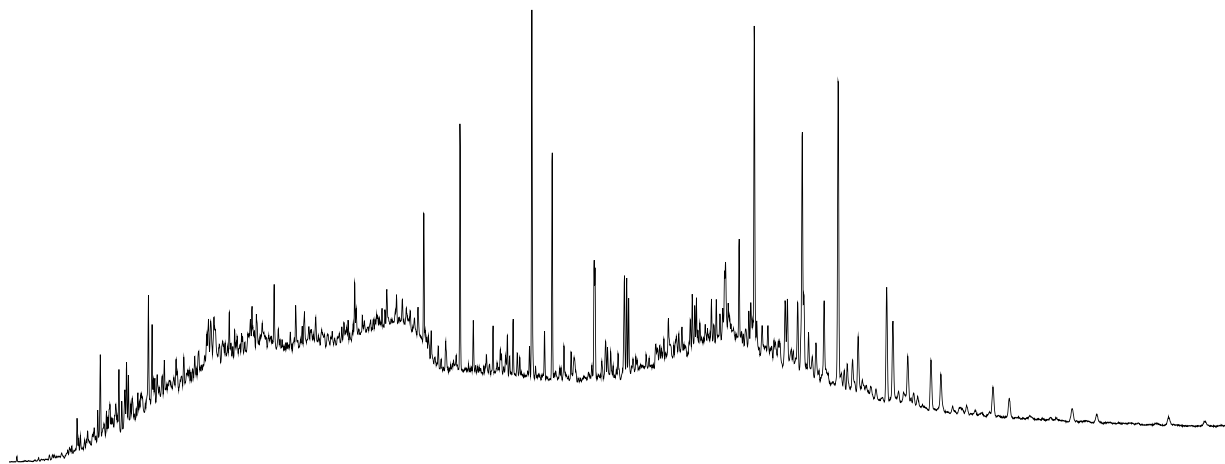
SR-209a



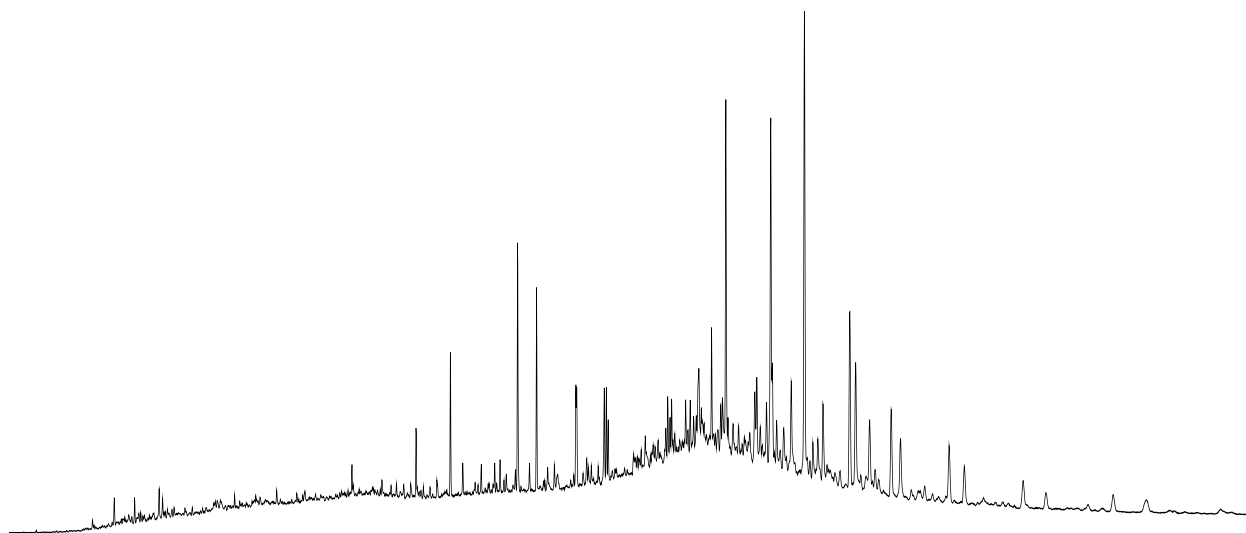
SR-210b



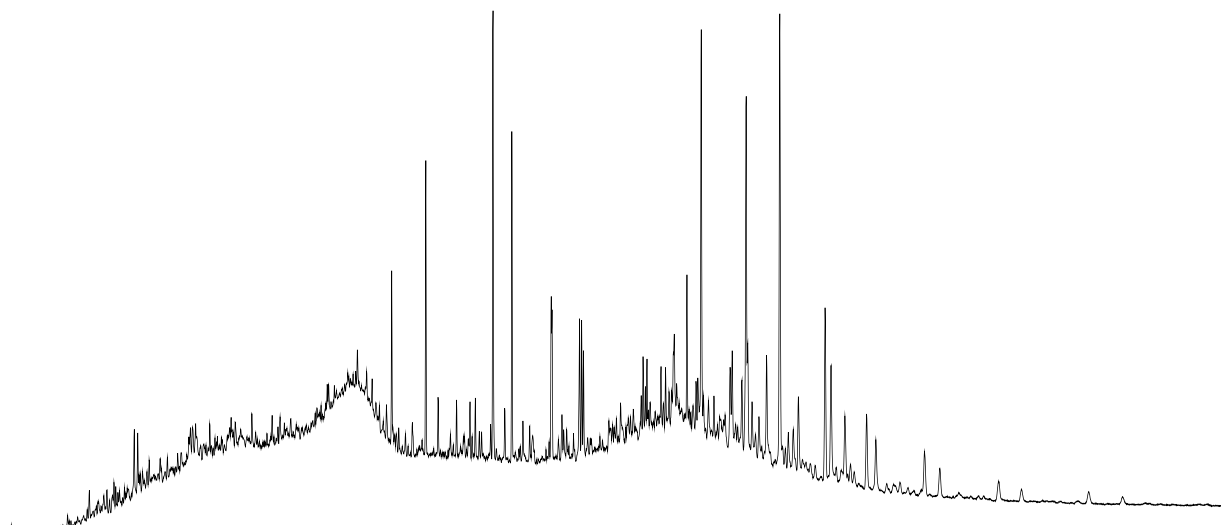
SR-211b



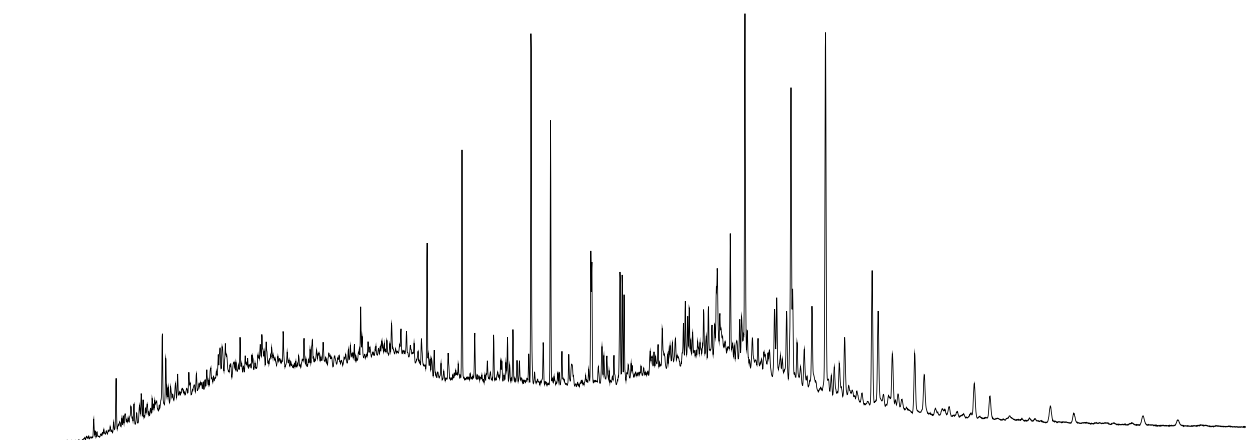
SR-212a



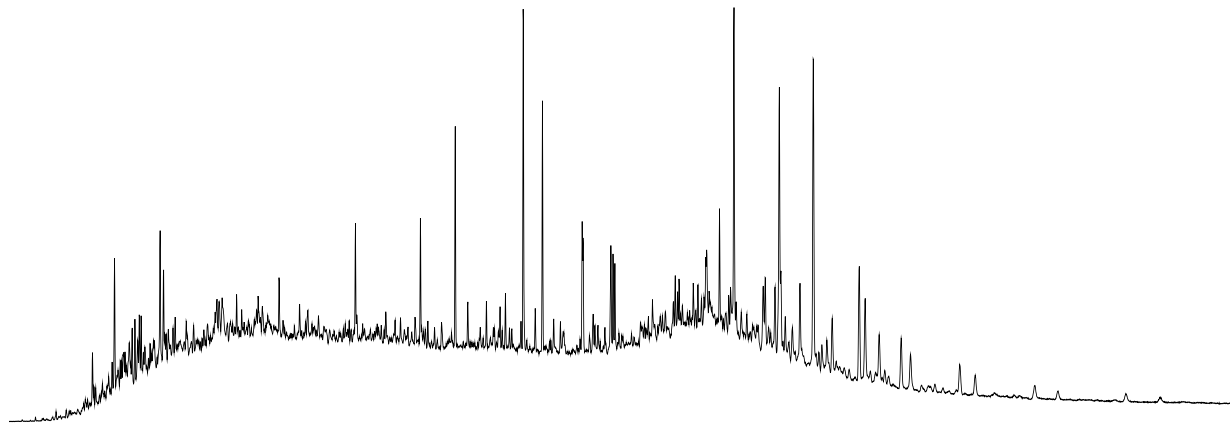
SR-213



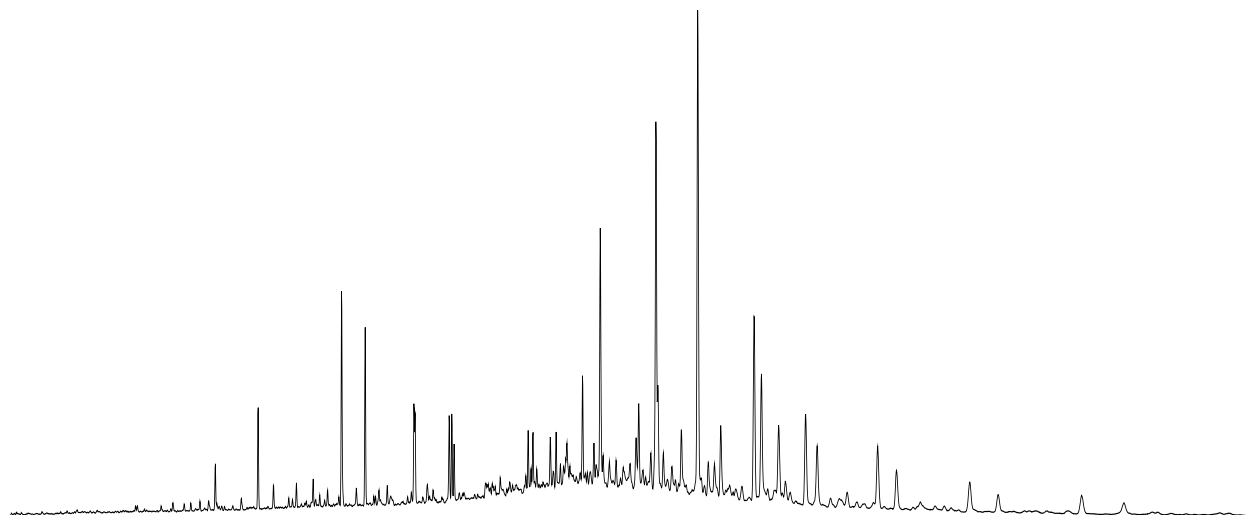
SR-214b



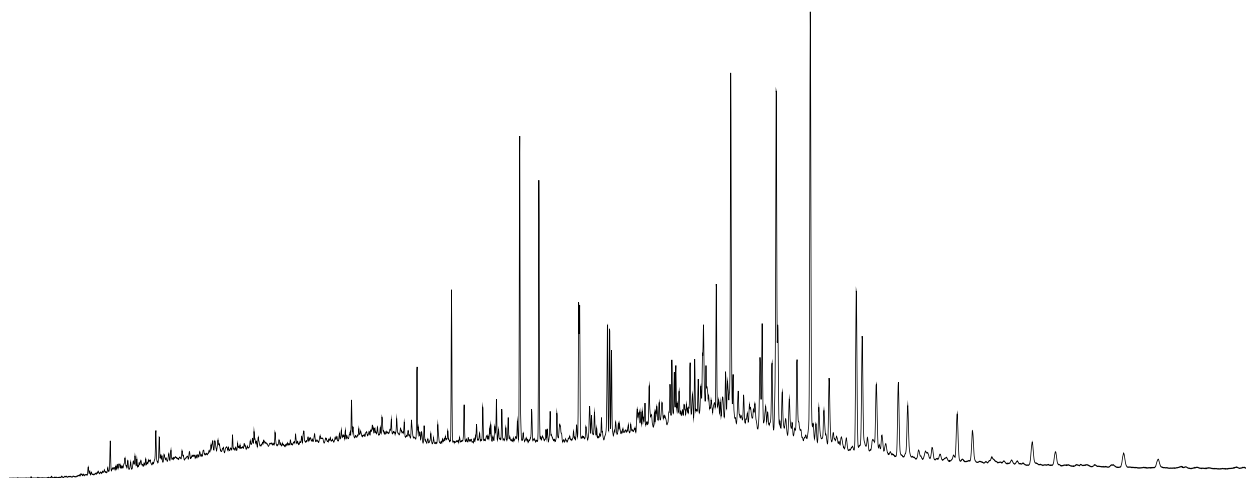
SR-215b



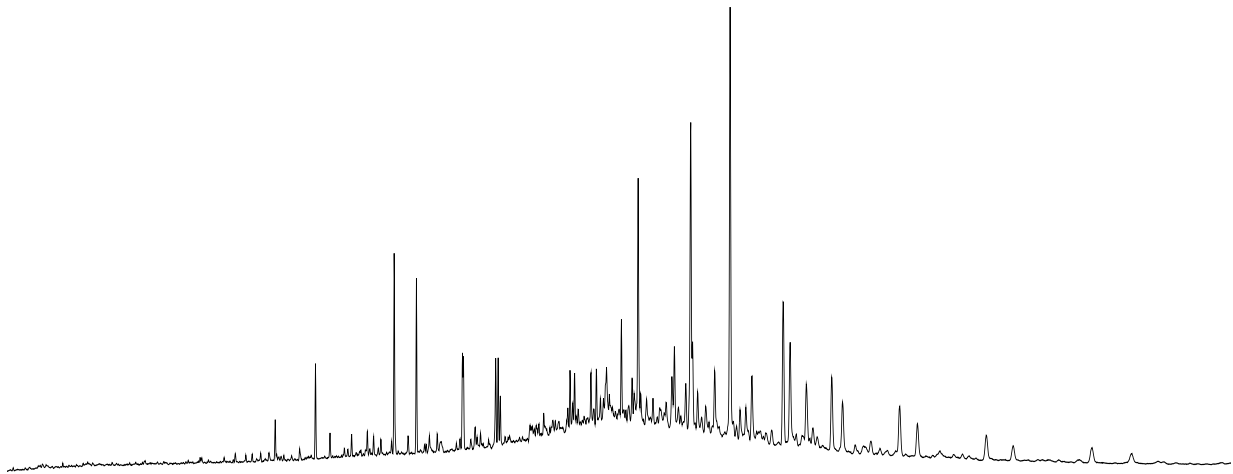
SR-219a



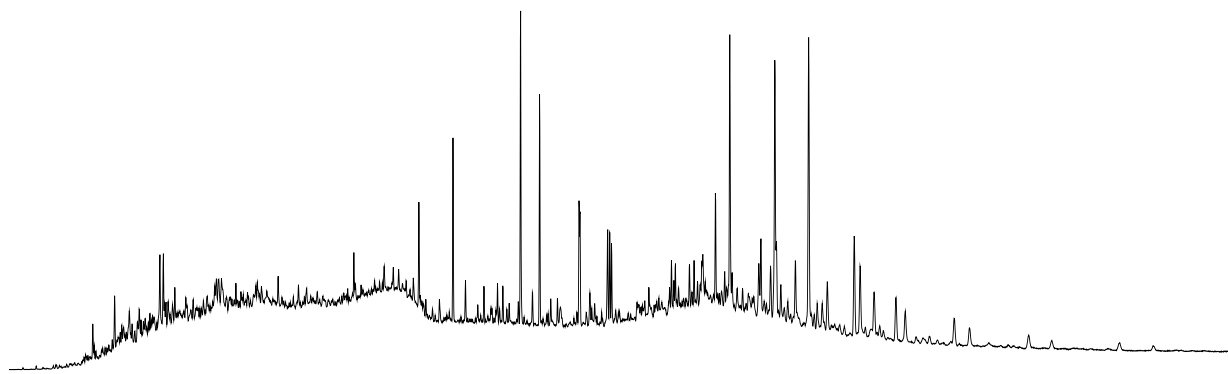
SR-221b



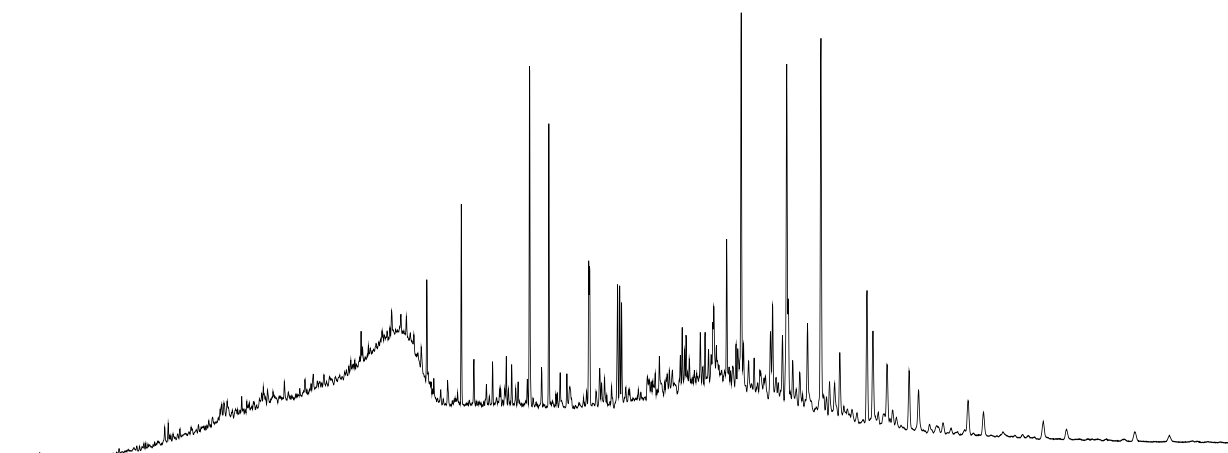
SR-222a



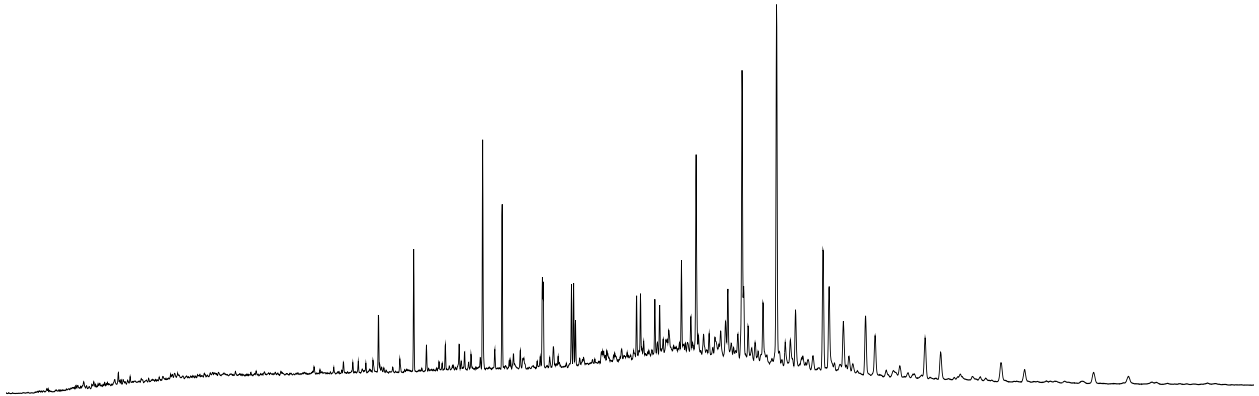
SR-224b



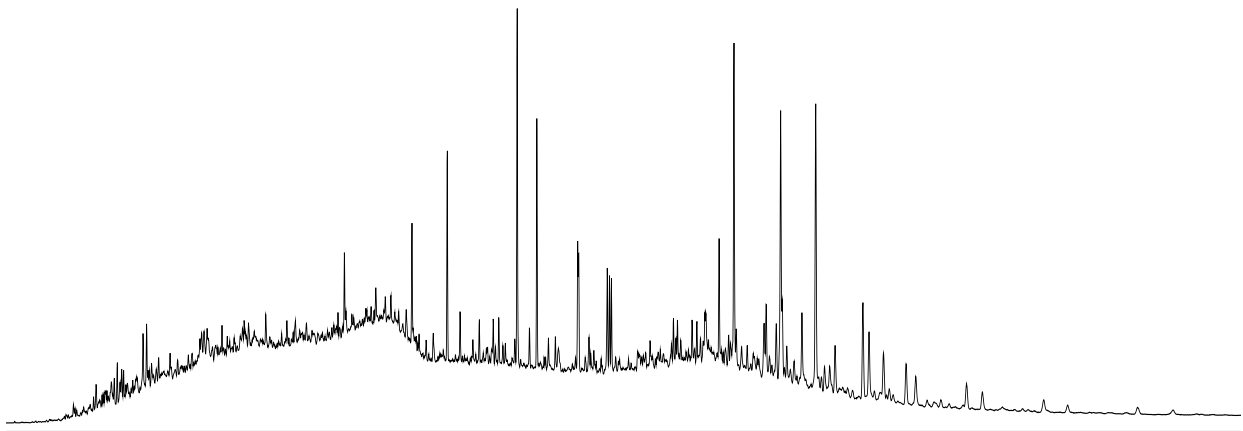
SR-225b



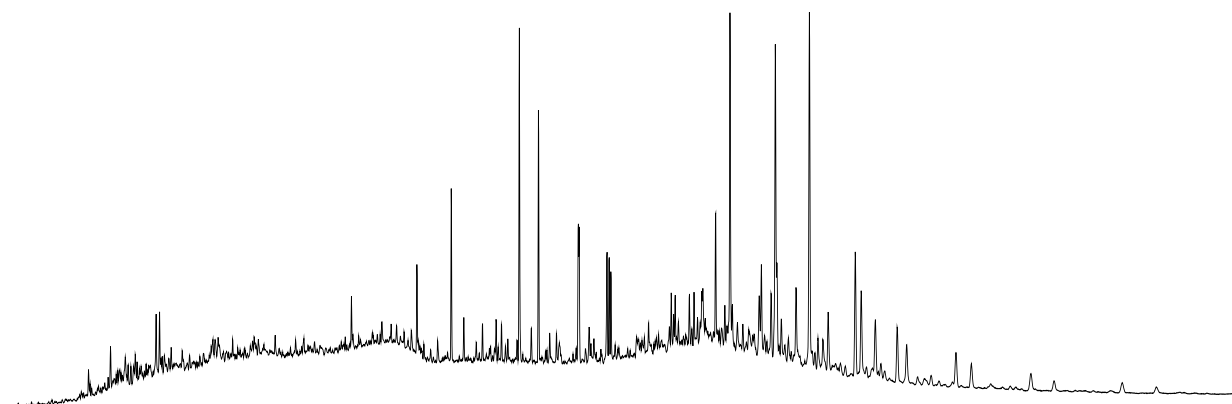
SR-226a



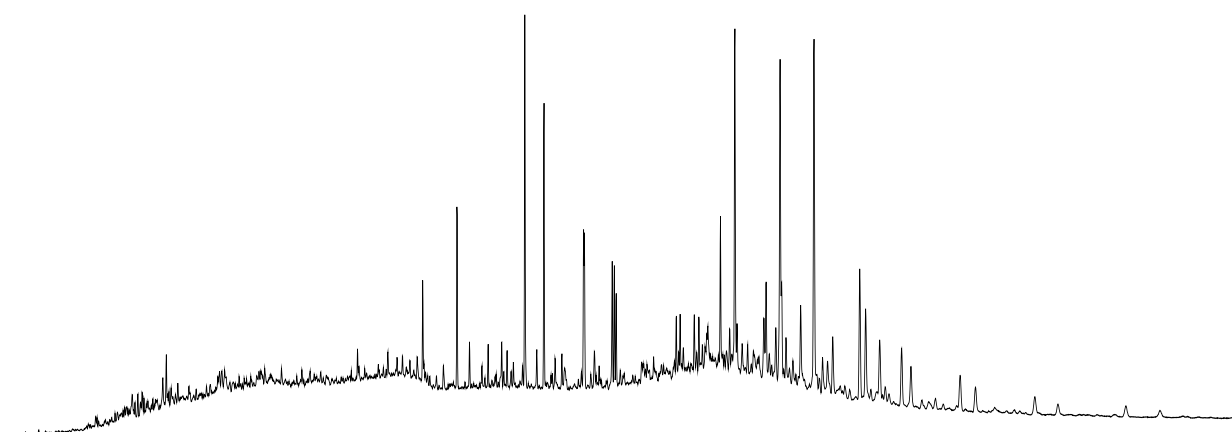
SR-227b



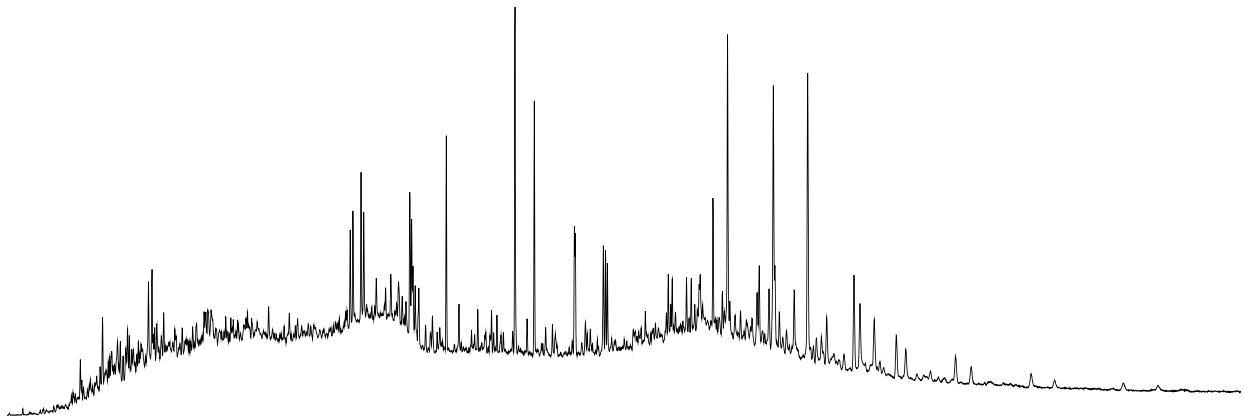
SR-228b



SR-229a

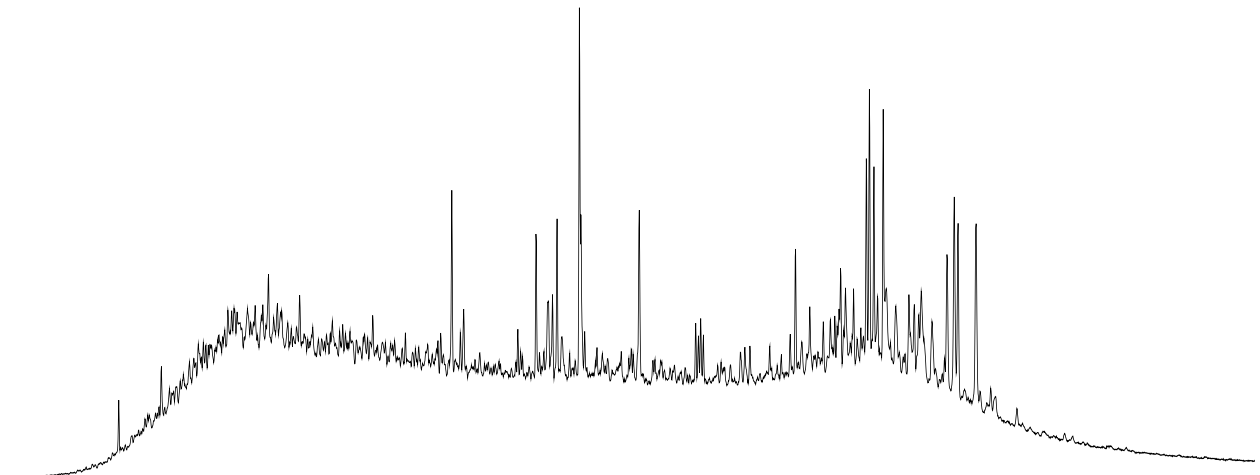


SR-230b

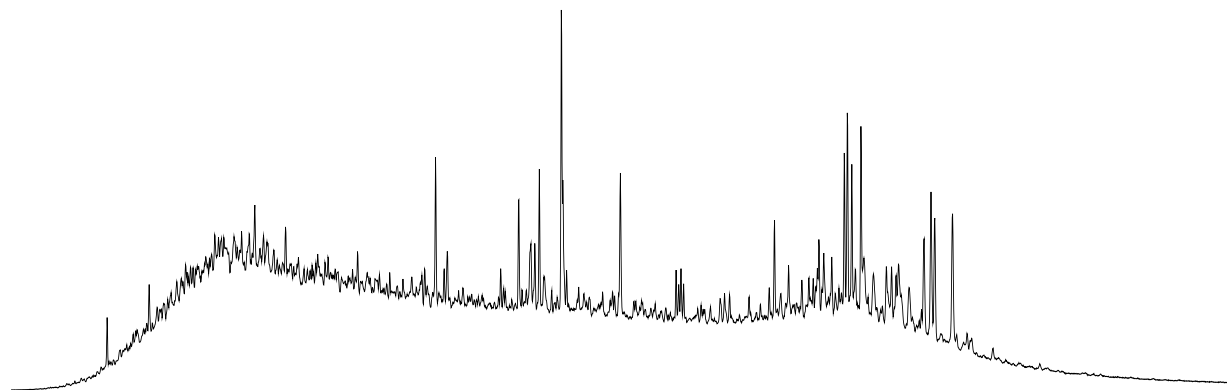


WDFD SATURATES M/Z 217

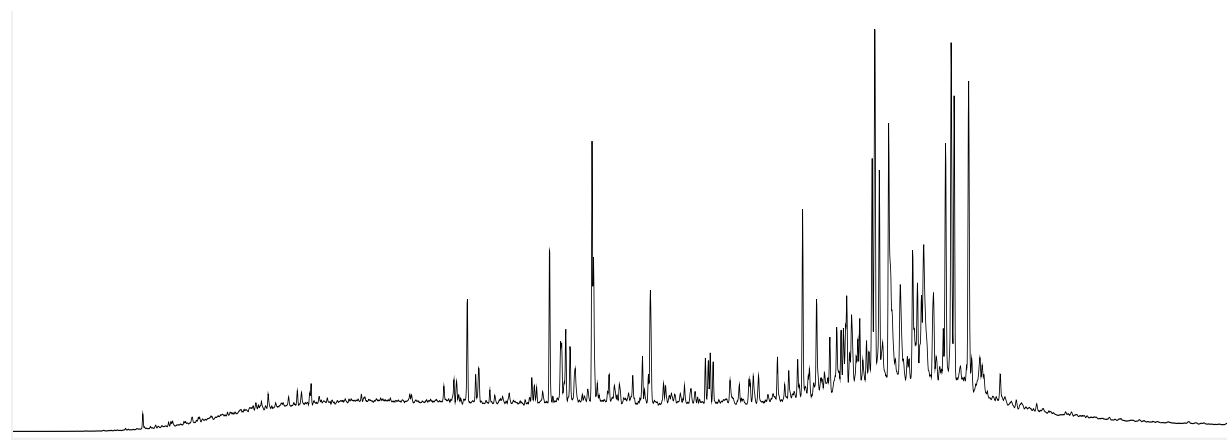
SR-190b



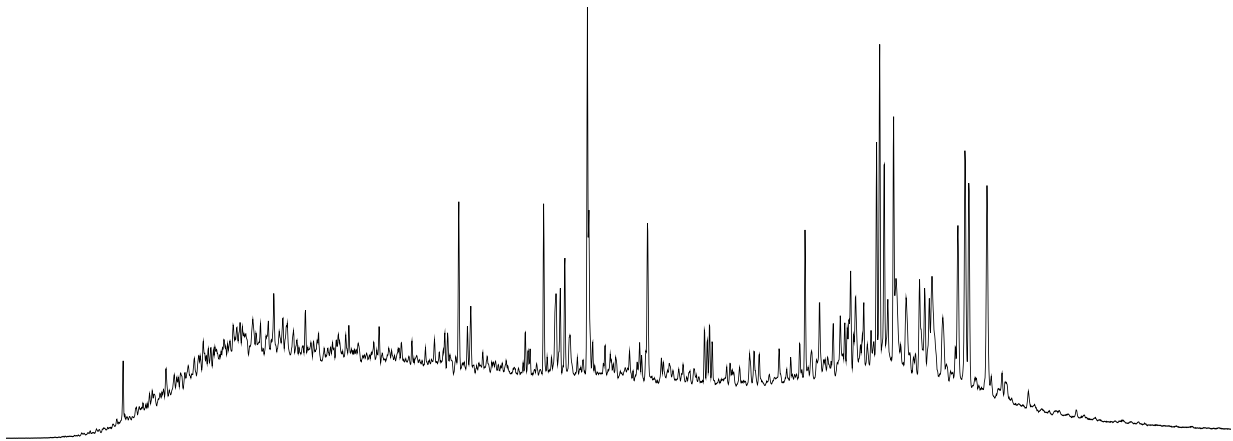
SR-191b



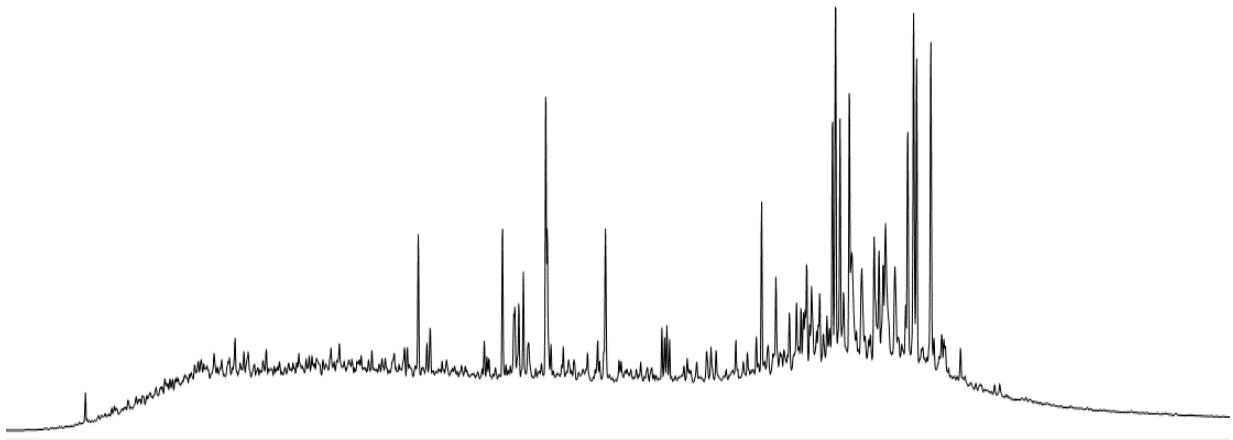
SR-192a



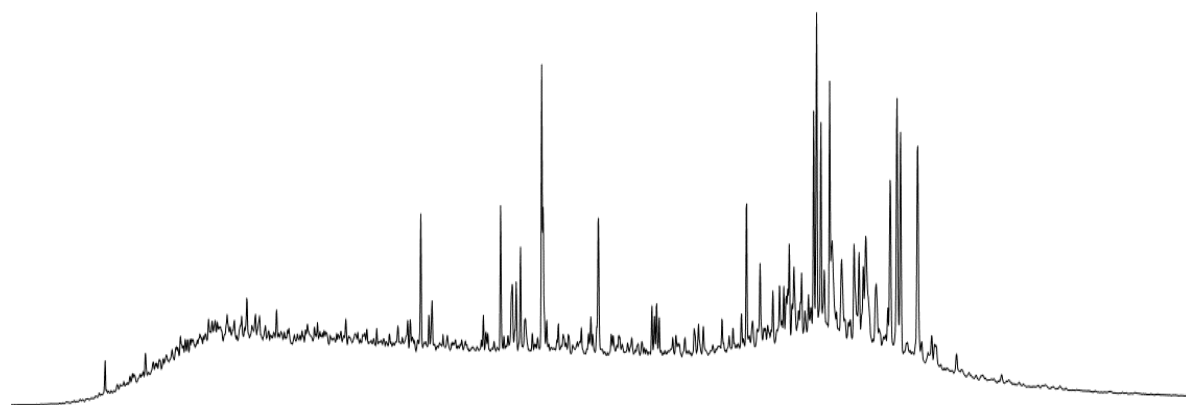
SR-193b



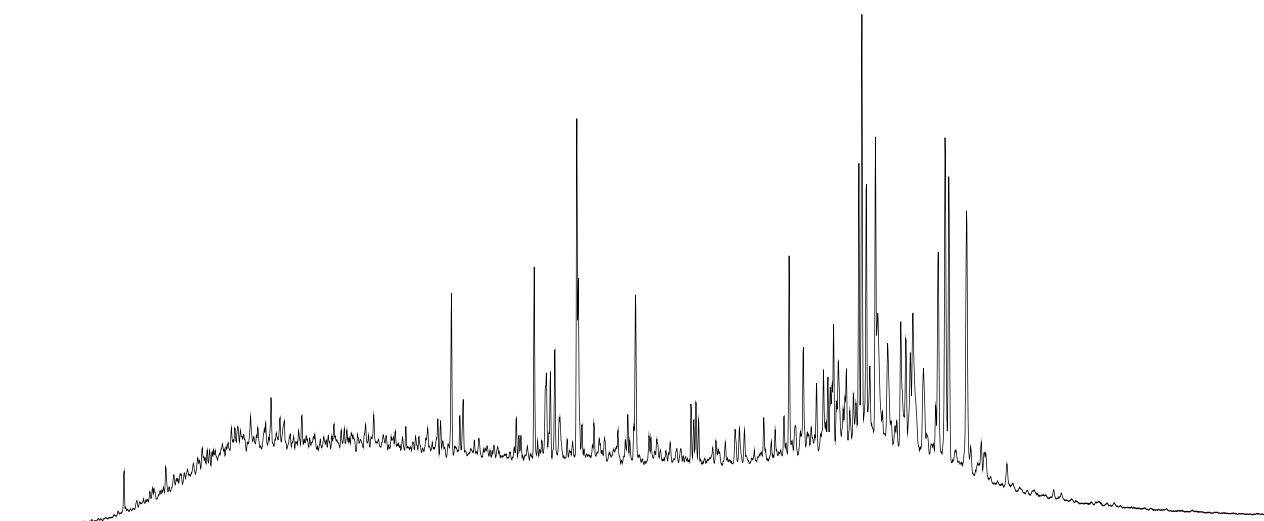
SR-194b



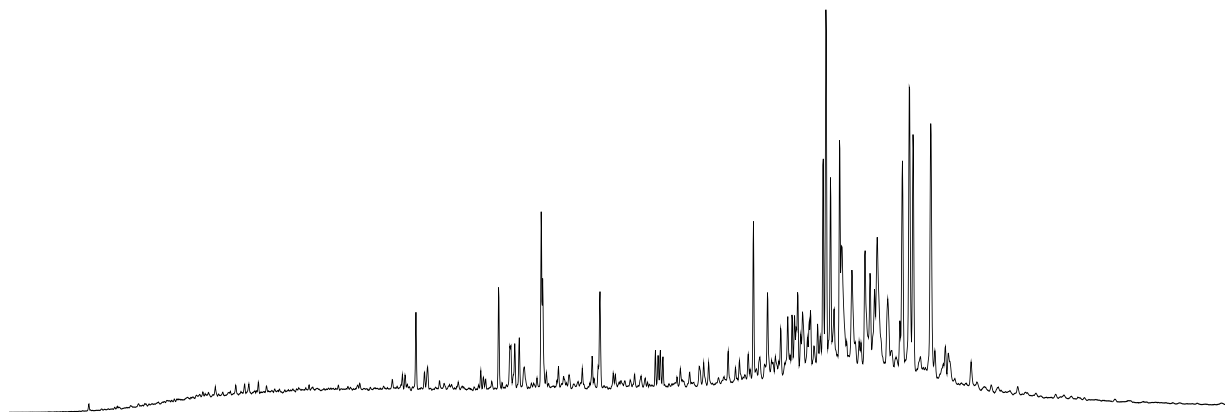
SR-195b



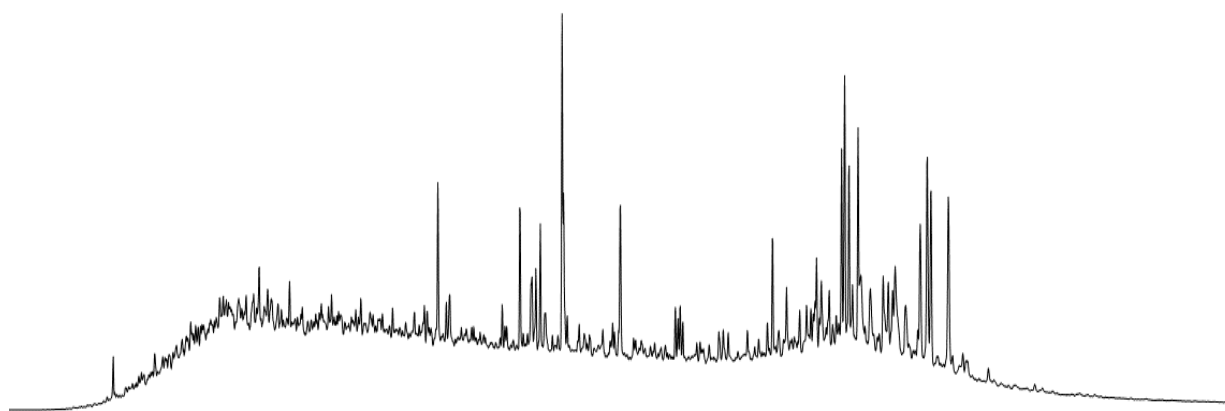
SR-197b



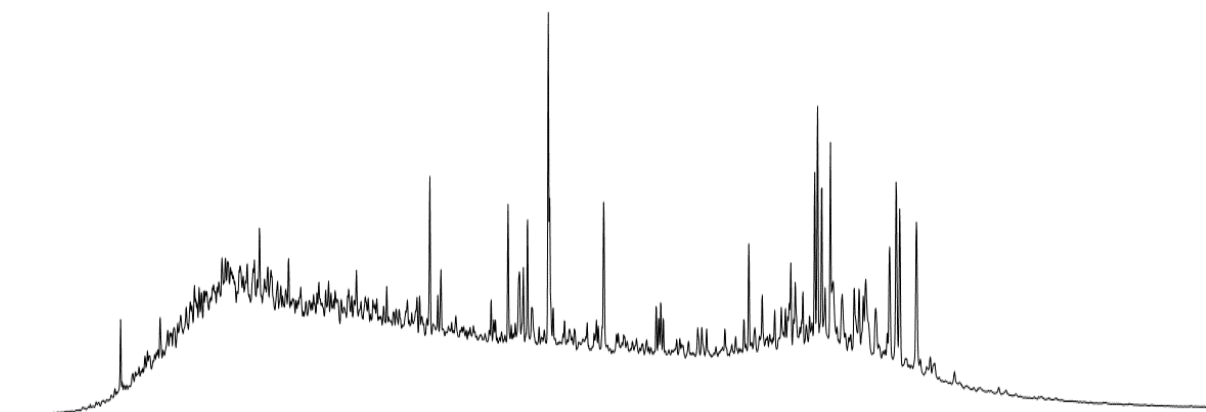
SR-198a



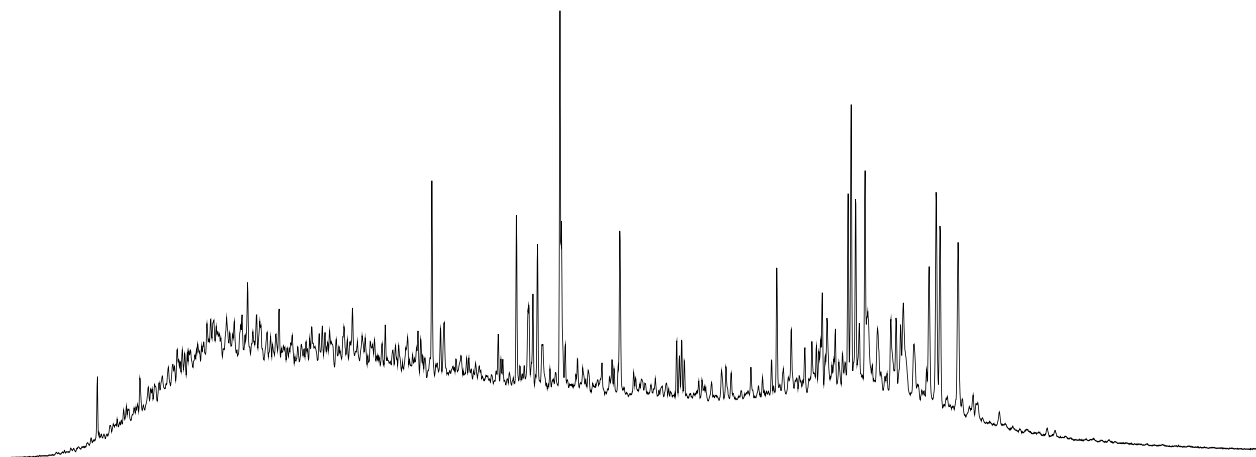
SR-199b



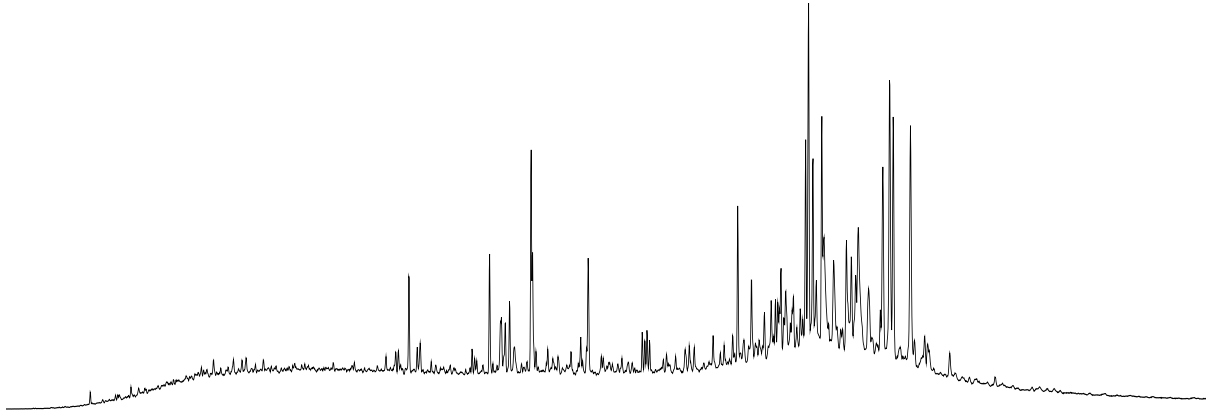
SR-200b



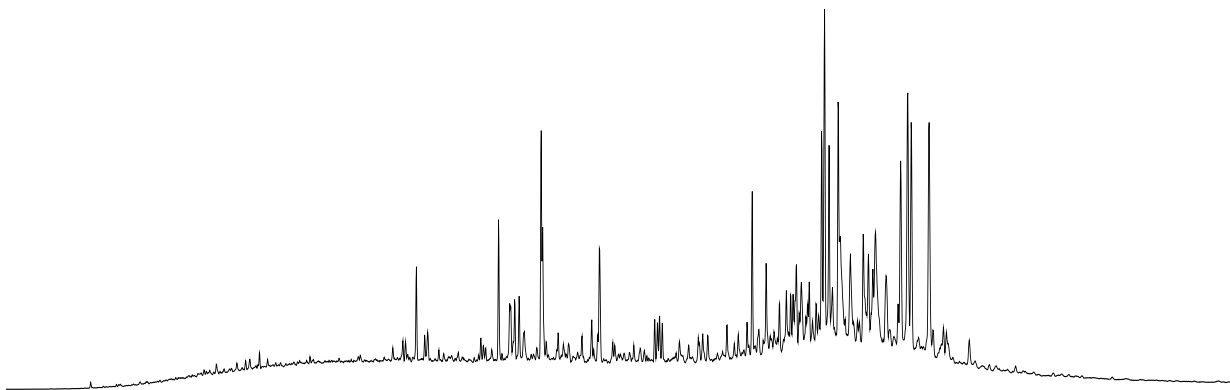
SR-204b



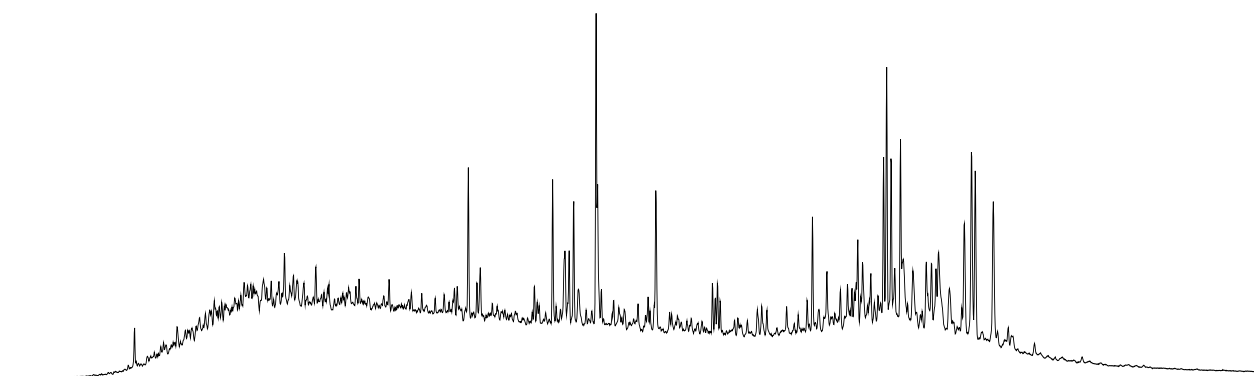
SR-205a



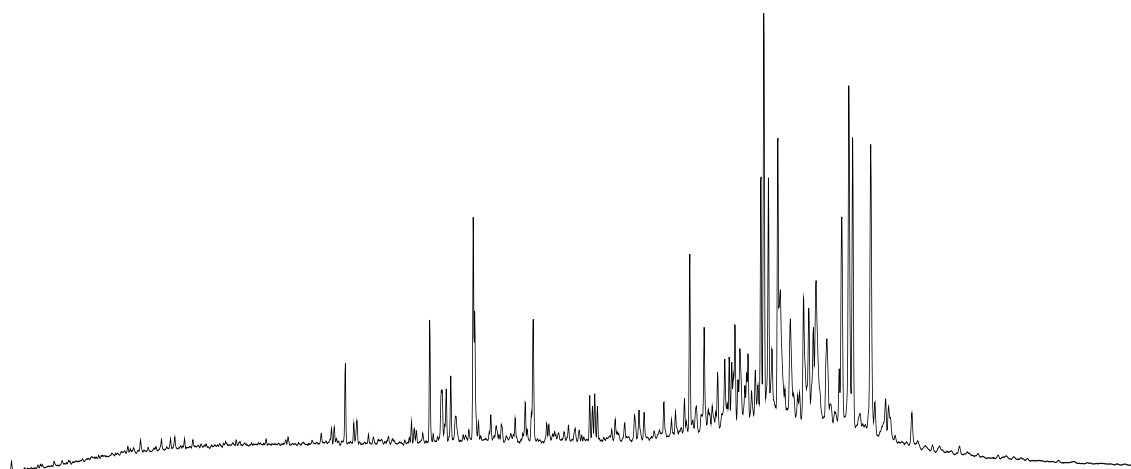
SR-207a



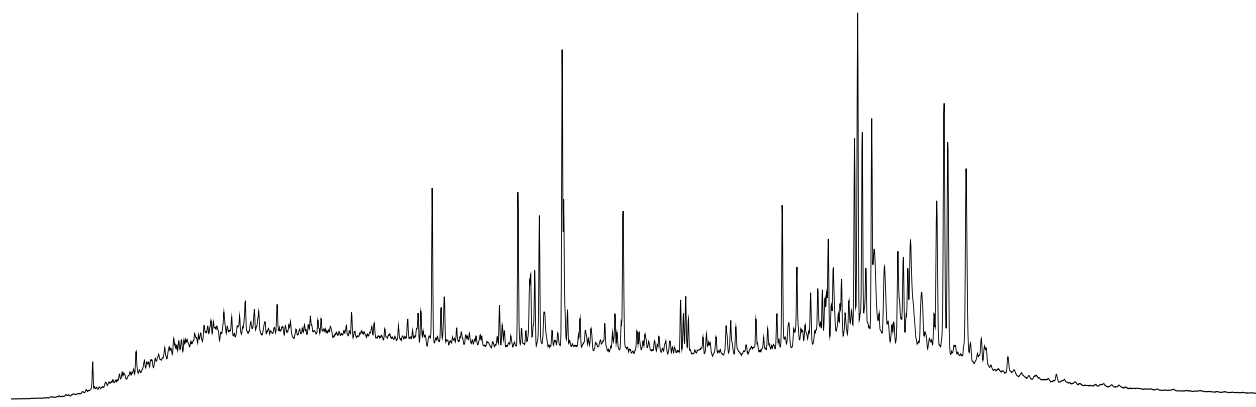
SR-208b



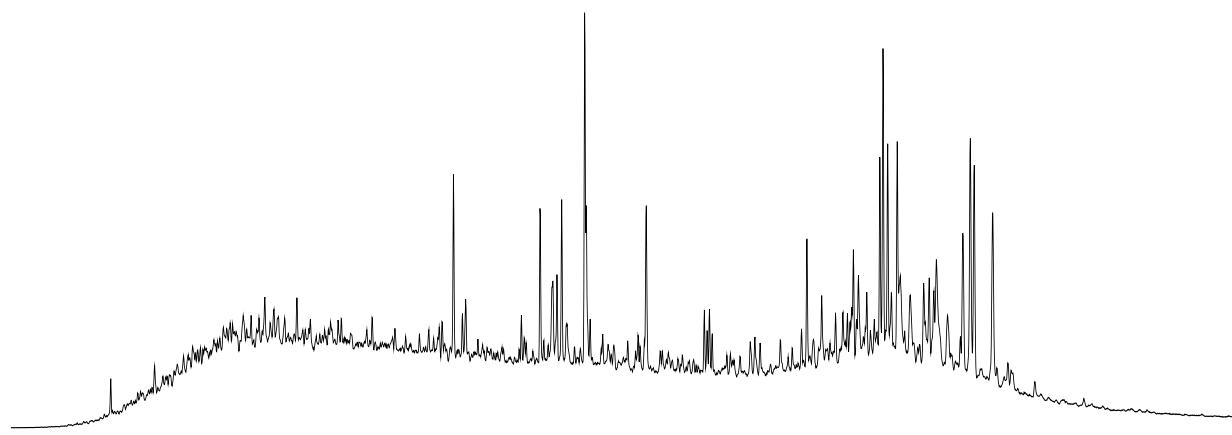
SR-209a



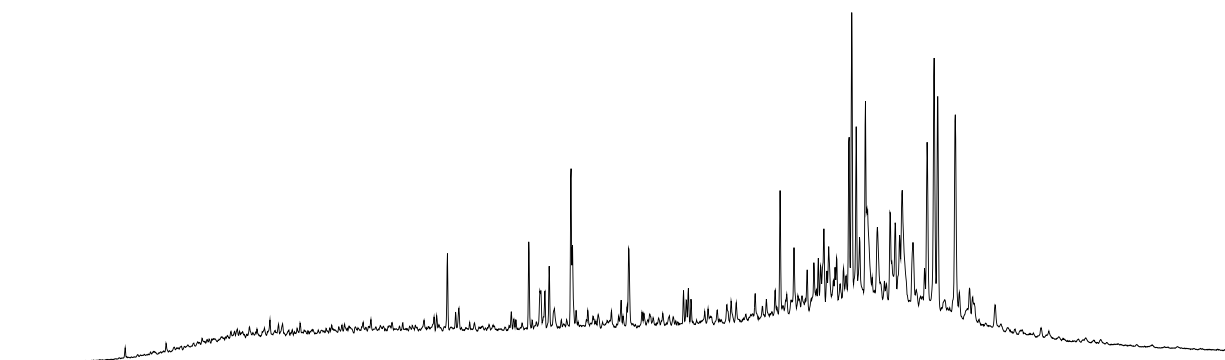
SR-210b



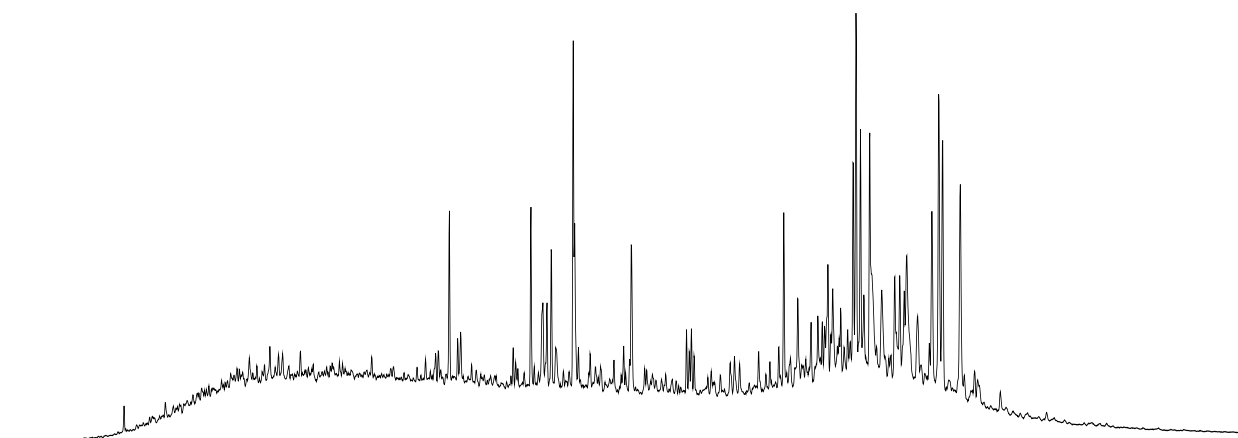
SR-211b



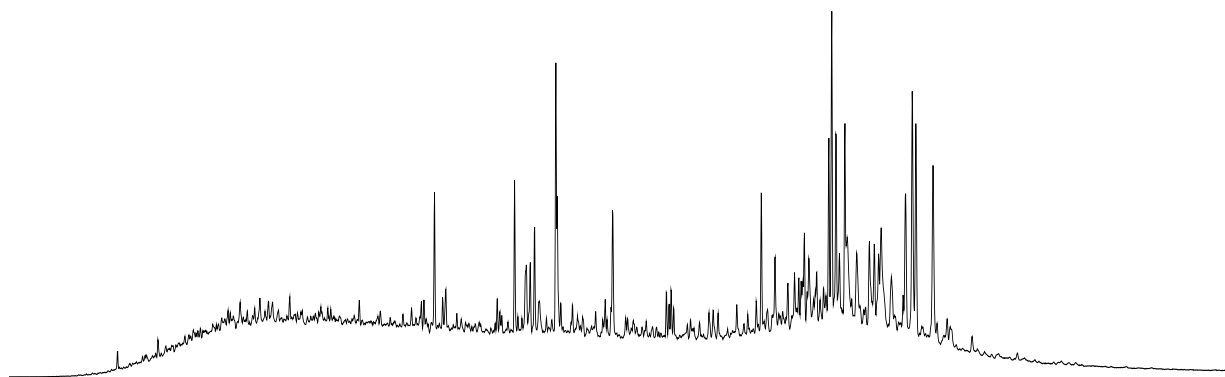
SR-212a



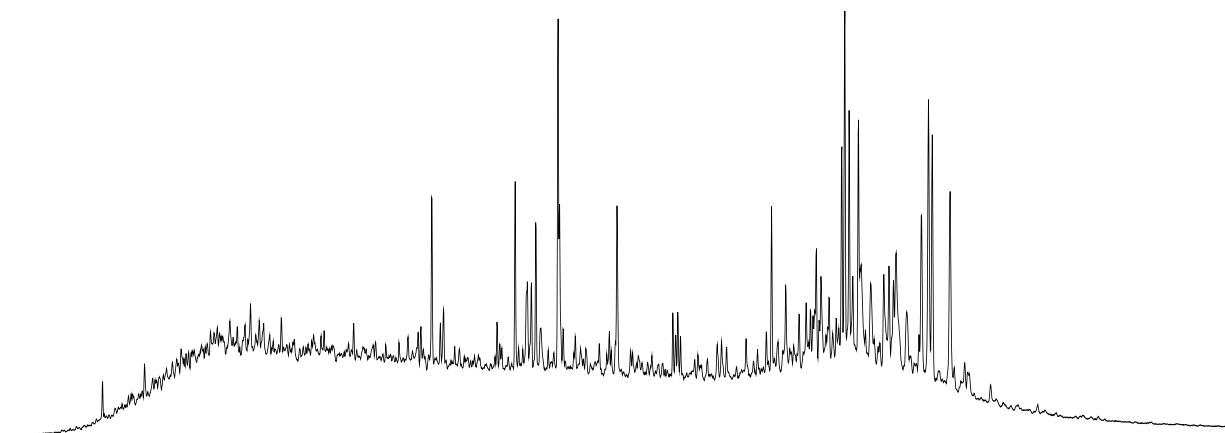
SR-213b



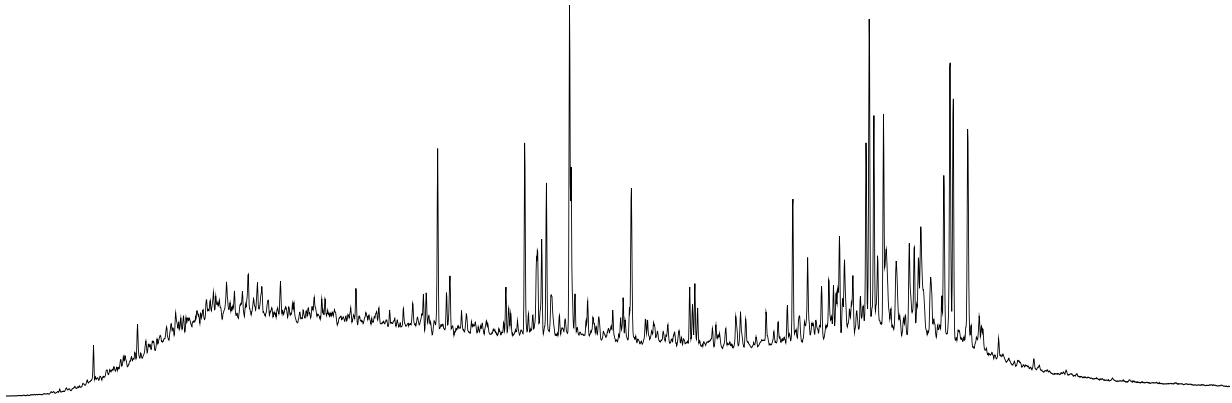
SR-214b



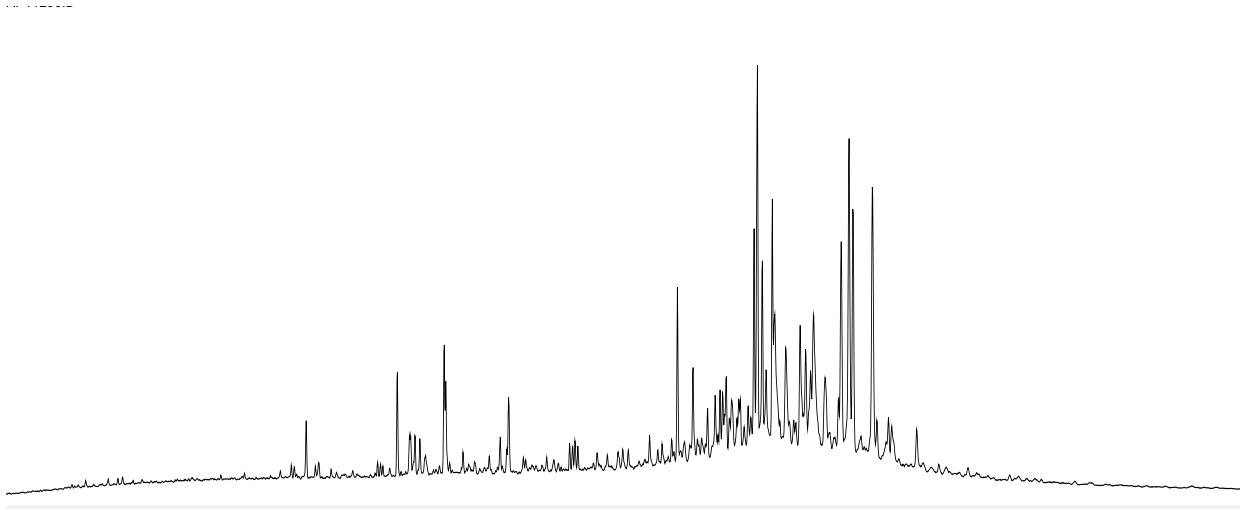
SR-215b



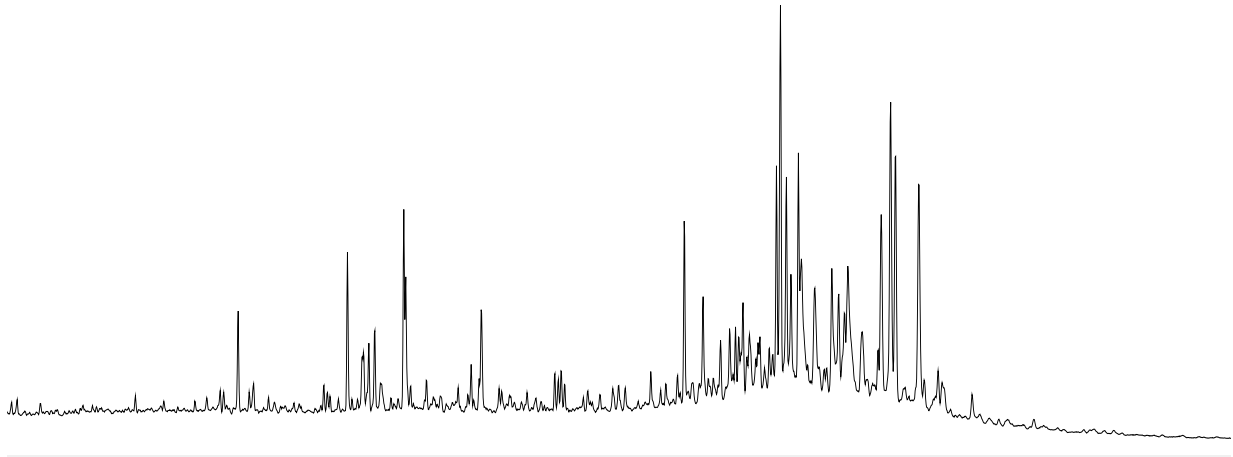
SR-217b



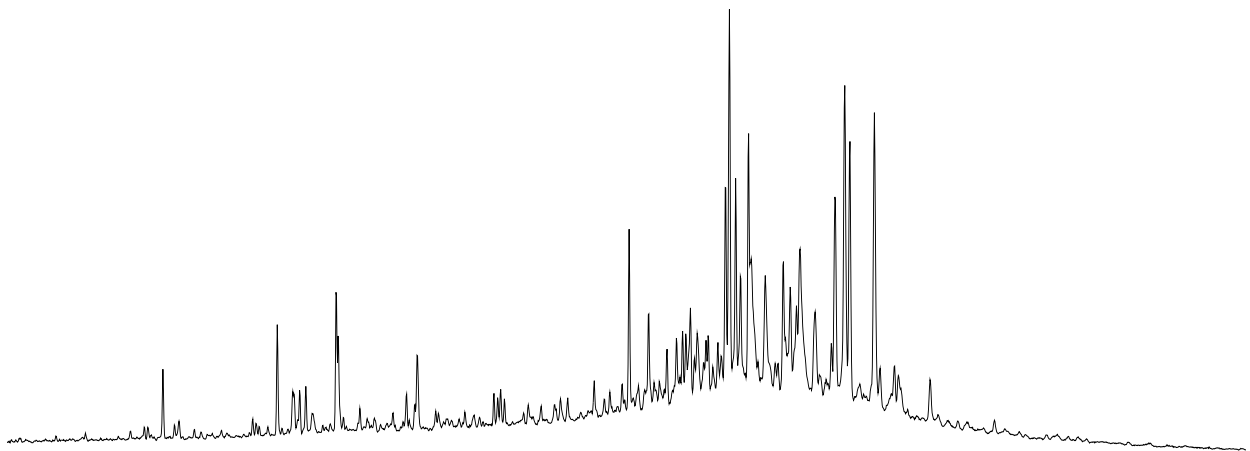
SR-219a



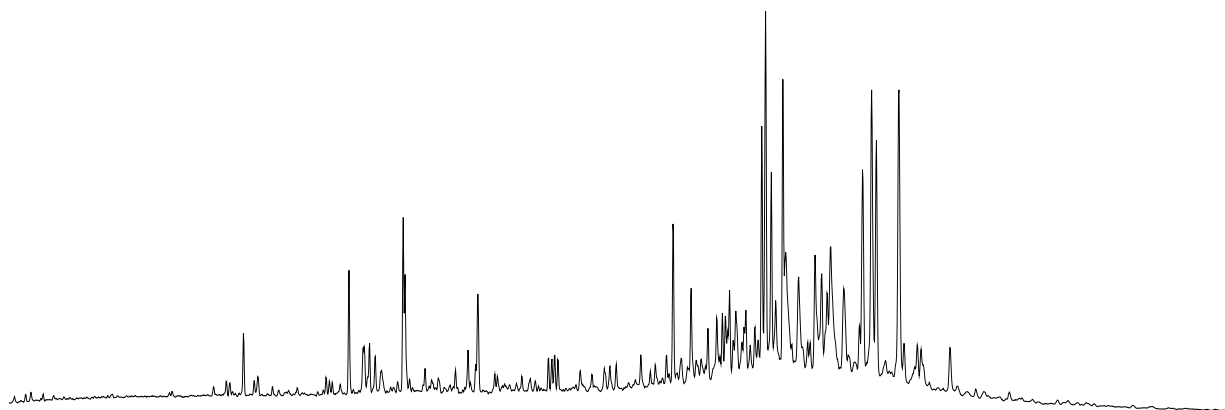
SR-221b



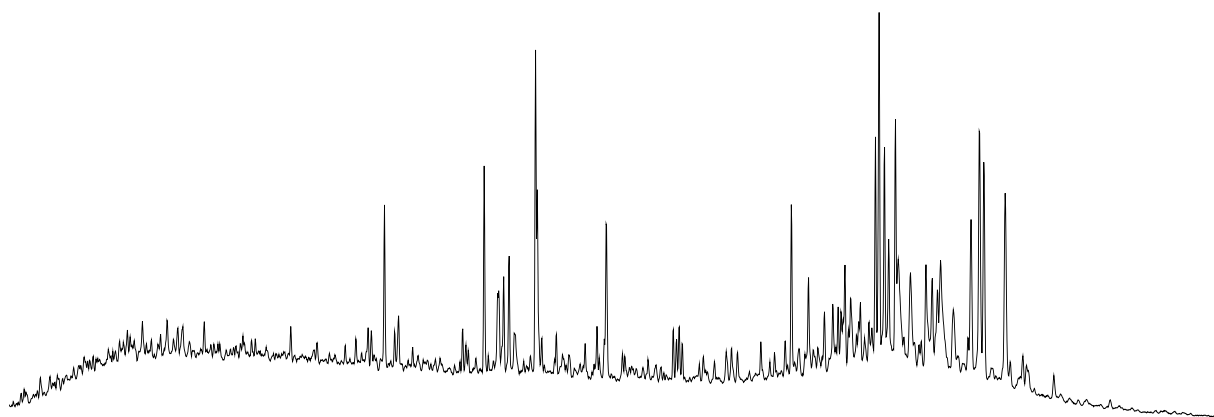
SR-222a



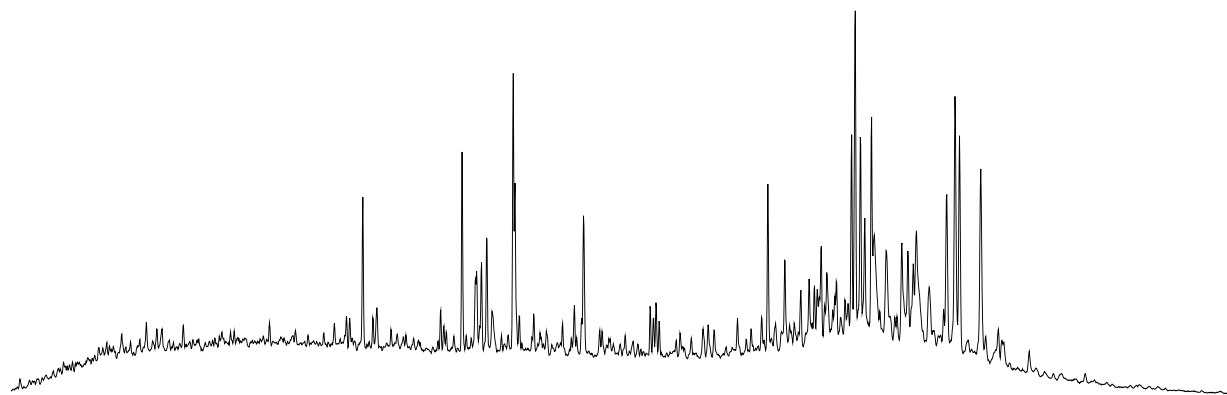
SR-223a



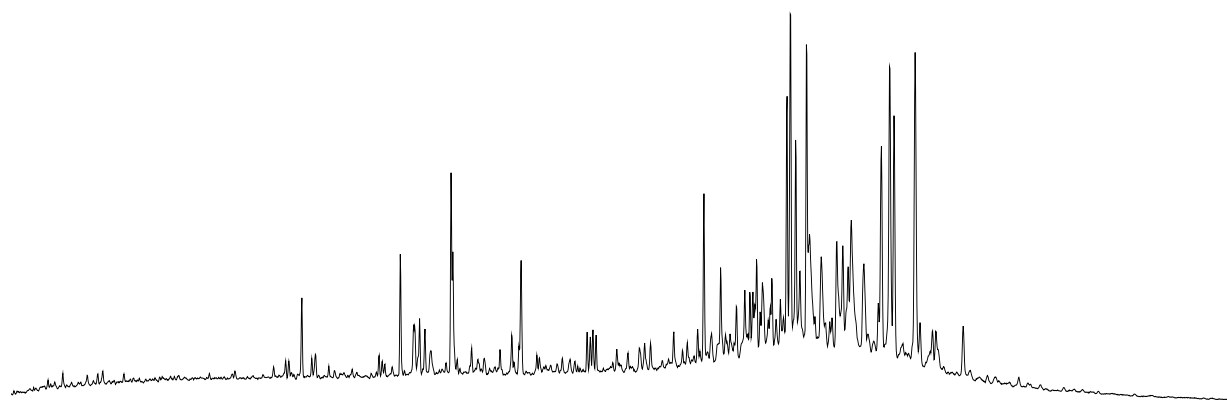
SR-224b



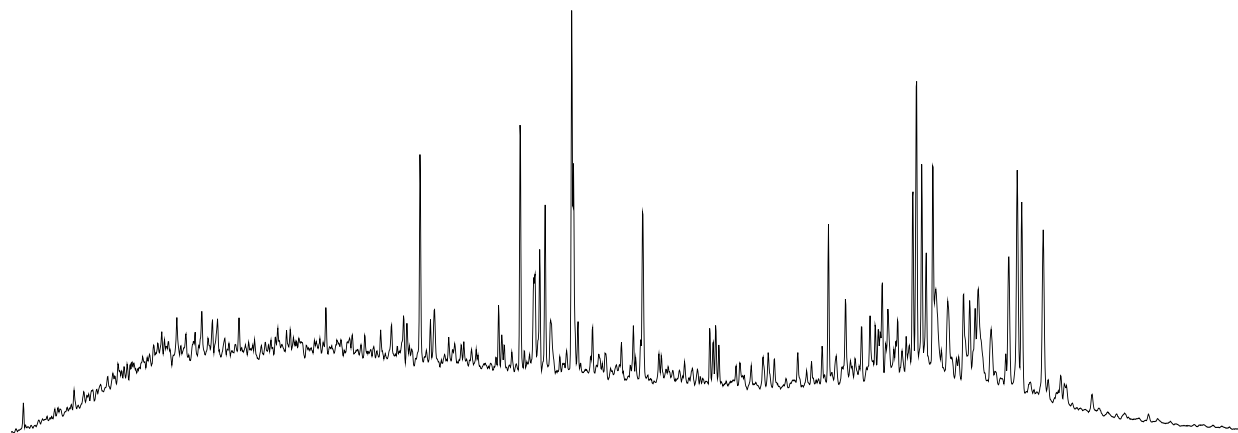
SR-225b



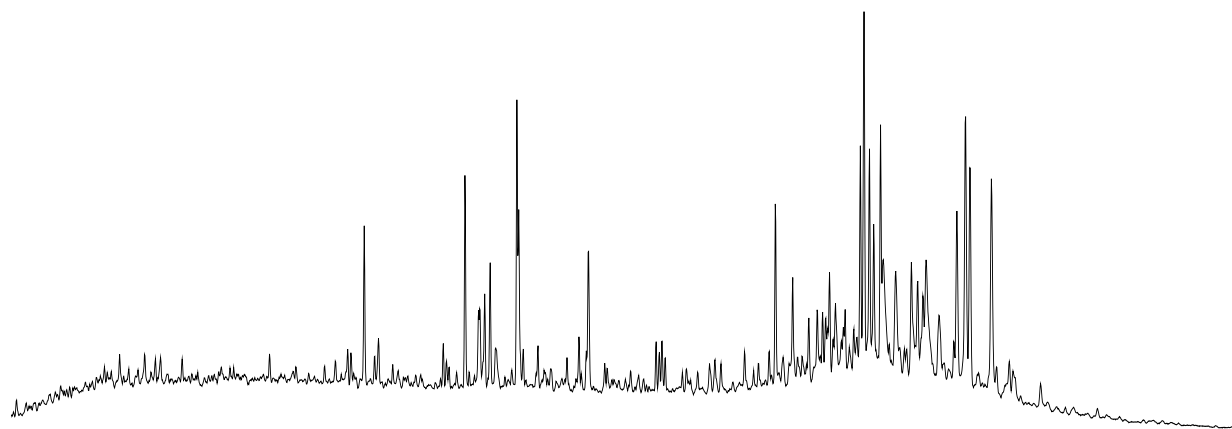
SR-226a



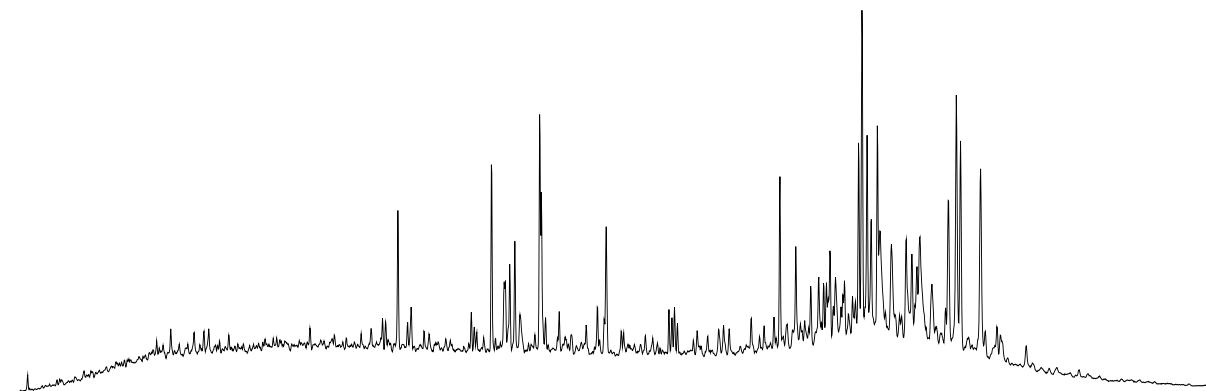
SR-227b



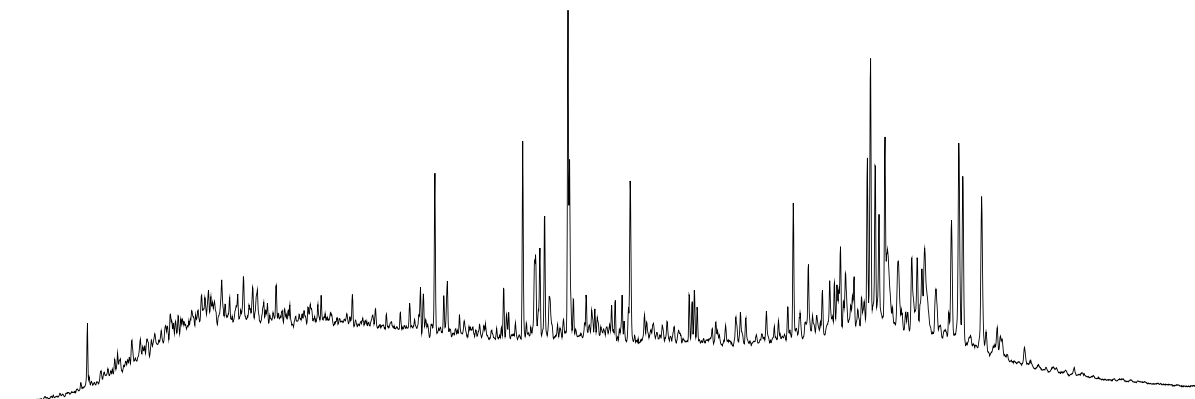
SR-228b



SR-229a

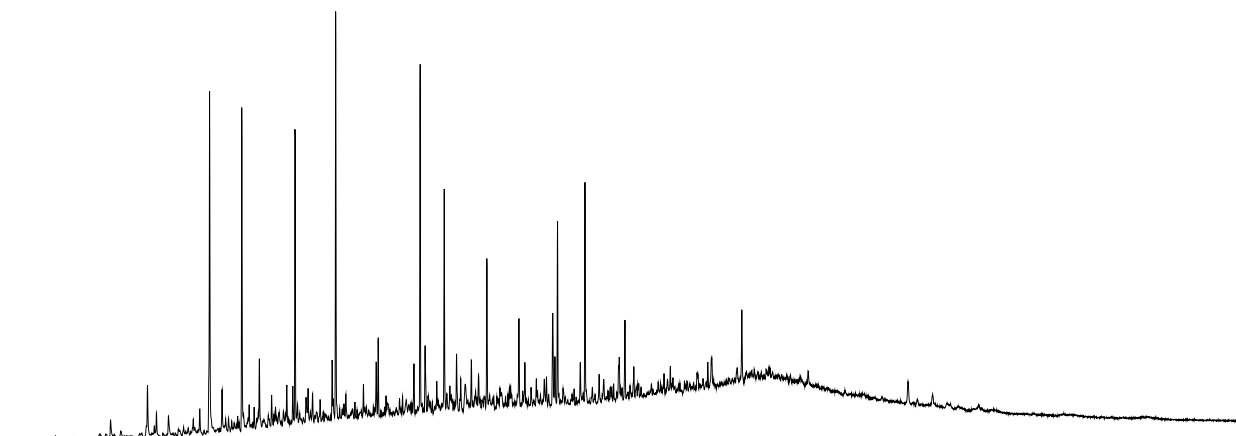


SR-230b

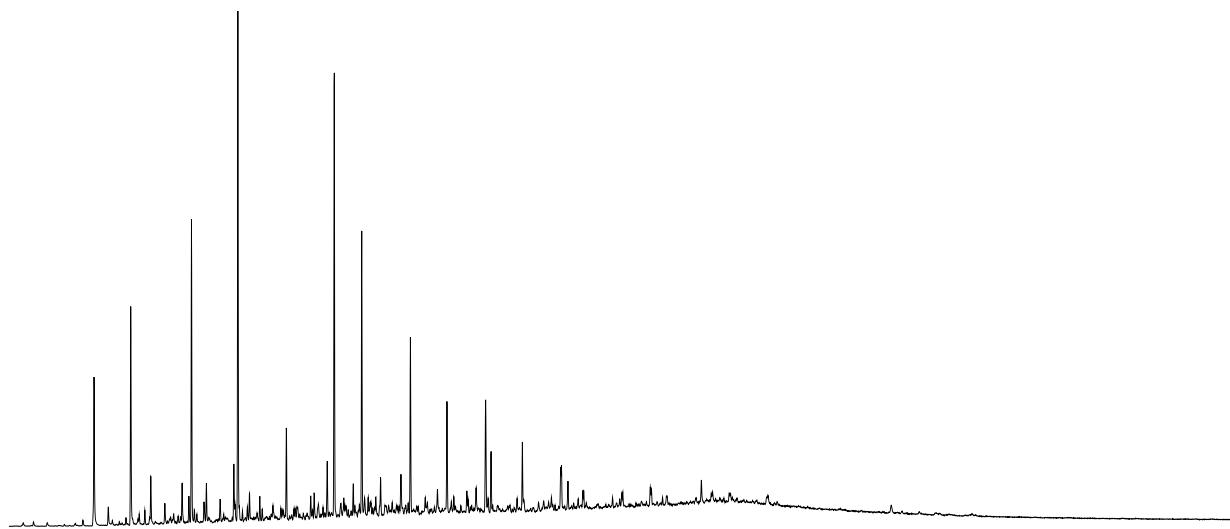


WDFD M/Z 133-134

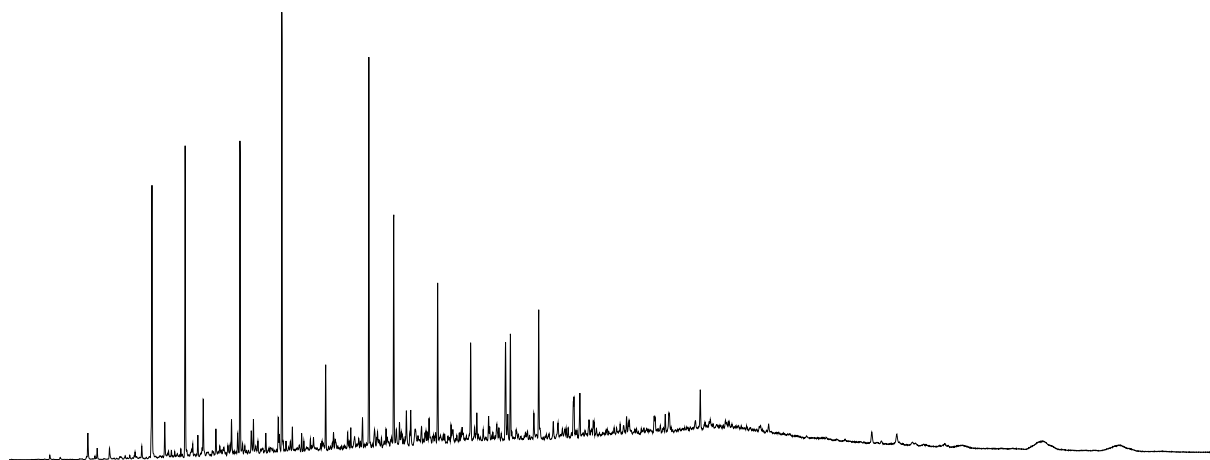
SR-190b



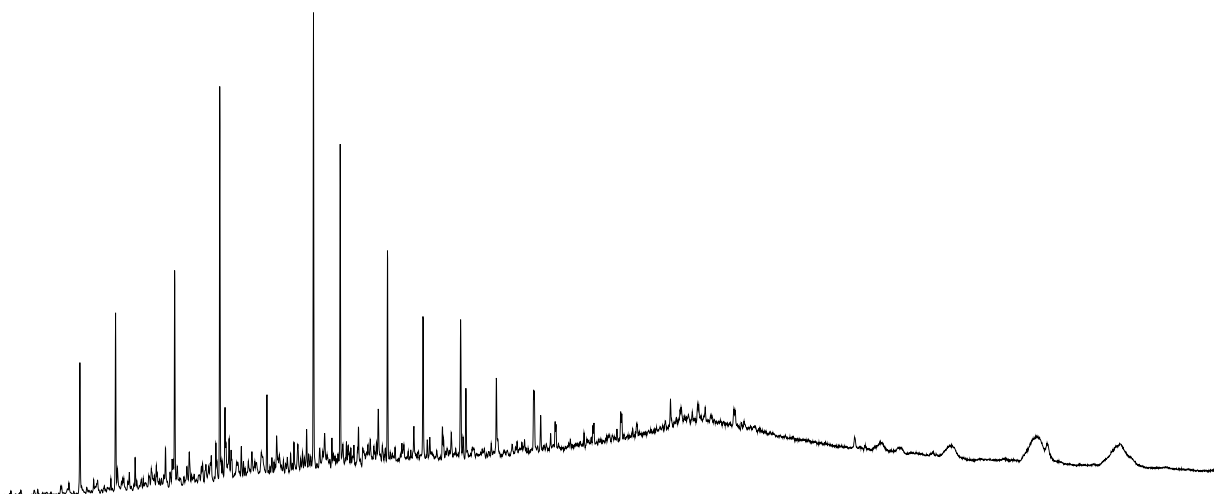
SR-191a



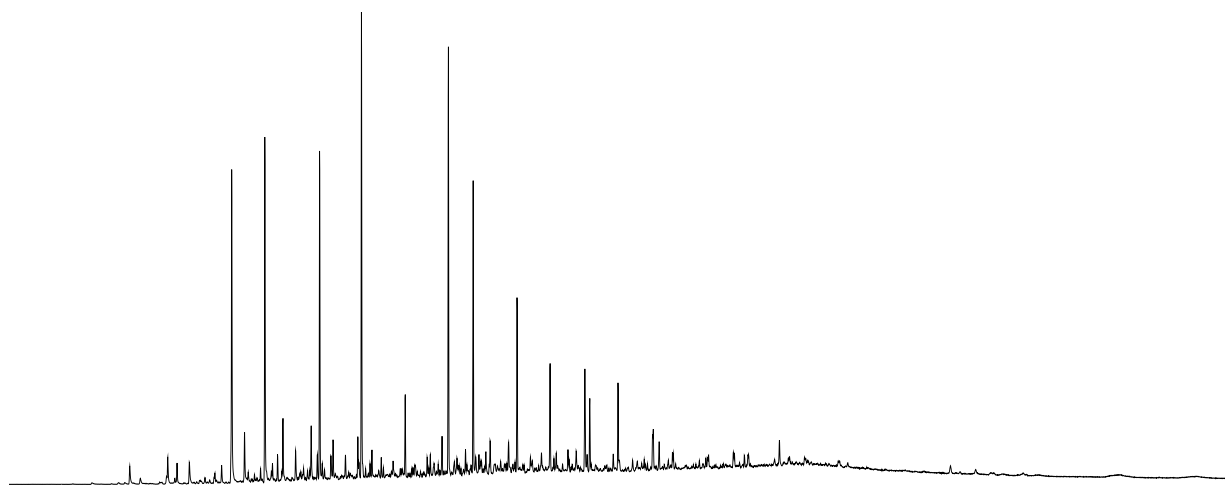
SR-191b



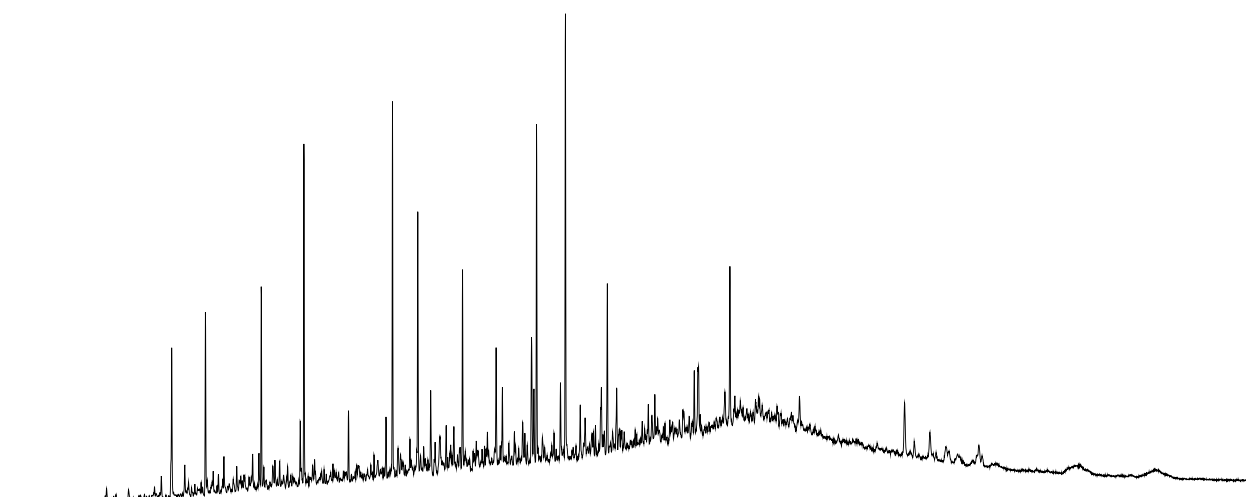
SR-192a



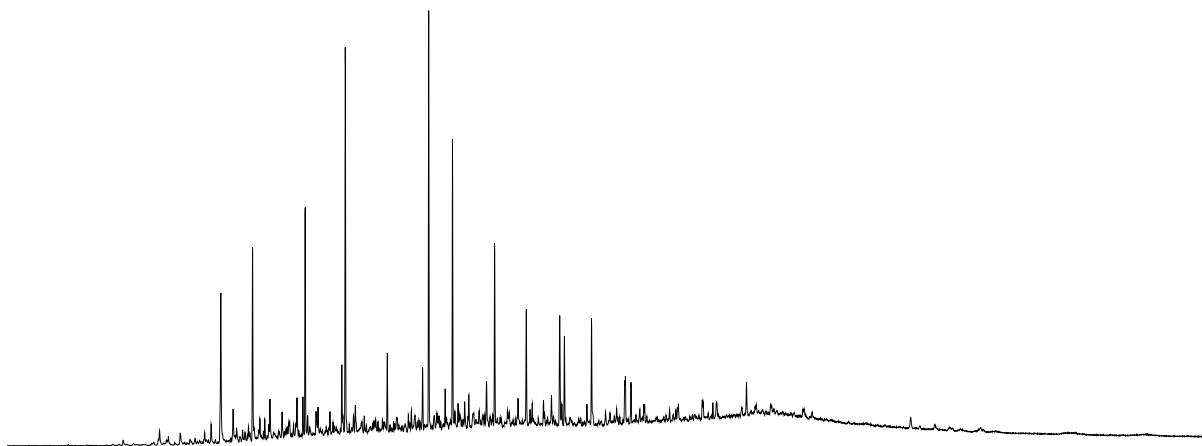
SR-193b



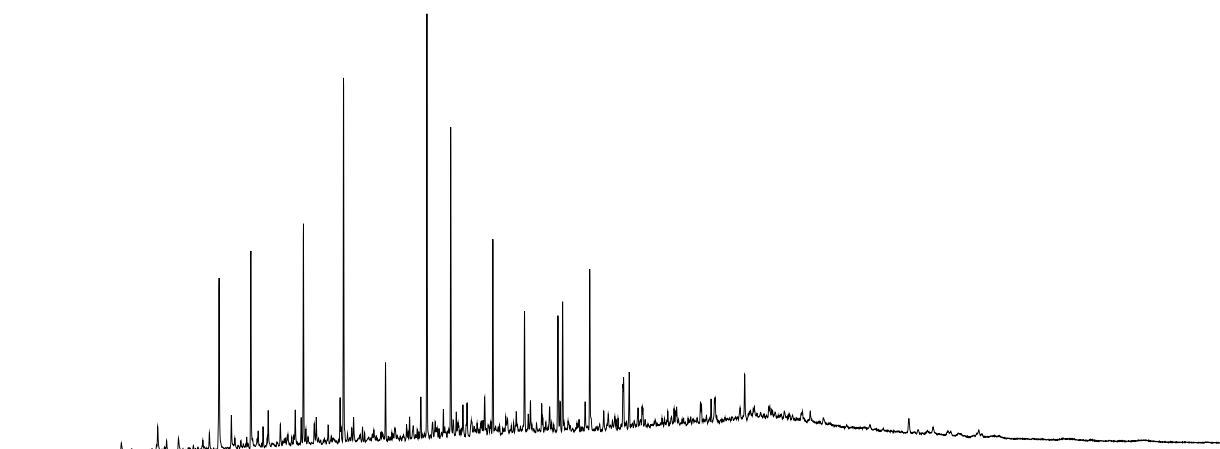
SR-194b



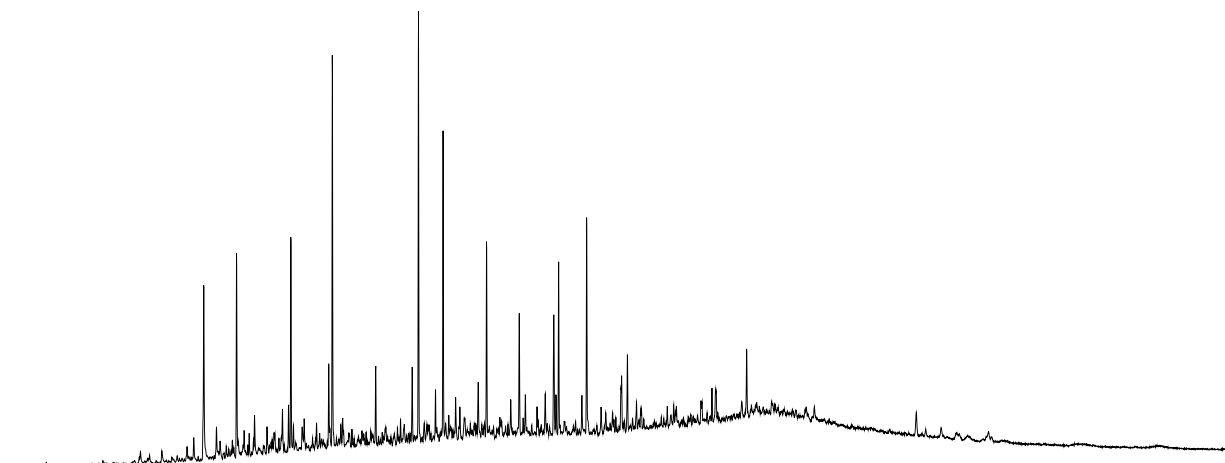
SR-195b



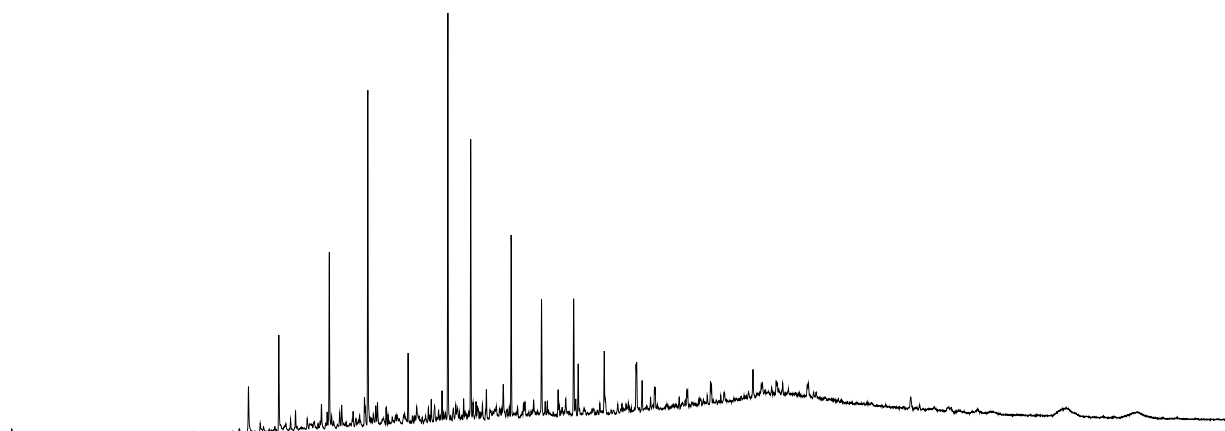
SR-196b



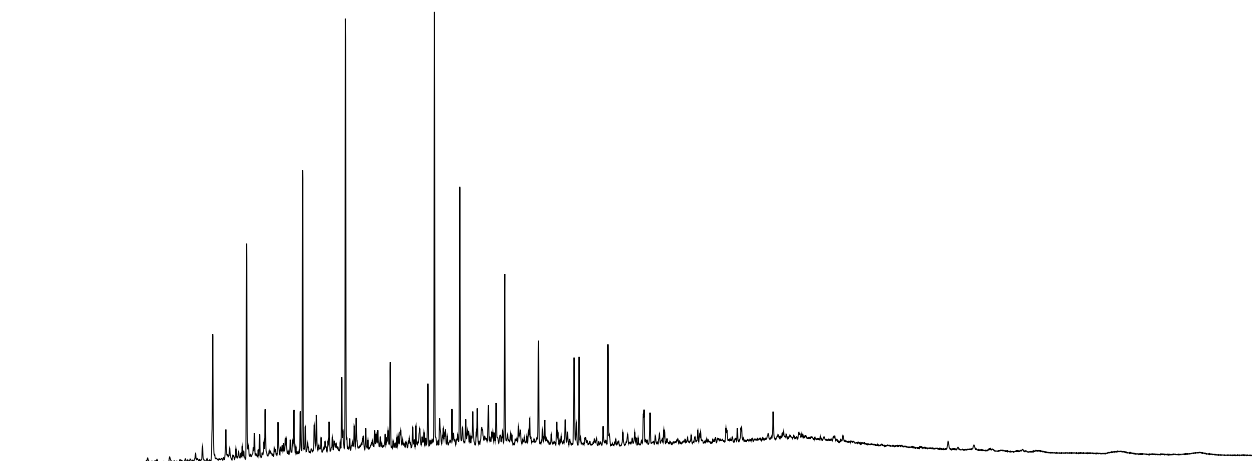
SR-197b



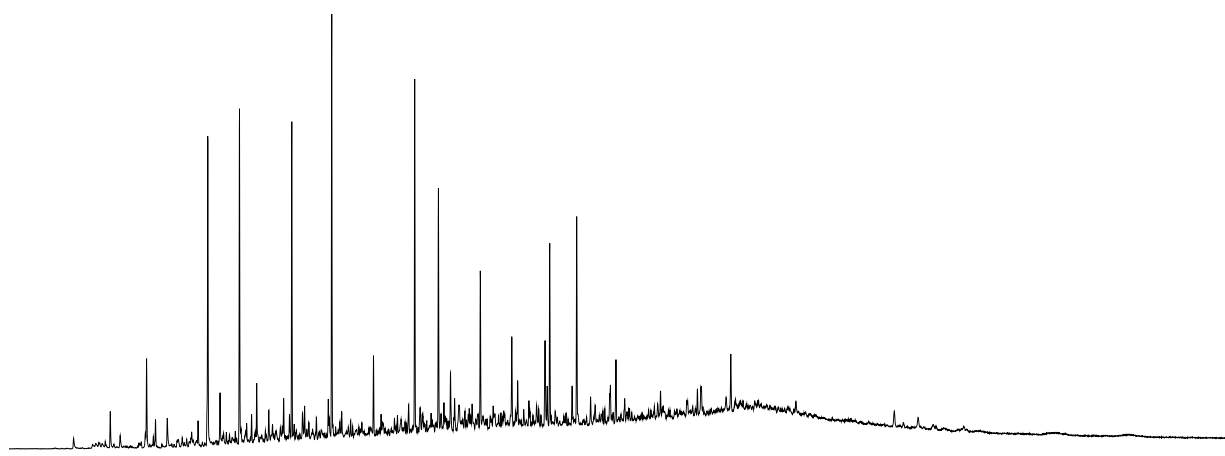
SR-198a



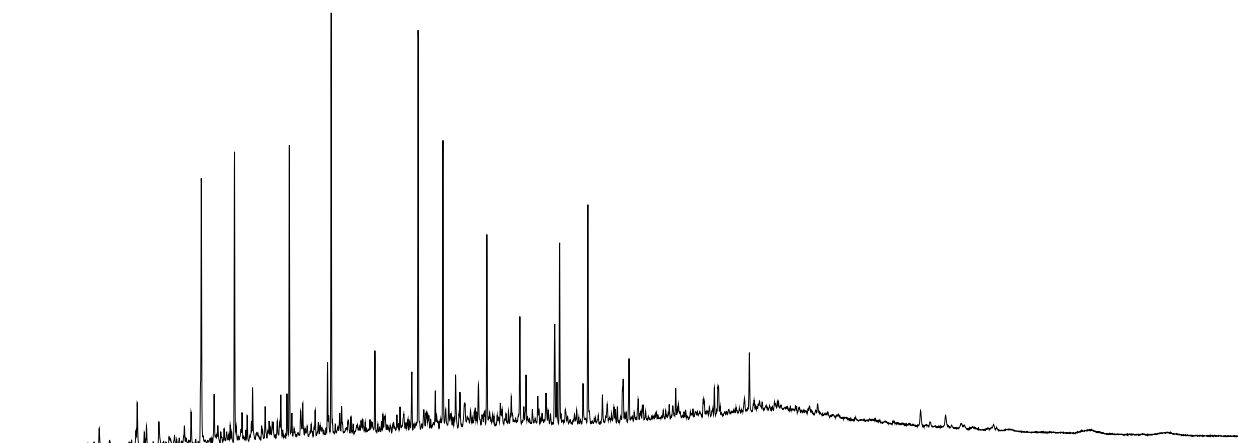
SR-199b



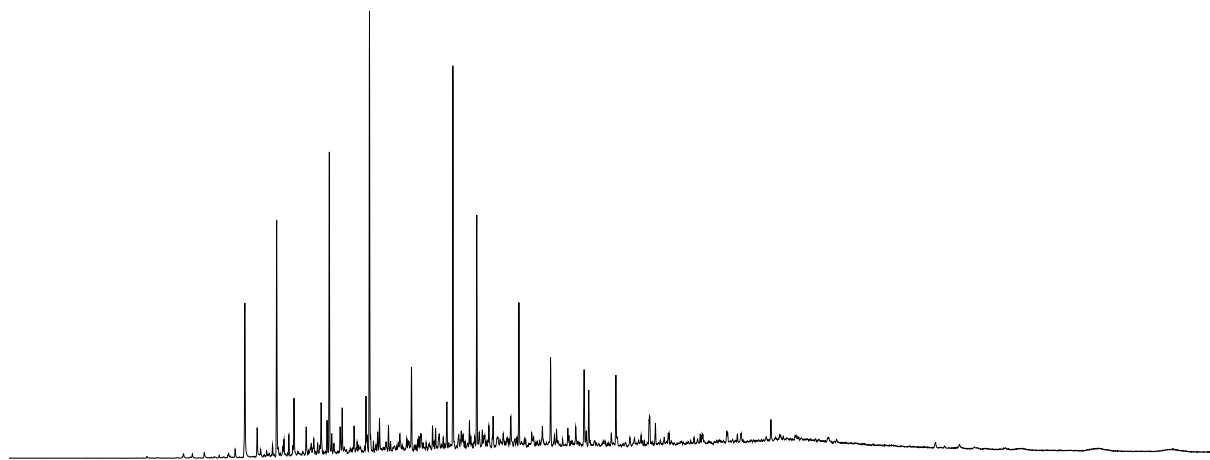
SR-200b



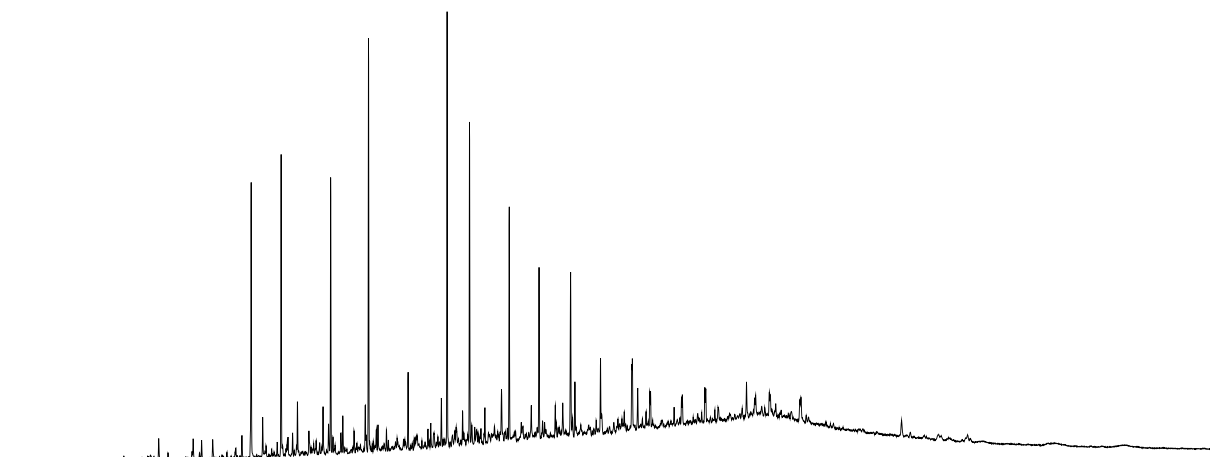
SR-204b



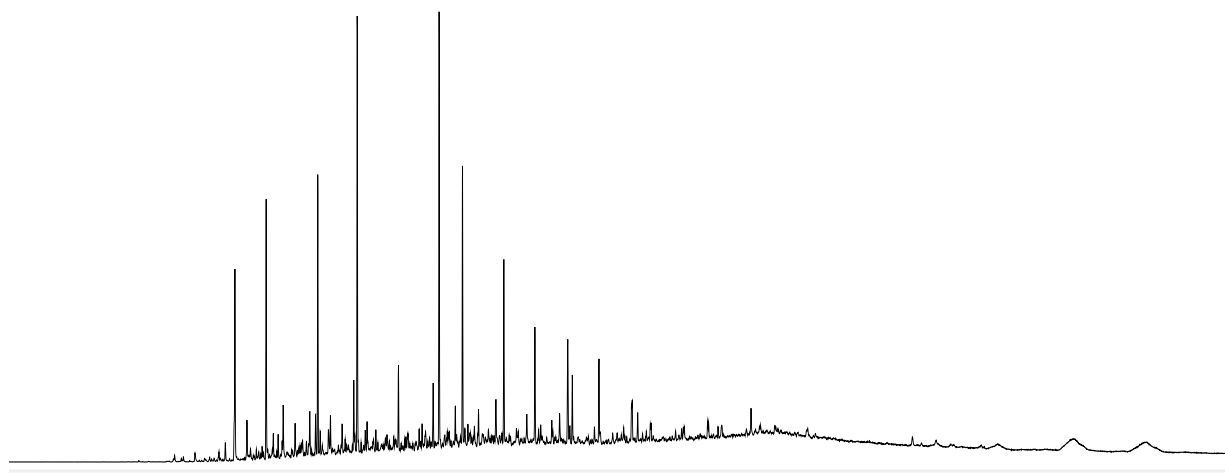
SR-208b



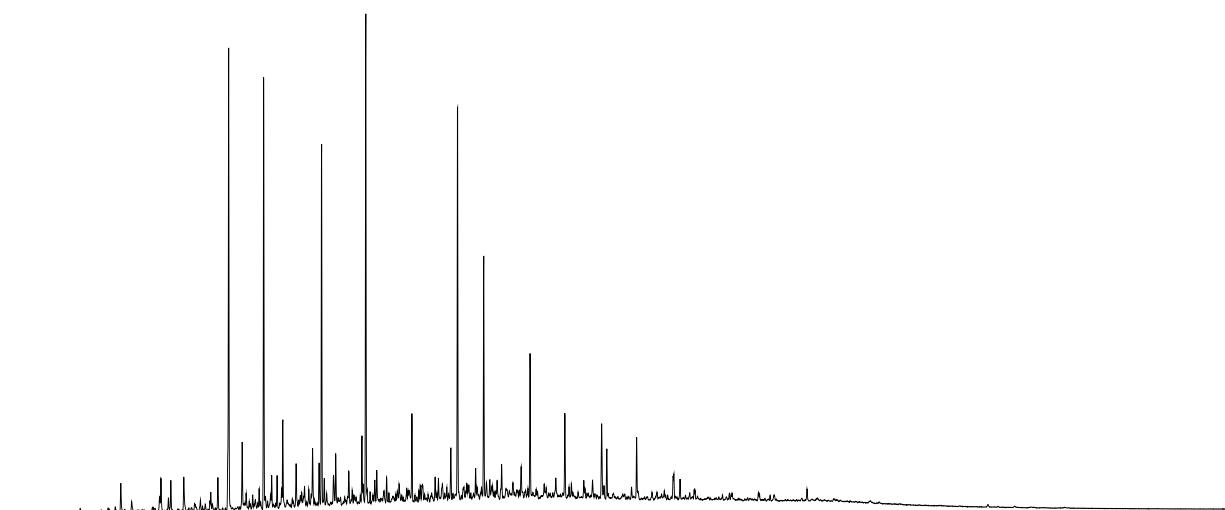
SR-209a



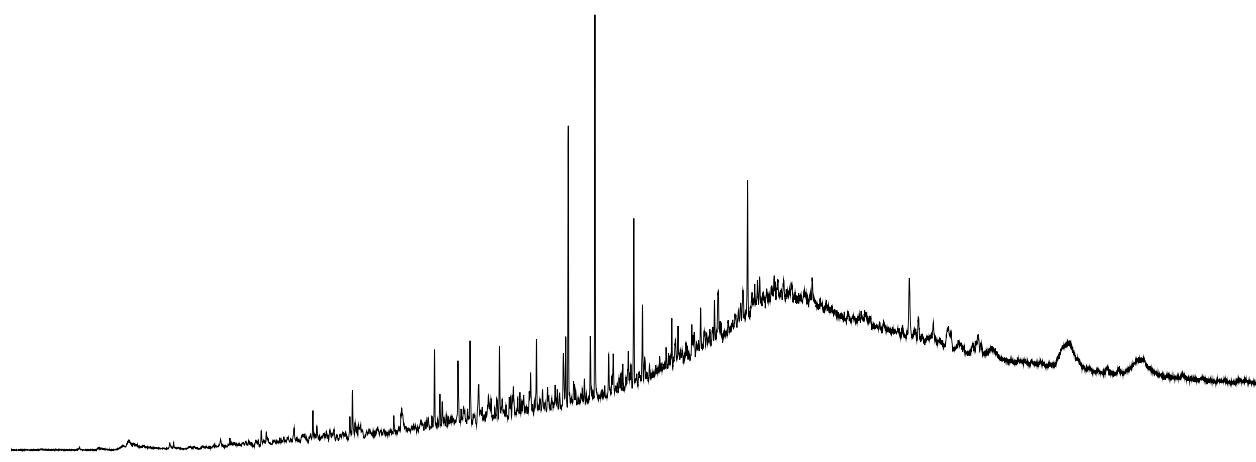
SR-210b



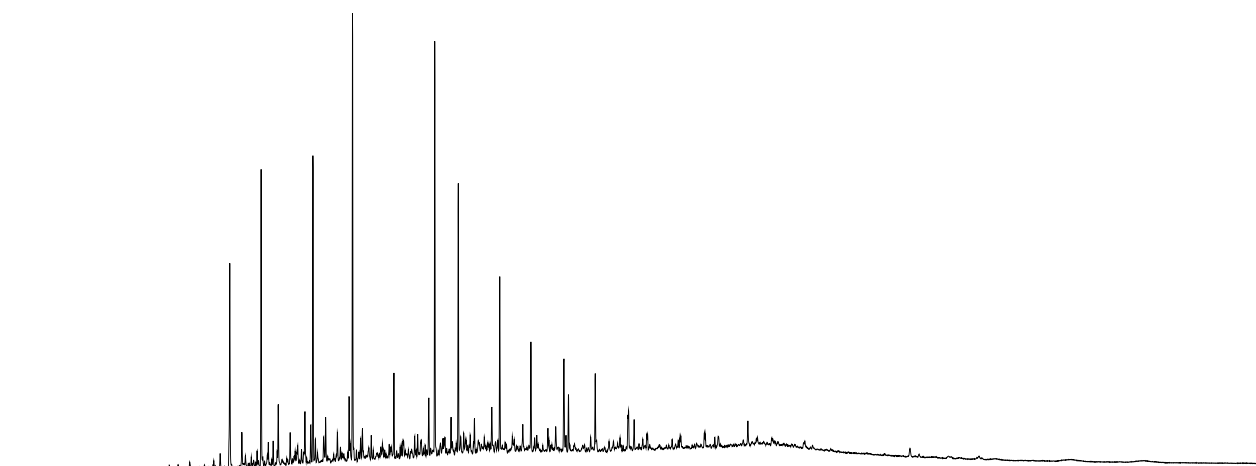
SR-211b



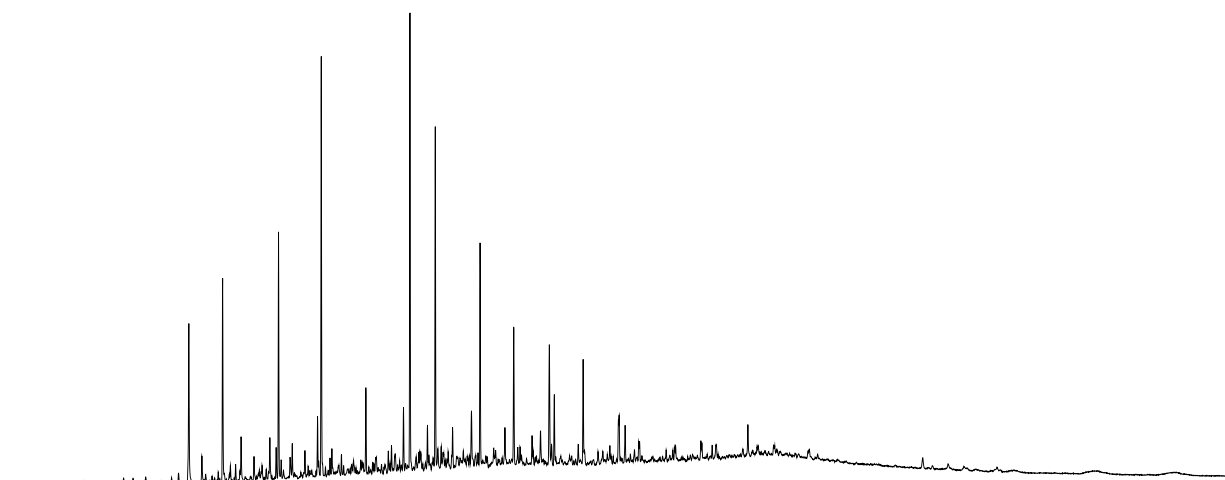
SR-212a



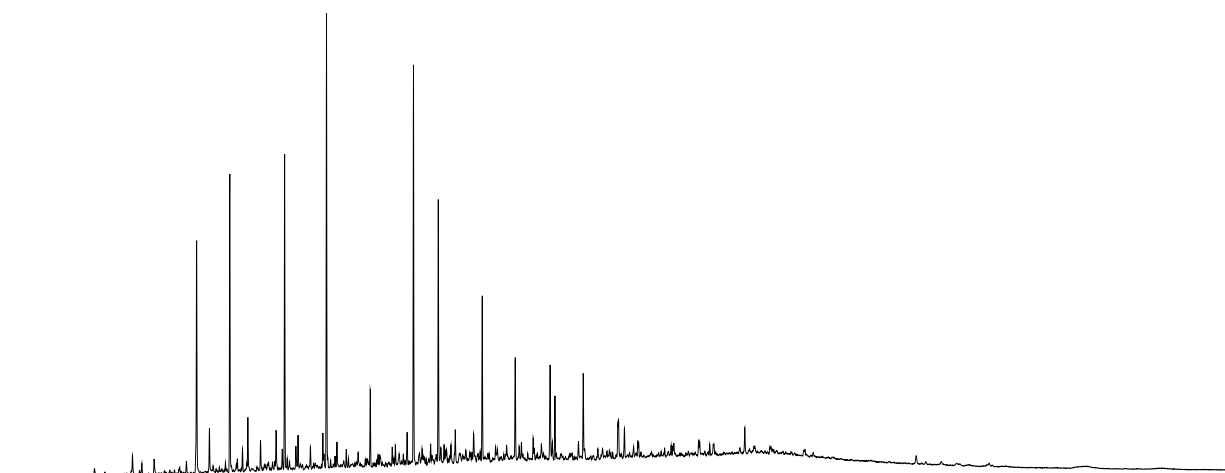
SR-213b



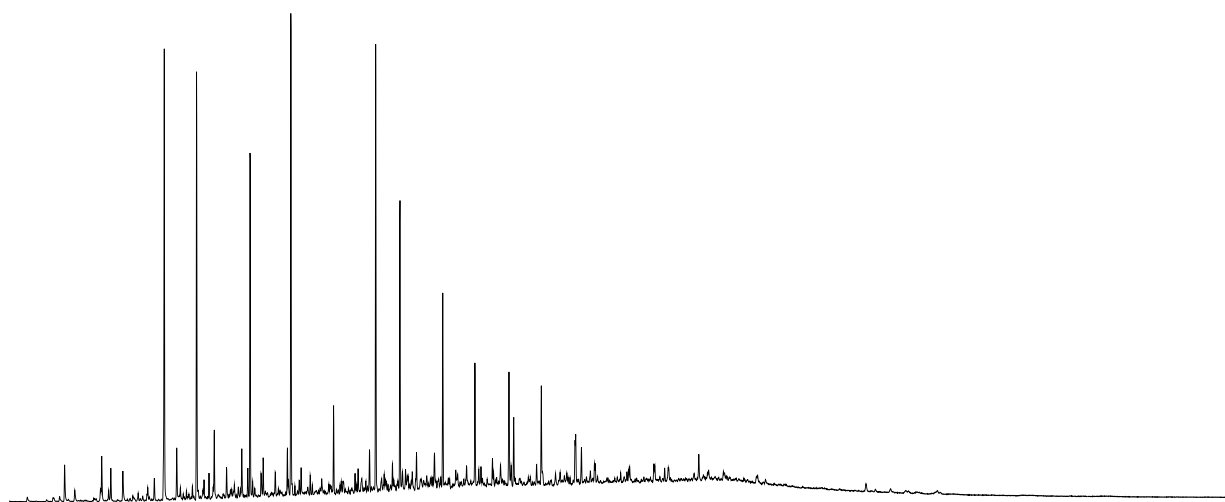
SR-214b



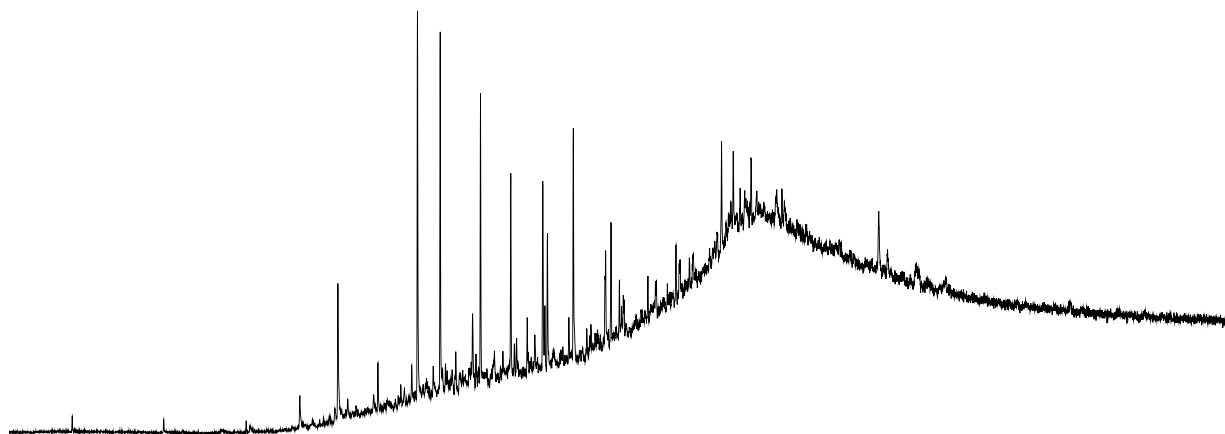
SR-215b



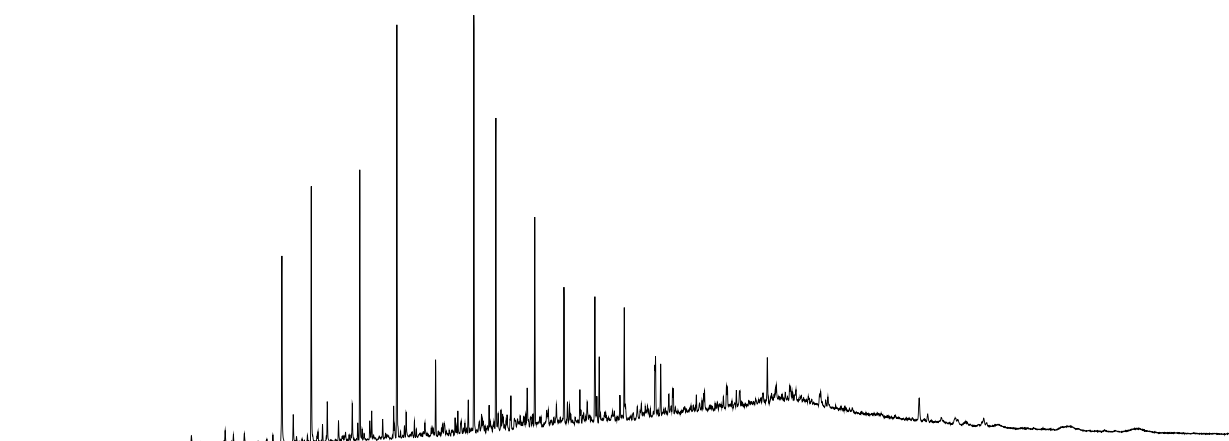
SR-217b



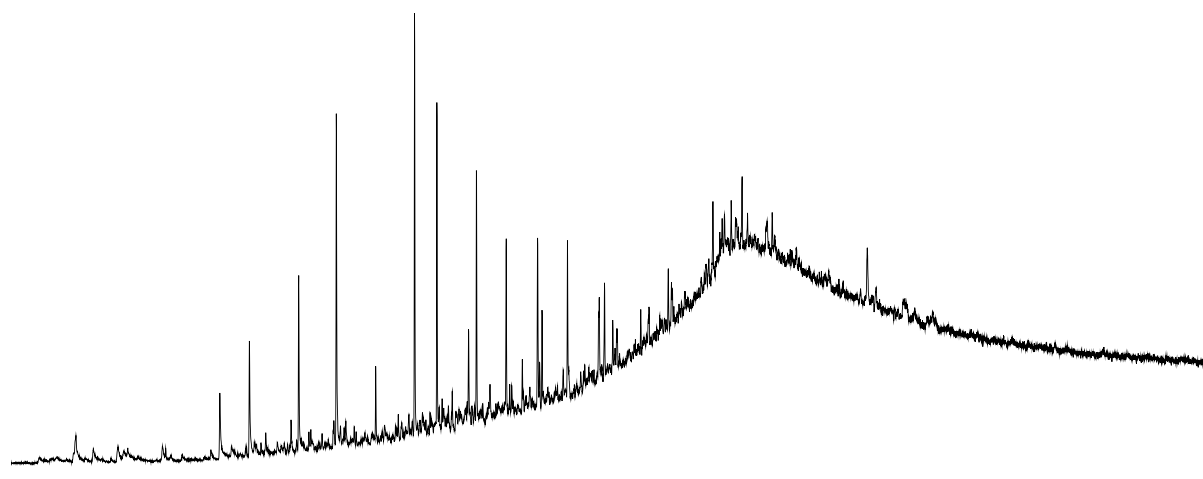
SR-219a



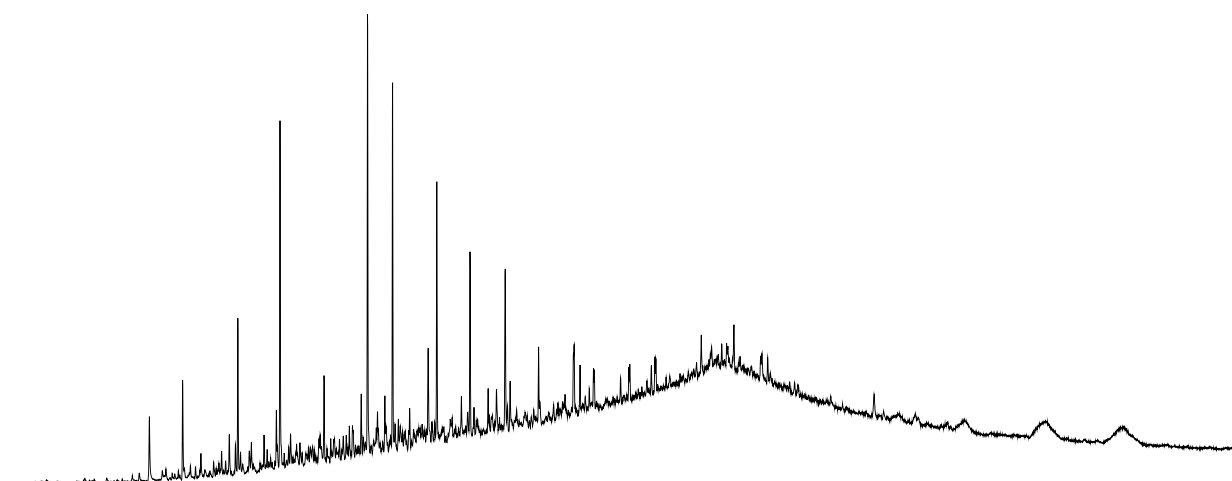
SR-221b



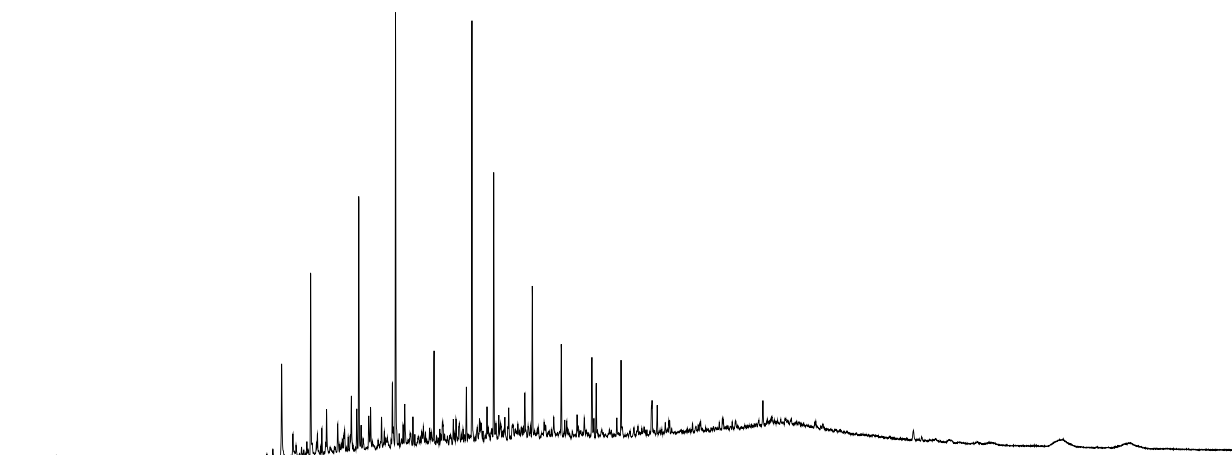
SR-222a



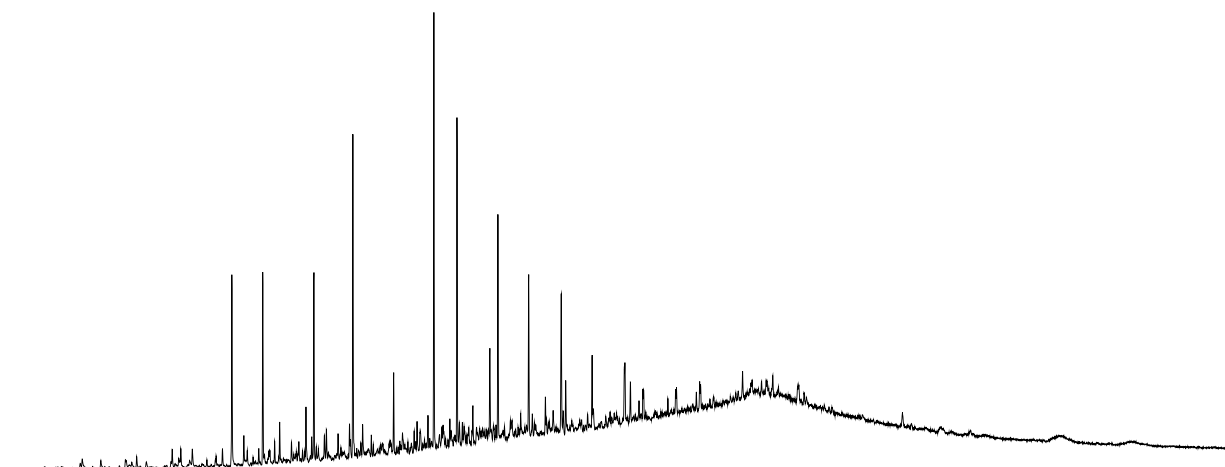
SR-223a



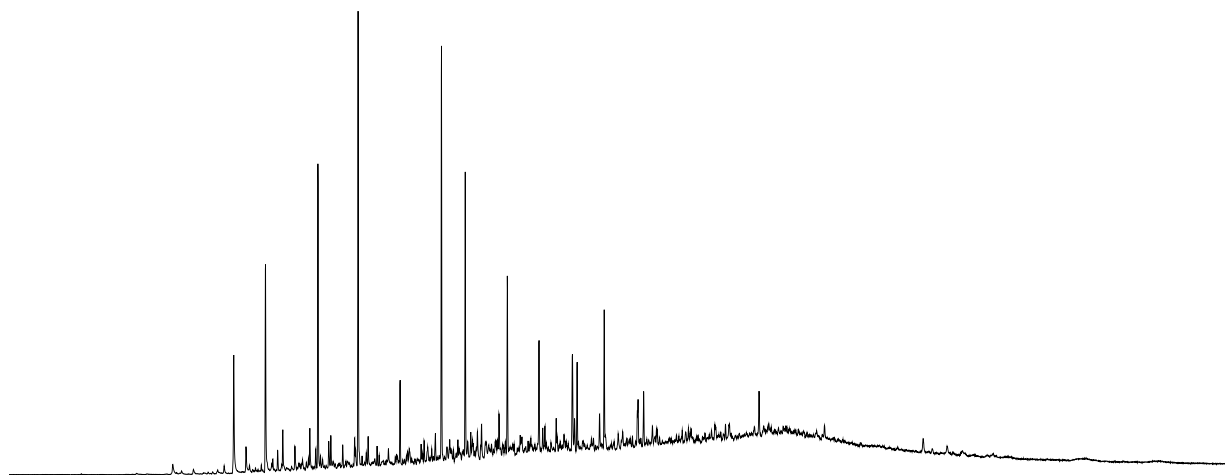
SR-225b



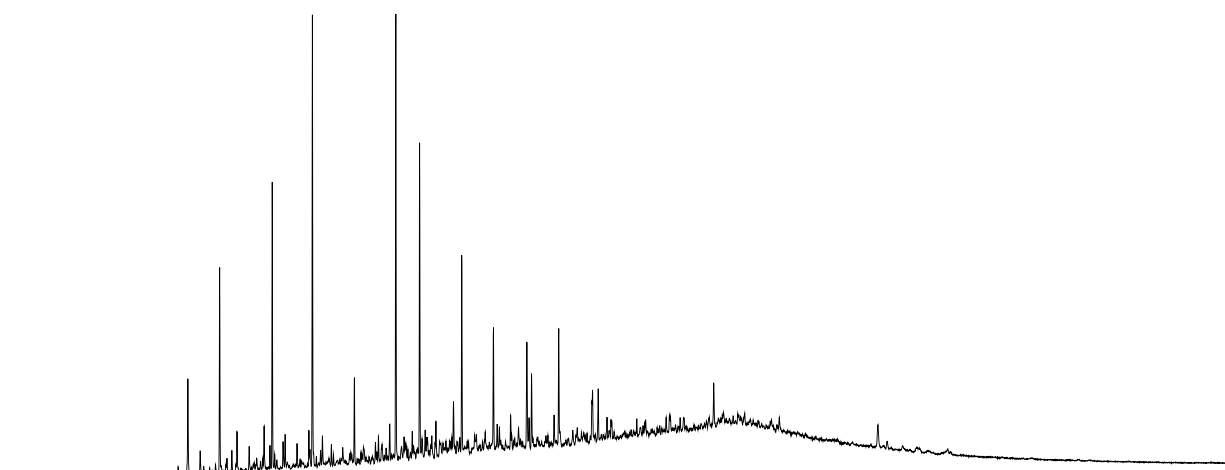
SR-226a



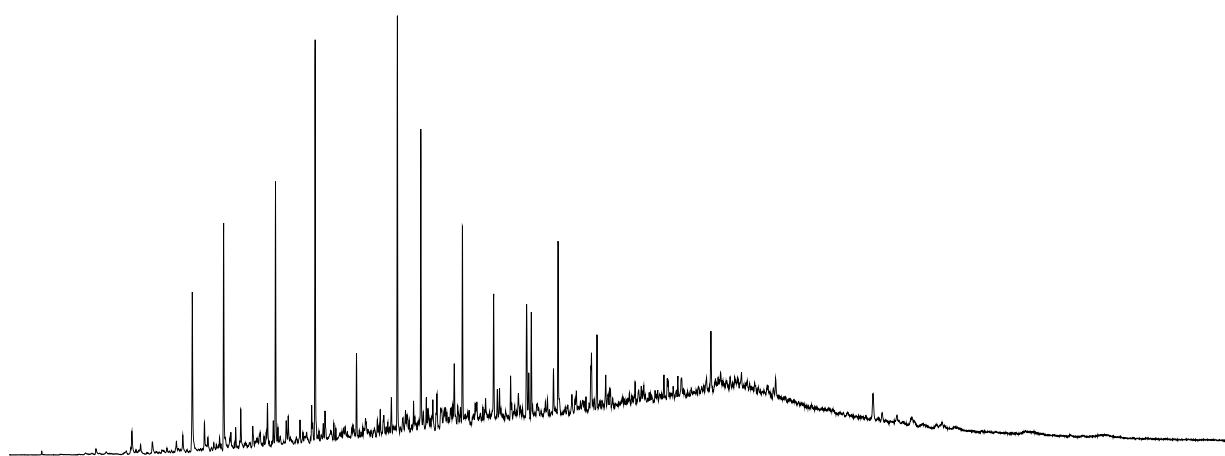
SR-227b



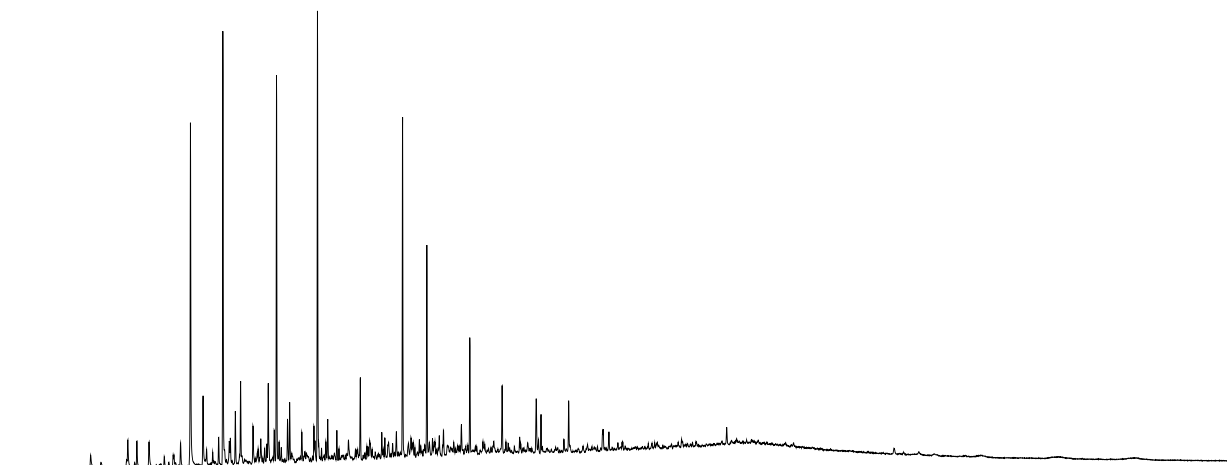
SR-228b



SR-229a

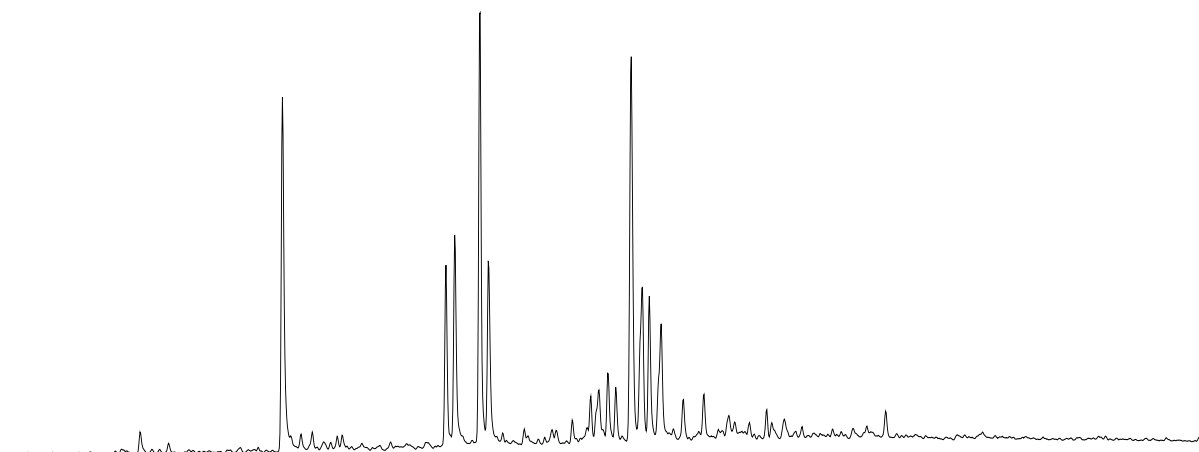


SR-230b

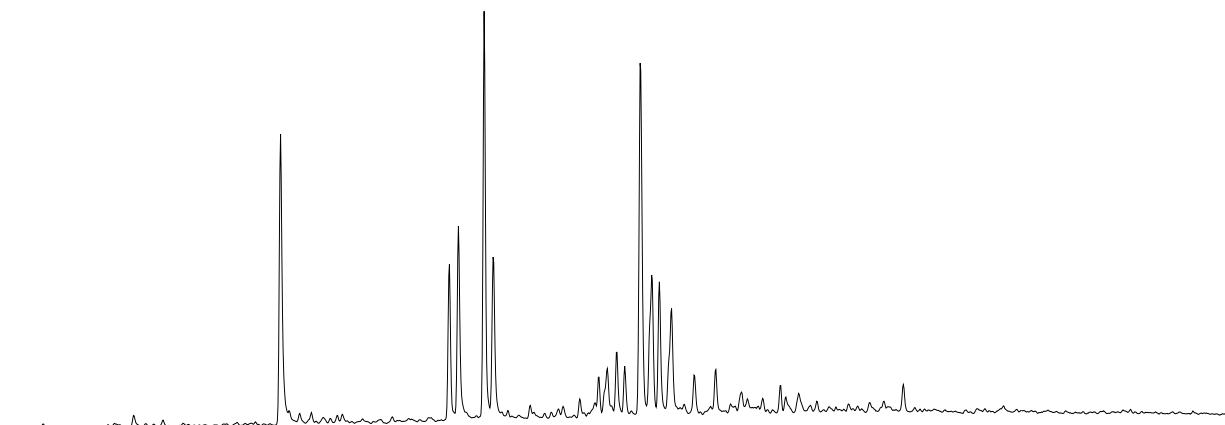


WDFD M/Z 178.3, 192.3, 206.3

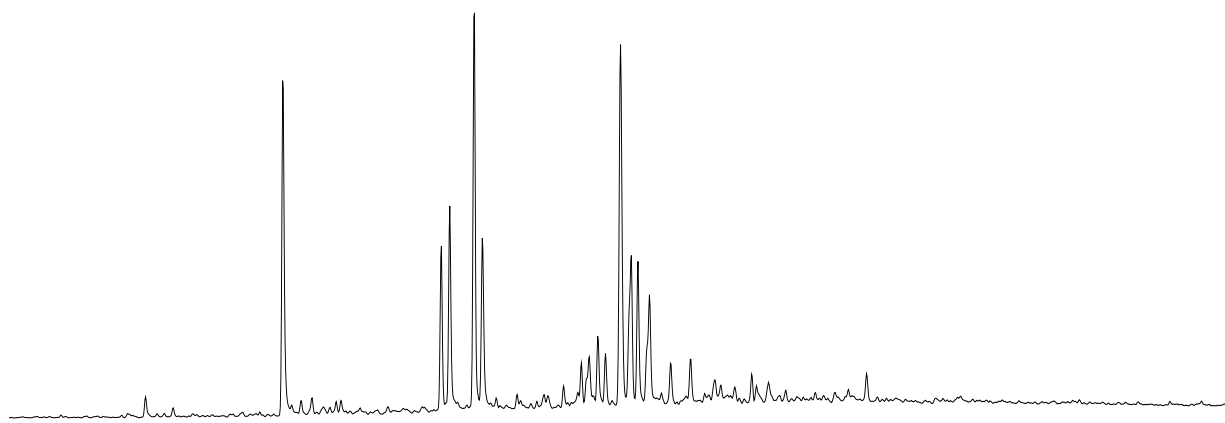
SR-190b



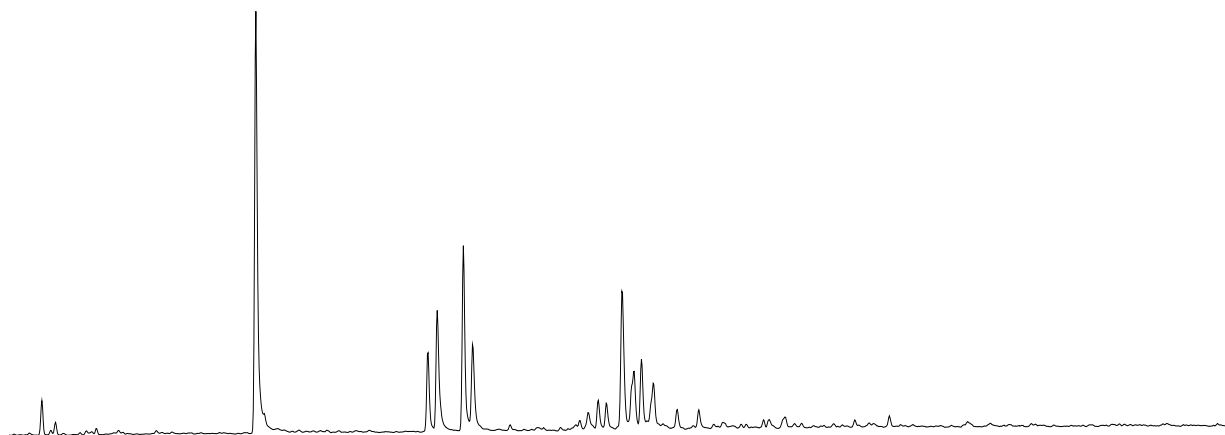
SR-191a



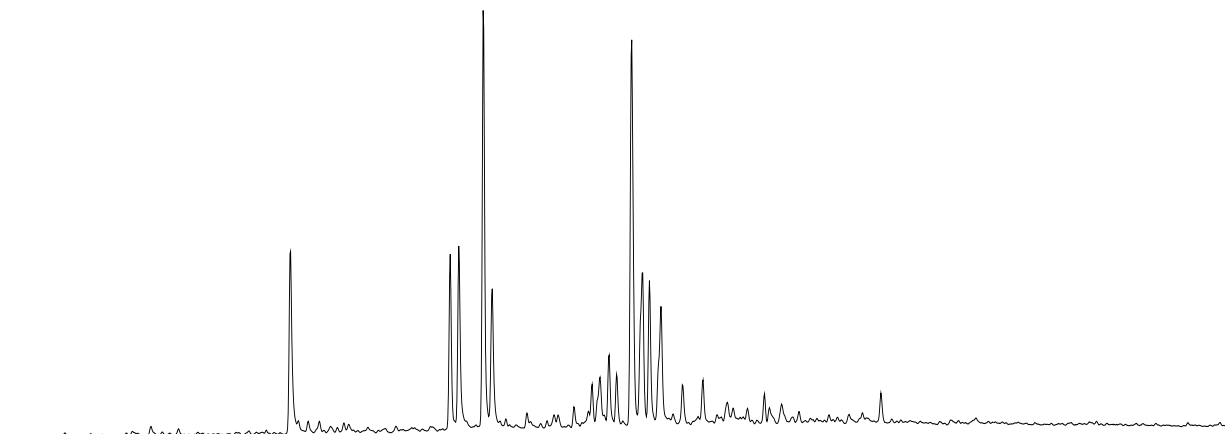
SR-191b



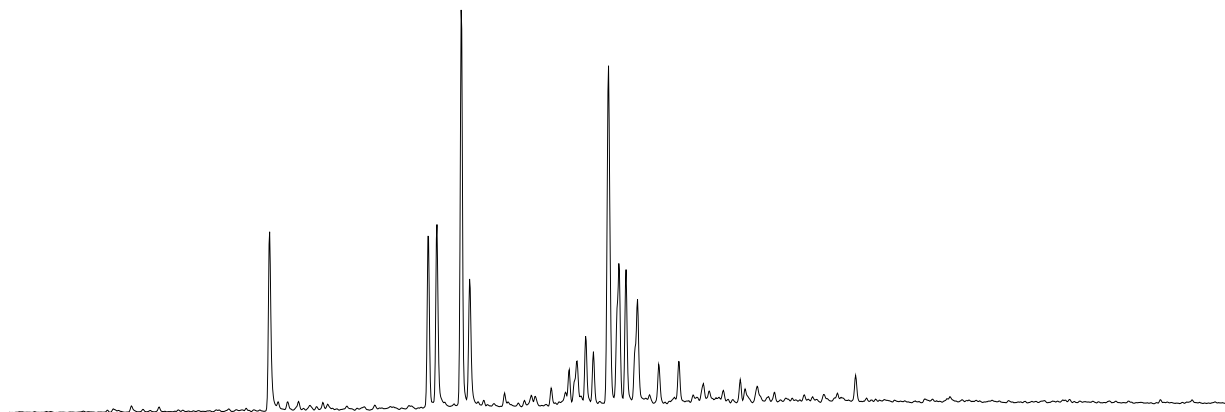
SR-192a



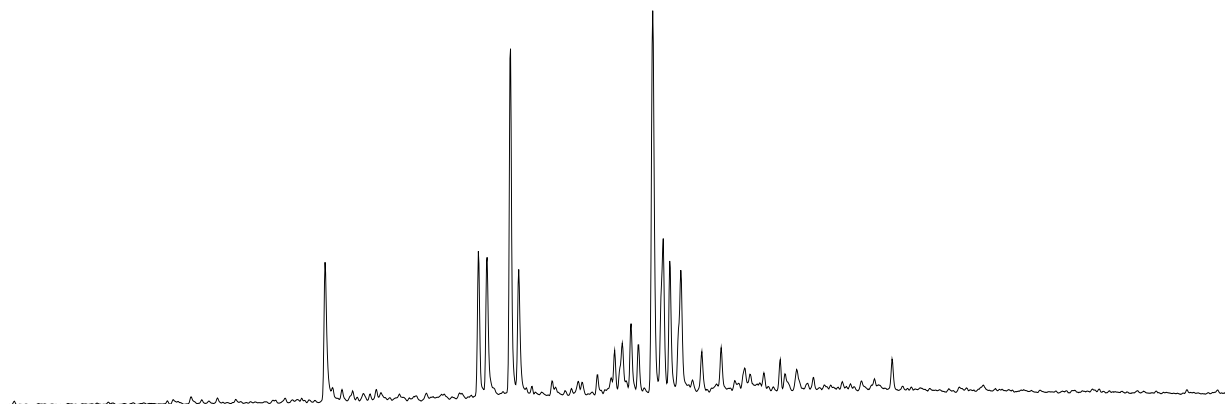
SR-193b



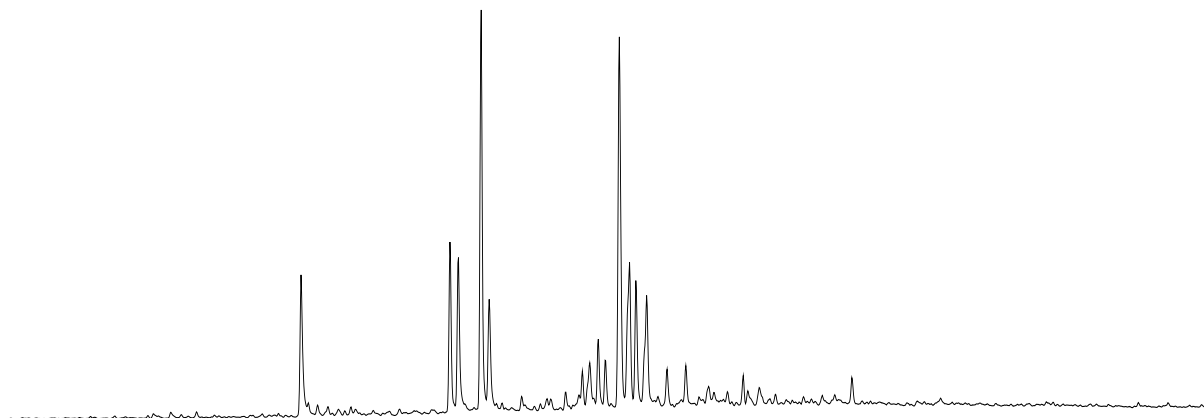
SR-194b



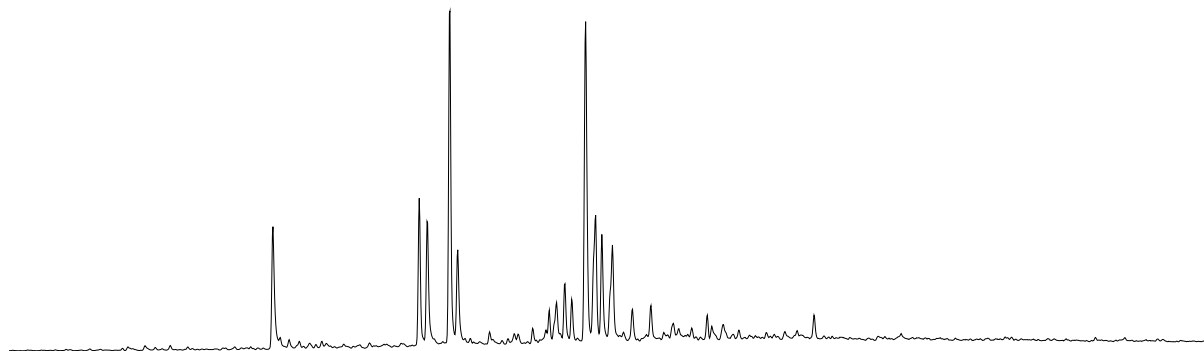
SR-195b



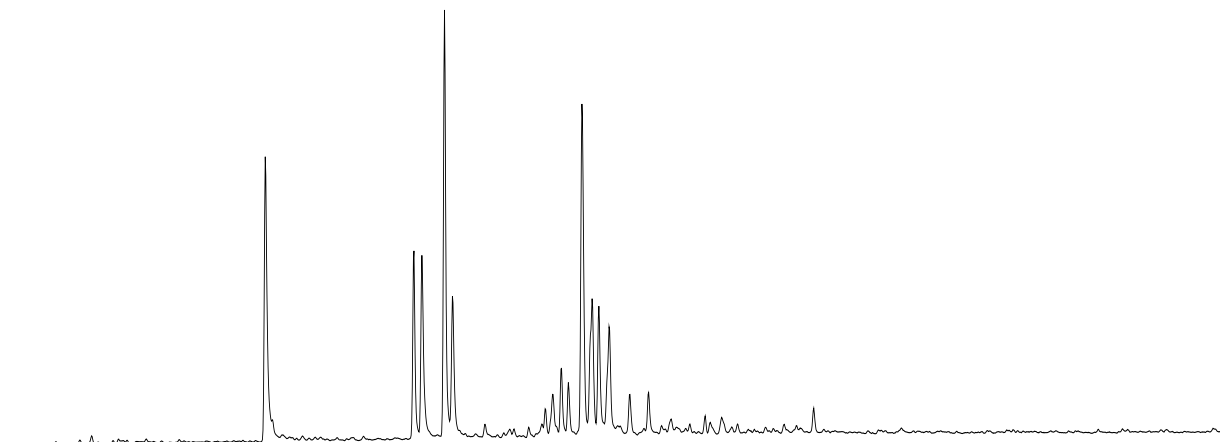
SR-196b



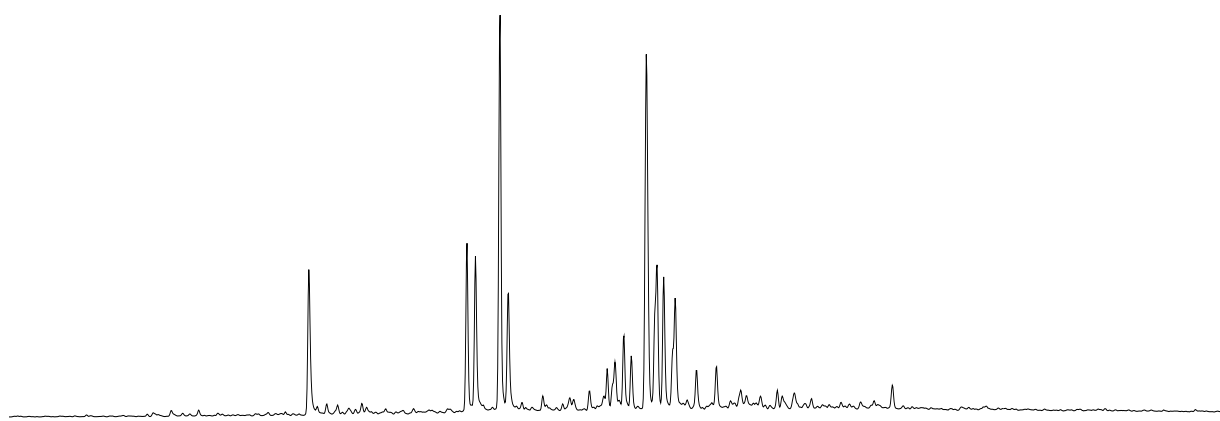
SR-197b



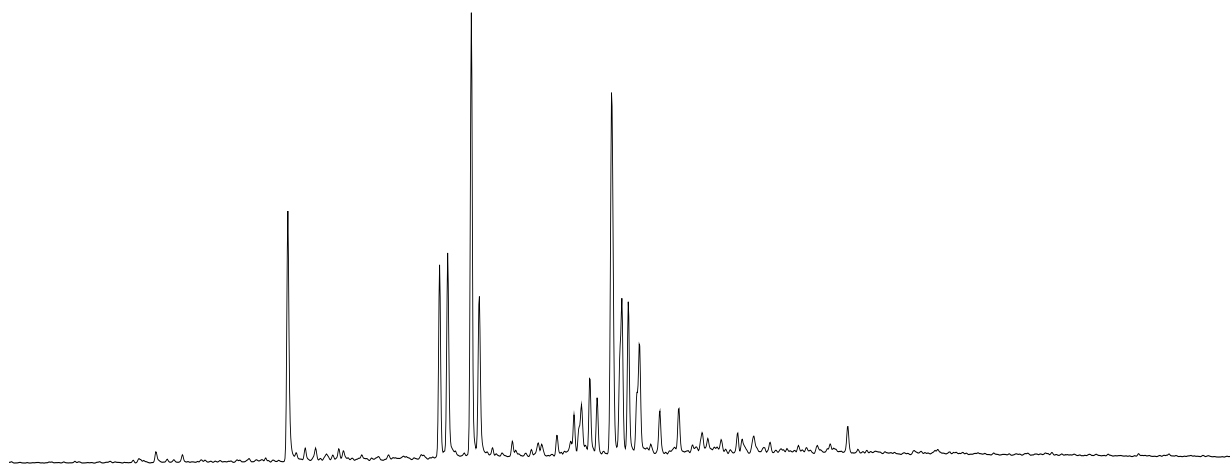
SR-198a



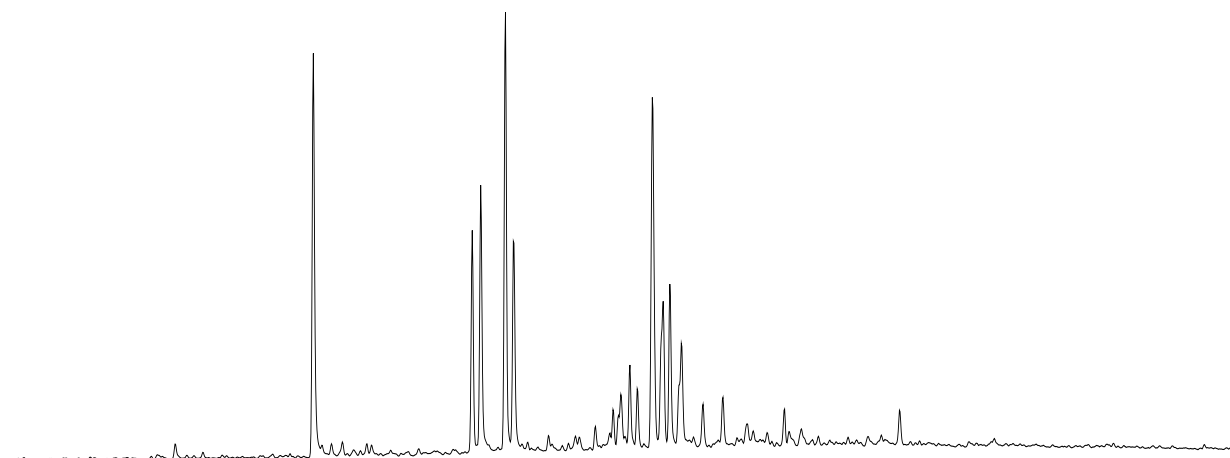
SR-199b



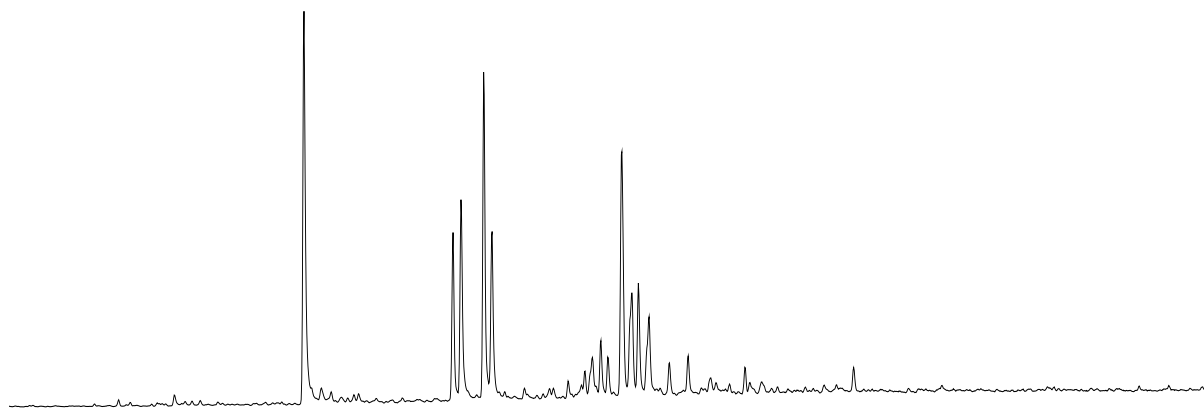
SR-200b



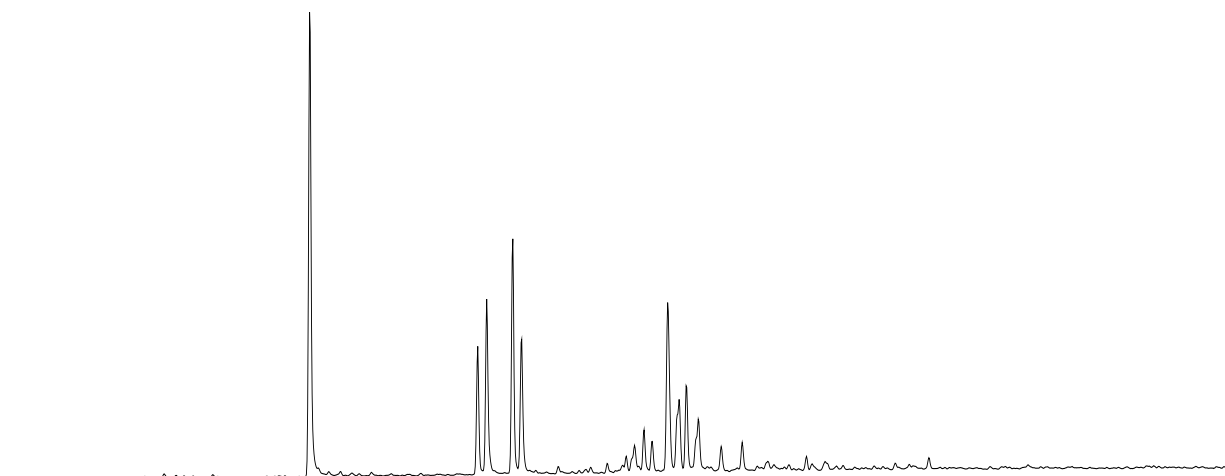
SR-204b



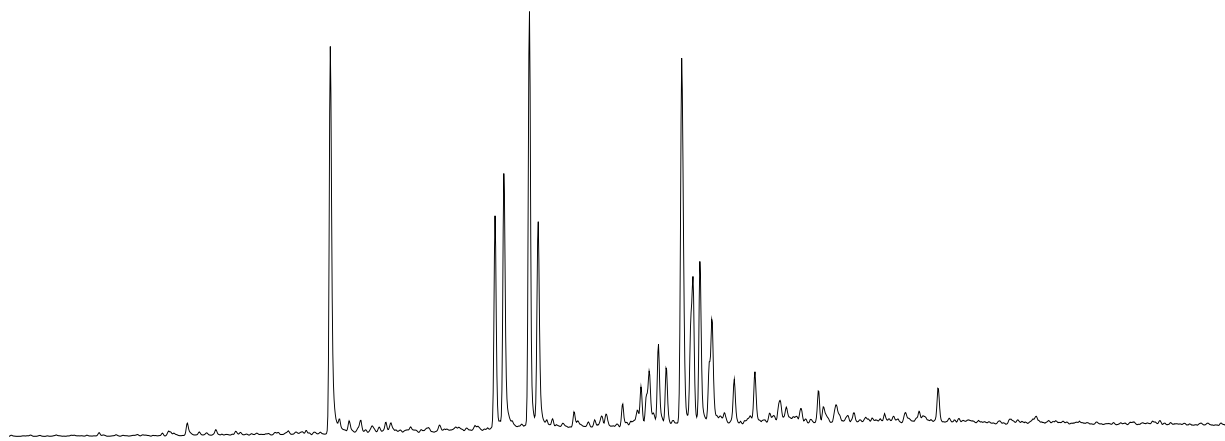
SR-205a



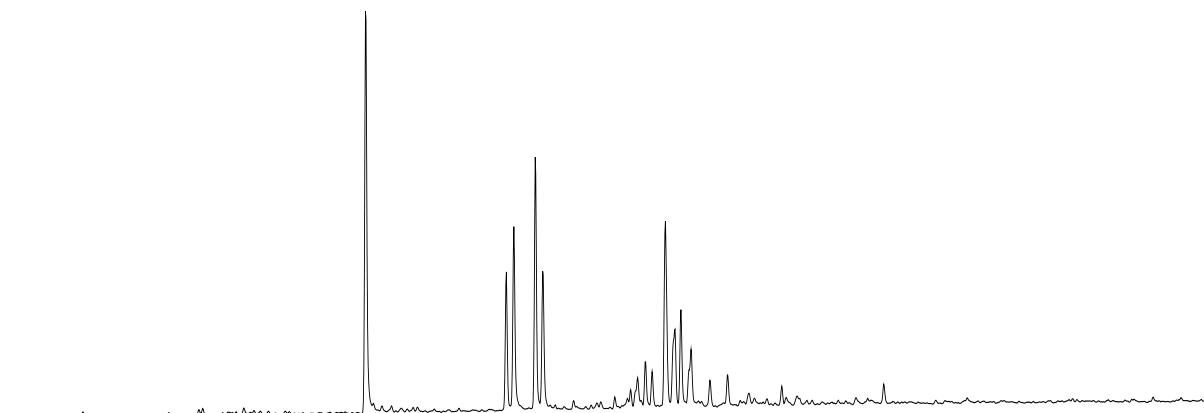
SR-207a



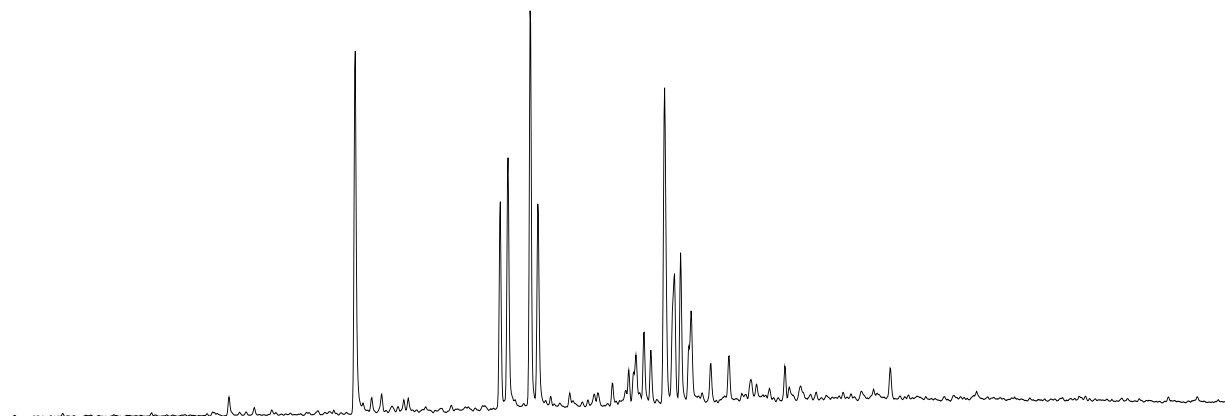
SR-208b



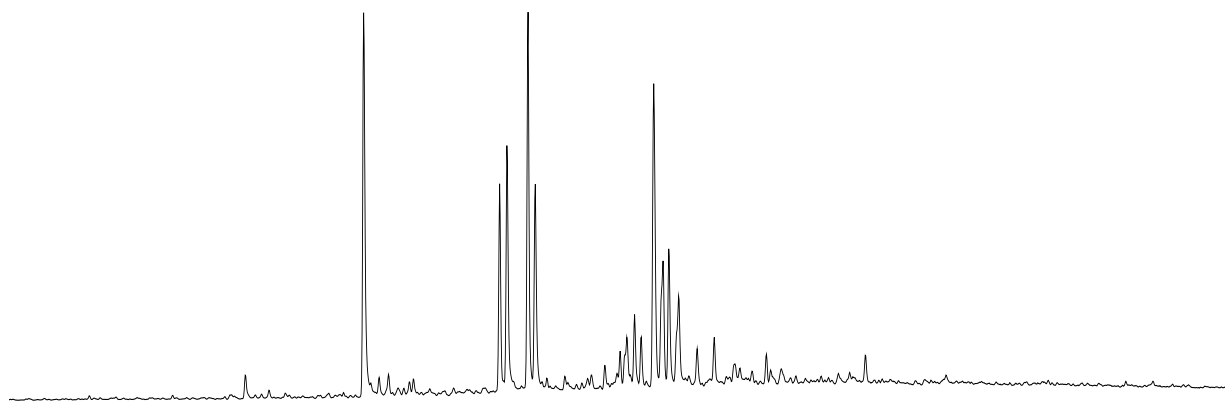
SR-209a



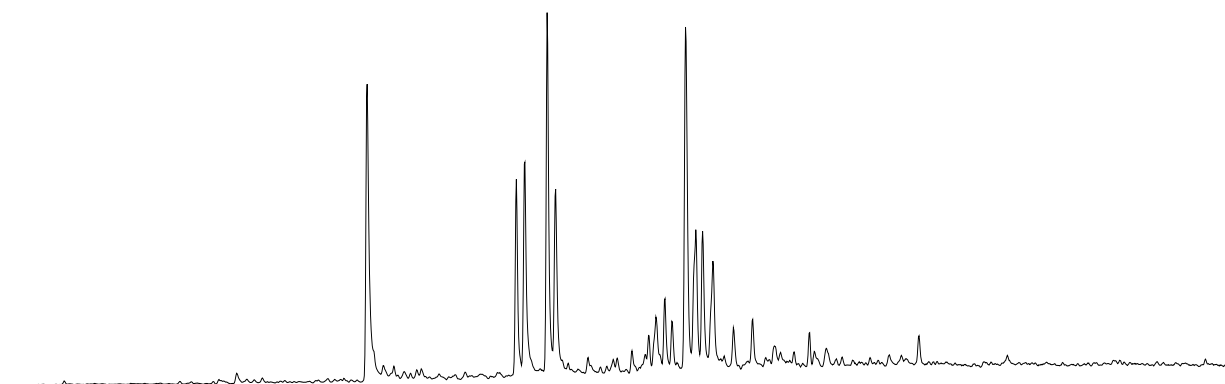
SR-210b



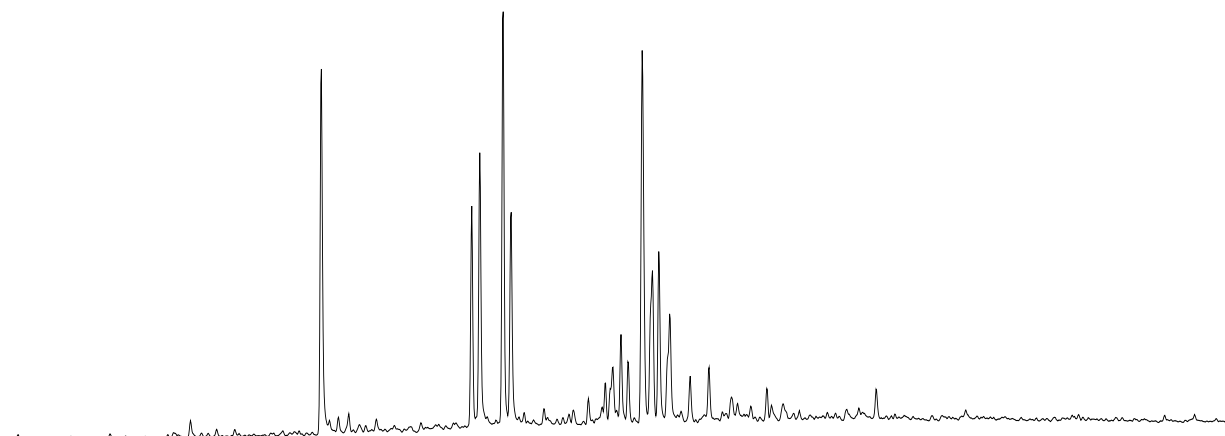
SR-211b



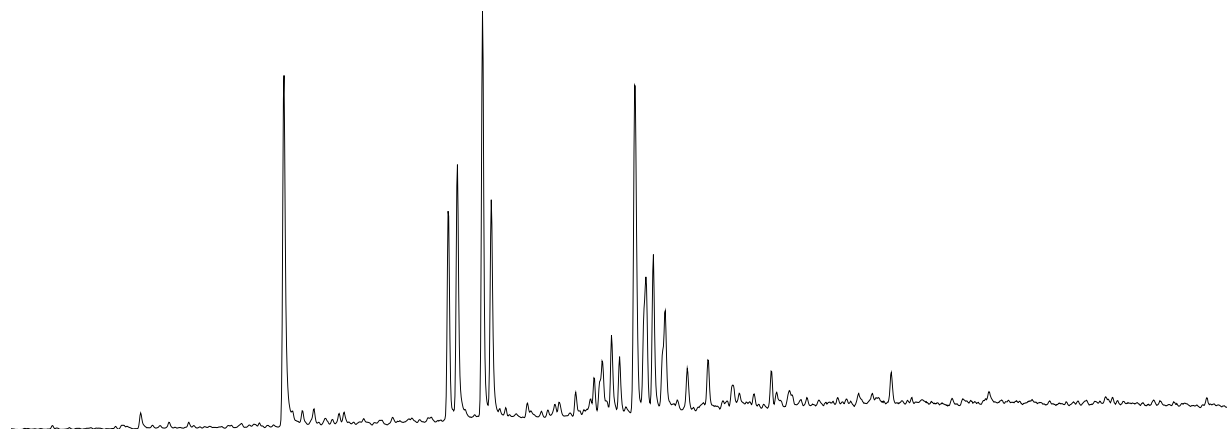
SR-212a



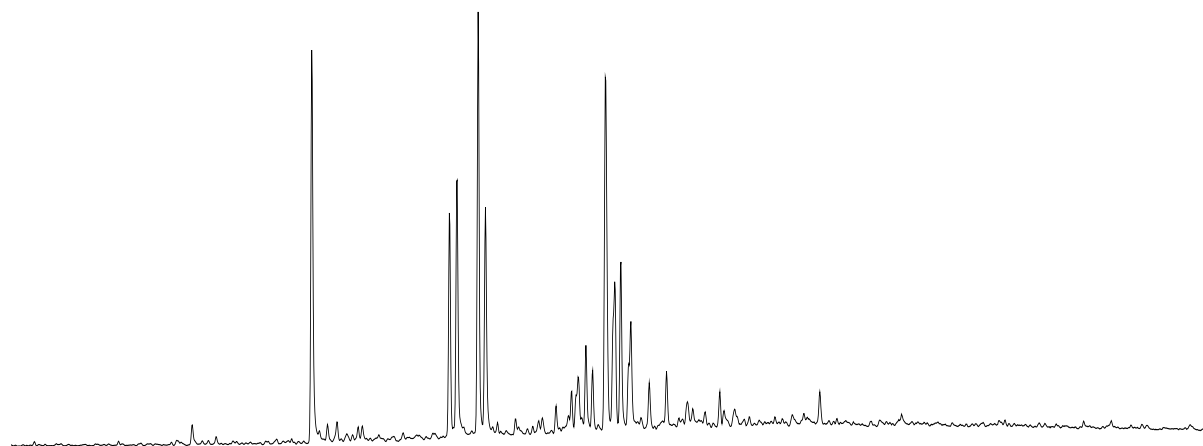
SR-213b



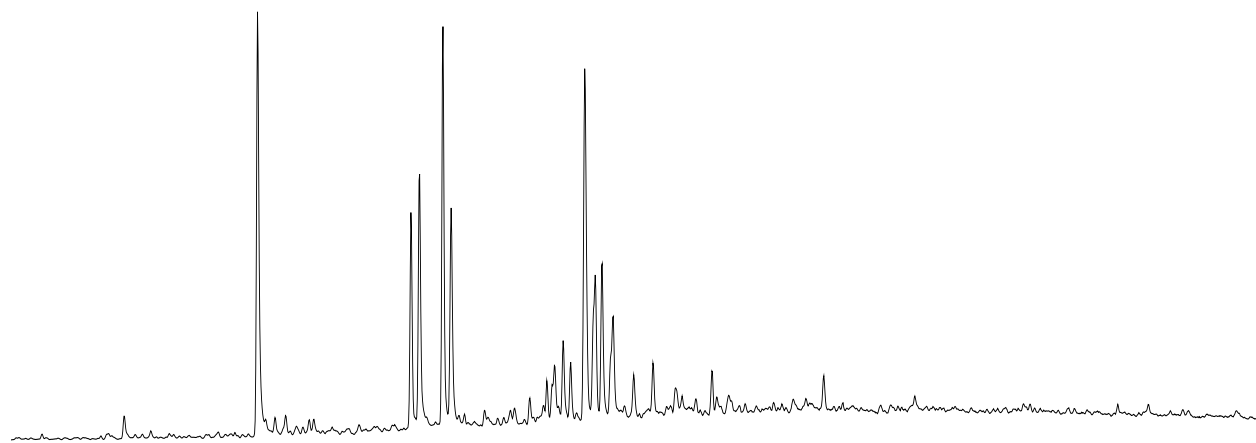
SR-214b



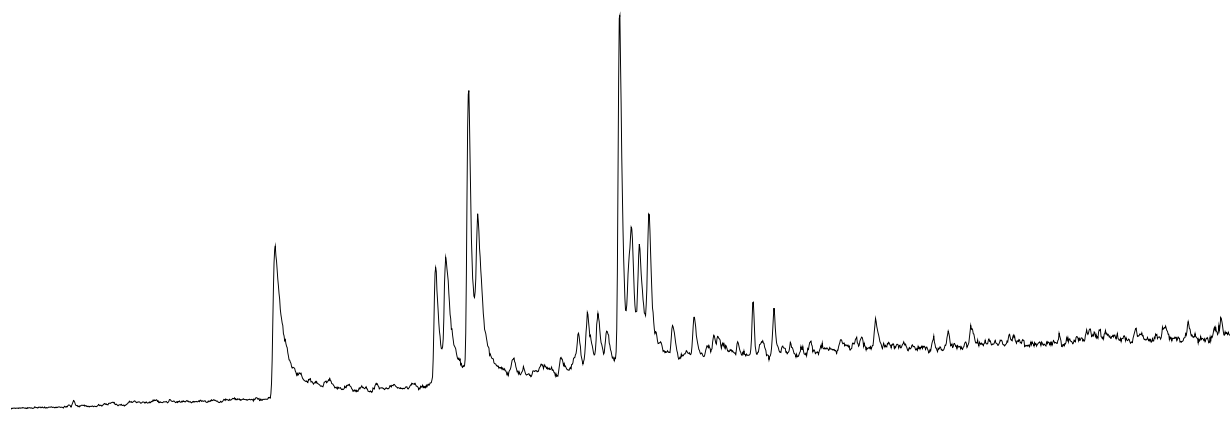
SR-215b



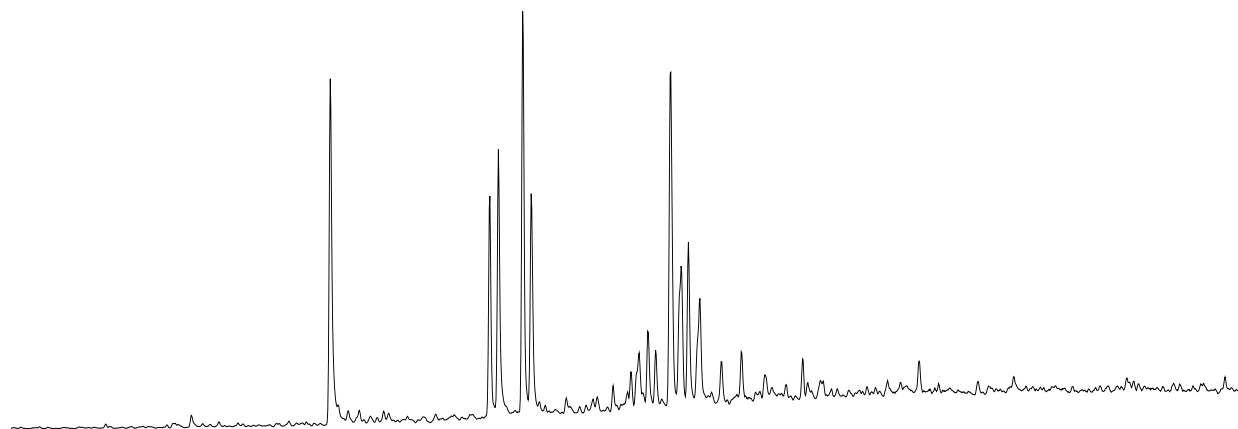
SR-217b



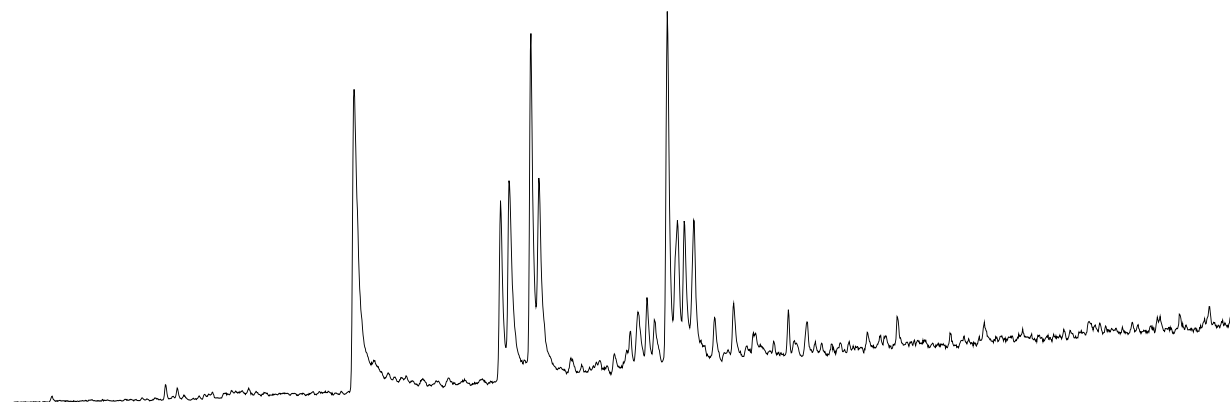
SR-219a



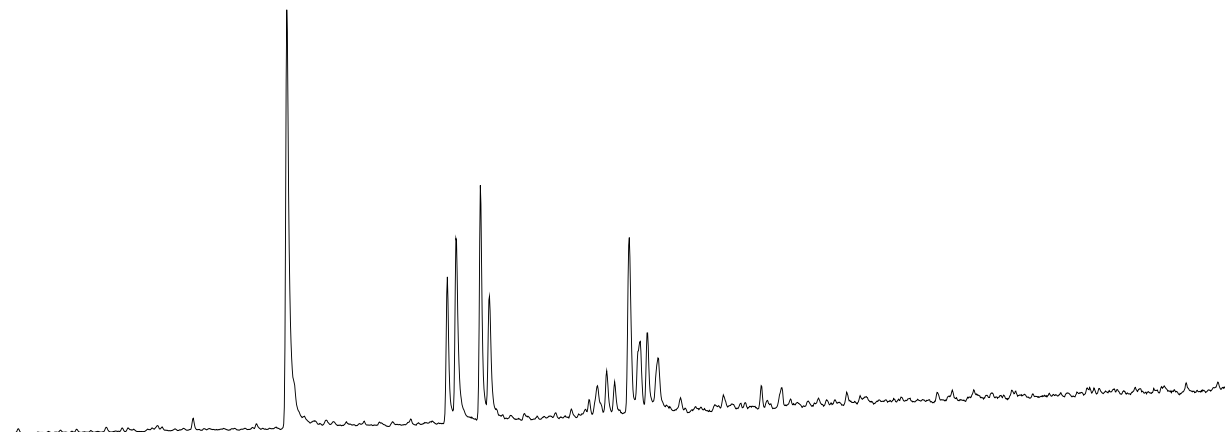
SR-221b



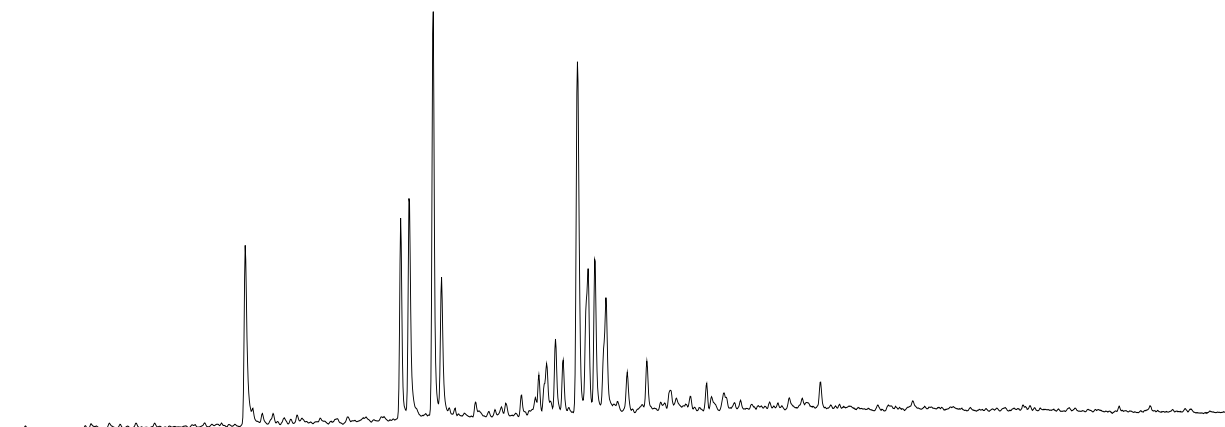
SR-222a



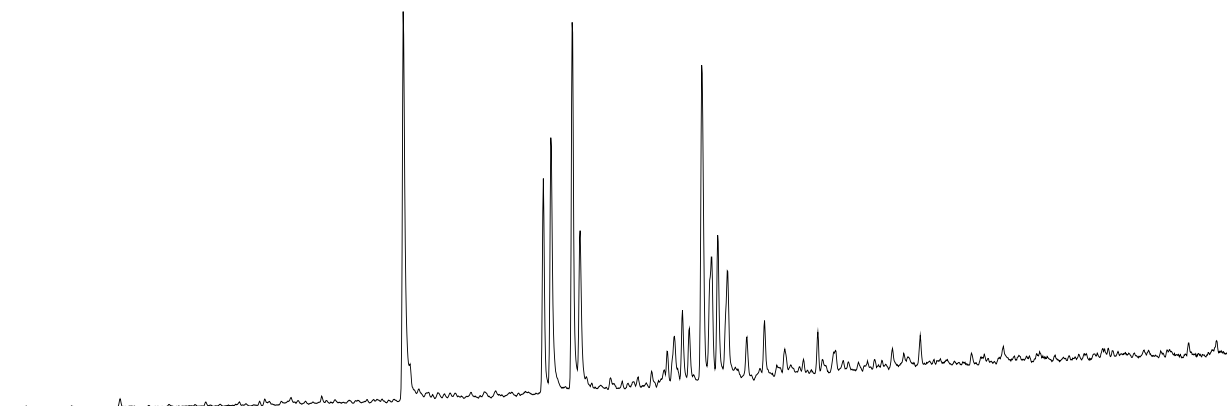
SR-223a



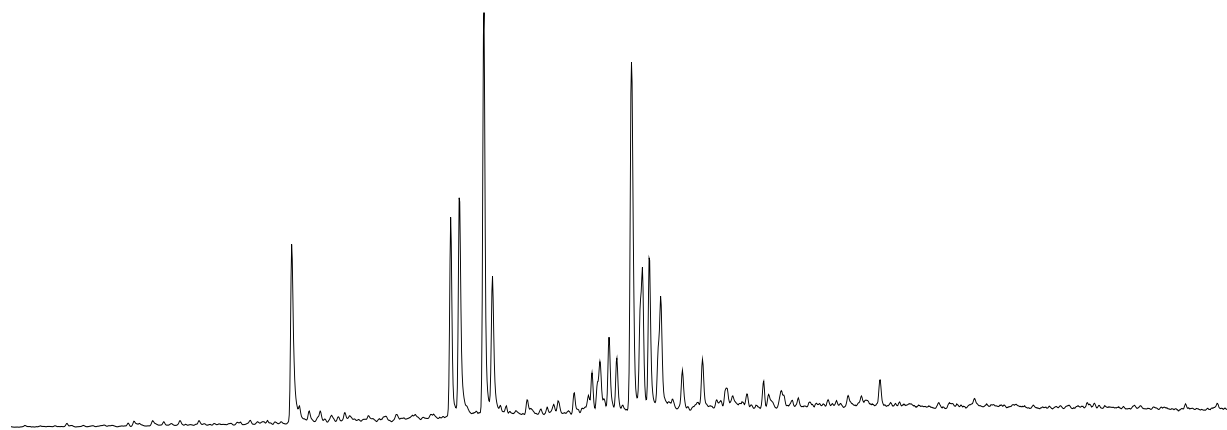
SR-225b



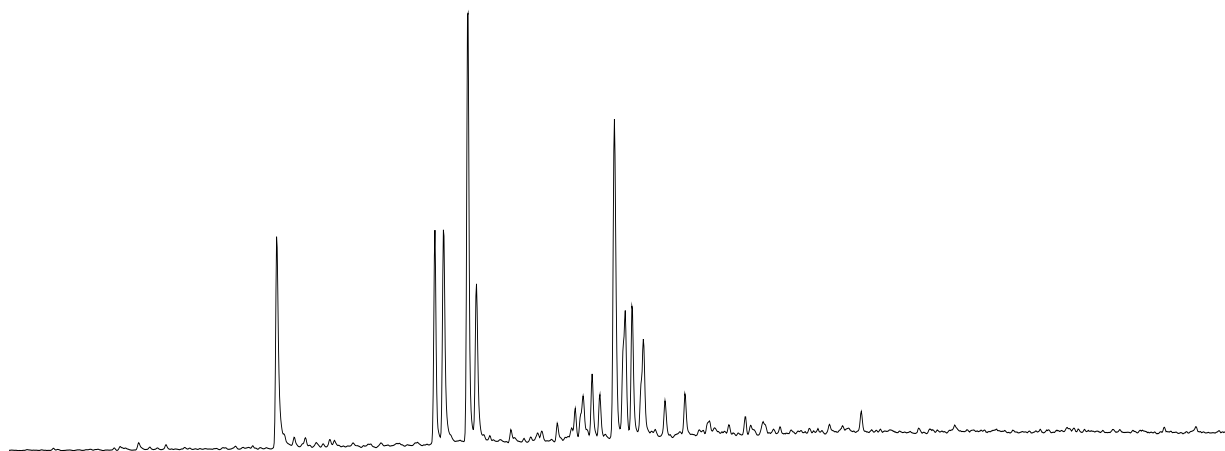
SR-226a



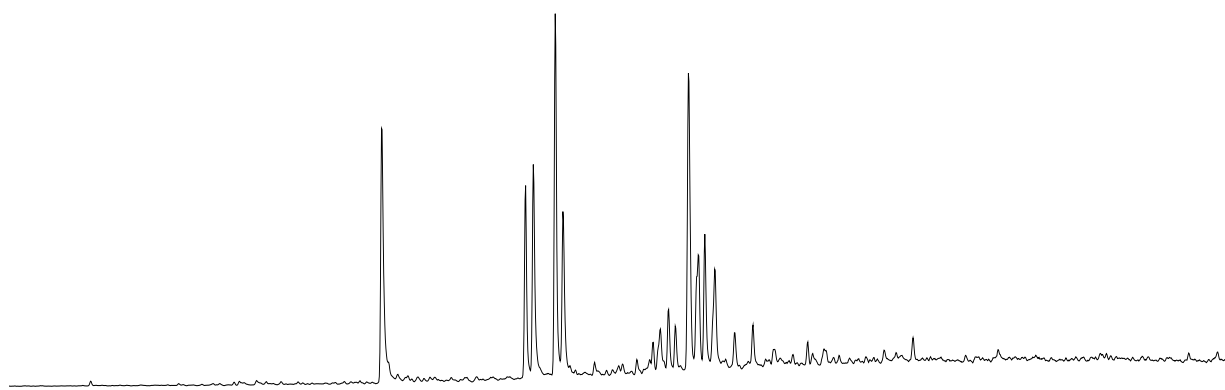
SR-227b



SR-228b



SR-229a



SR-230b

